

Planning and Optimization of Nuclear-Renewable Micro Hybrid Energy Systems for Off-Grid Applications

by

Md Rafiul Abdussami

A thesis submitted to the
School of Graduate and Postdoctoral Studies in partial
fulfillment of the requirements for the degree of

Master of Applied Science in Nuclear Engineering

Faculty of Energy Systems and Nuclear Science

University of Ontario Institute of Technology (Ontario Tech University)

Oshawa, Ontario, Canada

November 2020

© Md Rafiul Abdussami, 2020

THESIS EXAMINATION INFORMATION

Submitted by: **Md Rafiul Abdussami**

Master of Applied Science in Nuclear Engineering

Thesis title:

Planning and Optimization of Nuclear-Renewable Micro Hybrid Energy Systems for Off-grid Applications

An oral defense of this thesis took place on November 16, 2020 in front of the following examining committee:

Examining Committee:

Chair of Examining Committee Dr. Jennifer McKellar

Research Supervisor Dr. Hossam Gaber

Examining Committee Member Mr. John Froats

Thesis Examiner Dr. Jing Ren

The above committee determined that the thesis is acceptable in form and content and that a satisfactory knowledge of the field covered by the thesis was demonstrated by the candidate during an oral examination. A signed copy of the Certificate of Approval is available from the School of Graduate and Postdoctoral Studies.

ABSTRACT

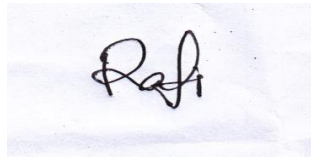
Resilient operation of medium/large scale off-grid energy systems is a key challenge for energy crisis solutions, which requires continuous and sustainable energy resources. In this context, microreactors are incorporated with renewables to provide a continuous, reliable, and sustainable energy supply. The research is apportioned into two parts. In the first part, the study proposes three methods of hybridization for planning and identifying the most efficient Nuclear-Renewable Micro Hybrid Energy System (N-R MHES). Based on proposed hybridization techniques, mathematical modeling of N-R MHES's economy is carried out. An artificial intelligence optimization technique is used to achieve the optimal system configurations of different N-R MHESs and determine the best hybridized nuclear-renewable system. In the second portion of the study, a traditional technology, diesel-fired Micro Energy Grid (MEG), is compared with the best configured N-R MHES. This study of the comparison indicates that microreactor-based MEGs could be a potential replacement for diesel-fired MEGs.

Keywords: Nuclear Power; Renewable Energy; Hybrid Energy System; Energy Management; Sensitivity Assessment.

AUTHOR'S DECLARATION

I hereby declare that this thesis consists of original work of which I have authored. This is a true copy of the thesis, including any required final revisions, as accepted by my examiners.

I authorize Ontario Tech University (UOIT) to lend this thesis to other institutions or individuals for the purpose of scholarly research. I further authorize Ontario Tech University (UOIT) to reproduce this thesis by photocopying or by other means, in total or in part, at the request of other institutions or individuals for the purpose of scholarly research. I understand that my thesis will be made electronically available to the public.

A photograph of a handwritten signature in black ink on a white piece of paper. The signature is stylized and appears to read 'Rafi'.

Md Rafiul Abdussami

STATEMENT OF CONTRIBUTIONS

Part of the work described in this thesis has been published as:

□ Conference Paper

- ✓ **C-01:** H. A. Gabbar and M. R. Abdussami, "Resilient Micro Energy Grids for Nuclear Power Plants During Normal and Emergency Operations," in *Recent Trends in Intelligent Computing, Communication and Devices*, vol. 1006, V. Jain, S. Patnaik, F. Popențiu Vlădicescu, and I. K. Sethi, Eds. Singapore: Springer Singapore, 2020, pp. 1047–1057.
- ✓ **C-02:** M. R. Abdussami and H. A. Gabbar, "Flywheel-based Micro Energy Grid for Reliable Emergency Back-up Power for Nuclear Power Plant," in *2019 IEEE International Conference on Smart Energy Systems and Technologies (SEST)*, Porto, Portugal, Sep. 2019, pp. 1–6, doi: 10.1109/SEST.2019.8849063.
- ✓ **C-03:** H. A. Gabbar and M. R. Abdussami, "Feasibility Analysis of Grid-Connected Nuclear-Renewable Micro Hybrid Energy System," in *2019 IEEE 7th International Conference on Smart Energy Grid Engineering (SEGE)*, Oshawa, ON, Canada, Aug. 2019, pp. 294–298, doi: 10.1109/SEGE.2019.8859925.
- ✓ **C-04:** M. R. Abdussami and H. A. Gabbar, "Nuclear-Powered Hybrid Energy Storage-Based Fast Charging Station for Electrification Transportation," in *2019 IEEE 7th International Conference on Smart Energy Grid Engineering (SEGE)*, Oshawa, ON, Canada, Aug. 2019, pp. 304–308, doi: 10.1109/SEGE.2019.8859878.
- ✓ **C-05:** M. R. Abdussami, Md. I. Adham, and H. A. Gabbar, "Modeling and performance analysis of nuclear-renewable micro hybrid energy system based on different coupling methods", in *TMREES Conference Series: Technologies and Materials for Renewable Energy, Environment and Sustainability - 2020*, June 25-27, Athens, Greece, Energy Report (Elsevier), In-Press. (**Best Paper Award**)

□ Journal Paper

- ✓ **J-01:** H. A. Gabbar, M. R. Abdussami, and M. I. Adham, "Techno-Economic Evaluation of Interconnected Nuclear-Renewable Micro Hybrid Energy Systems with Combined Heat and Power," *Energies*, vol. 13, no. 7, p. 1642, Apr. 2020, doi: 10.3390/en13071642.

- ✓ **J-02:** H. A. Gabbar, M. R. Abdussami, and M. I. Adham, "Micro Nuclear Reactors: Potential Replacements for Diesel Gensets within Micro Energy Grids," *Energies* 2020, 13, 5172, doi: 10.3390/en13195172
- ✓ **J-03:** H. A. Gabbar, M. R. Abdussami and M. I. Adham, "Optimal Planning of Nuclear-Renewable Micro-Hybrid Energy System by Particle Swarm Optimization," *IEEE Access*, doi: 10.1109/ACCESS.2020.3027524.
- ✓ **J-04:** H. A. Gabbar and M. R. Abdussami, "Grid-Connected Nuclear-Renewable Micro Hybrid Energy System," *IEEE Smart Grid Newsletter*, Issue- August 2019. (Available at: <https://smartgrid.ieee.org/newsletters/august-2019/grid-connected-nuclear-renewable-micro-hybrid-energy-system>)

□ **Book Chapter**

- ✓ **B-01:** H. A. Gabbar and M. R. Abdussami, "Planning of Decarbonized Hybrid Energy Systems for Smart Cities", smart cities with financial and policy, Elsevier (In submit).

I performed the majority of the tasks, such as idea formulation, simulation, and writing, in all published works.

ACKNOWLEDGEMENTS

I would like to thank and offer my sincerest gratitude to my thesis supervisor, Dr. Hossam Gaber, for his encouragement, supervision, and support. I cannot imagine having any better advisor for my thesis regarding his knowledge, perceptiveness, and motivation.

Besides, I would like to thank Professor John Froats for his timely guidance. I would also like to thank all of my lab members for their time and support.

I am indebted forever to my family members for their patience, understanding, and endless encouragement during this study.

Md Rafiul Abdussami
Oshawa, Ontario, Canada
November 2020

Table of Contents

AUTHOR'S DECLARATION.....	IV
STATEMENT OF CONTRIBUTIONS.....	V
ACKNOWLEDGEMENTS	VII
Table of Contents	VIII
List of Tables	XI
List of Figures	XI
Nomenclature	XV
Acronym Library	XVI
Chapter 1: Introduction	17
1.1. Background.....	20
1.2. Motivation.....	22
1.3. Problem Definition	24
1.4. Objectives	25
1.5. Thesis Outline.....	26
Chapter 2: Literature Review	27
2.1. Micro Energy Grid (MEG).....	27
2.2. Nuclear-Renewable Integration.....	29
2.2.1. Nuclear-Renewable Micro Hybrid Energy System.....	29
2.2.2. Micro Modular Reactor (MMR)	35
2.3. Combined Heat and Power/Cogeneration	40
2.4. Optimization Algorithms	41
2.4.1. Classical Optimization Techniques	42
2.4.2. Meta-heuristic Optimization Techniques	42
2.4.3. Computer Software	45
2.5. Key Performance Indicators (KPIs).....	45
2.5.1. Generation Reliability Factor (GRF).....	47
2.5.2. Loss of Power Supply Probability (LPSP).....	47
2.5.3. Surplus Energy Fraction (SEF)	48
2.5.4. Levelized Cost of Energy (LCOE).....	49

2.5.5. Level of Autonomy (LA)	49
2.5.6. Renewable Fraction (RF)	49
Chapter 3: Methodology	51
3.1. Research Framework	51
3.2. Methods of Data Collection.....	52
3.3. Methods of Analysis	52
3.4. Discussion on Methodological Choice	56
3.5. Assumptions Considered in Modeling	57
Chapter 4: Proposed System Architectures and Energy Management	59
4.1. Direct Coupling	59
4.2. Single Resource and Multiple Product-based Coupling.....	62
4.3. Multiple Resources and Multiple Product-based Coupling.....	64
Chapter 5: System Modeling.....	66
5.1. Nuclear Power Plant (Micro Modular Reactor).....	66
5.2. Solar Energy	69
5.3. Wind Energy.....	70
5.4. Hydro Power (Water Energy).....	72
5.5. Biomass Energy	73
5.6. Electrolyzer, Hydrogen Tank, and Fuel Cell (FC)	76
5.7. Energy Storage System.....	77
5.7.1. Electrochemical Energy Storage (EES)	77
5.7.2. Thermal Energy Storage (TES).....	78
5.8. H2E unit.....	79
5.9. E2H Unit.....	80
5.10. Diesel Generator	81
Chapter 6: Simulation Model.....	83
6.1. Objective Function.....	83
6.2. Constraints	86
6.3. Decision Variables.....	89
6.4. Implementation of Optimization Algorithm (Particle Swarm Optimization). 91	
Chapter 7: Results and Discussions	94
7.1. Comparison between the Proposed Hybridization Methods	96

7.1.1.	Assessment of Sensitivity to Shifting of Daily Peak Demand	107
7.1.2.	Assessment of Sensitivity to Shifting of Seasonal Demand	109
7.1.3.	Assessment of Sensitivity to Variation in Average Energy Demand....	110
7.1.4.	Assessment of Sensitivity to Variation in System Equipment Cost.....	112
7.1.5.	Assessment of Sensitivity to Variation in Economic Parameters	118
7.1.6.	Assessment of Sensitivity to Variation in Capacity Factor (MMR)	120
7.2.	Comparison between the Best Hybridized System and Diesel-based MEG	121
7.2.1.	Assessment of Sensitivity to Shifting of Daily Peak Demand	129
7.2.2.	Assessment of Sensitivity to Shifting of Seasonal Demand	129
7.2.3.	Assessment of Sensitivity to Variation in Average Energy Demand....	130
7.2.4.	Assessment of Sensitivity to Variation in System Equipment Cost.....	131
7.2.5.	Assessment of Sensitivity to Variation in Economic Parameters	133
7.2.6.	Assessment of Sensitivity to Variation in Renewable Resources	134
7.2.7.	Assessment of Sensitivity to Variation in PV panels and WT Availability	135
Chapter 8:	Conclusions and Recommendations.....	138
8.1.	Summary and Conclusions	138
8.2.	Contributions of the Thesis.....	139
8.3.	Safety Aspects of N-R MHES	140
8.4.	Future Work and Recommendations	142
REFERENCES	144

List of Tables

Table 2-1: A List of Microreactors [75].....	35
Table 2-2: A list of Meta-heuristic Optimization Techniques used in HESs.....	43
Table 5-1: Specification of the MMR Unit.....	67
Table 5-2: Parameters of the Solar PV Panel.....	70
Table 5-3: Parameters of the Wind Turbine.....	71
Table 5-4: Parameters of the Run-of-River System.....	73
Table 5-5: Parameters of the Biogas Plant.....	75
Table 5-6: Parameters of the Fuel Cell	76
Table 5-7: Parameters of the Electrolyzer.....	77
Table 5-8: Parameters of the Hydrogen Tank.....	77
Table 5-9: Parameters of the EES	78
Table 5-10: Parameters of the TES	79
Table 5-11: Parameters of the H2E Unit.....	80
Table 5-12: Parameters of the E2H Unit.....	80
Table 5-13: Parameters of the Diesel Generators	82
Table 7-1: A list of Studied Benchmark Functions	94
Table 7-2: Optimal Configuration of different Proposed N-R MHES.....	97
Table 7-3: KPIs of different Proposed N-R MHESs	98
Table 7-4: A Summary of the Sensitivity Analysis Conducted in Section 7.1	107
Table 7-5: Optimal Configuration of Diesel Genset-bases MEG	124
Table 7-6: Comparison of KPIs between Case-03 and Case-04.....	125
Table 7-7: A Summary of the Sensitivity Analysis Conducted in Section 7.2.....	128
Table 8-1: Different types of Events Associated with Microreactor Facility	140

List of Figures

Figure 1-1: Death Rates by Energy Production Sources.....	17
Figure 1-2: GHG Emissions by Energy Production Sources.....	19
Figure 1-3: Global Energy Share by Energy Production Sources	20
Figure 1-4: A Typical Interconnected N-R MHES.....	22
Figure 2-1: A Typical MEG.....	28
Figure 2-2: MMR Facility consisting of Main NPP and Adjacent Plant	36
Figure 2-3: MMR Plant/Main Nuclear Plant (Simplified Schematic)	37
Figure 2-4: Adjacent Plant (Simplified Schematic).....	39
Figure 2-5: Cutaway View of a TRISO Fuel Particle.....	40
Figure 2-6: Topping Cycle.....	41
Figure 2-7: Bottoming Cycle	41
Figure 2-8: Classification of Optimization Techniques.....	42
Figure 2-9: Implementation of the PSO Algorithm in the Problem.....	45

Figure 2-10: Classification of KPIs	46
Figure 3-1: Research Framework.....	51
Figure 3-2: Solar Irradiance	53
Figure 3-3: Temperature	54
Figure 3-4: Wind Speed	54
Figure 3-5: Electrical Load Profile	55
Figure 3-6: Thermal Load Profile.....	55
Figure 3-7: Streamflow Rate.....	56
Figure 4-1: Schematic of Direct Coupled N-R MHES	60
Figure 4-2: Energy Management Algorithm of Directly Coupled N-R MHES.....	61
Figure 4-3: Schematic of Single Resource and Multiple Products-based Coupled N-R MHES	62
Figure 4-4: Energy Management Algorithm of Single Resource and Multiple Products-based Coupled N-R MHES.....	63
Figure 4-5: Schematic of Multiple Resources and Multiple Products-based Coupled N-R MHES	64
Figure 4-6: Energy Management Algorithm of Multiple Resources and Multiple Products-based Coupled N-R MHES.....	65
Figure 5-1: Capital Cost Reduction for Different Learning Rates.....	67
Figure 5-2: A Typical Power Curve of Wind Turbine.....	71
Figure 5-3: Run-of-River System	72
Figure 5-4: Schematic of the Biogas Plant with CHP.....	74
Figure 5-5: Efficiency Curve of a Diesel Genset.....	82
Figure 7-1: Convergence Plot (Rosenbrock Function)	95
Figure 7-2: Convergence Plot (Ackley Function).....	95
Figure 7-3: Convergence Plot (Michalewicz Function).....	95
Figure 7-4: Convergence Plot (Eggholder Function).....	96
Figure 7-5: Comparison of NPC for the Proposed N-R MHES.....	96
Figure 7-6: Convergence Plot (Case-01)	99
Figure 7-7: Total Energy Generation and Consumption Scenario (Case-01).....	99
Figure 7-8: Energy Storage Operation (Case-01)	100
Figure 7-9: Convergence Plot (Case-02)	100
Figure 7-10: Total Electric Energy Generation and Consumption Scenario (Case-02) .	101
Figure 7-11: Total Thermal Energy Generation and Consumption Scenario (Case-02)	101
Figure 7-12: Energy Storage Operation (Case-02)	101
Figure 7-13: Convergence Plot (Case-03)	102
Figure 7-14: Total Electric Energy Generation and Consumption Scenario (Case-03) .	102
Figure 7-15: Total Thermal Energy Generation and Consumption Scenario (Case-03)	103
Figure 7-16: Energy Storage Operation (Case-03)	103
Figure 7-17: Electric Load Profile (for energy management algorithm verification)....	104
Figure 7-18: Thermal Load Profile (for energy management algorithm verification) ...	104
Figure 7-19: Energy Management Algorithm Verification (Case-01).....	105

Figure 7-20: Electric Energy Management Algorithm Verification (Case-02)	105
Figure 7-21: Thermal Energy Management Algorithm Verification (Case-02)	105
Figure 7-22: Electric Energy Management Algorithm Verification (Case-03)	106
Figure 7-23: Thermal Energy Management Algorithm Verification (Case-03)	106
Figure 7-24: Shifted Electric Peak Demand (daily)	107
Figure 7-25: Shifted Thermal Peak Demand (daily)	108
Figure 7-26: Impact of Variation in Daily Peak Demand	108
Figure 7-27: Shifted Electric Peak Demand (seasonal)	109
Figure 7-28: Shifted Thermal Peak Demand (seasonal)	109
Figure 7-29: Impact of Variation in Seasonal Peak Demand	110
Figure 7-30: Impact of Variation in Average Electric Demand	111
Figure 7-31: Impact of Variation in Average Thermal Demand	112
Figure 7-32: Impact of Variation in both Average Electric and Thermal Demand	112
Figure 7-33: Impact of Variation in System Equipment Cost (Case-01)	113
Figure 7-34: Impact of Variation in Different Types of Cost of MMR (Case-01)	114
Figure 7-35: Error Analysis of Microreactor Costs (Case-01)	114
Figure 7-36: Impact of Variation in System Equipment Cost (Case-02)	115
Figure 7-37: Impact of Variation in different types of Cost of MMR (Case-02)	115
Figure 7-38: Error Analysis of Microreactor Costs (Case-02)	116
Figure 7-39: Impact of Variation in System Equipment Cost (Case-03)	117
Figure 7-40: Impact of Variation in different types of Cost of MMR (Case-03)	117
Figure 7-41: Error Analysis of Microreactor Costs (Case-03)	118
Figure 7-42: Impact of Variation in Project Lifetime	119
Figure 7-43: Impact of Variation in Discount Rate	119
Figure 7-44: Impact of Variation in Inflation Rate	120
Figure 7-45: Impact of Variation in Capacity Factor (MMR)	121
Figure 7-46: Schematic of Diesel Genset-based MEG	122
Figure 7-47: Energy Management Algorithm of Diesel Genset-based MEG	123
Figure 7-48: Comparison of the NPC between Case-03 and Case-04	124
Figure 7-49: Convergence Plot (Case-04)	125
Figure 7-50: Total Electric Energy Generation and Consumption Scenario (Case-04) .	126
Figure 7-51: Total Thermal Energy Generation and Consumption Scenario (Case-04)	126
Figure 7-52: Energy Storage Operation (Case-04)	127
Figure 7-53: Electric Energy Management Algorithm Verification (Case-04)	127
Figure 7-54: Thermal Energy Management Algorithm Verification (Case-04)	128
Figure 7-55: Impact of the Shifting of Daily Peak Demand	129
Figure 7-56: Impact of the Shifting of Seasonal Peak Demand	130
Figure 7-57: Impact of Variation in Average Electric Demand	130
Figure 7-58: Impact of Variation in Average Thermal Demand	131
Figure 7-59: Impact of Variation in both Average Electric and thermal Demand	131
Figure 7-60: Impact of Variation in System Equipment Cost (Case-04)	132
Figure 7-61: Impact of Variation in Diesel Genset Cost	132

Figure 7-62: Impact of Variation in Project Lifetime	133
Figure 7-63: Impact of Variation in Discount Rate	133
Figure 7-64: Impact of Variation in the Inflation Rate	134
Figure 7-65: Impact of Variation in the Solar Irradiance.....	135
Figure 7-66: Impact of Variation in the Wind Speed.....	135
Figure 7-67: Impact of Variation in PV Panels Availability	137
Figure 7-68: Impact of Variation in WT Availability.....	137
Figure 7-69: Impact of Variation in both PV Panels and WT Availability	137

Nomenclature

$P_{PV}(t)$	Power generation (kW) by PV panel at time step t .
$P_W(t)$	Power generation (kW) by WT at time step t .
$P_{MMR}(t)$	Power generation (kW) by MMR at time step t .
$P_h(t)$	Power generation (kW) by hydro plant at time step t .
$P_{bio}(t)$	Power generation (kW) by BG at time step t .
$P_{diesel}(t)$	Total electric power generation (kW) by diesel Genset at time step t .
$T_{MMR}(t)$	Thermal power generation (kW) by MMR at time step t .
$T_{bio}(t)$	Thermal power generation (kW) by BG at time step t .
$T_{diesel}(t)$	Total thermal power generation (kW) by diesel Genset at time step t .
$P_{EL}(t)$	Electric load demand at time step t .
$P_{TL}(t)$	Thermal load demand at time step t .
$FC_{dch}(t)$	Available discharging power of FC at time step t .
$FC_{ch}(t)$	Available charging power of FC at time step t .
$EES_{dch}(t)$	Available discharging power of EES at time step t .
$EES_{ch}(t)$	Available charging power of EES at time step t .
$TES_{dch}(t)$	Available discharging power of TES at time step t .
$TES_{ch}(t)$	Available charging power of TES at time step t .
t_{total}	Total time.
$E2H(t)$	Generated power by E2H at unit time step.
$H2E(t)$	Generated power by H2H at unit time step.
$E_{dump}(t)$	Dumped power at electric dump load at time step t .
$T_{dump}(t)$	Dumped power at thermal dump load at time step t .
$H2E_{eff}$	Efficiency of H2E unit.

Acronym Library

BG	Biogas Generator
CHP	Combined Heat and Power
E2H unit	Electricity-to-Heat conversion unit
EES	Electrochemical Energy Storage
FC	Fuel Cell
GRF	Generation Reliability Factor
HES	Hybrid Energy System
HT	Hydro Turbine
H2E unit	Heat-to-Electricity conversion unit
KPI	Key Performance Indicator
LA	Level of Autonomy
LCOE	Levelized Cost of Energy
LPSP	Loss of Power Supply Probability
MEG	Micro Energy Grid
MMR	Micro Modular Reactor
NPC	Net Present Cost
N-R HES	Nuclear-Renewable Hybrid Energy System
N-R MHES	Nuclear-Renewable Micro Hybrid Energy System
O&M	Operations and Maintenance
PSO	Particle Swarm Optimization
PV	Photovoltaic
RES	Renewable Energy Source
SEF	Surplus Energy Fraction
SOC	State of Charge
TES	Thermal Energy Storage
UOIT	University of Ontario Institute of Technology
WT	Wind Turbine

Chapter 1: Introduction

Electricity is an essential precondition for global advancement and economic growth. Electricity demand is rising proportionally to the population and economic development. Currently, the world is undergoing two main challenges for managing high electricity demand. The first problem is how to support the increased demand for electricity without exploiting finite energy resources (mainly fossil fuels). Another challenge is how to produce electricity without affecting the environment [1].

Energy crisis leads to most of the challenges and opportunities that the world is facing nowadays. All energy production sources have shortcomings, such as air pollution, accidents, and GHG emissions. About five million premature deaths has been occurred every year due to air pollution [2], and fossil fuel is the main contributor to air pollution. Mining of fossil fuel and uranium, raw material transportation, construction, oil and gas extraction, and deployment involve accidents. Though there are numerous downsides in energy generation, it varies significantly depending on generation sources. Clearly, fossil fuel is the deadliest and dirtiest form of energy production source, while nuclear and Renewable Energy Source (RES)-based generation are the cleanest and safest form of energy production. Fig. 1-1 represents the death rate percentage per TWh from different energy production sources in Europe [3]. It should be noted that anti-pollution regulations are already well-established in Europe. Hence, the death rate caused by fossil fuel may increase for other regions.

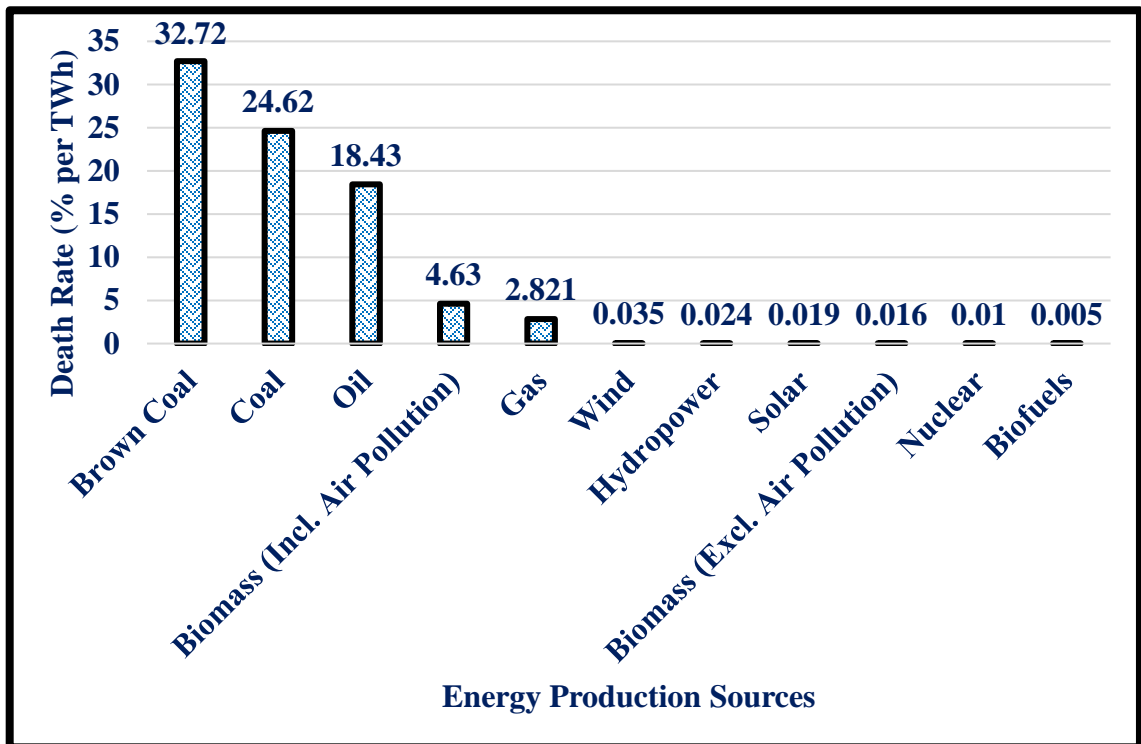


Figure 1-1: Death Rates by Energy Production Sources

A substantial amount of electric energy is currently produced from conventional sources like coal, gas, and oil. Generation of electricity by using these resources tends to increase Greenhouse Gas (GHGs) in the atmosphere. Research is ongoing to lessen the environmental impact of traditional source usages for electricity generation. For instance, one such initiative is the implementation of Carbon Capture and Storage (CCS). In this process, the waste carbon dioxide from power plants can be captured and transported to a storage site for disposal. Thus, carbon dioxide is restricted from dispersion in the environment [4].

In recent times, the world is looking for sustainable energy sources that will be used to meet today's demand without putting the sources into a threat to future usages. Consequently, RESs, such as solar, wind, geothermal, hydropower, and ocean energy, are recognized as sustainable sources for electric energy production [5]. RESs are intermittent, and electricity cannot be stored economically for a lengthened period. Therefore, some other energy sources are needed to provide back-up for RESs during their unavailability period and act as a base load or critical load supplier.

Affordable, resilient, and carbon-free electricity generation is the most vital determinant to achieve a sustainable energy system. Mostly, RESs are recognized as carbon-free energy resources to meet electric demand. Due to nearly zero carbon emissions from nuclear plants, there is a worldwide tendency to move towards nuclear energy. The hybridization between RESs and nuclear reactors may result in a carbon-free, reliable, and innovative energy infrastructure.

Public perspectives on nuclear energy vary widely from country to country, and nuclear energy policies are not friendly in several countries. After the Fukushima-Daiichi nuclear disaster in 2011, Germany planned to phase out 10 out of 17 nuclear plants from 2011 to 2017. Germany intends to shut down the remaining nuclear facilities by 2022. It is estimated that the phase-out policy of nuclear plants will cause more than 1,100 new deaths in Germany due to air pollution from other conventional generation sources [6]. A study reports that around two million lives would have been saved if fossil fuel-based generation had been replaced by nuclear [7].

Energy sources also have long-term consequences on climate change. Fossil-fired based generations release a significant amount of GHGs. The energy resources emitting the least carbon are considered the safest and cleanest form of sources. Several co-benefits regarding public health, safety, and environmental impact have been reported if fossil-fired generations are substituted by either renewables or nuclear [8],[9]. Fig. 1-2 represents the amount of carbon dioxide generation by sources per kWh [3]. It can be concluded by comparing Fig. 1-1 and Fig. 1-2 that safer resources have lower pollution. Coal, oil, and natural gas are still the highest contributors to environmental pollution depicted in Fig. 1-2. Though technology deployment depends on several factors, e.g., capital cost, construction time, and project location, nuclear and renewables are the most appropriate technologies in terms of human health and environmental issues.

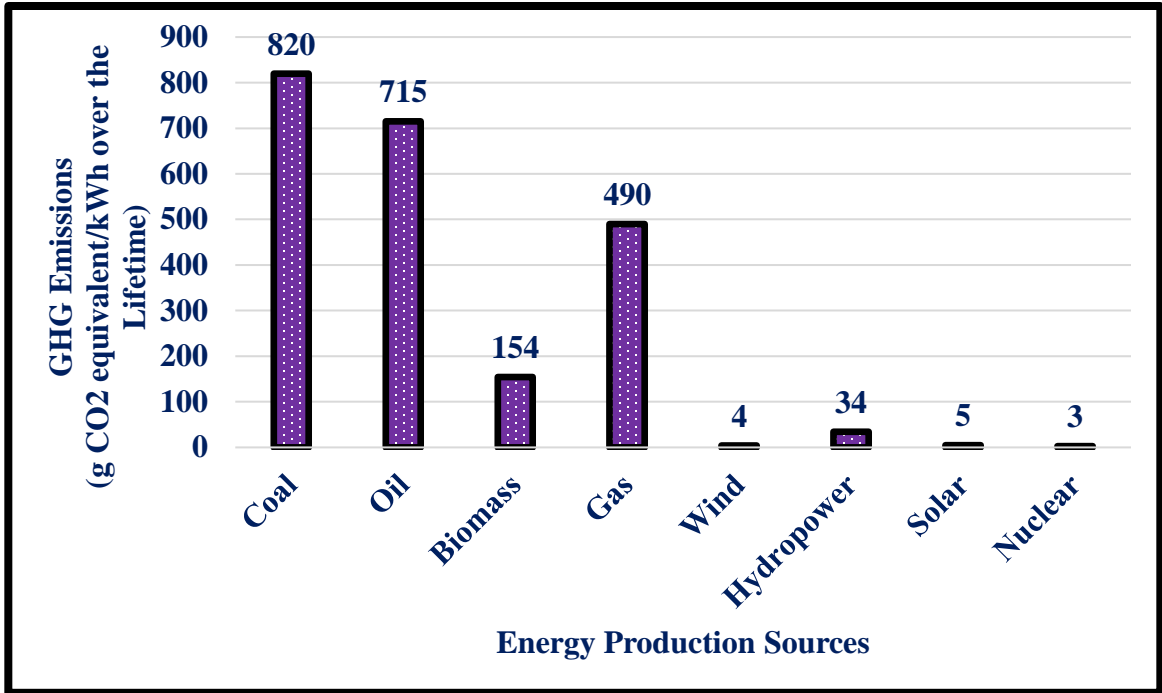


Figure 1-2: GHG Emissions by Energy Production Sources

Fig. 1-3 exhibits the energy share by different sources from 1975-2020 [10]. It is important to note that the summation of individual percentage by the sources will not give 100% since some other resources are not placed in Fig. 1-3. The International Energy Agency (IEA) is expecting that global energy share by renewables will take the lead over the coal-powered generation by 2020. It is also predicted that coal-powered generation share will fall at the highest margin in 2020 for the first time in the last 45 years. Renewables have already taken the lead over coal in 2019. Renewables are expected to increase more since several projects will be completed in the upcoming years [10]. Because of minimal GHG emissions, affordability, and sustainability, nuclear and RESs have become vital energy sources. Therefore, nuclear and renewables should go hand-in-hand to maximize the benefits and provide an innovative energy crisis solution.

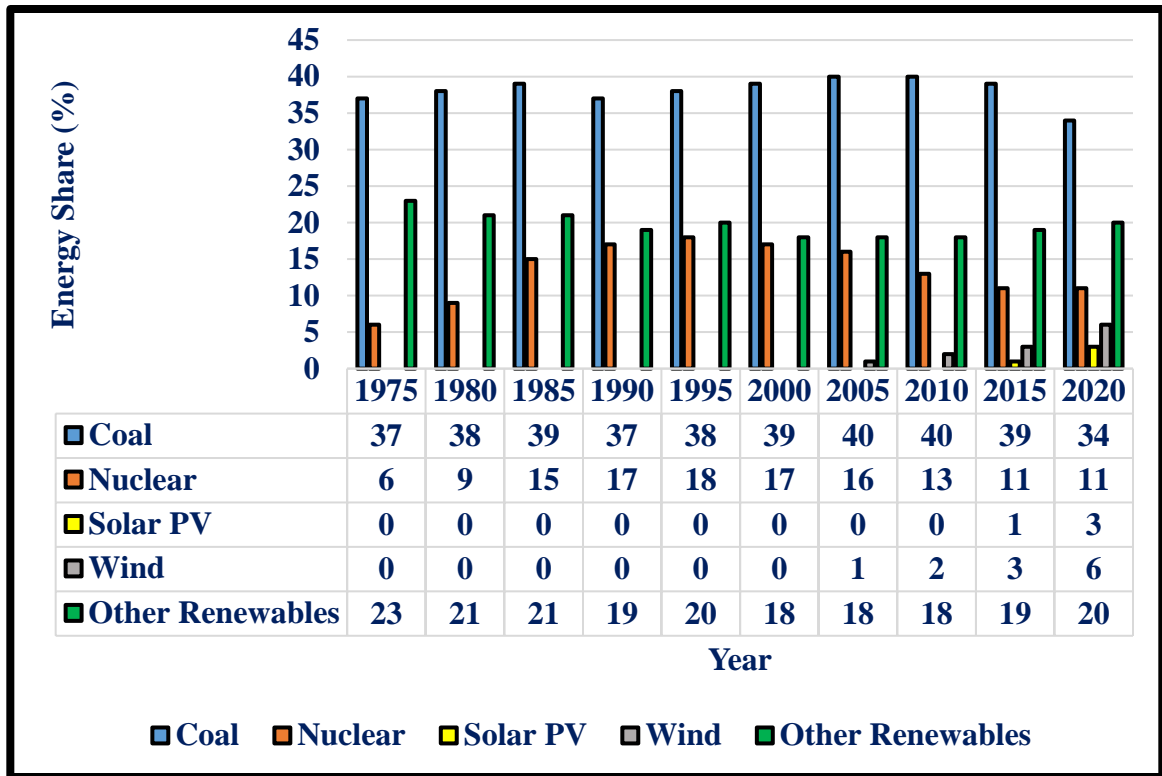


Figure 1-3: Global Energy Share by Energy Production Sources

This study concentrates on micro-scale nuclear-renewable integration for off-grid applications. Different coupling approaches for off-grid applications are proposed and discussed in this research. Efficient and straightforward energy management techniques have also been offered for integrated systems. A robust optimization technique is applied to obtain the best system configuration. The study also investigates the techno-economic feasibility of Nuclear-Renewable Micro hybrid Energy Systems (N-R MHESs) by comparing traditional fossil-fired technologies.

1.1. Background

Electric demand for distant locations is typically served by Micro Energy Grid (MEG) since the electric grid footprint is not available. MEG refers to an energy network that links local RESs to support electrical and thermal demand. The generation side of an MEG involves fossil-fired internal combustion engines, microturbines, fuel cells, and RESs. The sizing of microgrids solely depends on assessment and understanding of system load and geographical characteristics; a specific sizing of MEG does not fit all types of system demand [11]. The "Combined Heat and Power (CHP)" and the "Distributed Generation (DG)" concepts are employed together in MEG to generate electric and thermal energy. An MEG can operate both grid-connected and off-grid mode. MEG allows high penetration of RESs, reduces transmission losses, enhances system reliability by operating in island mode during the fault, and improves energy management capability [12].

The CHP is also known as "Cogeneration"- concomitant generation of electric and thermal power from the same energy source. In a CHP facility, the waste heat is recovered and used as valuable thermal power for heating and cooling. Most of the electricity generation plant utilizes heat engines to produce electricity from heat. The theoretical heat-to-electricity conversion efficiency for modern combustion plants range from 30% to 60%; practical efficiency can be even less than the theoretical. CHP facility can improve the overall system efficiency of up to 90% and, CHP's benefits are widely recognized. Nevertheless, recovered waste heat is not usually considered for large-scale electricity generation plants since traditional generation plants are located far from the consumer end. Therefore, decentralized generation at the consumer end has a great potential to use waste heat by CHP units [13].

Microreactors can replace fossil fuel-based generators within MEG to reduce GHG emissions significantly and improve system operating conditions. An MEG, along with microreactors, is termed as " N-R MHES." N-R MHES is a combination of very small-scale nuclear reactors, called Micro Modular Reactor (MMR), and different RESs. N-R MHES provides a resilient energy supply for electric and thermal demand for off-grid applications. DG principle is also implemented in N-R MHES. CHP criteria are often applied in N-R MHES, but there are no binding rules for CHP implementation. In traditional MEG, RESs and fossil fuel-based generators are regarded for energy production. At the same time, nuclear reactors and RESs are considered as generators in N-R MHESs instead of fossil-fired generators [14]. An N-R MHES provides virtually zero carbon footprint since no fossil fuel is burnt within the system. However, some GHGs are released at mining, construction phase of the system, fuel and raw materials shipment, decommissioning, and waste management [15].

N-R MHES can offer several secondary commodities. Fig. 1-4 represents a typical interconnected N-R MHES with possible resources and applications [16]. An interconnected Nuclear-Renewable Hybrid Energy System (N-R HES) can serve several applications, such as seawater desalination, electric transportation, district heating, and calcination. It is also economical to produce secondary commodities with N-R HES rather than only satisfying electrical and thermal demand [8].

to achieve a 100% RES-based energy system. The flexibility measures, such as energy storage, can respond to the intermittency of RES in this type of scenario [21]. Stand-alone RES-based HES, combined with energy storage, is possible to some extent to serve small-scale energy demand. However, the sizing of energy storage, e.g., electric battery, Pumped Hydro Storage (PHS), and hydrogen, is critical for a microgrid. Moreover, there is no large-scale storage available currently, and a few large scales (in MW scale) electric batteries are being proposed to develop some areas [22]. Large-scale PHS is available, but PHS is site-specific and has a high capital cost [23]. Hydrogen can be a possible massive energy storage media. Fuel Cell (FC) utilizes the stored hydrogen to generate electricity. Nonetheless, FC's efficiency is significantly low (around 30%-60%), and it is under the research and development (R&D) stage [24]. It is recommended to allow high penetration of renewables and install energy storage systems to overcome intermittency drawbacks. Therefore, energy storage systems are always indispensable, but a clean and continuous form of energy source is also required to minimize the vast energy storage requirement.

Typically, MEG's operating strategy comprises diesel generator and energy storage to support energy demand and ensure system reliability. Due to lower initial cost and fast response characteristics, diesel Genset is usually integrated with RESs to meet small scale demands (in a kW). Diesel Genset has high fuel and maintenance cost, and it produces a notable amount of GHGs, e.g., carbon monoxide, black carbon, sulfur dioxide, nitrogen oxide, and particulate matter [25]. Diesel Genset can operate from 15,000 to 50,000 hours in its' lifetime [26]. However, the continuous operation for serving medium/high energy demand reduces the lifetime of a Genset.

Because of the high fixed cost, high capacity factor, and base-load supply capability of MMR, stand-alone off-grid MMR-based energy systems do not provide flexible and economic operation [27]. A vast amount of energy will be wasted in this type of off-grid energy systems even if energy storage systems are included. Stand-alone off-grid MMR-based energy systems also elongate the energy storage sizing unnecessary since the surplus energy can not be sold to electric grids [28]. Hence, energy-mix is an essential pathway for the global energy crisis solution. In [29], it is stated that the optimal range of contribution of renewable, nuclear, and gas technology in a hybrid system should be 50%, 50-60%, and 70-80%, respectively. However, gas technologies produce a significant amount of GHG emissions.

Bragg-Sitton et al. (2014) addressed a few challenges for integrating clean and reliable baseload generation sources, Nuclear Power Plants (NPPs), with intermittent RESs. It is also not an economical approach to run a baseload energy system into load-following to handle variable resources. Underutilized resource capacity and cycling cost can also make a system economically extravagant [30].

In these circumstances, it is imperative to introduce an energy source that will provide continuous electric and thermal energy supply for medium/large-scale demand. Usually, RESs cannot provide a constant supply for a longer duration. Hence, a nuclear microreactor, a continuous mode of power supply with essentially zero carbon emissions,

is aimed to combine with RESs and energy storage systems. Nuclear-renewable integrated systems assure continuity, reliability, and resiliency for off-grid applications. An efficient energy management and control algorithm is also required to minimize the challenges of a nuclear-renewable integrated system.

1.3. Problem Definition

Though integrated nuclear-renewable energy systems have been addressed in a few pieces of literature, precise hybridization techniques for micro-scale nuclear-renewable integrated systems need to be focused on. Research on the modeling of generic N-R HES is going on at Idaho National Laboratory (INL), Oak Ridge National Laboratory (ORNL), and Argonne National Laboratory (ANL) to test the economic viability of integrated systems [31]. Some researchers aim to develop a few interconnected nuclear-renewable hybridization models for large-scale integration [17]. Still, small-scale integrated systems might provide different innovations due to the unique characteristics of MMR. Therefore, specific hybridization techniques of N-R MHES for off-grid applications are required. The nuclear-renewable interconnection techniques also need to be verified through engineering approaches.

Simulation platforms of nuclear-renewable hybrid systems require modeling of system architecture to implement the energy management algorithm and assess the techno-economic feasibility. The techno-economic evaluation does not require dynamic modeling of each system component. However, the system component design needs power balance models, reliability parameters, and different cost models associated with system performance.

Identification of Key Performance Indicators (KPIs) is necessary to assess system performance, and KPIs must comprise technical and economic criteria. Besides, since the coupling techniques offer compact and efficient energy management algorithms for different HESs, a robust optimization technique is demanded to achieve the systems' optimal configuration. Optimal system configuration is a prerequisite to analyze interconnected nuclear-renewable hybrid systems. The interconnected systems involve a massive amount of data and sophisticated energy management techniques. Traditional optimization techniques are not adequate to find the best solution composing of a large amount of data. In this situation, an intelligent optimization technique is a right choice.

Sensitivity analysis is another fundamental approach for evaluating this type of study. The objective function of N-R MHES optimization depends on several sensitivity variables. Average energy demand fluctuation, peak demand shifting, component cost, project lifetime, discount rate, inflation rate, generator capacity factor, and system reliability constraints have a significant impact on the fitness function of the hybrid system optimization problem. The analysis results of N-R MHES must be confirmed through sensitivity assessment. This type of evaluation helps the user to strengthen the decision-making framework.

The techno-economic feasibility assessment of a micro-scale nuclear-renewable integrated system has not been conducted yet. Economic aspects and system reliability need to be evaluated for the proposed N-R MHESs. Besides, as N-R MHESs could be an excellent replacement of fossil-fired MEGs for off-grid applications, a comparative study based on selected KPIs between the proposed methods and traditional technologies is compulsory. The comparative research must evaluate the system's output sensitivity to all possible input variables.

1.4. Objectives

The study's primary goals are to develop and identify the most effective nuclear-renewable hybridization technique and compare the competency of the best N-R MHES with traditional technologies. To achieve the goals, the study will cover the following objectives:

- Development of different coupling/hybridization methods for integrating nuclear and renewable resources within Micro Energy Systems (MESs).
- Modeling of N-R MHESs based on the developed coupling methods.
- Identification of KPIs for techno-economic evaluation of N-R MHESs.
- Optimization and sensitivity analysis of the micro hybrid energy systems in view of evaluating the system performance.
- Utilization of the proposed optimal N-R MHES to compare with conventional technologies.

Three different coupling methods are proposed for micro-scale nuclear-renewable hybridized systems in the first step. Three distinct types of energy management algorithms are also developed for each system configuration. In the next level, economic modeling of each system component is accomplished in the MATLAB simulator for the techno-economic assessment. A list of KPIs is identified to evaluate the cost-efficiency and reliability of the systems. Later, a robust optimization technique, titled Particle Swarm Optimization (PSO), is implemented to obtain the best system configurations for three different hybridized systems in terms of Net Present Cost (NPC). System reliability constraints and energy balance constraints are employed in the optimization problem. System performance is evaluated based on the selected KPIs and sensitivity analysis.

In the following step, the best N-R MHES, among the three proposed hybridized nuclear-renewable systems, is used to compare it with other possible technologies. A diesel Genset is used as a convenient surrogate technology for this study. Diesel Genset is inserted into the best N-R MHES to replace MMR, while the rest of the system components are kept the same. The new system arrangement is labeled "Diesel Genset-based MEG." An identical energy management algorithm and reliability constraints are also used here to obtain the optimal configuration of the diesel-based MEG. In the later section, the best N-R MHES and the optimal diesel Genset-based MEG are compared to recognize these two systems' superiority. Sensitivity analyses are conducted in all sections to strengthen the achieved results.

1.5. Thesis Outline

The thesis is structured in chapters, which include sections and sub-sections. The total number of chapters of this thesis is seven. The current chapter holds the "Introduction" chapter.

The second chapter aims to provide a brief literature review of the research. The section covers fundamental concepts and state-of-arts of MEG, N-R HES, MMR, CHP, optimization algorithms, and system KPIs.

The third chapter contains the research methodology. The research framework, data collection methods, methods of analysis, discussion on methodological choice, and assumptions are discussed in detail here.

The proposed N-R MHESs based on distinct hybridization methods are outlined in Chapter-04. The system working principle and energy management algorithms are described in this section. A detailed representation of diesel-fired MEG is also shown here.

The components of the system architecture are identified and discussed in Chapter-05. Required mathematical equations, system sizing, and component cost of each element are presented in this chapter.

Chapter-06 interprets the mathematical details of the optimization problem formulation. The objective function, optimization constraints, and decision variables are listed in this chapter. The implementation steps of optimization techniques are also shown in this section.

Chapter-07 holds the results and discusses the research findings. The effectiveness of the proposed hybridization techniques is compared and analyzed in this section based on system KPIs. The diesel-fired MEG is also examined in the second part of this chapter.

Finally, Chapter-08 concludes with a summary and direction of the intended future works of this study. This chapter also summarizes the main contribution of the research carried out.

Chapter 2: Literature Review

The literature reviewed for this research is presented in four main sections. Section 2.1 provides an overview of MEGs and their advantages over conventional energy infrastructure. It also discusses the research works done in MEG. Section 2.2 offers detail on previous research activities on nuclear-renewable integration. This study intends to integrate MMR with renewables, and MMR is a new concept. Therefore, MMR's brief idea is also provided in this section. A concise description of cogeneration, also known as CHP, is stated in Section 2.3. Different types of optimization techniques are reviewed in the subsequent section, Section 2.4. Finally, Section 2.5 lists the system performance indicators considered for the study.

2.1. Micro Energy Grid (MEG)

MEGs are a new form of microgrids (power grids) that simultaneously supply electric and heat energy [30]. MEGs add CHP units to provide thermal energy. An MEG combines different types of fossil-fired energy generation resources and RES, and it is located at the consumer end. The "Distributed Generation (DG)" concept is applied in MEGs. MEGs are considered as a potential solution for low-cost energy supply and reduction of GHG emissions. Uniqueness, diversity, controllability, interactivity, and independence are the main features of MEGs. Energy storage systems are installed in MEGs to confirm the energy grid's stability and reliability. Energy storage systems also supply energy to grids and loads in case of emergencies. MEGs can perform both at the grid-connected mode as well as at the islanded mode. Bidirectional power supplies are available between MEGs and traditional grids, and it provides outstanding support for conventional grids during a blackout [12], [32]. A typical MEG is presented in Fig. 2-1 [33]. The benefits of MEGs can be explained as follows [34], [35].

- *Reduction of Energy Loss:* Since the distance between generation sources and loads is minimal, MEGs reduce the transmission losses of electric and heat energy significantly.
- *Capability of high RES penetration:* MEGs can handle high penetration of RESs with Electrochemical Energy Storage (EES), Thermal Energy Storage (TES), and plug-in electric vehicles. It also utilizes the intermittent nature of RESs efficiently.
- *Improvement of Energy Management:* Planning of an MEG includes the optimal number of system components. Therefore, electric and heat energy are utilized properly within an MEG.
- *Contribution to Secondary Production:* Since an MEG generates electric and thermal energy simultaneously, excess electrical and thermal power can contribute to forming secondary products, such as hydrogen and water.

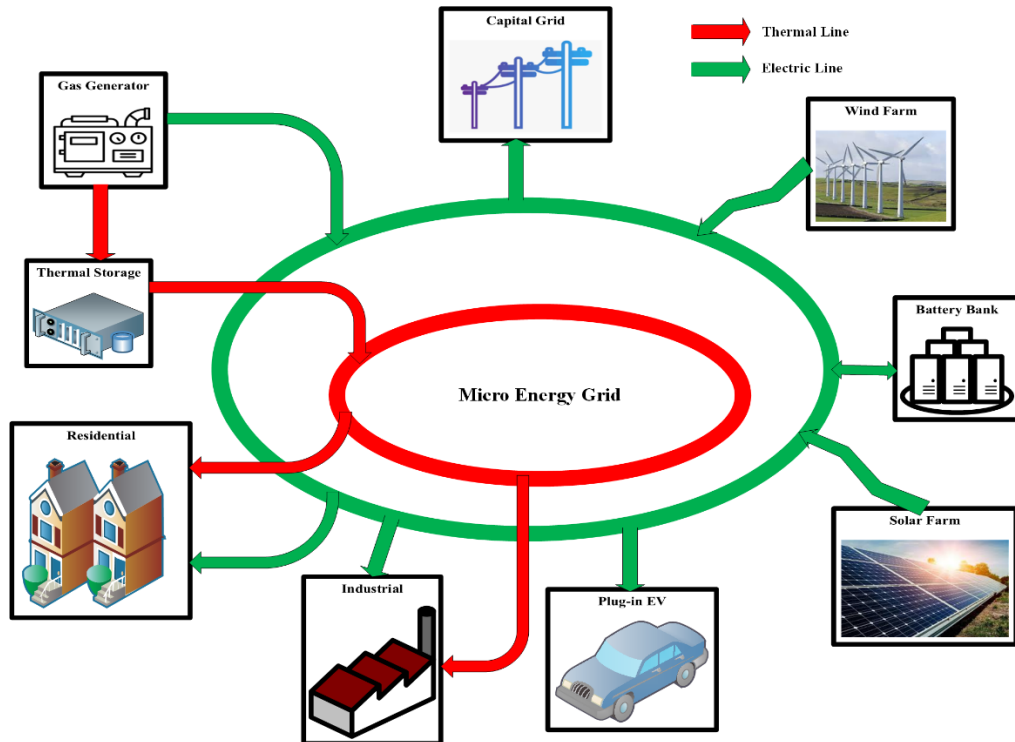


Figure 2-1: A Typical MEG

An HES is a single facility that includes multiple energy resources as inputs and produces one or more products as outputs. Among the output products, there must be at least one commodity like electricity or transportation fuel. HESs include multiple energy conversion subsystems. In HESs, the products might be coupled behind electric transmission buses or electric grids. An electric grid is regarded as a single entity and an immensely dynamic and responsive subsystem for supplying electrical energy. Several types of integration are possible in HESs, such as electrical, mechanical, thermal, chemical, and hydrogen. An advanced control system is used in HESs to maintain energy demand, energy conversion strategy, and subsystems' operating principles. Moreover, HESs produce many non-energy outputs whose outputs are energy-intensive; this increases the system performance and overall profitability [14].

Different manufacturers are designing several types of power supply facilities, such as mobile microgrids with portable energy storage systems, for off-grid applications. These facilities need extensive energy storage systems, fuel storage, and diesel generators for continuous power supply. It might be a suitable solution for a small community with minimal energy demand [36]. Still, a traditional microgrid is not competent in handling large scale commercial and industrial loads in a remote area.

Several pieces of research have been carried to identify the optimal system configuration to provide a resilient electric supply. Giatrakos et al. (2009) predicted the viability of a Photovoltaic (PV)/diesel Genset/batteries-based HES [37]. Mohammed et al. (2019) optimized a Wind Turbine (WT)/tidal turbine/PV panel/batteries-based HES to provide a

reliable electricity supply to a distant area in Brittany, France. The PSO was used as an optimization technique in [38]. Ming et al. (2017) proposed optimal design methods for a PV/WT/batteries-based HES for both grid-connected and islanded modes of operation. A Multi-Objective Evolutionary Algorithm (MOEA) was used in [39] to minimize system cost and fuel emissions. An and Tuan (2018) proposed an HES optimization method based on a dynamic programming method to reduce system cost for a location in Vietnam [40]. Al-Masri et al. (2019) addressed the advantages of the inclusion of pumped hydro storage with WT for the Jordanian utility grid. Al-Masri et al. (2019) reported that emissions and grid purchase reductions were 24.69% and 24.68% for the WT/pumped hydro-based HES of the project location [41]. Halabi et al. (2017) studied different configurations of HES in HOMER Pro software for Sabah, Malaysia. The study results demonstrated that HES, consisting of PV/diesel/batteries, showed the best result in terms of economic, environmental matrix, and sustainability [42].

Researches on optimal sizing and operation of MEGs have also been conducted in some literature. Abdollahi et al. (2014) studied a CHP system to determine the optimal functioning and sizing of thermal energy storage. The Linear Programming (LP) algorithm was adopted in [43] to minimize the objective function- the total fuel cost. Razavi et al. (2018) carried out a case study comprising of electricity-only units, heat-only units, and CHP units to determine the optimal operating point of CHP units. The research was conducted in the General Algebraic Modeling System (GAMS) software based on Mixed-Integer Nonlinear Programming (MINLP) [44]. Hu et al. (2020) proposed a modified optimized algorithm, a combination of PSO and Genetic Algorithm (GA), to obtain the optimal configuration of a wind/solar/hydro-based CHP hybrid system based on heat-electric coordinated dispatch [45]. Awad et al. (2016) optimized the operation of a PV/thermal/micro-turbine CHP system to fulfill electric and thermal demand by utilizing heat from a CHP unit. The research was conducted in the AnyLogic and the MATLAB simulator [46]. Fang and Lahdelma (2016) optimized a CHP model with thermal energy storage to maximize the system revenue and minimize the system production cost using a sliding time window method [47].

2.2. Nuclear-Renewable Integration

2.2.1. Nuclear-Renewable Micro Hybrid Energy System

Bragg-Sitton et al. (2014) have defined nuclear-renewable hybrid systems as an energy network that fundamentally accomplishes the grid electricity demand and drives an additional industrial product generation process by surplus thermal or electric energy [48]. The secondary industrial process may include upgradation of synthetic fuel by heating, desalinated water production by electricity and heat, titanium dioxide production by thermal energy, district heating, and productions in paper mills [49]. A nuclear-renewable integrated system is proficient in optimal energy distribution to multiple production scheme for maximizing the profit. Ruth and Cutler (2017) defined N-R HESs as a single energy

generation interface consisting of a nuclear reactor, at least one renewable resource, and an industrial process that utilizes electric or thermal energy, or both [50].

An N-R HES is a collaborative network of different RESs, nuclear reactors, energy storage systems (ESSs), power electronic devices, and various energy users (e.g., electric, thermal, and hydrogen). Since no fossil fuel is combusted in N-R HESs, it is the cleanest HES with virtually zero GHG emissions. N-R HESs utilize a substantial amount of waste heat energy from thermal generators (e.g., nuclear reactor, geothermal energy, concentrated solar power, and biomass) to generate different commodities. Several advanced control algorithms are used in N-R HESs to ensure the security and reliability of the system. Based on the size of a hybrid system, the coupling scheme can be categorized into two types [51], as discussed below.

❖ ***Large-scale Coupling***

In large-scale coupling, a traditional large-scale NPP is collocated with regionally available RESs. The coupling may occur at either the electrical, thermal, or electrical-thermal levels. For example, the International Atomic Energy Agency (IAEA) recommends that a conventional large-scale NPP must have a bare area called an "exclusion zone" around NPPs for safety purposes. A part of this exclusion zone can be used to install wind turbines to extract wind energy and integrate it with NPP generations or electric grids [52]. Since the exclusion zone is typically a large empty area, it might be a favorable space for achieving high wind speeds, implying a high wind energy potential. However, the exclusion zone requirement for small-scale reactors has been changed in the new regulation [53]. The sizing of an exclusion zone for a small reactor is nearly reduced to non-existent. Hence, the cost of real state for WT and solar panels needs to be considered. Moreover, PV panels can be fitted on different facilities of NPPs to harness solar power. The large-scale coupling also includes Mobile Microgrids (MMs) with traditional NPPs for various purposes. An MM is an HES consisting of different RESs, such as wind and PV, with intelligent remote-control capabilities for resilient off-grid power supplies [54]. An MM can also be linked with large-scale NPP for emergency cases to support the essential electric system, Class I power supply, of NPP. Class I power class, associated with a battery bank, is the most sensitive power class in NPPs, and it can never be interrupted. Hence, a battery fast charging mechanism powered by MMs can solve the drawbacks of battery banks and ensure the safety of NPPs. In summary, the integration of MMs with traditional NPPs works for both objectives – load demand fulfillment and NPP emergency back-up support [55].

❖ ***Modular-scale Coupling***

In modular-scale coupling, a small-scale reactor, such as Small Modular Reactor (SMR) or MMR, is conjoined with RESs at a site where RESs are mostly available. MMRs are moveable and modular in size. MMRs are towed into a suitable location to combine with RESs in modular-scale coupling schemes. HESs that use a

modular-scale coupling method are called N-R MHESs. N-R MHESs have immense applications in remote communities, transportation electrification, distant oil and gas mining facilities, and remote chemical industries. A grid-connected N-R MHES also provides an excellent energy solution to the medium-level electricity demand with the lowest NPC and COE [51].

Suman (2018) highlighted the critical challenges of nuclear-renewable integration, such as integration values, regulatory, financial, technological, plant testing, and plant operation. The author suggested that the information linkage-based nuclear-renewable coupling would overcome the complexities of the integration process [27].

Ruth et al. (2014) classified the nuclear-renewable integration process into six: electrical, thermal, chemical, hydrogen, mechanical, and information. A combination of RESs, nuclear reactors, and industrial processes, including the versatility of grids and making the best possible use of investment, was explored in [56]. The study concluded that nuclear and renewable energy integration could be a potential solution for a long-term and ample amount of power and heat supply. The integrated system is free from sudden price changes, such as fossil-fuels price fluctuations. The document also pointed out that the nuclear-renewable hybrid system can supply load-following power, and excess energy can be used to produce secondary energy-intensive products. Nevertheless, the authors recommend system analysis, technical advancement, and optimization to implement this hybrid system in practice [56].

Rabiti et al. (2015) highlighted a generic strategy for designing, simulation, co-simulation, and control of N-R HESs. They addressed system design requirements, Figure of Merits (FOMs), required system constraints, grid modeling, and market analysis procedures. They also defined design objectives, solution approaches, computational tools, and data collection criteria. Existing gaps between available software framework and required tools were also addressed in this study. The authors also recommended several tools, such as Adams, Amesim, ANSYS, CarMaker, Dymola, EnergyPlus, MATLAB/Simulink, Hopsan, LMS Virtual.Lab, MapleSim, NI LabVIEW, OpenModelica, SimulationX, and xMOD, which need to be thought for future works [57].

Though several computational tools are available, such as HOMER, HOGA, Hybrid2, SOLSIM, and RAPSIM, for non-nuclear HESs, very few numbers of computational tools are available for N-R HESs. For example, MODELICA, Excel, and RAVEN are used to design and interpret the N-H HES although these tools are not explicitly developed for nuclear hybrid energy systems [58], [59], [60]. Modelica is broadly used for the development of dynamic systems consisting of small components. An HES was effectively modeled in [59] by using Modelica. Only NPP and WT were considered as inputs in this study, while electricity and synthetic fuel were accepted as output. Control algorithms of the HES were assessed in Modelica comprehensively. The developed HES would be needed to optimize for estimating profitability. Currently, all of the physical models are designed in Modelica.

Sabharwall et al. (2015) observed three possible cases in [61] on nuclear-renewable integration for financial analysis. The cases were (1) standalone nuclear generation system, (2) nuclear/wind generation system, and (3) nuclear/wind/hydrogen generation system. A sensitivity analysis was conducted by varying the discount rate, depreciation rate, and energy market to compare the Net Present Value (NPV), Internal Rate of Return (IRR), Cost of Energy (COE), and payback period of the three cases. It was inferred that the nuclear/wind/hydrogen system could be a profitable project for future energy generation.

A comprehensive research and development program on dynamic modeling, simulation, component development, and testing of N-R HESs was articulated in [17], which provided a useful background to support the analysis of N-R HESs. N-R HESs have been categorized into three classes: tightly coupled N-R HES, thermally coupled N-R HES, and loosely coupled N-R HES. The potential benefits of N-R HESs include GHG-free electricity, a resilient electric grid, and low COE. The authors have also regarded the integration of SMRs and RESs for future work. It is expected to demonstrate N-R HESs infrastructure by 2030.

Baker et al. (2017) quantified the benefits of a flexible Nuclear Hybrid Energy System (NHES) integrated with a grid. An SMR, battery storage, wind power generation source, and a desalination plant were studied within the NHES. The SMR was regarded as a primary generation source, and the sizing of the SMR (300 MWe) was discussed in this study. The authors concluded that battery investment was only justifiable for higher levels of renewable energy penetration [62].

A grid-connected N-R HES has been assessed in [63] with a flexible load, named high-temperature steam electrolysis (HTSE). The research primarily concentrates on the modeling and control of the system equipment in Modelica. The study claimed a reliable steady-state operation of NPPs, high-penetration of RESs with resiliency, and efficient production of alternative commodities, such as oxygen and hydrogen. Since a Light Water Reactor (LWR) was used in this study, and the HTSE required high input temperature, it was suggested to include temperature-boosting technology with the HTSE system. Furthermore, the investigation asserted grid stability by satisfying demand and system constraints.

Garcia et al. (2016) configured an NHES with multiple commodities production and grid stability. The NHES model was also capable of planning uncertainly, KPI optimization, and real-time energy management. The NHES was superior to conventional energy systems in terms of identifying uncertainly and high-level penetration of RESs. Besides, the NHES could significantly reduce GHG emissions by serving electric grids and industrial demand with a baseload heat generator, i.e., nuclear reactor and RESs. However, the simulation carried out by Garcia et al. was not verified with real data obtained from industries. The probabilistic modeling and uncertainly of the sources were also overlooked in the study [64].

Mag et al. (2016) investigated the concept of a hybrid nuclear plant where an SMR and solar PV were considered. This hybrid plant also consisted of a molten salt thermal energy storage system. Electricity from photovoltaic was converted into heat and used for the superheating of nuclear steam. The investigation determined that the hybrid nuclear power plant was more efficient than a standalone NPP. Molten salt storage served as extensive and indirect electric energy storage. The authors proved that thermal storage was more cost-effective than compressed air storage and competitive with pumped hydro storage in terms of capital cost and round-trip efficiency. The study also concluded that the hybrid nuclear power plant has a lower initial cost per kilowatt than the standalone nuclear power plant. However, the nuclear reactor considered in this study was not commercially available [65].

Epiney et al. (2020) stated the necessity of installing a large-scale flexible generator, such as gas turbines, for absorbing electricity demand fluctuation that can also be reduced by the concept of N-R HESs. A RAVEN/Modelica-based software framework was demonstrated in [66] to appraise the economic aspects of N-R HESs. The research asserted that financial profits could be attained by incorporating the proper industrial process into nuclear reactors. The study also examined a general case for implementing the proposed framework. Nevertheless, the methodology needed validation by real data, such as wind speed and industrial load demand, which are typically dependent on geographical conditions.

Chen et al. (2016) optimized two configurations of NHESs to understand system complexities, difficulties, and opportunities in Texas and Arizona, USA. The heat generation plant consisted of an SMR, wind energy, solar PV, electric grid, and additional energy conversion units that produced chemical products, such as gasoline, Liquefied Petroleum Gas (LPG), and freshwater. The research demonstrated that the proposed optimizer could achieve economic gain. The study also supported the view that higher gain could be achieved if the system decreased its' participation to produce electricity and increased its' participation to generate alternative commodities like gasoline, freshwater, and LPG. The research recommended that online optimization should be developed to work with real-time commodity prices and energy markets [58].

Gabbar et al. (2020) revealed and compared five different cases, such as traditional fossil fuel-based energy systems, fossil fuel/RESs-based HESs, standalone RESs-based energy systems, independent nuclear energy systems, and N-R MHESs in [28]. Small-scale N-R HESs could be an excellent prospect of continuous electricity supply for off-grid applications in terms of the discount rate, inflation rate, and project lifetime. N-R MHESs provided the best resiliency and reliability to the demand for long term energy policy. Besides, modular N-R HESs have the potential to reduce the amount of GHG significantly.

The flexible operation of nuclear reactors with variable renewable sources has been presented in [67]. The mixed-integer linear programming (MILP) was implemented to evaluate the nuclear reactor's operating constraints, such as core reactivity. The investigation claimed that the flexible nuclear reactor operation would provide less

operating expenses and higher system revenue. The flexible nuclear reactor also has increased the energy generation contribution of renewable resources.

Progresses on the development of N-R HESs were exhibited in [68] by modeling a small scale reactor in Modelica software. The demonstration illustrated the design simplicity of the reactor model and simple module alteration in Modelica. However, the model has focused more on the features of Modelica software than the development and integration of a complete N-R HES. Currently, the International Atomic Energy Agency (IAEA) has issued a report on nuclear-renewable integration [69]. The report has comprised several case studies, prospects, applications of N-R HESs, opportunities and challenges of nuclear-renewable integration, and the role of small-scale reactors in nuclear-renewable hybridization. The document also points out the nuclear energy policy of different countries to accelerate the innovation of nuclear-renewable integration.

Epiney et al. (2018) described a case study on the installation of a Reverse Osmosis (RO) plant for water supply, collaborated with Arizona Public Supply (APS). The study mainly focused on applying N-R HESs software framework to conduct the case. Three different cases were developed and analyzed in this study. A sensitivity analysis was carried out at the end of the investigation by varying different system parameters, such as discount rate, wholesale electricity price, project lifetime, net demand projection, and amount of salty water. However, N-R HES modeling was not presented in the study [70]. A similar case study has been conducted by Kim and Garcia (2015) in [71]. They also proposed a nuclear/PV HES for water desalination plants by the RO process. The HES was modeled in an object-oriented Modelica interface. Moreover, the authors evaluated the system response due to step-changes in variable electrical load and PV penetration. Technical issues were the main interests of this study.

Ruth et al. (2016) has analyzed two scenarios of N-R HESs. The first scenario considered a nuclear reactor, thermal power cycle, WT, and synthetic gasoline production plant in Texas. The second scenario included a nuclear reactor, a PV panel, a thermal power cycle, and a desalination plant. The economies of the N-R HESs were compared with available natural gas systems for both scenarios. The N-R HESs of the study primarily focused on serving industrial processes. The research team found the N-R HESs as a potentially profitable candidate system compared to other technologies [72]. The authors extended this research in [50], and this document highlighted the economic potential of N-R HESs for hydrogen production.

Three scenarios of N-R HESs for supplying thermal energy were mentioned in [73]. The first arrangement constituted a nuclear reactor, thermal power cycle, wind power plant, and electric boiler. The second scenario comprised a nuclear reactor, thermal power cycle, wind power plant, and electric thermal storage. The last configuration was a combination of a nuclear reactor, thermal power cycle, wind power plant, electric boiler, and thermal storage. The electric thermal storage stored thermal energy that was generated by electricity. The financial performance analysis indicated that the third arrangement has the lowest NPV, lowest IRR, and highest TCI. The analysis results were evident because the

thermal power supply was elevated significantly by introducing the electric boiler and the thermal storage simultaneously in the third scenario. The result was also apparent since the authors assumed that the cost of heat generated from the nuclear reactor was less than the price of heat generated from gas (electric boiler) [73].

Redfoot and Borrelli (2018) indicated the similarities between the Nuclear Fuel Cycle Simulator (NFCS) and the required modeling features of N-R HESs. The authors addressed the necessary functionalities of N-R HESs and the already developed software used to model N-R HESs. The required functionalities of an N-R HES included dynamic feature, component optimization, stochastic model of renewables, grid demand model, economic KPIs, and sensitivity analysis. Redfoot and Borrelli recommend incorporating new components, flexibility provision, financial tools, open-source tools, physical modeling tools, and uncertainty tools into the NFCS in the future to get benefits in N-R HESs modeling [74].

2.2.2. Micro Modular Reactor (MMR)

A very few literature and resources are found that talked about MMRs. According to the IAEA, NPPs rated under 300 MWe can be interpreted as "small" NPPs. The IAEA defines NPPs as "medium" if reactors have a power rating up to 700 MWe. The "small" and "medium" NPPs collectively have been referred to as "small and medium reactor (SMR)," but commonly, they are termed as "Small Modular Reactor (SMR)." One subclass of SMRs is "very small reactors (vSMRs)" that are rated under 15 MWe [75].

MMRs are somewhat different from SMRs in terms of power rating, and microreactors are defined differently in various literature. According to [116], the sizing of MMRs is below 10 MWe. In [76], the electric and the thermal power rating of MMRs are defined as below 30 MWe and 100 MWt, respectively. Small-scale nuclear reactors like MMRs are currently getting attention for their small size, affordability, security, reliability, and innovativeness. Several manufacturers are working to develop and bring microreactors into the market. A list of microreactors (under-development) is presented in Table 2-1.

Table 2-1: A List of Microreactors [75]

Name	Capacity (MWe)	Type	Developer
eVinci	0.2-5	Heatpipe FNR	Westinghouse, USA
NuScale micro	1-10	Heatpipe	NuScale, USA
Aurora	1.5	Heatpipe FNR	Oklo, USA
Sealer	3-10	Lead FNR	LeadCold, Sweden
Holos Quad	3-13	HTR	HolosGen, USA
U-battery	4	HTR	Urenco-led consortium, UK
MMR-5	5	HTR	UltraSafe Nuclear, USA
Starcore	10-20	HTR	Starcore, Quebec
Gen4 module	25	Lead-bismuth FNR	Gen4 (Hyperion), USA

MMRs are fourth-generation micro-scale nuclear reactors that afford clean, reliable, and cost-efficient electric and thermal power. MMRs are specially designed for remote residential and industrial applications where there is no footprint of electric grids. It has a CHP provision that facilitates MMRs to generate electrical and thermal energy simultaneously. It reduces electric and thermal power generation by up to 50%. Since MMRs do not release any GHG emissions during operation, it reduces 100% carbon emissions. MMRs are developed in industries and brought it as a package at project locations. It requires a small size of concrete foundation. Microreactors are sized concerning the international standard of portable containers so that the reactor can be exported to any license location by ship, rail, or road. The reactor is sealed and does not require to refuel during its lifetime. Thus, it assures the utmost security of fuel supply. The fuel module is discharged from MMRs facility at the end of its lifetime and kept in a commissioned nuclear waste management facility. A new fuel module replaces the old module; no engineering work is done with the fuel module at the site. In addition, no spent fuel facility is located at the reactor site. Hence, MMRs' design provides excellent environmental protection. The development cost of MMRs is also lower compared to SMRs and other fourth-generation nuclear reactors. As a large portion of MMRs' expenses is related to sunk cost, the energy cost and economic risks are entirely predictable for MMRs. MMRs can provide flexible operation of NPP [77].

Microreactors are high-temperature and gas-cooled modern reactors. An MMR facility consists of a main nuclear plant (MMR plant) and an adjacent plant. Main nuclear plants generate heat, and the heat is transferred to adjacent plants. Adjacent plants consist of all components required to convert the heat into electricity and process heat depending on customer requirements. A schematic of an MMR facility is shown in Fig. 2-2.

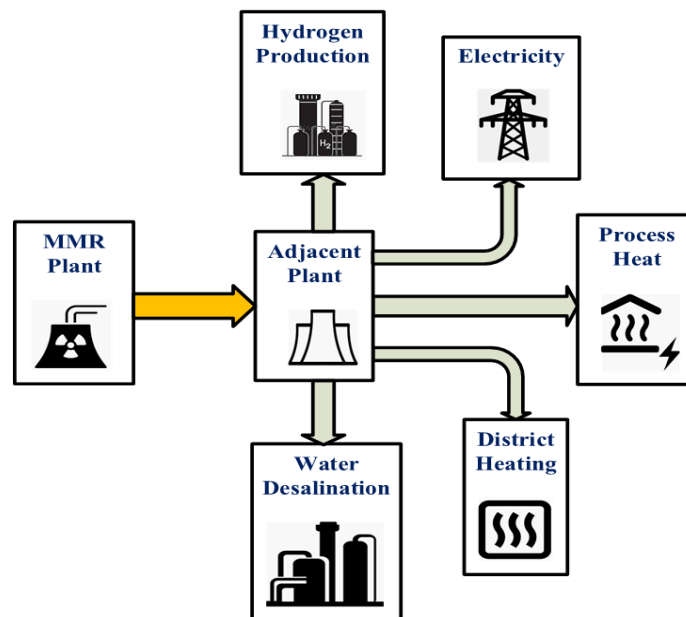


Figure 2-2: MMR Facility consisting of Main NPP and Adjacent Plant

Main nuclear plants consist of three main components: Closed-loop Helium Cycle, Intermediate Heat Exchanger (IHX), and Molten Salt System. In an MMR facility, helium is used as the primary coolant, while molten salt is utilized as the secondary coolant. MMR plants employ a closed-loop helium cycle to extract and transfer the generated process heat. Helium circulates through the reactor core and removes heat from the core. Cold helium passes through the nuclear reactor core and gets heated by a controlled fission reaction. The hot helium goes through the IHX and transfers heat to the molten salt system. The cold helium is recirculated through the reactor core by an electric-powered circulator after losing heat to the molten salt system. In a molten salt system, cold molten salt enters the IHX, absorbs heat from helium, and passes out to adjacent plants [78]. A simplified diagram of a main nuclear plant is presented in Fig. 2-3.

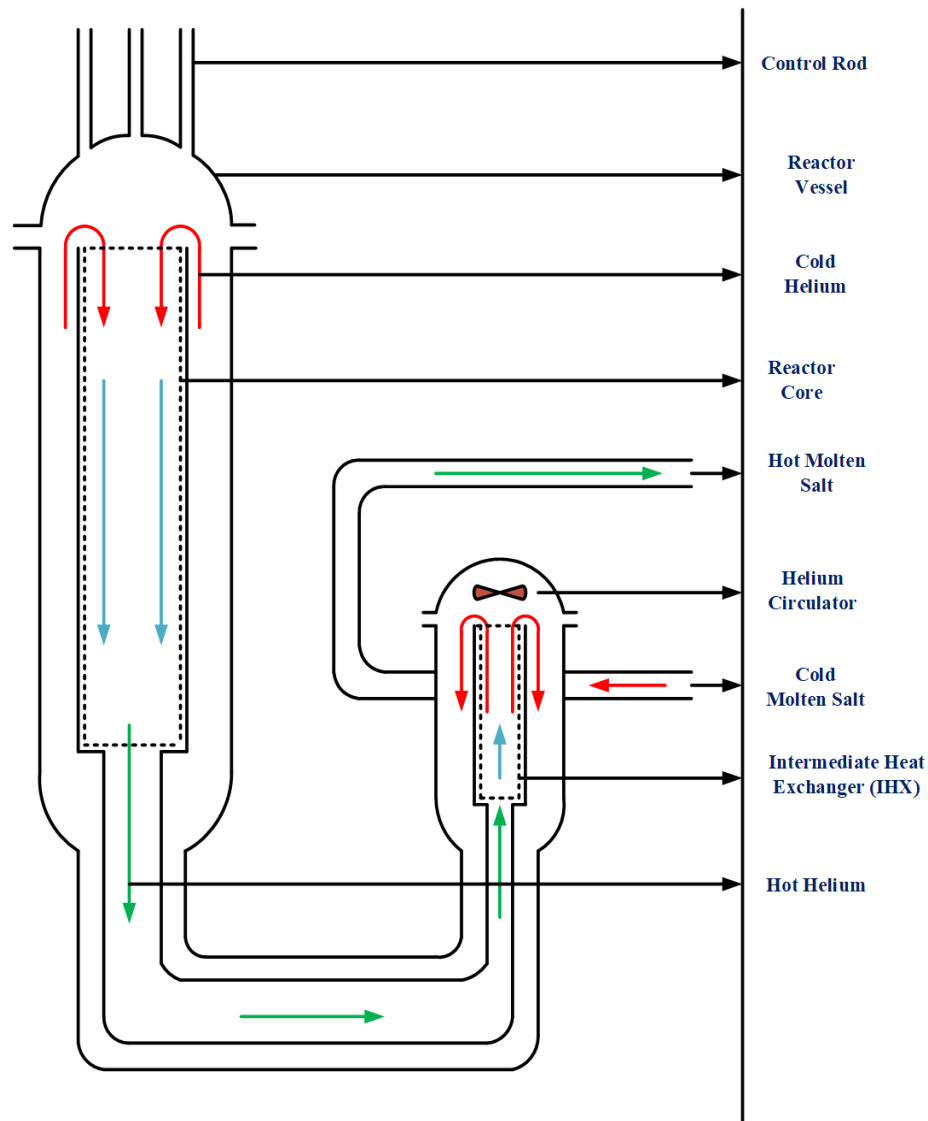


Figure 2-3: MMR Plant/Main Nuclear Plant (Simplified Schematic)

Main NPPs are chemical facilities, and adjacent plants are non-nuclear facilities. The IHX separates the chemical process from power blocks (adjacent plants). It mitigates the potential risks of contaminating radioactive materials into power blocks. In a hybrid energy system, molten salt is utilized differently for electricity generation, process heat, and thermal energy storage [79].

Adjacent plants are solely used to utilize the thermal energy extracted from molten salt and produce electricity as well as process heat. All the equipment required to generate electricity are installed in adjacent plants. The offices, parking lots, transmission lines, and visitors and training centers are also located at adjacent plants. Adjacent plant areas are enclosed with a dedicated security fence. However, infrastructure design depends on locations and design requirements.

Adjacent plants are divided into two cycles: molten salt cycle and steam cycle. A molten salt cycle acts as an intermediate medium to exchange the generated heat from MMR plants to the steam cycle through a heat exchanger. The purpose of the heat exchanger is to supply electricity and thermal power to the customers. A molten salt system consists of hot salt tank, hot salt pump, cold salt tank, cold salt pump, gas furnace, and pipes. The molten salt is pumped to the hot salt tank, and then it is pumped to a steam generator. After that, the cold molten salt is transferred to the cold salt tank before reheating in MMR plants. The connector between cold and hot molten salt tanks is a nuclear plant bypass. A bypass allows molten salt from the cold reservoir to be pumped directly to the hot reservoir. Therefore, it enables molten salt circulation without the molten salt passing through nuclear plants. This bypass serves many operational purposes, for example, during start-ups or the adjustments of tank temperature. A gas furnace is used in the molten salt cycle to manage the temperature of molten salt during MMR plants' unavailability.

A steam cycle/power generation cycle consists of turbine, generator, air-cooled condenser, and additional required structures. The purpose of this cycle is to generate electricity and process heat. Bleed steam is extracted from turbines at a specific pressure and temperature for thermal applications depending on requirements. Typically, a modern MMR can supply process heat at 710°C [80]. An electric grid can be located near to adjacent plants for a grid-connected mode of operation. An air-cooled condenser is used to remove the heat generated during steam condensation without the help of any external sources. Superheaters convert the wet steam or saturated steam into dry steam or superheated steam. Superheated steam is used in turbines to generate electricity. Preheaters recover the heat from flue gases and increase thermal efficiency [81, p.], [82]. A simplified schematic of an adjacent plant is presented in Fig. 2-4.

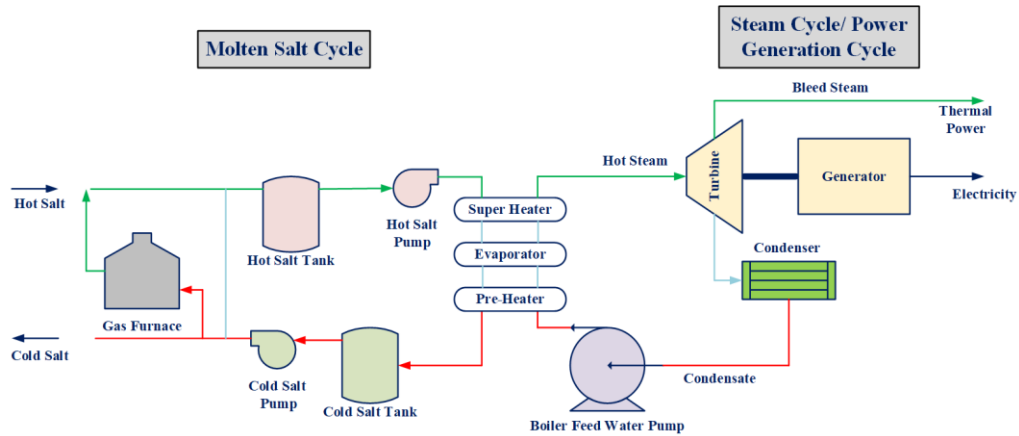


Figure 2-4: Adjacent Plant (Simplified Schematic)

Nuclear cogenerations have several advantages, such as reduction of GHG emissions, improvement of overall plant efficiency by utilizing waste heat or low-grade thermal energy, curtailment of energy generation cost, and lowering environmental impact [83]. Since NPP efficiency is between 30-40%, a massive amount of energy is wasted in nuclear generation. A cogeneration process can enhance NPP efficiency by up to 80% by utilizing the waste thermal energy. However, the integration of a cogeneration subsystem must be chosen sensibly [84]. MMRs can save the cost of heat and electricity, up to 50% [77].

MMRs are powered by Tristructural Isotropic (TRISO) fuel. The uranium enrichment of TRISO fuel is 9-12% [85]. The primary objective of using TRISO fuel is to retain radioactive materials, high coolant temperature, and minimize an emergency shut-down system's requirement. TRISO fuel can only generate heat; it can not be re-processed. TRISO fuel can proliferate its reaction, and the reaction can not go out of control. A traditional operating reactor adds highly complex and specialized safety systems. On the contrary, the TRISO fuel module itself maintains the fission product retention during accidents and normal conditions. Thus, TRISO fuel is secured. TRISO particles are combined to structure the fuel pellets.

TRISO fuel is composed of five regions. The spherical center of TRISO fuel, called fuel kernel, is the uranium. A porous carbon buffer encircles the fuel kernel. The carbon buffer aims to accommodate internal gas buildup and reduce the speed of the fission fragment. The carbon layer is surrounded by low-density pyrolytic carbon (PyC) or inner PyC (IPyC), followed by silicon carbide (SiC), followed by high-density pyrolytic carbon (PyC) or outer PyC (OPyC) [86]. PyC layers safeguard the SiC layer from chemical attack during fuel operation. It also provides extended protections to fission products. Corrosive gases are used to store SiC, and IPyC protects the center from these corrosive gases. SiC works as a primary pressure vessel for the particle. It also strengthens the fuel against building up the gas pressure. Furthermore, it provides a diffusion barrier for metallic and gaseous fission products [87]. A TRISO fuel particle's cutaway view is pictured in Fig. 2-5, as redrawn from [88].

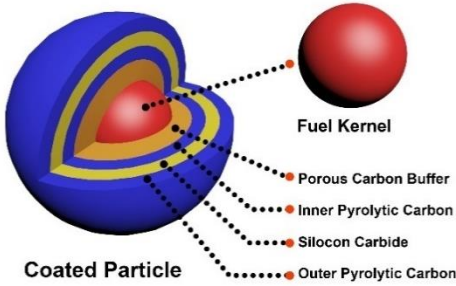


Figure 2-5: Cutaway View of a TRISO Fuel Particle

2.3. Combined Heat and Power/Cogeneration

A CHP unit provides both thermal and electric power concurrently from a single generation unit. The generation sources involve fossil fuel (e.g., coal and natural gas), nuclear fuel, and renewable resources (e.g., geothermal, biomass, and concentrated solar thermal power). The most popular renewables, such as wind, hydro, and solar PV, are not involved in thermal generation. Hence, the deployment of CHP units is not possible for these types of renewables [89]. A CHP unit consists of five main components: prime mover, electric power generation unit, waste heat recovery unit, energy management unit, and thermally activated equipment [90], [91].

The proximity between heat production and demand is one of the critical factors in CHP. Since heat energy can not be transported in a long-distance, it is mandatory to install CHP units close to the thermal demand site. It is also always economical to supply both electricity and heat generated from CHP units to the same customer. CHP technologies can be divided into two categories: topping cycle and bottoming cycle [92].

- ❖ **Topping Cycle CHP:** In a topping cycle CHP, the primary or top objective is to generate electricity. The energy left over after generating electricity will be used to produce valuable thermal energy for heat users. Typically, gas turbines and reciprocating engines are used in a topping cycle. The waste thermal energy rejected from a generating station is captured to produce useable thermal energy. Topping cycle CHP generally produces relatively low-grade heat. Trilateral flash cycle, with the help of a Convergence-Divergence (CD) nozzle, can generate power from low-grade heat. However, high-grade heat can also be obtained from the topping cycle CHP by balancing the generation between power and heat [93], [94]. A schematic of a simplified topping cycle CHP is presented in Fig. 2-6 [95].

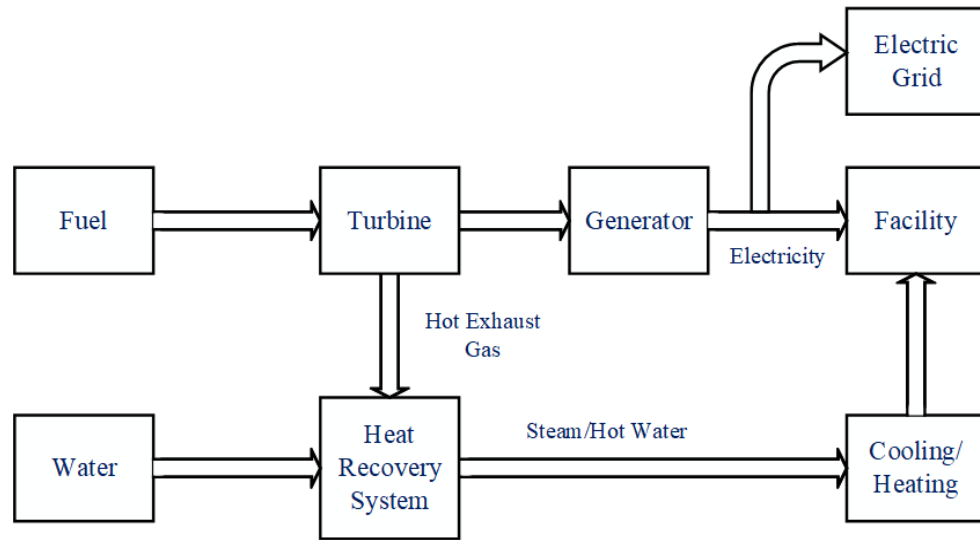


Figure 2-6: Topping Cycle

- ❖ **Bottoming Cycle CHP:** In a bottoming cycle CHP, electricity production is the bottom-line priority. The main target of the bottoming cycle CHP is to generate heat for industrial applications. The waste heat recovered from heat engines is used to generate electricity. Bottoming cycle CHP provides proper quality heat for the industrial process and driving steam turbines. If the heat energy has a comparatively low temperature, an Organic Rankin Cycle turbine can be used to convert lower grade heat into electric power. It is also possible to extract combustible gas, e.g., blast furnace, from a bottoming cycle CHP to drive gas turbines [96], [97]. A generic layout of a bottoming cycle is presented in Fig. 2-7 [95].

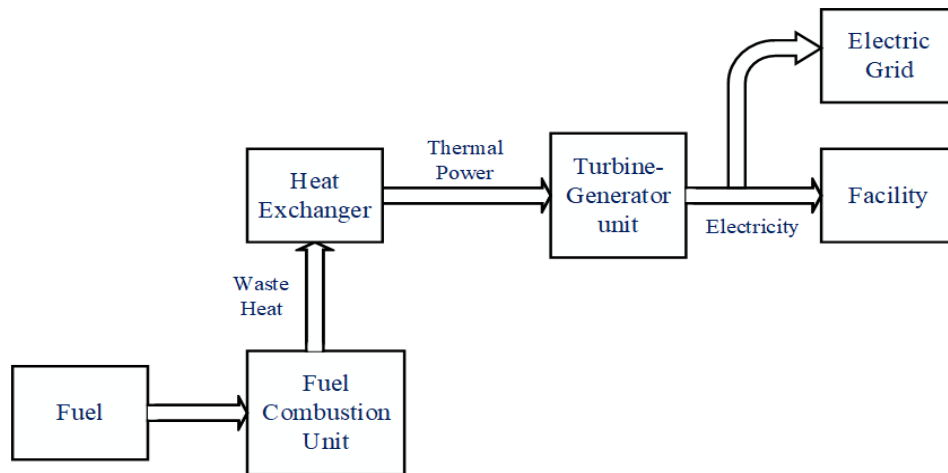


Figure 2-7: Bottoming Cycle

2.4. Optimization Algorithms

Numerous optimization techniques have already been explored and utilized in HESs to achieve optimal sizing and operation. The main goal of the optimization is to find system

configuration with minimum cost and maximum reliability. Optimization techniques can be classified into three categories [98]. Fig. 2-8 summarizes the types of optimization techniques.

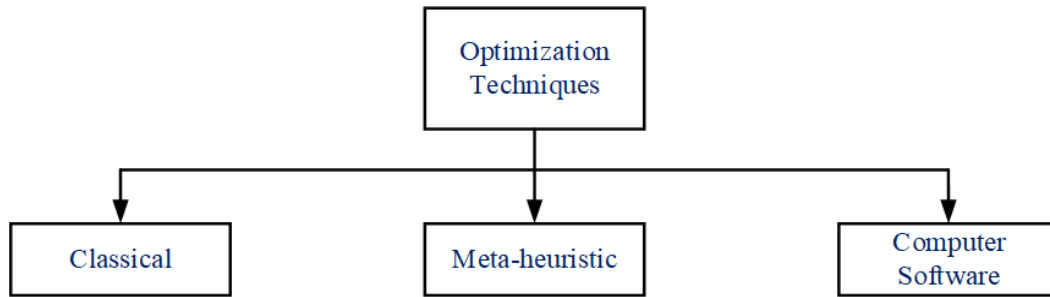


Figure 2-8: Classification of Optimization Techniques

2.4.1. Classical Optimization Techniques

Classical optimization techniques rely on numerical analysis, iterative methods, and graphical analysis [99]. It solves differential equations to determine the optimal solution [100]. Classical optimization techniques include Linear Programming (LP), Mixed Integer Linear Programming (MILP), Nonlinear Programming (NLP), Dynamic Programming (DP), and analytical methods. If the objective function and the constraints are linear, LP and MILP are used to solve the problem.

LP is employed in [101] to minimize the NPC of Wind/PV-based hybrid energy system in three different sites in India. The optimization constraints incorporate battery autonomy, energy balance equation, and PV capacity. Theo et al. (2016) has introduced MILP in [102] to obtain the optimal size of an on-grid hybrid energy system with minimum NPV and optimum energy storage. A multi-objective MLIP is applied in [103] to find locations and Distributed Generation (DG) system sizing based on the least total system cost and CO₂ emissions. MLIP is also used in [104] to minimize the total operating cost and CO₂ emissions in a grid-connected PV/fuel cell/battery-based hybrid energy system. However, classical optimization techniques could not regard system characteristics, such as WT installation height, the PV panel's tilt angle, and the number of battery chargers. But all of these parameters have an impact on energy production [105].

2.4.2. Meta-heuristic Optimization Techniques

Meta-heuristic optimization techniques can be grouped into two categories: single algorithm and hybrid algorithm. In the single algorithm, one artificial intelligent-based algorithm is used to find the optimal solution. It has better accuracy and convergence capability compared to classical methods. The single algorithm includes Genetic Algorithm (GA), Ant Colony Optimizer (ACO), PSO, Artificial Bee Colony (ABC) optimization, Cuckoo Search (CS), Simulated Annealing (SA), and other meta-heuristic methods. The hybrid algorithm combines two or more single algorithms, either classical or meta-heuristic, to find the optimal solution. Hybrid Big Bang-Big Crunch (HBB-BC), Hybrid

Teaching-Learning-based Optimization (HT-LBO), Hybrid GA and an Exhaustive-Search (HGA-ES), Iterative-Pareto-Fuzzy (IPF), Modified Electric System Cascade Analysis (MESCA), Hybrid Simulated Annealing-Tabu Search (HAS-TS), MarKov-based GA (MarKov-GA), Discrete Chaotic HS-based Simulated Annealing (DCHSSA), Improved Simulated Annealing Particle Swarm Optimization (ISAPSO), and Hybrid Flower Pollination Algorithm and Simulated Annealing (HFPA-SA) are some of the examples of hybrid algorithm. These hybrid algorithm is more efficient than the single algorithm, and it overcomes the drawbacks of the single algorithm [98]. Some of the meta-heuristic optimizations used in HESs are listed in Table 2-2.

Table 2-2: A list of Meta-heuristic Optimization Techniques used in HESs

Objective Function	Optimization Technique	Results	Reference
COE	PSO, GA	Solar/diesel/hydro/biomass/biogas-based energy system was developed to serve the system demand with the least COE. Reliability criteria, economic parameters, renewable factor, and CO ₂ emissions were incorporated as optimization constraints.	[106]
NPC, Availability of electricity	MOGA ¹	The grid-connected PV/wind system was analyzed to minimize total system cost and availability of electricity.	[107]
LCC ² , Reliability	PSO	A PV/wind/battery-based system was optimized to obtain minimum LCC and highest reliability.	[108]
TPC ³	HBB-BC ⁴	HBB-BC, a combination of BB-BC and PSO, was used to find the optimal size of the stand-alone PV/WT/battery-based energy system.	[109]
TAC ⁵ , LPSP, fuel cost	HT-LBO ⁶	Sizing optimization of a stand-alone PV/WT/diesel/battery-based energy system was carried out with reliability constraints.	[110]
COE	HAS-TS ⁷	A WT/PV/diesel/biodiesel/FC/battery-based small autonomous energy system was optimized, which also provided better performance compared to individual SA or TS in terms of convergence and quality.	[111]
LPSP, Payback Period	HFPA-SA ⁸	A RES-based hybrid has been studied to obtain the optimal PV panel tilt angle, the number of batteries, and the number of PV panels in Tehran, Iran.	[112]

¹Multi-objective GA, ²Life Cycle Cost, ³Total Present Cost, ⁴Hybrid Big Bang-Big Crunch, ⁵Total Annualized Cost, ⁶Hybrid Teaching-Learning-based Optimization, ⁷Hybrid Simulated Annealing–Tabu Search, ⁸Hybrid Flower Pollination Algorithm and Simulated Annealing

PSO algorithm was chosen in this study. The algorithm was developed by Kennedy and Eberhart in 1995, and it is a metaheuristic optimization technique. PSO's underlying idea is based on social intercommunication by a group of the population, called a swarm, and evolutionary computation. The two best values are measured in the PSO algorithm for each particle's location. The first value is the best value for a particle that has been obtained so far by that individual particle or swarm; this is called personal best, and the value is stored. PSO optimizer discovers the best value among the population that is called the global best. Individual particle directs towards the personal best and global best based on its position and velocity. Fitness function is used in PSO to find out the best solution among all the possible solutions. Constrains can be incorporated into the objective function. PSO algorithm can be explained in three steps [113].

- Assess the fitness of an individual particle.
- Upgrade the global and personal best fitness and location.
- Upgrade each particle's position and velocity.

Every particle identifies the best fitness value. During the iteration, the particle with the best fitness value is compared to other particles and upgraded. This process proceeds until it gets some concluding criteria, like predefined fitness value or iteration number. The particle position is updated by using Eq. 2-1 [114].

$$y_{k+1}^i = y_k^i + v_{k+1}^i \quad \text{Eq. 2-1}$$

Where, y is the particle position, and v is the particle velocity. i and k denote the number of particles and the number of iterations.

The velocity of a particle in the swarm is updated using the following equations.

$$v_{k+1}^i = K[v_k^i + c_1 r_1 (p_k^i - y_k^i) + c_2 r_2 (p_k^g - y_k^i)] \quad \text{Eq. 2-2}$$

$$K = \frac{2k}{|2 - \varphi - \sqrt{\varphi^2 - 4\varphi}|} \quad \text{Eq. 2-3}$$

$$\varphi = c_1 + c_2 > 4 \quad \text{Eq. 2-4}$$

Where, c_1 is the individual acceleration coefficient, c_2 is the social acceleration coefficient, K is the constriction coefficient, r_1 and r_2 are the random number between 0 to 1, p^i is the personal best position, and p^g is the global best position.

The PSO principle, as stated above, is followed in this study to solve the problem. The problem is formulated in the MATLAB environment based on requirements. The implementation algorithm of PSO in the defined problem is outlined in Fig. 2-9.

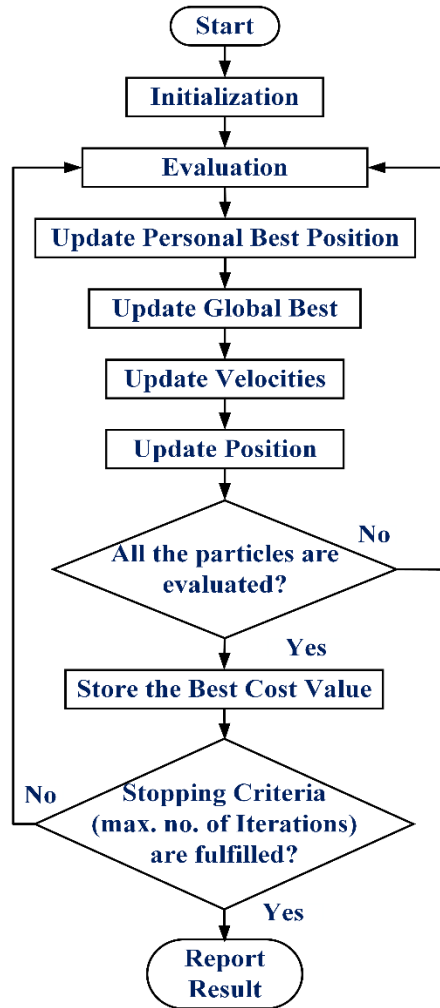


Figure 2-9: Implementation of the PSO Algorithm in the Problem

2.4.3. Computer Software

Several computer software tools are available for hybrid energy system analysis. Hybrid Optimization Model for Electric Renewable (HOMER) is one of the most extensively used software packages for optimizing HESs [115]. Some other available software packages for HES optimization include SOLSTOR, HYBRID2, *RETScreen*, *SOMES*, *HYSYS*, *HOGA*, *iHOGA*, and *iGRHYSO* [116].

2.5. Key Performance Indicators (KPIs)

KPIs evaluate the benefits and the drawbacks of a system. KPI works as an essential decision-making factor for designers. Since an N-R MHES is a complex integrated system, it is mandatory to identify and evaluate KPIs for system deployment. By conducting a comprehensive literature review, KPIs of a hybrid energy system are categorized in mainly four sections: Technical, Economical, Environmental, and Socio-Economical. A list of KPIs is shown in Fig. 2-10.

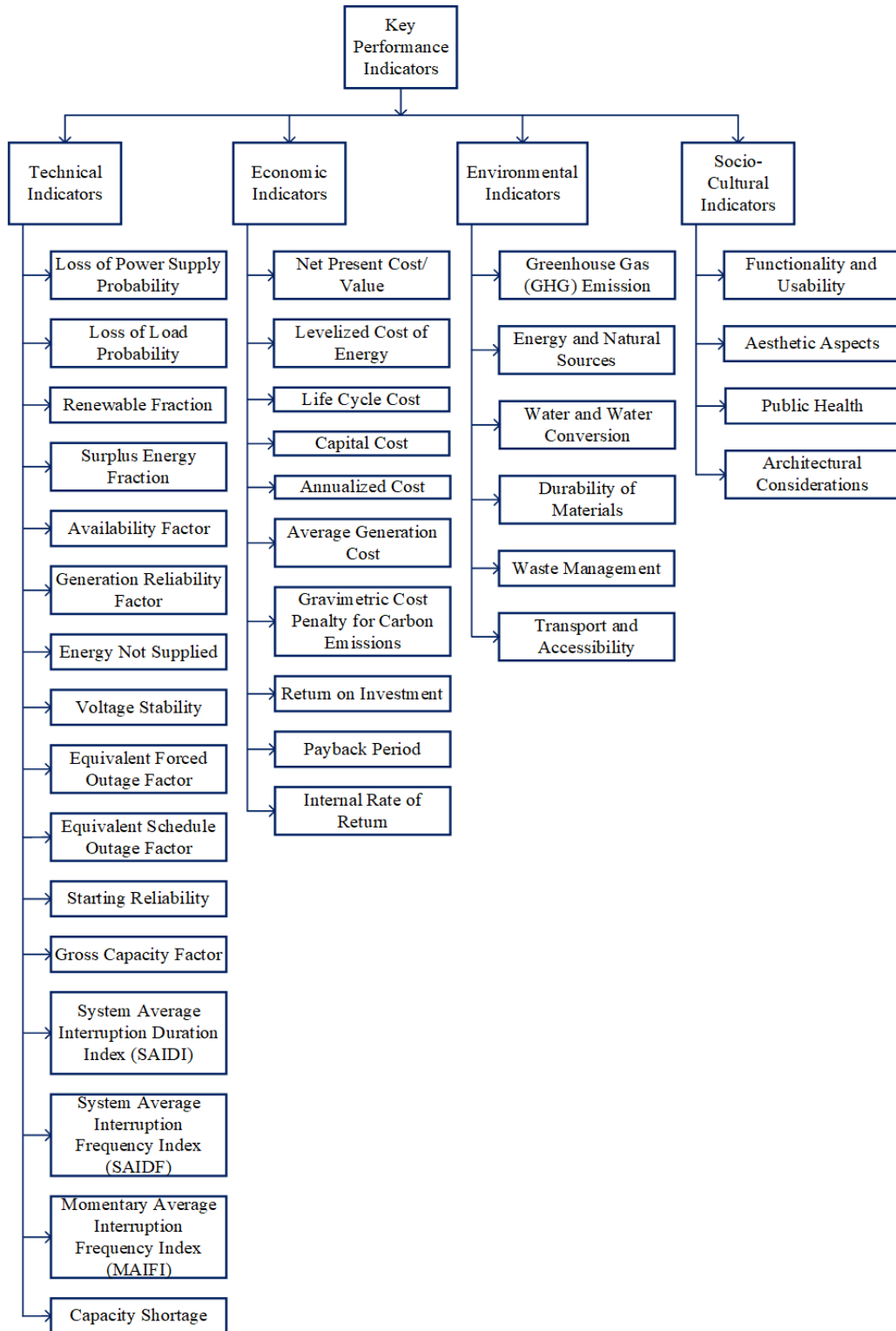


Figure 2-10: Classification of KPIs

The study primarily focuses on technical and economic KPIs. The discussion of environmental and socio-cultural indicators is beyond this study. Some critical KPIs considered in this study are discussed as follows.

2.5.1. Generation Reliability Factor (GRF)

GRF is an indication of how much demand is supported by an energy system. The following equations calculate GRFs for both electric and thermal demand of the system studied here [117].

$$GRF_{elec} = \frac{\sum_{t=1}^{t_{total}} P_{gen}(t) \times \Delta t}{\sum_{t=1}^{t_{total}} P_{EL}(t) \times \Delta t} \times 100\% \quad \forall t \in t_{total} \quad Eq. 2-5$$

$$P_{gen}(t) = P_{pv}(t) + P_w(t) + P_{MMR}(t) + P_h(t) + P_{bio}(t) \text{ (for MMR-based MEG)}$$

$$P_{gen}(t) = P_{pv}(t) + P_w(t) + P_{diesel}(t) + P_h(t) + P_{bio}(t) \text{ (for diesel-based MEG)}$$

$$\forall t \in t_{total} \quad Eq. 2-6$$

$$GRF_{ther} = \frac{\sum_{t=1}^{t_{total}} T_{gen}(t) \times \Delta t}{\sum_{t=1}^{t_{total}} P_{TL}(t) \times \Delta t} \times 100\% \quad \forall t \in t_{total} \quad Eq. 2-7$$

$$T_{gen}(t) = T_{MMR}(t) + T_{bio}(t) \text{ (for MMR-based MEG)}$$

$$T_{gen}(t) = T_{diesel}(t) + T_{bio}(t) \text{ (for diesel-based MEG)}$$

$$\forall t \in t_{total} \quad Eq. 2-8$$

Where, $P_{gen}(t)$ is the total electric energy generation (kW) within a system at time step t , $T_{gen}(t)$ is the total thermal energy generation (kW) within a system at time step t , and Δt is the time step considered in the analysis.

2.5.2. Loss of Power Supply Probability (LPSP)

A loss of power supply occurs when the system demand is higher than the system generation. It is necessary to keep the loss of power supply within a specific margin for ultimate system reliability. The least loss of power supply implies the most reliable system. Hence, another reliability constraint, LPSP, is introduced in the study. LPSP is also considered a constraint in the optimization problem.

LPSP is the ratio of summation of power shortage at each time step and summation of demand at each time step. The maximum and minimum values of LPSP are 100% and 0%, respectively. The lower value of LPSP indicates a more reliable energy system. LPSP can be expressed by the following equations [118],[119].

$$LPSP_{elec} = \frac{\sum_{t=1}^{t_{total}} (P_{dem}(t) - P_{gen}(t))}{\sum_{t=1}^{t_{total}} P_{EL}(t)} \times 100\% \quad P_{dem}(t) > P_{gen}(t) \quad Eq. 2-9$$

$$P_{dem}(t) = P_{EL}(t) + P_{EES,SOC}^{min}(t) + P_{Htank,SOC}^{min}(t) \quad \forall t \in t_{total} \quad Eq. 2-10$$

$$LPSP_{ther} = \frac{\sum_{t=1}^{t_{total}} (T_{dem}(t) - T_{gen}(t))}{\sum_{t=1}^{t_{total}} P_{TL}(t)} \times 100\% \quad P_{dem}(t) > T_{gen}(t) \quad Eq. 2-11$$

$$T_{dem}(t) = P_{TL}(t) + P_{TES,SOC}^{min}(t) \quad \forall t \in t_{total} \quad Eq. 2-12$$

Where, $LPSP_{elec}$ and $LPSP_{ther}$ are the loss of power supply probability for electric and thermal demand, respectively, $P_{EES,SOC}^{min}(t)$ is the required power to maintain minimum State of Charge (SOC) of the EES, $P_{Htank,SOC}^{min}$ is the minimum power required for generating hydrogen to maintain the minimum SOC of hydrogen tank, and $P_{TES,SOC}^{min}(t)$ is the required power to maintain minimum SOC of the TES.

2.5.3. Surplus Energy Fraction (SEF)

It is requisite to maintain surplus energy within a nuclear-renewable hybrid system for optimal planning. It is not expected to generate a large amount of surplus energy without being stored in a storage. Though it is quite challenging to maintain zero surplus energy in a nuclear-renewable integrated system due to the variable nature of RESs, it is essential to keep the excess energy generation within a specific limit. Therefore, a KPI, namely SEF, is regarded in this study. SEF is another constraint employed in the optimization problem.

SEF is the ratio of total excess energy in a specific period to the total energy production within that particular time. SEF must be limited to a particular percentage, and a larger percent of SEF is not acceptable for an optimal and reliable energy system. SEF can be calculated from the following equations [119], [120].

$$SEF_{elec} = \frac{\sum_{t=1}^{t_{total}} (P_{gen}(t) \times \Delta t - P_{con}(t) \times \Delta t)}{\sum_{t=1}^{t_{total}} P_{gen}(t) \times \Delta t} \times 100\% \quad P_{gen}(t) > P_{con}(t) \quad Eq. 2-13$$

$$P_{con}(t) = P_{EL}(t) + P_{EES,SOC}^{max}(t) + P_{Htank,SOC}^{max}(t) \quad \forall t \in t_{total} \quad Eq. 2-14$$

$$SEF_{ther} = \frac{\sum_{t=1}^{t_{total}} (T_{gen}(t) \times \Delta t - T_{con}(t) \times \Delta t)}{\sum_{t=1}^{t_{total}} T_{gen}(t) \times \Delta t} \times 100\% \quad T_{gen}(t) > T_{con}(t) \quad Eq. 2-15$$

$$T_{con}(t) = P_{TL}(t) + P_{TES,SOC}^{max}(t) \quad \forall t \in t_{total} \quad Eq. 2-16$$

Where, SEF_{elec} and SEF_{ther} are the surplus electric energy fraction and surplus thermal energy fraction, respectively, $P_{EES,SOC}^{max}(t)$ is the required power to maximize the EES's SOC, $P_{Htank,SOC}^{max}(t)$ is the required power to maximize the hydrogen storage's SOC, and $P_{TES,SOC}^{max}(t)$ is the required power to maximize the TES's SOC.

2.5.4. Levelized Cost of Energy (LCOE)

LCOE is a fundamental economic matrix to compare different generation sources and energy systems. It accounts for capital cost, replacement cost, Operations and Maintenance (O&M) cost, and other financial indices throughout the project lifetime. Lower LCOE resembles a higher profit for investors.

LCOE (\$/kWh) is the average cost per unit of electricity or energy (kWh). The following equation is used to calculate LCOE [118].

$$LCOE = \frac{NPC_{total}}{\sum_{t=1}^{8760} (P_{EL}(t) + P_{TL}(t)) \times \Delta t} \times \frac{i(1+i)^n}{(1+i)^n - 1} \quad Eq. 2-17$$

Where, NPC_{total} is the system total NPC (\$), i is the real interest rate (%), and n is the project lifetime (years).

2.5.5. Level of Autonomy (LA)

LA is defined as the ratio of the number of hours when a loss of load does not occur and the total number of system operation hours. The higher value of LA defines better system reliability. The maximum and minimum values of LA are 100% and 0%, sequentially. LA is expressed by the following equations [118].

$$LA_{elec} = \frac{H_{total} - H_{LOL}^{elec}}{H_{total}} \times 100\% \quad Eq. 2-18$$

$$LA_{ther} = \frac{H_{total} - H_{LOL}^{ther}}{H_{total}} \times 100\% \quad Eq. 2-19$$

Where, H_{total} is the total operation hour of an energy system (hours), H_{LOL}^{elec} is the total number of hours when a loss of electric load occurs (hours), and H_{LOL}^{ther} is the total number of hours when a loss of thermal load occurs (hours).

2.5.6. Renewable Fraction (RF)

RF defines as the percentage of total generated energy that comes from RESs. RF value of a fully RESs-based energy system is 100%, whereas 0% RF value implies that none of the

RESs-based generators are installed within a system [121]. The following equation determines the RF of an HES [122].

$$RF = 1 - \frac{\sum_{t=1}^{t_{total}} P_{nonrenew}(t) + \sum_{t=1}^{t_{total}} T_{nonrenew}(t)}{\sum_{t=1}^{t_{total}} P_{EL}(t) + \sum_{t=1}^{t_{total}} P_{TL}(t)} \times 100\% \quad Eq. 2-20$$

Where, $P_{nonrenew}(t)$ is the electricity production from non-renewable resources (kW), and $T_{nonrenew}(t)$ is the thermal energy production from non-renewable resources (kW). RF is calculated only in the second part of this study.

Chapter 3: Methodology

In this chapter, the research framework is presented by a flowchart in section 3.1. Methods of data collection are covered in section 3.1. Section 3.3. discusses the technique of analysis adopted in this research. The evaluation and justification of methodology is provided in section 3.4. A list of assumptions of this research is noted in section 3.5.

3.1. Research Framework

This section identifies the problem and the potential framework to solve the problem. Fig. 3-1 presents a flowchart of the research framework. The research framework systematically explained a new research topic named N-R MHES. The study needed quantitative primary data for a specific project location to conduct a case study. The data served as surrogate data to evaluate system performance. Since a nuclear-renewable integrated system experiences demand fluctuation, component cost variations, economic index variations, and system reliability constraints, the sensitivity analysis has been conducted in both parts of the study to strengthen the research.

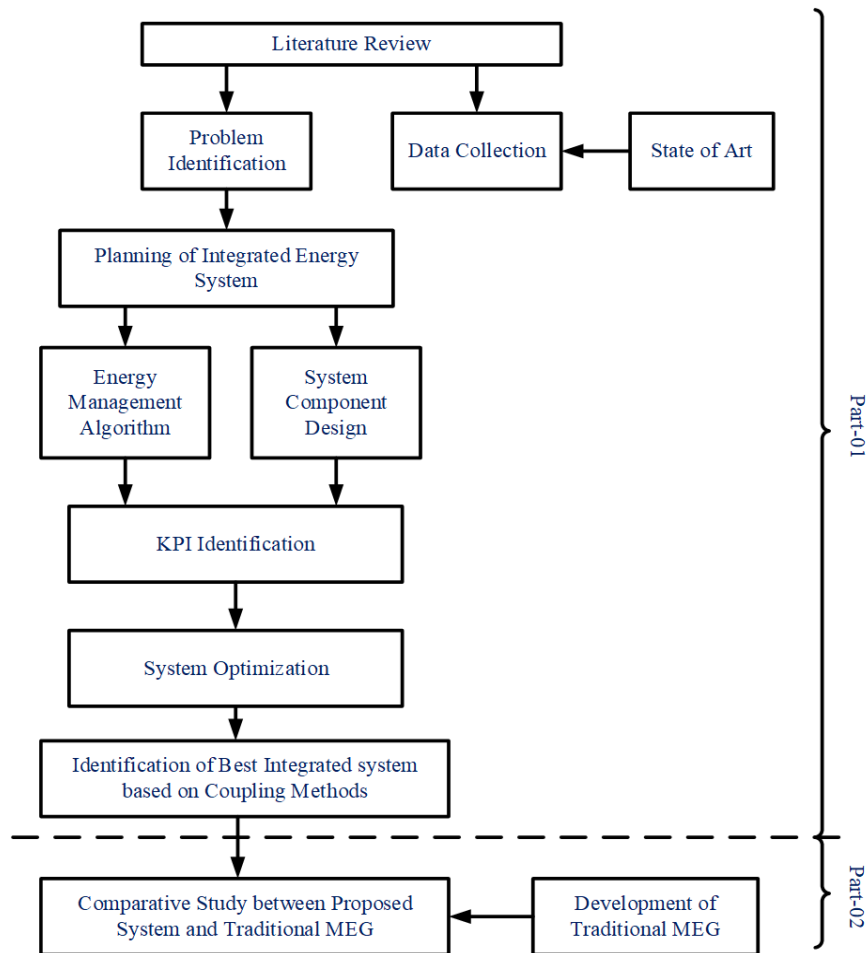


Figure 3-1: Research Framework

3.2. Methods of Data Collection

This research required several quantitative data, such as electric load profile, thermal load profile, solar irradiance, temperature, wind speed, and streamflow. The needed data related to MMRs have been collected by conducting an extensive investigation from literature reviews, websites, and manufacturers. Since MMRs' data are sensitive and subjected to change from manufacturer to manufacturer, the base-case is taken very carefully by viewing all aspects. Several communications were done through emails with different research organizations and manufacturers to get more realistic data. The most trustworthy and popular websites were chosen to get the data of solar irradiance, temperature, wind speed, and streamflow. The average monthly electric load data has been obtained from Ontario Tech University (UOIT) campus. As the exact thermal load demand has not been received for the UOIT campus, a typical thermal demand was considered for the study. The thermal load profile was taken from the Hybrid Optimization Model for Multiple Energy Resources (HOMER) Pro software library. HOMER Pro is one of the most standard and widely used software developed by the National Renewable Energy Laboratory, U.S.A. HOMER has a robust library comprising residential, commercial, industrial, and community-type load profiles [123]. The thermal demand profile was a combination of residential and industrial load demand.

The data of capital cost, replacement cost, O&M cost, and component lifetime were collected from different manufactures and industry partners. Several cross-checked were made with other manufactures to confirm the most realistic equipment prices. The data are properly acknowledged and referenced in the later sections.

3.3. Methods of Analysis

The hourly data for one year contains a total of 8760 data points ($365 \text{ days} \times 24 \text{ hours/day}$). Investigation of an HES with 8760 data and a large number of variables significantly increased the simulation time. To reduce the simulation time, it was necessary to lessen the number of data points with conservative assumptions. Therefore, the daily data (24 data points) for each month (total 12 months) of a year was assumed to be identical; this guided to use of 288 data points ($12 \text{ month} \times 1 \text{ day/month} \times 24 \text{ hours/day}$) rather than considering 8760 data points in the simulation [124]. For example, the daily profile (24 data point) of January was the same throughout January; this held for the rest of the months. But, the daily load profile of January was not the same as the rest of eleven months. So, the assumption directed to work with only 288 data ($12 \text{ month} \times 1 \text{ day/month} \times 24 \text{ hours/day}$) in simulation instead of 8760 data; this reduced the simulation times three-folded.

The following steps have been considered to convert the resources data (solar irradiance, temperature, and wind speed) from 8760 data points to 288 data points.

- The yearly (8760 data points) resources data (solar irradiances, temperature, and wind speed) were gathered from different websites.
- Eight thousand seven hundred sixty (8760) data sets were divided into 12 sections to categorize each section into one month.
- This data processing technique aimed to represent each month by hourly data of a single day; each month was represented with 24 data points. The 24 data points for each month were the hour-by-hour average of each day. For example, to measure the first data point of (among 24 data points) January, each first hour data of each day (total 31 days) of January was taken and made the average. Similarly, January's second resource data point (among 24 data points) was the average of each second-hour data of each day (total 31 days) of January. The entire data processing was carried out by MATLAB programming.

The solar irradiance, temperature, and wind speed data are represented in Fig. 3-2, Fig. 3-3, and Fig. 3-4, respectively [125].

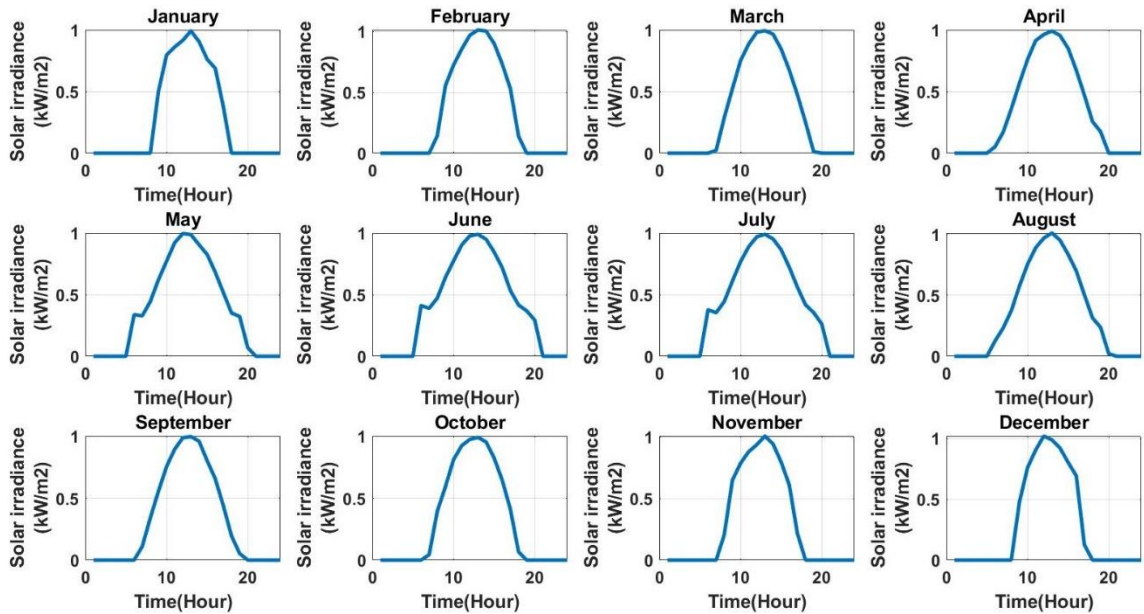


Figure 3-2: Solar Irradiance

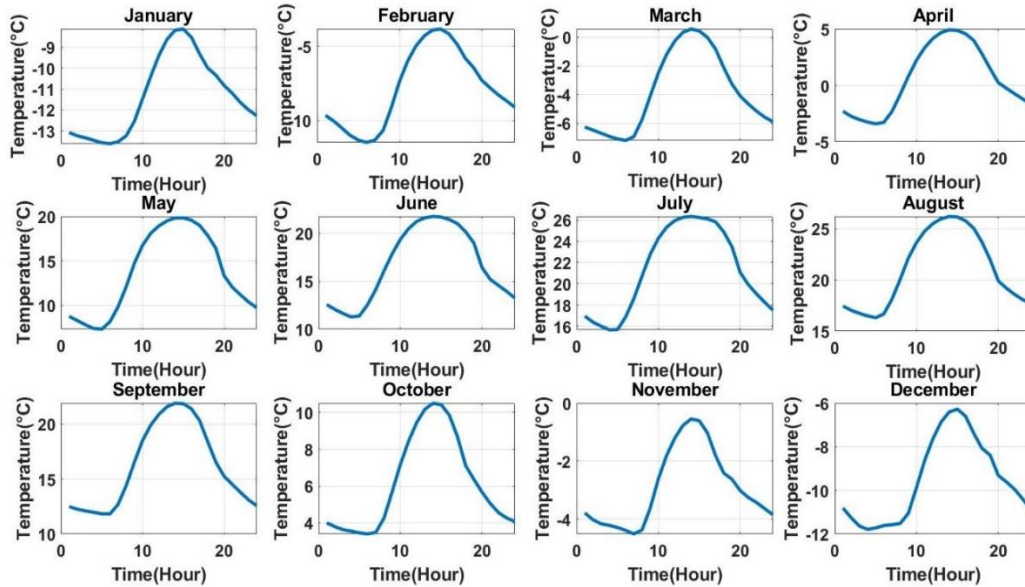


Figure 3-3: Temperature

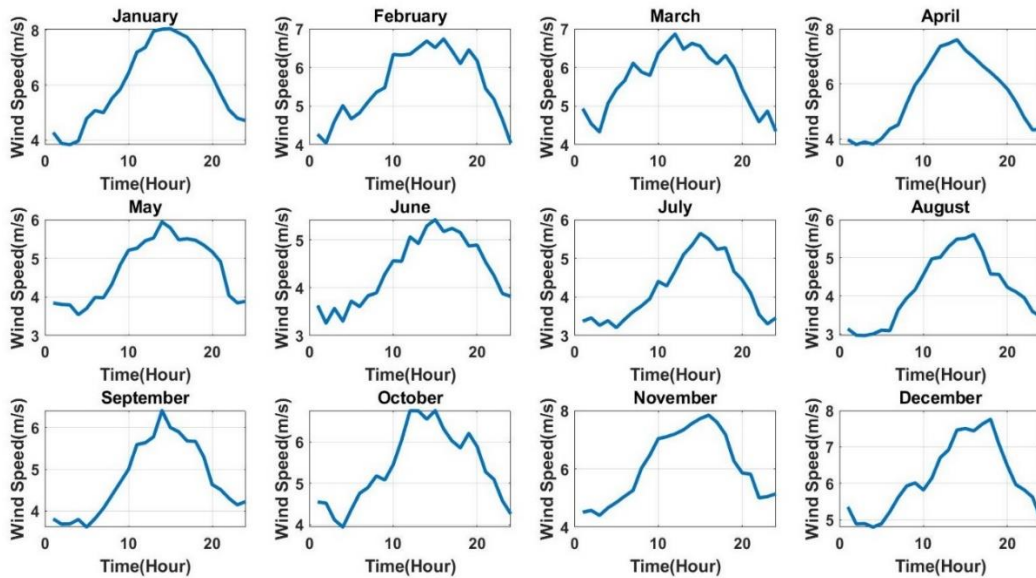


Figure 3-4: Wind Speed

The hourly load profile of a year was not available for the UOIT campus. Therefore, the monthly average data of electric demand for the year 2018 has been obtained for the UOIT campus. A typical electrical load profile, an aggregate of residential and industrial demand, was captured from the HOMER Pro software library and scaled to reflect the monthly average load demand of UOIT. Since the HOMER Pro library provides hourly data of a year (total 8760 data points), it was required to convert 8760 data points into 288 data points for simulation. The data processing techniques explained above were followed here for data conversion. Hence, each month's daily load profile was assumed to be the same, but the monthly load profile would be changed throughout the year. For example, the daily

demand profile (24 data point) of January was the same throughout the whole month of January; this held for the rest of the months. But, the daily load profile was not the same as the rest eleven months. This assumption was conservative since the real-life load profile mostly experiences seasonal changes, not the daily changes. Fig. 3-5 presents the electric load profile of the UOIT campus (2018) regarded in the study.

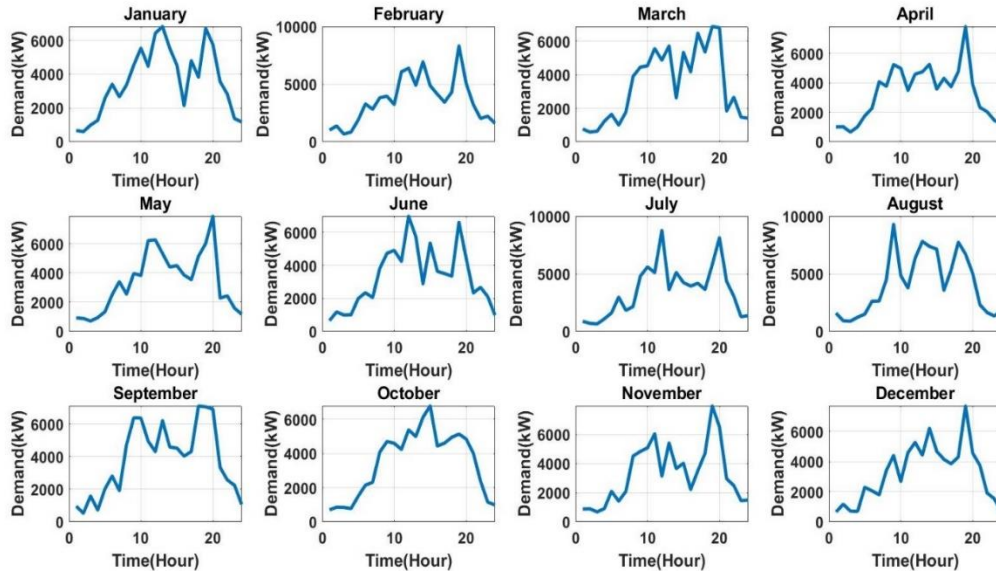


Figure 3-5: Electrical Load Profile

Since the exact thermal load profile was not available for the UOIT campus, a typical thermal demand profile, a combination of residential and industrial demand, was collected from the HOMER Pro software library. The same steps were followed for the thermal data set to convert 8760 data points into 288 data points. The synthesized thermal load profile is displayed in Fig. 3-6.

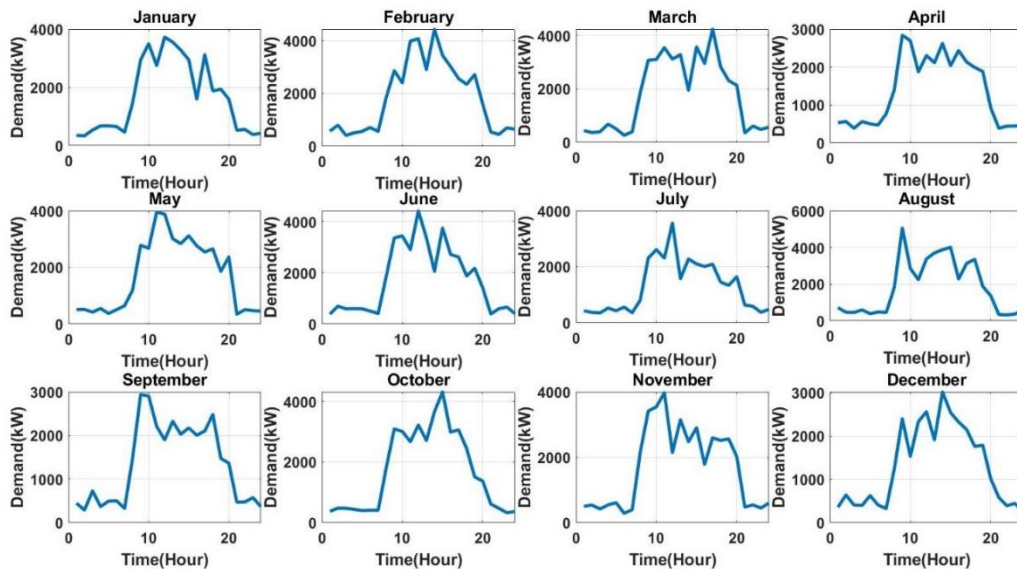


Figure 3-6: Thermal Load Profile

The monthly average streamflow data of the year 2018 were collected from Lake Ontario, Oshawa, Ontario, Canada. The nearest watercourse to the UOIT campus is Lakeview Park, situated at the shore of Lake Ontario. Lakeview Park is around 10 km far from UOIT Campus [126]. The monthly average data of Lake Ontario were collected and processed in MATLAB to convert the monthly average data into the hourly time step data (8760 data points) and 288 data points. MATLAB functions named "*datetime*," "*timetable*," and "*retime*" were used for monthly average data conversion into hourly data. The streamflow rate, available on the website [127], was the total water flow rate of Lake Ontario. Therefore, the data is scaled down to reflect a maximum of 1000.64 kW hydropower plant. The hourly streamflow data (8760 data points) of a year were converted into 288 data points by following the technique, as mentioned earlier. Though hydro dams provide a baseload supply to demand, the streamflow's actual intermittency was reflected in the scaled data. The variability in hydropower generation made the analysis more robust and practical. The streamflow data used in the study is shown in Fig. 3-7. Each month in Fig. 3-7 indicates the daily mass flow rate (24 data points) for that particular month.

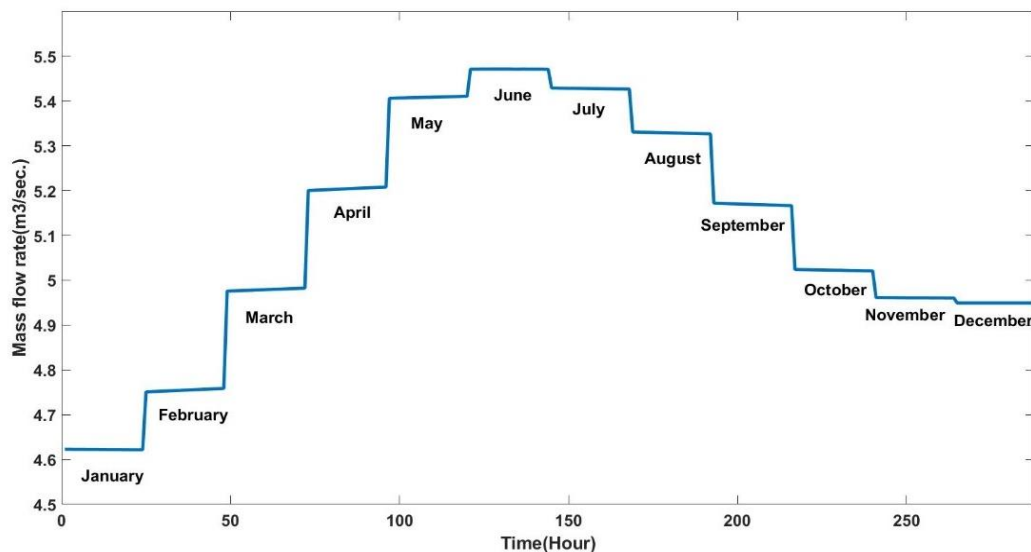


Figure 3-7: Streamflow Rate

3.4. Discussion on Methodological Choice

Though a large-scale nuclear-renewable integration was addressed in [128], this study discussed, modeled, and optimized three specific coupling methods for a micro-scale nuclear-renewable integration. To compare the three hybridization methods, system demand was kept fixed for all cases; the resources were arrayed in all possible combinations to support the load. It was imperative to develop and optimize all proposed hybridization techniques-based HESs before comparing the systems with conventional technologies.

Since the nuclear-renewable integrated systems depend on multiple variables, a sensitivity analysis has been conducted in the study to validate the assumptions. The sensitivity assessment evaluated the impact of different system variables, confirmed the methodology, and strengthened the research results.

Due to versatility, simplicity, and large-scale open resources, MATLAB simulator was used in this study. MATLAB allows users to accomplish with mathematical modeling-based simulation and object-orientated simulation (MATLAB SIMULINK). Since object-oriented simulation has pre-defined parameters and less library support, the numerical modeling-based simulation was adopted in this study. The mathematical modeling-based simulation provides excellent flexibility to users; users can include different parameters and variables depending on overall system requirements.

PSO performs perfectly in a non-smooth global optimization problem. It has several advantages over traditional optimization algorithms. The key benefits of PSO are as follows [129].

- PSO does not include derivatives in a mathematical formulation.
- PSO programming and implementation are more straightforward than other heuristic optimization algorithms.
- PSO is affected insignificantly by the characteristic of the objective function. On the contrary, mathematical optimization algorithms and other metaheuristic algorithms are quite sensitive to the objective function's nature.
- PSO includes few parameters, such as inertia weight factor and two acceleration coefficients.
- The influence of parameters on the solution is more limited for PSO compared to other metaheuristic algorithms.
- PSO has a robust convergence algorithm.
- PSO produces high-quality results and a steady convergence curve within a quicker simulation time.
- PSO has a roughly 80% better time rate than conventional optimization techniques [130].

By considering all circumstances, PSO is selected for this study.

Moreover, a single objective PSO with several reliability constraints was implemented in this research. It eliminated the necessity of a multi-objective PSO technique. In multi-objective PSO for hybrid system problems, both economic matrix and reliability indexes are considered as objective functions. On the other hand, an economic matrix, called NPC, was regarded as the objective function in this study. Multiple reliability indexes were considered as constraints; this served the purpose of multi-objective PSO without any cumbersome process and with less simulation time.

3.5. Assumptions Considered in Modeling

The study addressed several assumptions. Each assumption related to a specific topic is indicated in the designated section in the latter part of the study. However, the key assumptions that were made in this study can be summarized as follows.

- The daily electric demand (hourly) and the daily thermal demand (hourly) for a month were the same.
- It is only possible to guess the anticipated annual variability of the resources data for the entire project lifetime. To estimate the uncertainty and the variability of the yearly resource data, it is required to interpret the past data for at least ten years. It is also difficult to guess the resource input's uncertainty since it follows an intricate meteorological pattern [131]. Therefore, solar irradiance, temperature, wind speed, and streamflow rate were identical for each year of the total project lifetime.
- The only available MMR size for this study was 1000 kW.
- The capacity factor of the MMR is considered as 95% for the base case analysis [132].
- The nuclear reactor is unavailable during the period of fuel module replacement. The diesel Genset is unavailable when generators complete their lifespan and require replacement. The WT, PV panels, and other equipment are also inaccessible during the component replacement period. This replacement period for the nuclear fuel module, the diesel Genset, and components may offer alternative generation sources to support the system demand. But, the cost associated with alternative sources is not considered in any of the cases in the study for simplicity.
- The main shortcomings of a large-scale Genset are high fuel cost and high O&M cost. On the other hand, a very small-scale Genset needs to adjust the output voltage, and multiple units of Gensets take a considerable amount of space. By regarding all benefits and drawbacks of Gensets, a trade-off was made between large-scale Genset and very Small-scale Genset. Therefore, only three types of diesel Genset, rated as 50 kW, 30 kW, and 20 kW, were available for diesel-fired MEG.
- It is very unusual to get an NPP that provides a vast amount of thermal supply to the demand [133], and NNPs accomplish a large share of thermal demand in this study. Hence, the monthly average thermal demand was less than the electric demand.
- The quality of heat generated from the CHP unit is beyond this study.

Chapter 4: Proposed System Architectures and Energy Management

The first part of the analysis develops, discusses, and compares the three N-R MHESs that are modeled based on the proposed hybridization methods. The second part of the research extends the discussion and provides a comparative study between the best nuclear-renewable hybridized system and a traditional technology-based MEG. Since the study focused on off-grid applications, no electric grid is regarded in this study. The proposed hybridization methods are explained in section 4.1, 4.2, and 4.3.

4.1. Direct Coupling

The direct coupling method is a conventional hybridization means of nuclear reactors and RESs. In this coupling, electricity is generated from different RESs and nuclear reactors, and the resources simultaneously serve electrical and thermal requirements by utilizing only electricity. CHP facilities and by-product commodities are not regarded in this configuration. Hence, thermal generation is not available in this infrastructure. As there is no direct thermal generation within this HES, the system architecture does not include any thermal energy storage. Electrochemical, chemical, electrical, and mechanical energy storage systems might be added to store the excess electricity. Fig. 4-1 depicts a system schematic of directly coupled N-R MHES.

Any types of RESs, e.g., solar, wind, hydro, biomass, and geothermal, can be counted within the directly coupled HES. One of the conventional renewable sources, geothermal energy, is not added in Fig. 4-1 since geothermal energy depends on geographical conditions. For the same reason, pumped hydro energy storage is not considered in the case study. The thermal demand may involve residential energy demand, district heating, calcination plant, and seawater desalination plant. In a directly coupled N-R MHES, the electric requirement is met by direct electricity production, while the thermal demand is accomplished by Electricity-to-Heat (E2H) unit. E2H unit converts electric energy into thermal energy. It should be noted that the required thermal energy to produce biogas is obtained from N-R MHESs; this also holds for other coupling methods discussed in the following sections.

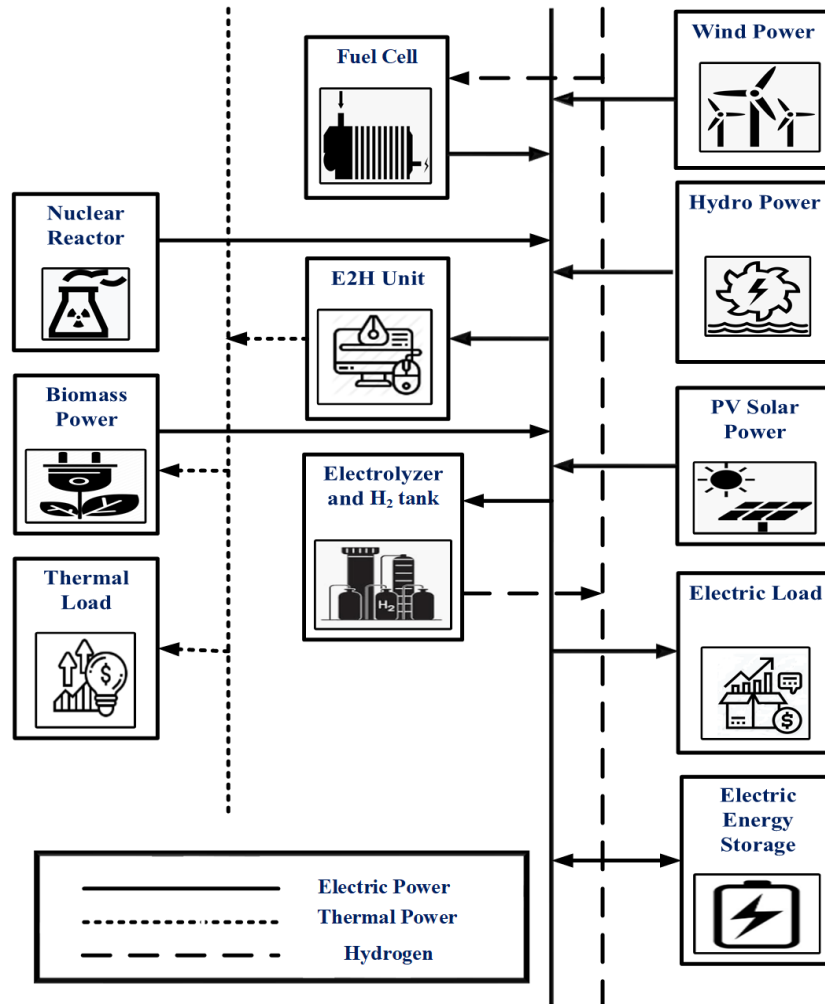


Figure 4-1: Schematic of Direct Coupled N-R MHES

In the energy management algorithm, a hierarchy is maintained in the charging and discharging of storage systems. As stated in the earlier section, hydrogen storage is introduced in the proposed HES to reduce EES sizing. It has a higher priority than EES in the charging and discharging mechanism. If there is any surplus electricity available, it will be stored in the hydrogen tanks, followed by the EES. Similarly, the deficit amount of electric and thermal demand will be fulfilled by FCs, followed by the EES. FCs utilize the stored hydrogen to generate electricity. After charging the hydrogen tanks and EES, if there is any excess electric energy available, it will be consumed by electrical dump loads. The energy management strategy is outlined in Fig. 4-2.

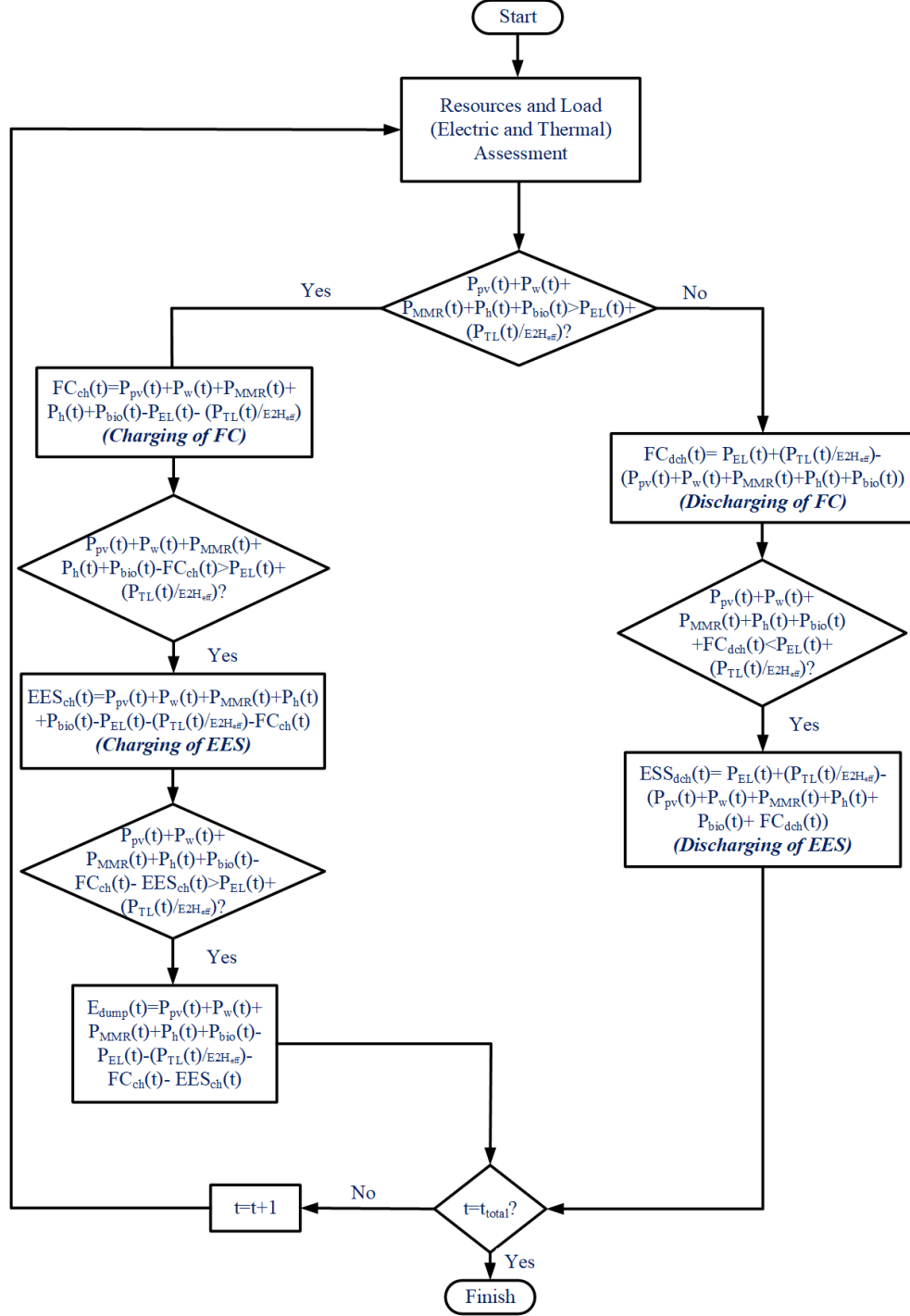


Figure 4-2: Energy Management Algorithm of Directly Coupled N-R MHES

Any combination of renewables, energy storages, and loads is plausible within this type of N-R MHES. The arrangement of different equipment is not limited to the proposed N-R MHES shown in this study. However, energy management fundamentals must be maintained in extended or reduced types directly coupled N-R MHESs.

4.2. Single Resource and Multiple Product-based Coupling

In this kind of hybridization, electrical and thermal load are served by nuclear reactors and Biogas Generators (BGs); no other renewables are involved in this HES. Generated electricity from nuclear reactors and biomass directly serves the electric load. In contrast, CHP's recovered thermal power from nuclear reactors and BGs is supplied to thermal load. Since electrical and thermal generators are available within the HES, this system configuration can combine electric, electrochemical, thermal, and mechanical energy storage systems. Heat-to-Electricity (H2E) units and E2H units are inserted to ensure the ultimate reliability of energy supply. However, the H2E unit and the E2H unit will have the least preference and will be operated in extreme cases. The detailed architecture of this coupling is shown in Fig. 4-3.

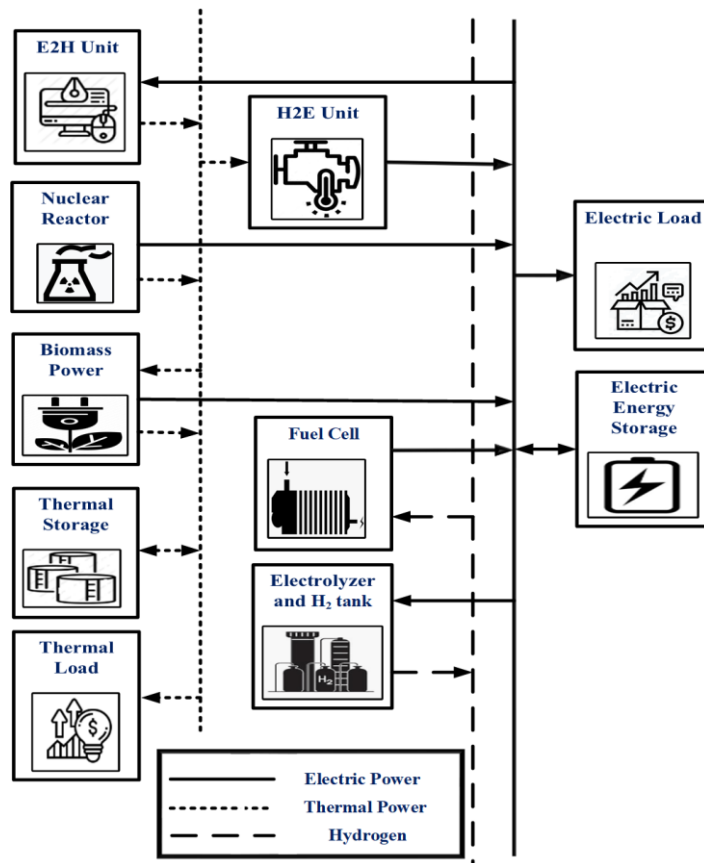


Figure 4-3: Schematic of Single Resource and Multiple Products-based Coupled N-R MHES

The energy management flowchart of this coupling is shown in Fig. 4-4. For electrical energy management, if there is any surplus electrical energy within the system, it will be stored in the hydrogen tanks and EES. Still, if there is excess energy after charging the hydrogen tanks and EES, and there is a requirement from thermal demand, it will be used to serve the thermal load through the E2H unit. Electric dump loads will consume the

additional excess electric energy. Likewise, if there is any shortage of electrical energy management demand, the hydrogen tanks and EES will be discharged to fulfill the electrical need. The H2E unit will be operated if the hydrogen tanks and battery banks cannot support the deficit electric demand. Since BGs depend on thermal power, it is reasonable to integrate BGs with nuclear generation so that the nuclear reactors can partially/fully support the BGs with thermal energy. There are no traditional RESs, such as solar, wind, and hydro, in this system architect, except BGs.

In thermal energy management, the surplus thermal energy will be stored in TES. The further excess heat will be supplied to serve electric demand by the H2E unit if there is any electrical demand shortage. The rest of the excess thermal power, if available, will be consumed in thermal dump loads. On the other hand, the deficit thermal demand will be satisfied by discharging of the TES. After discharging the TES, the deficit thermal demand will be accomplished by the E2H unit, provided there is excess electric energy. Both H2E and E2H units have the least precedence in the energy management algorithm.

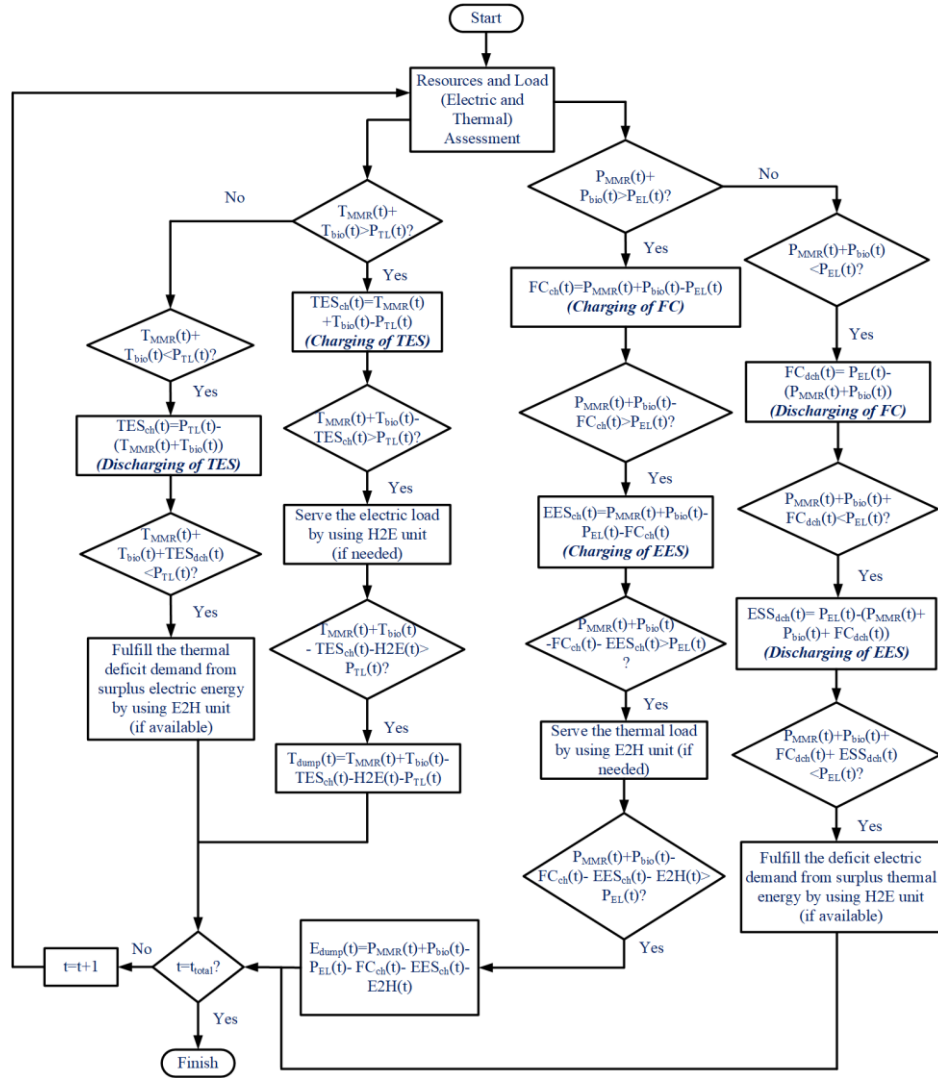


Figure 4-4: Energy Management Algorithm of Single Resource and Multiple Products-based Coupled N-R MHES

4.3. Multiple Resources and Multiple Product-based Coupling

Multiple Resources and Multiple Products-based coupling is a blended hybridization technique of direct coupling and single resource and multiple products-based coupling method. In this type of hybridization, electrical load is served by MMRs, PV panels, WTs, Hydro Turbines (HTs), and BGs, while thermal load is met by recovered heat from MMRs and BGs. The purpose of the rest of the system equipment, e.g., hydrogen tank, FC, EES, TES, E2H, and H2E, is similar to the single resource and multiple products-based coupling method. CHP and by-product commodities are considered in this type of hybridization process. Fig. 4-5 and Fig. 4-6 illustrate the schematic and the energy management strategy, respectively, of the "multiple resources and multiple products-based coupling method."

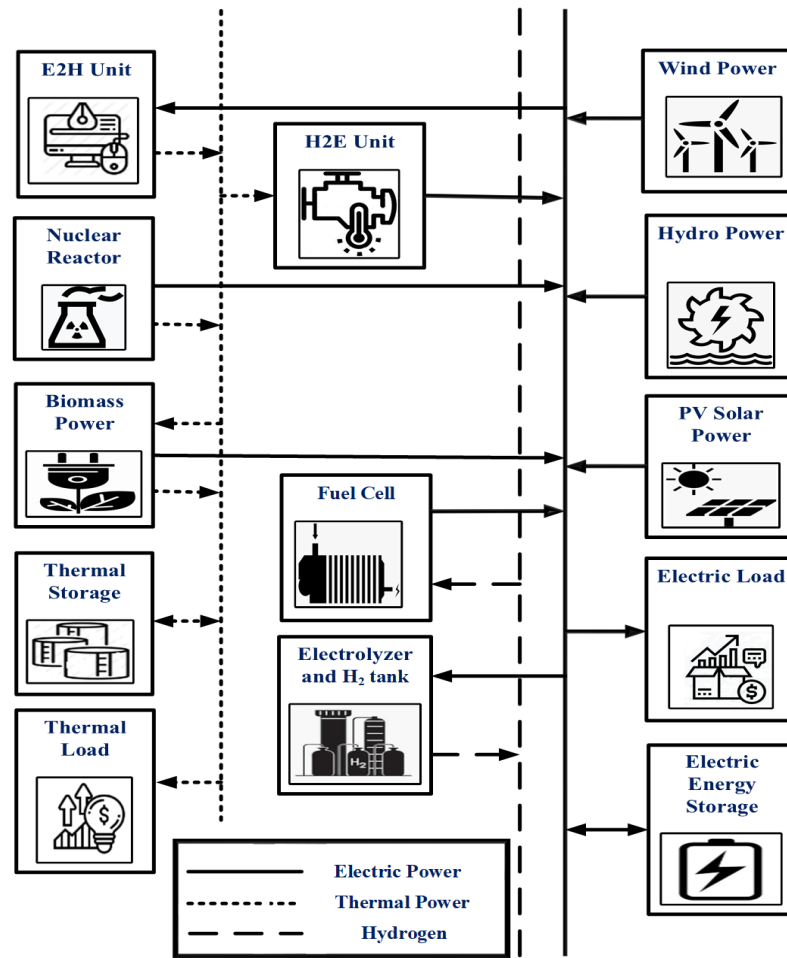


Figure 4-5: Schematic of Multiple Resources and Multiple Products-based Coupled N-R MHES

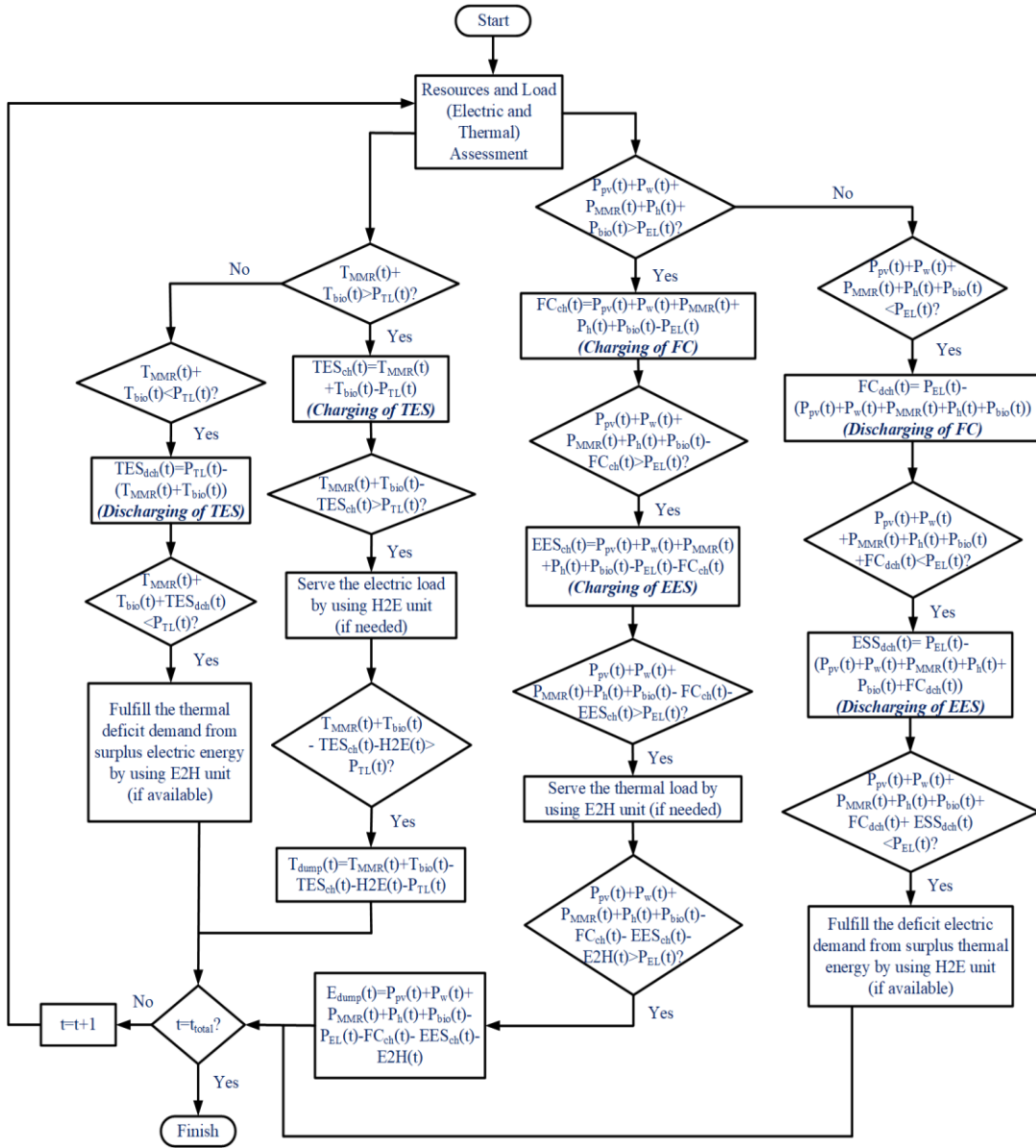


Figure 4-6: Energy Management Algorithm of Multiple Resources and Multiple Products-based Coupled N-R MHES

Chapter 5: System Modeling

5.1. Nuclear Power Plant (Micro Modular Reactor)

This study principally focuses on the economic model of MMRs. The discussions on the licensing processes and the regulations are beyond this study. MMR deployment cost depends on several determinants, such as technology, plant design, civil works, licensed site location, environmental qualifications, transport facility, financing organization, and labor. Transmission and Distribution (T&D) cost is excluded in this research since the T&D cost is associated with all types of technology. The deployment of MMRs qualifies for Production Tax Credits (PTCs). PTCs are the per kWh tax credit for the selected energy system, mainly for RES-based energy systems [134]. The PTCs are available for nuclear generation also up to 6000 MWe at USD 0.018/kWh. However, the inclusion of PTCs in an MMR cost model has an insignificant impact. Thus, PTCs are not contemplated in this study [132].

The installation cost of a first-of-a-kind any equipment is higher than the next deployment. Similarly, the overnight capital cost of an MMR decreases with lessons learned. The learning rate is the fraction of cost reduction per doubling the cumulative capacity/unit, with experience gained in a production plant [135]. The relationship between lessons learned and cost reduction of a technology can be expressed by the following “one-factor learning curve” equation [136].

$$LR = 1 - 2^{-R} \quad \text{Eq. 5-1}$$

Where, LR is the learning rate (%), and R is the rate of cost reduction (%). The exact learning rate is always case-specific. The N th-of-a-kind cost, the stabilized cost of technology for a particular learning rate, depends on project locations and design complexities. For example, an MMR produced in a factory has a higher learning rate than an MMR produced on-site. Besides, the learning rate will be higher in a dedicated MMR production factory than a mixed MMR production factory with other commodities.

Depending on the learning rate, the overnight capital cost of an MMR unit will be decreased. Eq. 5-2 represents the relationship between cost reduction and MMR capital cost [137].

$$C_u = C_{1st} \times N_{th}^{-R} \quad \text{Eq. 5-2}$$

Where, C_u is the unit cost of an MMR of N_{th} number MMR unit (\$), and C_{1st} is the cost of the 1st MMR unit (\$). Since R is the rate of cost reduction, R is negative in Eq. 5-2.

The detailed input parameters of the MMR studied in the study are listed in Table 5-1 [132]. The input values are collected from several MMR developers.

Table 5-1: Specification of the MMR Unit

Parameters	Value
Reactor size (kW_e)	1000
Plant lifetime (Years)	40
Core lifetime (Years)	10
Capacity factor (%)	95
Nominal overnight capital cost ($$/kW_e)$	15,000
Fixed O&M cost ($$/kW_e)$	350
Fuel cost ($$/MWh)$	10
Decommissioning cost ($$/MWh)$	5
Refueling cost of fuel module (\$)	20 million
Plant efficiency (%)	40

Fig. 5-1 represents the impact of learning rates on the number of MMR deployment. Factory fabricated product-based industries, such as automotive, aerospace, and shipbuilding, have a learning rate between 15% to 20% [138]. Since MMRs are also factory-made products, MMRs’ learning rate is expected to 5%-15%. Besides, the “Korea Hydro & Nuclear Power” has encountered a learning rate of 10% for nuclear reactors [139]. By considering all viewpoints, a 10% learning rate is considered in this study. The fuel price and the O&M cost of MMRs are also expected to reduce with operational experience gained. However, since these costs contribute to the total cost insignificantly [140] and the overnight cost is the primary driver of the value for MMRs, the fuel cost and the O&M cost reduction are not included to avoid undesirable complexities in the study.

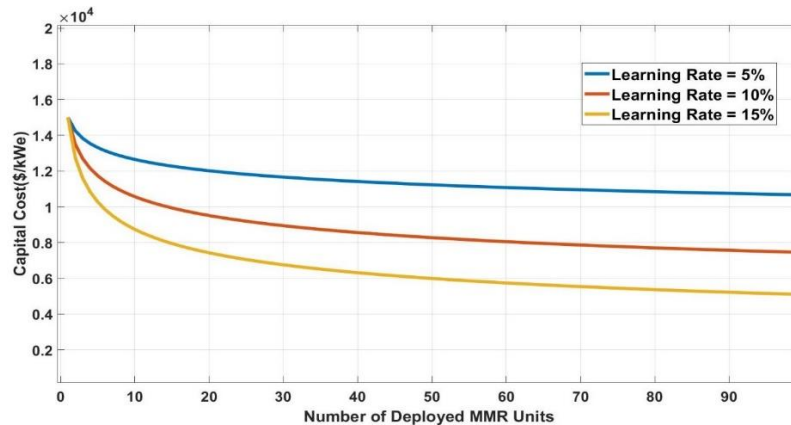


Figure 5-1: Capital Cost Reduction for Different Learning Rates

The analysis incorporates site engineering and MMR licensing cost in the MMR capital cost. Due to various technologies and manufacturers, refurbishment cost may not fit in a fixed economic model of MMR. Some may replace the entire nuclear reactor, refurbish it at the central facilities, refuel it, and then reuse it. On the other hand, some may only refuel the reactor in-place and not carry out any refurbishment. Therefore, the refurbishment cost is managed into the fixed O&M cost in the analysis rather than handling it separately. The

fuel cost, listed in Table 5-1, includes the fuel management cost as well. Decommissioning cost is accrued during the operation of MMRs. Hence, it is considered as evenly spread over the project lifetime. The refueling cost is the sum of expenses to transport the fuel module from the factory to the licensed site and install it at a dedicated location. The refueling cost does not include the MMR fuel cost since it is captured in the “Fuel Cost.” The cost associated with “exclusion zone” for microreactors is not considered in this study since “exclusion zone” concept is near non-existence for microreactors. As research is going on to develop regulatory documents for microreactors, detailed requirements and specifications on “exclusion zone” are hardly known. However, it can be added in future microreactor economic models depending on the required ratio of “exclusion zone” area and costs related to the site real estate.

Nuclear power plant operation is primarily categorized into two sections: baseload operation and load-following operation [141]. MMR-based NPPs are also capable of operating in both modes. The baseload MMR operation always provides a constant power level at its maximum capacity. Baseload MMRs are only unavailable during the maintenance or refurbishment period. On the other hand, load-following MMRs change their output depending on the system demand variation for the long or short term. Though traditional large-scale reactors are not operated in load-following mode, the modern microreactor has the capability of load-following operation. Load-following of microreactors is performed by adjusting reactor control rods, bypassing steam turbines, and making one or multiple units offline [142].

Load-following MMR is a complex mechanism and likely to face high thermo-mechanical stress. Microreactor vendors claim that the main steam supply and reactor coolant systems will be affected by the load-following strategy, which may lead to frequent replacements. The load-following technique also affects heat exchangers due to the rapid rate of temperature change. Small/micro-scale reactors can perform load-following from 100% to as low as 20% power. The power ramp of this kind of reactors is linear, and it is around 5% per minute. Rates of power ramp and duration of low power operation are restricted with a defined limit. Another critical issue with load-following is Fuel Pellet Cladding Interaction (PCI) at greater than 5% per minute power ramp. But lower reactor power density, like a micro-scale reactor, reduces the risk [142]. Adjustment of a baseload system, such as NPP, to handle a variable demand causes significant wear and tear on systems and increases O&M cost [143].

The capital cost is the main contributor to MMR's total deployment cost. The O&M cost and the fuel cost do not depend on the amount of generated electricity. Hence, load-following, reduction of electricity production, is not cost-efficient. However, secondary commodities production by excess thermal generation utilizing CHP units may lead to improve the investment economics [140]. On the contrary, base-load plant operation is straightforward; it always provides a specific amount of energy supply over a period. For HESs, the rest of the demand is met by dispatchable generation sources and variable RESs

along with energy storage systems. The appropriate energy mix depends on total system cost, availability, and optimal system configuration [144].

Moreover, load-following NPP is required if a significant portion of energy contribution comes from nuclear generation [145]. The energy mix of renewables with nuclear reduces a substantial contribution of nuclear generation in HESs. By considering the circumstances mentioned above, MMR's baseload operation, linked with electric and thermal energy storage, is adopted in this study. The waste heat is recovered and utilized in cogeneration to produce useable thermal power.

5.2. Solar Energy

Solar energy can be utilized in two ways to generate electricity: Concentrated Solar Power (CSP) and Solar Photovoltaic (PV). The solar PV system is considered in this study. Solar PV panels absorb photons from solar energy by utilizing semiconductor materials and convert the solar energy into Direct-Current (DC). A solar PV system comprises several components, such as PV modules, power electronics equipment, and mounting equipment. The semiconductor materials used in a PV module include amorphous silicon, polycrystalline silicon, monocrystalline silicon, and cadmium telluride [146].

Solar power generation by PV panels largely depends on solar irradiance, ambient temperature, and PV panel surface area. The PV panel's precise modeling to extract solar power from the UOIT location is represented below [147].

$$P_{PV}(t) = N_{PV} \times \eta_{PV}(t) \times PV_{area} \times G_t(t) \quad \forall t \in t_{total} \quad Eq. 5-3$$

$$\eta_{PV}(t) = \eta_{ref} \times \eta_{MPPT} \times [1 + \beta(T_c(t) - T_{cref})] \quad \forall t \in t_{total} \quad Eq. 5-4$$

$$T_c(t) = T_a(t) + \left(\frac{NOCT - 20}{800} \right) \times G_t(t) \quad \forall t \in t_{total} \quad Eq. 5-5$$

Where, N_{PV} is the number of the PV panels, $\eta_{PV}(t)$ is the instantaneous PV panel efficiency (%), PV_{area} is the area occupied by the unit PV panel (m^2), $G_t(t)$ is the solar irradiance (kW/m^2), η_{ref} is the reference efficiency of the PV panel (%), η_{MPPT} is the efficiency of the Maximum Power Point Tracking (MPPT) unit (%), β is the temperature coefficient ($^{\circ}C^{-1}$), $T_a(t)$ is the ambient temperature ($^{\circ}C$), T_{cref} is the PV panel reference temperature ($^{\circ}C$), and $NOCT$ is the nominal operating cell temperature ($^{\circ}C$).

Table 5-2 lists a detailed specification of the solar PV panel considered in this study. Disposal cost of PV panels after completion of lifetime is not considered. PV panels can be installed either on roof-top or other dedicated places. Therefore, real estate cost related to PV panel is not also considered in this study.

Table 5-2: Parameters of the Solar PV Panel

Parameter	Value	Reference
Area Occupied by unit PV panel (m^2)	5	N/A
Capital Cost (\$/kW)	1200	[148]
Replacement Cost (\$/kW)	1000	[148]
O&M Cost (\$/kW/Year)	12	[149]
Lifetime (Years)	25	[150]
Reference Efficiency of PV Panel (%)	17.3	[151]
Efficiency of the MPPT unit (%)	95	[151]
Temperature Coefficient ($^{\circ}C^{-1}$)	-0.41	[151]
PV panel reference temperature ($^{\circ}C$)	25	[151]
Nominal Operating Cell Temperature ($^{\circ}C$)	45	[151]

5.3. Wind Energy

The wind is abounding in the environment, and it has great potential to generate electricity with zero fuel cost. To determine the exact amount of wind power derived by a WT, the wind speed is first estimated at the hub height for the project site. Eq. 5-6 calculates the wind speed at hub altitude [152].

$$V(t) = V_{ref}(t) \times \left(\frac{h_{hub}}{h_{ref}} \right)^a \quad \forall t \in t_{total} \quad Eq. 5-6$$

Where, $V(t)$ is the calculated wind speed (m/s), $V_{ref}(t)$ is the wind speed at the anemometer height (m/s), h_{hub} is the hub height (m), h_{ref} is the anemometer height (m), and a is the power-law exponent.

The wind speed measured at the hub height is used to calculate the actual wind power generation. The system designers must comply with the wind turbine power curve and wind speed to select the WT. Wind turbine power curves provide an initial idea of what size the WT should have. Depending on the maximum, minimum, and average wind speed, the designers select the WTs. A typical power curve of a WT is given in Fig. 5-2.

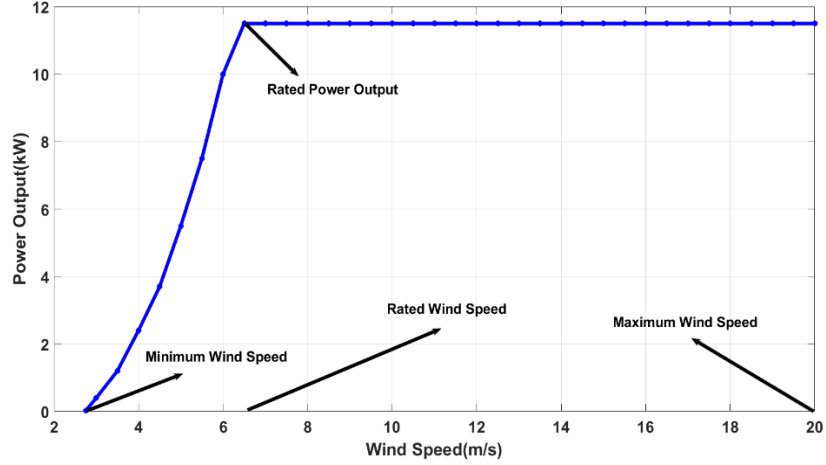


Figure 5-2: A Typical Power Curve of Wind Turbine

Wind power generated by the selected WT is measured from the following equation [153].

$$P_W(t) = \begin{cases} 0, & V(t) < V_{min}, V > V_{max} \\ \frac{P_r}{V_r^3 - V_{min}^3} \times V^3(t) - \frac{V_{min}^3}{V_r^3 - V_{min}^3} \times P_r, & V_{min} \leq V(t) \leq V_r \\ P_r, & V_r \leq V(t) \leq V_{max} \end{cases} \quad \text{Eq. 5-7}$$

Where, V_{min} is the minimum wind speed (m/s), V_{max} is the maximum wind speed (m/s), V_r is the rated wind speed (m/s), and P_r is the rated power of the WT (kW).

Table 5-3 presents different parameters of the WT studied in this research. Decommissioning cost of WTs is not regarded in this study. Since installation of WTs depends on project location and user requirements, real estate cost associated with WTs is not considered here.

Table 5-3: Parameters of the Wind Turbine

Parameter	Value	Reference
Nominal Capacity (kW)	10	N/A
Capital Cost (\$/kW)	1130	[148]
Replacement Cost (\$/kW)	1130	[148]
O&M Cost (\$/kW/Year)	48	[154]
Lifetime (Years)	25	[155]
Hub Height (m)	16	[156]
Anemometer Height (m)	50	[125]
Minimum wind speed (m/s)	2.75	[156]
Maximum wind speed (m/s)	20	[156]
Rated wind speed (m/s)	6	[156]
Power Law Exponent	1/7	[152]

5.4. Hydro Power (Water Energy)

A hydropower plant can operate at both baseload and load-following mode. Hydroelectric plants can change the power output instantly by opening turbine valves [145]. A run-of-river hydroelectric plant is considered in this study with a baseload mode of operation. In a run-of-river hydro, the natural streamflow of a river is redirected downwards by penstocks, and the penstock heads to the power generating house (turbine house). Streamflow is utilized to generate electricity by using turbines and generators. The used water is fed back to the main watercourse further downstream. A run-of-river system is also ecology-friendly since fishes can bypass through ladders of the system [157]. A schematic of a run-of-river hydroelectric plant is drawn in Fig. 5-3.

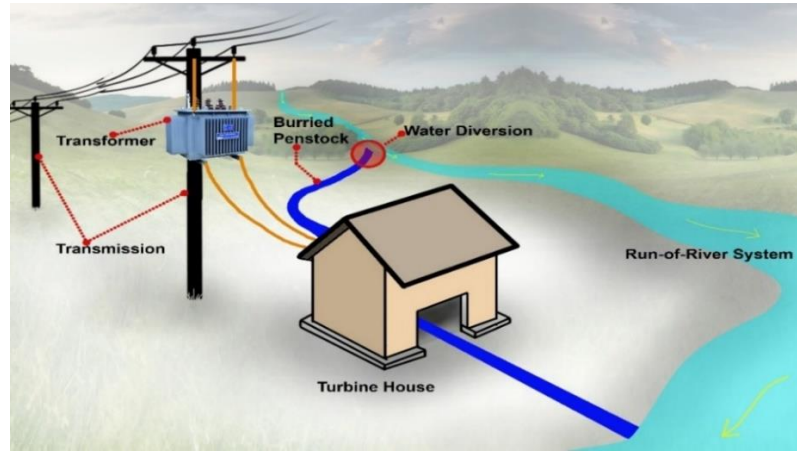


Figure 5-3: Run-of-River System

The monthly mass flow rate of Lake Ontario, located near the UOIT campus, for one year is collected and synthesized for the simulation. The maximum nominal capacity of the hydro plant is 1000.64 kW in this study. The mass flow rate data is scaled to ensure the nominal sizing of the hydroelectric plant. The nominal power of the hydropower plant can be determined from the following equations [158].

$$P_h(t) = H_{eff} \times \rho_w \times g \times Q_{turbine}(t) \times \eta_{HT} \quad \forall t \in t_{total} \quad Eq. 5-8$$

$$H_{eff} = H_a(1 - H_{loss}) \quad Eq. 5-9$$

Where, H_{eff} is the effective water head (m), ρ_w is the water density ($1000 \frac{kg}{m^3}$), g is the gravitational constant ($9.81 \frac{m}{s^2}$), $Q_{turbine}(t)$ is the mass flow rate ($\frac{m^3}{s}$) at time step t , η_{HT} is the HT efficiency (%), H_a is the available water head (m), and H_{loss} is the pipe head loss (%).

The mass flow rate or HT flow rate is the amount of water that passes through the HTs. In this study, the mass flow rate is calculated using the following equation.

$$Q_{turbine} = \begin{cases} 0, & Q_{available} < Q_{min} \\ Q_{available}, & Q_{min} \leq Q_{available} \leq Q_{max} \\ Q_{max}, & Q_{available} > Q_{max} \end{cases} \quad Eq. 5-10$$

Where, $Q_{available}$ is the available mass flow rate to the HTs ($\frac{m^3}{s}$), Q_{min} is the available minimum mass flow rate to the HTs ($\frac{m^3}{s}$), and Q_{max} is the available maximum mass flow rate to the HTs ($\frac{m^3}{s}$).

A detailed specification of the hydroelectric plant is shown in Table 5-4.

Table 5-4: Parameters of the Run-of-River System

Parameter	Value	Reference
Nominal Capacity (kW)	1000.64	N/A
Capital Cost (\$/kW)	2500	[159]
Replacement Cost (\$/kW)	250	[159]
O&M Cost (\$/kW/Year)	100	[159]
Lifetime (Years)	40	[159]
Efficiency (%)	80	[160]
Pipe Head Loss (%)	15	[158]
Available Water Head (m)	25	[158]
Design Flow Rate (m^3/s)	5.1	N/A
Minimum Mass Flow Ratio (%)	50	[158]
Maximum Mass Flow Ratio (%)	150	[158]

5.5. Biomass Energy

Biogas is produced in the Anaerobic Digestion (AD) process, where microorganisms split the organic matters into smaller chemical substances in the absence of oxygen. The AD process produces biogas as well as digestate as a by-product [161]. It could be a suitable replacement for natural gas. It could also be a potential solution for reducing GHG emission projects [162]. In the biogas generation process, manure is mixed with water to produce slurry. The slurry is pumped to deliver it in a digester and heated in the digester at a specific temperature to generate biogas.

A schematic of a biogas production plant from cow manure is outlined in Fig. 5-4 [163]. A digester is an insulated, sealed, and concrete-made vessel. A gas storage is integrated with digesters to store the generated biogas. Therefore, the digester's roof is made of a flexible double membrane roof. The biogas generated in the digester is cooled down and supplied to CHP units. The CHP unit utilizes the biogas to produce electricity and heat energy. The generated electric power serves the electrical demand. The thermal energy is mainly used to heat the digester, and the rest of the thermal energy is used for heating or other thermal applications

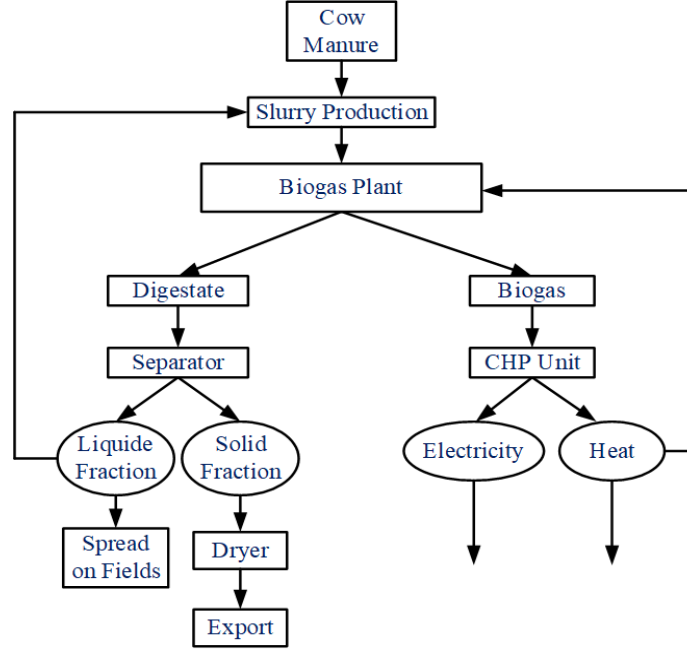


Figure 5-4: Schematic of the Biogas Plant with CHP

The study considers a farm-based small-scale biogas plant. The biogas is produced from cow manure, and the dairy farm consists of 150 cows. The nominal capacity of the BG is 65.10 kW. Eq. 5-11 can estimate the biogas production of the dairy farm in a year [164].

$$BG = N_i \times m_i \times k_{DSi} \times k_{OSi} \times v_{Bi} \times 365 \quad \text{Eq. 5-11}$$

Where, BG is the amount of biogas production ($m^3/year$), N_i is the number of animals in a specific group, m_i is the manure produced per animal (37 kg/day) [165], k_{DSi} is the dry substance content in the manure of particular animal (0.23) [163], k_{OSi} is the organic substance content in dry substance (0.85) [163], and v_{Bi} is the specific biogas output from the organic substance ($0.3 m^3/kg$) [163].

Total energy production from biogas is calculated from the following equation.

$$E = BG \times e_{Bi} \quad \text{Eq. 5-12}$$

Where, E is the energy generated from biogas ($kWh/year$), and e_{Bi} is the specific heat energy obtained from manure ($6 kWh/m^3$) [166]. The amount of energy generated from Eq. 5-12 is the input energy of the CHP unit.

The expression of electric power and thermal power generated from the CHP unit can be presented as follows, respectively.

$$P_{bio,elec}(t) = \frac{E \times K_e}{T_c} \quad \forall t \in t_{total} \quad \text{Eq. 5-13}$$

$$P_{bio,ther}(t) = \frac{E \times K_t}{T_c} \quad \forall t \in t_{total} \quad Eq. 5-14$$

Where, $P_{bio,elec}(t)$ and $P_{bio,ther}(t)$ are the electric and thermal power output of the CHP unit (kW), respectively, K_e and K_t are the electric and thermal efficiency of the CHP unit (%), respectively, and T_c is the number of operational hours of the plant during the year (4380 hours/year). The electrical efficiency of a biogas plant usually varies from 30% to 40%, while the thermal efficiency is 35-55% [167].

The AD unit requires heat energy to increase and maintain the digester temperature at a certain level. Eq. 5-15 measures the heat energy needed by the digester. As a rule of thumb, 30% extra energy is added to Eq. 5-15 by considering the losses [168].

$$Q_d = M \times s_{sub} \times (T_d - T_{sub}) \times 1.3 \quad Eq. 5-15$$

Where, Q_d is the required thermal energy to heat the substrate material (kJ/year), M is the total mass flow rate that is a combination of manure and water (kg/year), s_{sub} is the specific heat capacity of substrate/feed ($kJ.kg^{-1}.^{\circ}C^{-1}$) [169], T_d is the required temperature in digester ($^{\circ}C$), and T_{sub} is the substrate/feed temperature ($^{\circ}C$). The mixture of manure and water has a ratio of 1:1 to maintain 12% total dry solid content in the AD process [170]. As a rule of thumb, the feed's specific heat is the value of water ($4.18 kJ.kg^{-1}.^{\circ}C^{-1}$). The slurry, mixture of manure and water, is pumped and kept in the digester at $35^{\circ}C$ [171]. The minimum substrate/feed temperature implies the maximum heat energy consumption in the digester. Hence, $0^{\circ}C$ is assumed as the substrate/feed temperature in this study, which could be the lowest substrate/feed temperature.

The capital cost of the biogas plant incorporates AD unit cost, CHP unit cost, and other cost. The AD unit cost is the summation of construction cost of the digester, mixer, and accessories. The purchase cost and installation cost of the CHP unit are merged in the total CHP unit cost. The "others cost" covers civil work, management cost, backup storage cost, safety system, piping, and grid connection cost. The replacement cost is the summation of scheduled maintenance cost, labor cost, and insurance cost.

Table 5-5 outlines the different parameters of the biogas plant.

Table 5-5: Parameters of the Biogas Plant

Parameter	Value	Reference
Nominal Capacity (kW)	65.10	N/A
Capital Cost (\$/kW)	4000	[172]
Replacement Cost (\$/kW)	2500	[164]
O&M Cost (\$/kW/Year)	300	[172]
Lifetime (Years)	25	[172]
Electric Efficiency (%)	40	[167]
Thermal Efficiency (%)	30	[167]

In this study, the BG is performed when the solar irradiance becomes insignificant. The BG provides uniformity on the generation side. Usually, solar radiation reaches zero in the evening time and starts increasing in the morning. Therefore, the BG is scheduled from 7.00 p.m. to 7.00 a.m. to produce electricity from biogas. If there is any shortage of required thermal energy to heat the digester, the deficit thermal energy will be supplied from N-R MHESs.

5.6. Electrolyzer, Hydrogen Tank, and Fuel Cell (FC)

Alternative energy storage, other than battery storage, is considered in this study to reduce the battery sizing. Hydrogen storage is installed in the studied HESs to store excess electricity in the form of hydrogen. In this type of energy storage, the surplus electricity is used to produce hydrogen by electrolyzers. An electrolyzer is an electrochemical device, which dissociates water into oxygen and hydrogen by utilizing electrical current. Electrolyzers produce hydrogen by low-temperature electrolysis processes and stores in hydrogen tanks. FCs use hydrogen to generate electricity if there is energy need in N-R MHESs. The amount of hydrogen produced by the electrolyzer is formulated as follows [173], [174].

$$\begin{aligned} H_{production}(t) &= \{H_{tank}(t) - H_{tank}(t - 1)\} \\ &= \eta_{elec} \times E_{elec}(t) \times \frac{H_2 \text{ density } (kg/m^3)}{H_2 \text{ heating value } (kWh/m^3)} \quad \forall t \in t_{total} \quad Eq. 5-16 \end{aligned}$$

Where, $H_{tank}(t)$ is the amount of hydrogen (kg) at time t , η_{elec} is the electrolyzer efficiency (%), $E_{elec}(t)$ is the input energy to the electrolyzer (kWh), H_2 heating value is $3.4 kWh/m^3$ in standard condition, and H_2 density is $0.09 kg/m^3$.

Electric energy produced by the FC is determined from the following equation [174]:

$$\begin{aligned} E_{FC}(t) &= \{H_{tank}(t - 1) - H_{tank}(t)\} \times \eta_{FC} \\ &\times \frac{H_2 \text{ heating value } (kWh/m^3)}{H_2 \text{ density } (kg/m^3)} \quad \forall t \in t_{total} \quad Eq. 5-17 \end{aligned}$$

Where, η_{FC} is the efficiency of the FC (%).

A detailed specification of the FC, electrolyzer, and hydrogen tank are outlined in Table 5-6, Table 5-7, and Table 5-8, respectively.

Table 5-6: Parameters of the Fuel Cell

Parameter	Value	Reference
Capital Cost (\$/kW)	600	[175]
Replacement Cost (\$/kW)	500	[175]
O&M Cost (\$/kW)	0.0153	[175]
Lifetime (Years)	4.5	[175]
Efficiency (%)	50	[176]

Table 5-7: Parameters of the Electrolyzer

Parameter	Value	Reference
Capital Cost (\$/kW)	1500	[177]
Replacement Cost (\$/kW)	1000	[177]
O&M Cost (\$/kW/Year)	20	[177]
Lifetime (Years)	15	[175]
Efficiency (%)	80	[178]

Table 5-8: Parameters of the Hydrogen Tank

Parameter	Value	Reference
Rated Capacity (kg)	25	N/A
Capital Cost (\$/kg)	1200	[177]
Replacement Cost (\$/kg)	800	[177]
O&M Cost (\$/kg/Year)	15	[177]
Lifetime (Years)	25	[177]
Minimum SOC (%)	5	N/A
Maximum SOC (%)	100	N/A

5.7. Energy Storage System

5.7.1. Electrochemical Energy Storage (EES)

EES stores electric energy in the form of chemicals and supplies as electricity. EES can be categorized as conventional batteries and flow batteries. The selection and the compatibility of either EES or TES entirely depend on technical advancements, environmental impacts, economic feasibility, policy and market constraints, and logistic limitations. It can not be said in general indeed for single storage to be the best one [179]. Therefore, selection and recommendation of energy storage are beyond this study. A generic EES is considered and model in this research.

The battery capacity of a system depends on the demand and the days of autonomy. The following equation can measure the EES (battery) capacity (kWh) [121].

$$EES_{capacity} = \frac{P_{EL,avg} \times AD \times N_{bat}}{DOD \times \eta_{inv} \times \eta_{ESS}} \quad Eq. 5-18$$

Where, $P_{EL,avg}$ is the average electric demand (kW), AD is the autonomy days (typically 3 to 5 days), N_{bat} is the number of the battery bank, DOD is the depth of discharge of the battery (%), η_{inv} is the inverter efficiency (%), and η_{ESS} is the battery efficiency (%).

The maximum and minimum SOC of the EES are subjected to the following equations [174].

$$EES_{SOC,max} = EES_{capacity} \times DOD \quad Eq. 5-19$$

$$EES_{SOC,min} = EES_{capacity} \times (1 - DOD) \quad Eq. 5-20$$

The following equations describe the EES charging and discharging scheme (17) and (18), respectively.

$$E_{EES}(t) \leq E_{EES}^{rated} \quad \forall t \in t_{total} \quad Eq. 5-21$$

$$E_{EES}(t) = E_{EES}(t - 1) + E_{EES,in}(t)\eta_{EES} \quad \forall t \in t_{total} \quad Eq. 5-22$$

$$E_{EES}(t) = E_{EES}(t - 1) - \frac{E_{EES,out}(t)}{\eta_{EES}} \quad \forall t \in t_{total} \quad Eq. 5-23$$

Where, E_{EES}^{rated} is the rated energy of the battery (*kWh*), $E_{EES,in}(t)$ is the available battery charging energy (*kWh*), η_{EES} is the battery efficiency (%), and $E_{EES,out}(t)$ is the possible battery discharging energy (*kWh*).

Parameters of the EES studied in this research are listed in table 5-9.

Table 5-9: Parameters of the EES

Parameter	Value	Reference
Capital Cost (\$/kWh)	398	[175]
Replacement Cost (\$/kWh)	398	[175]
O&M Cost (\$/kWh/Year)	10	[179]
Lifetime (Years)	5	[175]
Efficiency (%)	85	[180]
Days of Autonomy (Days)	3	[121]
Depth of Discharge (%)	80	N/A
Inverter Efficiency (%)	95	[181]

5.7.2. Thermal Energy Storage (TES)

TES is mainly classified into two categories based on types of heat: sensible heat and latent heat. Sensible heat-based TES covers Underground Thermal Energy Storage (UTES), Hot/Cold water storage, and solid media storage. Latent heat-based TES includes Thermochemical Storage (TCS), Molten Salts, Liquid Air Energy Storage (LAES), and Phase Change Materials (PCMs) [179].

The selection of TES wholly depends on energy and power capacity, energy and power capacity cost, discharge time, response time, storage degradation rate, energy and power density, specific energy and power, round-trip efficiency, cycle life, technology lifetime,

O&M cost, technology readiness level, and storage output temperature. By considering all determinants, a generic hot and cold-water TES is adopted in this study. A hot and cold-water TES has reasonable expenses, short discharge and response time, moderate round-trip efficiency, average technology lifetime, and medium-level technology readiness. Parameters of the TES with load-following capability are listed in Table 5-10. The TES charging and discharging scheme can be expressed by Eq. 5-25 and Eq. 5-26, sequentially [182].

$$E_{TES}(t) \leq E_{TES}^{rated} \quad \forall t \in t_{total} \quad Eq. 5-24$$

$$E_{TES}(t) = E_{TES}(t-1) + E_{TES,in}(t)\eta_{TES} \quad \forall t \in t_{total} \quad Eq. 5-25$$

$$E_{TES}(t) = E_{TES}(t-1) - \frac{E_{TES,out}(t)}{\eta_{TES}} \quad \forall t \in t_{total} \quad Eq. 5-26$$

Where, E_{TES}^{rated} is the rated energy of the TES (*kWh*), $E_{TES,in}(t)$ is the available charging energy of the TES (*kWh*), η_{TES} is the efficiency of the TES (%), and $E_{TES,out}(t)$ is the output energy of the TES (*kWh*).

Table 5-10: Parameters of the TES

Parameter	Value	Reference
Capital Cost (\$/kWh)	5	[183]
Replacement Cost (\$/kWh)	5	[183]
Lifetime (Years)	30	[184]
Efficiency (%)	80	[185]
Days of Autonomy (Days)	2	N/A
Depth of Discharge (%)	80	N/A

5.8. H2E unit

H2E unit is considered to generate electricity from excess thermal power if required by the electric load. The H2E unit will be operated when there is no alternative to serve the electrical demand except excess thermal energy. The H2E unit consists of steam generators, steam turbines, and electric generators. The steam generator produces high-pressure steam, which is supplied to the steam turbine. The steam turbine is coupled with an electric generator. The high-pressure steam is used to rotate the turbine, and electricity is eventually produced from the electric generator. The following equations measure the electric power generated from the H2E unit.

$$H2E(t) = \eta_{H2E} \times P_{excess}(t) \quad \forall t \in t_{total} \quad Eq. 5-27$$

$$\eta_{H2E} = \eta_{SG} \times \eta_{ST} \times \eta_{EG} \quad \text{Eq. 5-28}$$

Where, η_{SG} is the steam generator efficiency (%), η_{ST} is the steam turbine efficiency (%), η_{EG} is the electric generator efficiency (%), and $P_{excess}(t)$ is the surplus thermal power at time step t .

The technical and economic parameters of the H2E unit are listed in Table 5-11.

Table 5-11: Parameters of the H2E Unit

Parameter	Value	Reference
Capital Cost (\$/kW)	1932	[186], [187]
Replacement Cost (\$/kW)	1932	[186], [187]
O&M Cost (\$/kW/Year)	0.9	[186], [187]
Lifetime (Years)	15	[186], [187]
Steam Generator Efficiency (%)	40	[188]
Steam Turbine Efficiency (%)	40	[189]
Electric Generator Efficiency (%)	95	[190]

5.9. E2H Unit

An E2H is also regarded in this research to produce thermal energy from surplus electric power. The E2H unit will come to the operation in extreme cases, similar to the H2E unit. The working principle of the E2H unit is identical to an electric boiler. The surplus electrical energy is used to serve the deficit thermal demand by the E2H system if there is any shortage in meeting the thermal power. The thermal power production by the E2H unit can be represented by Eq. 5-29.

$$E2H(t) = \eta_{E2H} \times T_{excess}(t) \quad \forall t \in t_{total} \quad \text{Eq. 5-29}$$

Where, η_{E2H} is the efficiency of E2H unit (%), and $T_{excess}(t)$ is the surplus electric power at time step t .

Table 5-12 shows parameters of the E2H unit considered here.

Table 5-12: Parameters of the E2H Unit

Parameter	Value	Reference
Capital Cost (\$/kW)	54	[191]
Replacement Cost (\$/kW)	54	[191]
O&M Cost (\$/kW/Year)	0	[191]
Lifetime (Years)	20	[191]
Efficiency (%)	98	[192]

5.10. Diesel Generator

Diesel Gensets are usually diesel engines that are coupled with generators. In this study (the second part of the analysis), diesel generators are used as a surrogate component of the conventional fossil-fired energy-generating technology to compare the MMR-based MEG for off-grid applications. Standalone off-grid RES-based HESs are hardly capable of fulfilling the medium/large-scale energy demand [158]. A typical fossil-fired microgrid includes diesel generators as a back-up power supply when renewables are unavailable. But diesel generators are included in this study to operate accompanying with renewables. The surplus energy generated from the MEGs will be stored in the EES. PSO finds out the minimum number of Gensets that need to be included within the system with the lowest NPC.

MMRs will be replaced in the second part of this study by different diesel Gensets to meet the load. Three types of small size Gensets are chosen for this study rather than using a large-size Genset. Large-scale Genset contributes to an extensive amount of capital cost, installation space, and fuel cost. Optimal sizing of diesel Gensets in a hybrid energy system requires the assessment of daily and yearly demand and growth rate. The peak demand of a remote community is typically 5 to 10 times higher than the average demand [193]. So, if the peak demand is considered in the optimal sizing of Gensets, the system will be oversized. Research reveals that it is economical and reliable to use different sizes of Gensets rather than using several equal-sized Gensets to optimize the Genset-loading and obtain maximum fuel efficiency [194]. The typical size of a Genset that is transported to remote locations is within 15-2500 kW. The smaller size of Gensets is also simpler to install [195]. Moreover, a small-size generator has less operating and fuel cost than a large-scale generator [196]. Small-size generators also need to regulate the voltage with inverters and battery chargers' output [197]. Therefore, by considering all perspectives, a trade-off is made between very large-scale Gensets and very small-scale Gensets. This study considers three reduced-sized diesel Gensets, rated as 50 kW, 30 kW, and 20 kW, by observing the system demand. When diesel Gensets work with renewables, it is typically designed to run at 80-100% of their rated power [198]. The diesel Gensets, considered in this study, run at the rated power to maximize the Genset efficiency. Light-load operation of diesel Gensets can cause premature aging, and it also stimulates the risk of machine failure [194]. A typical efficiency curve of a diesel generator is presented in Fig. 5-5 [199].

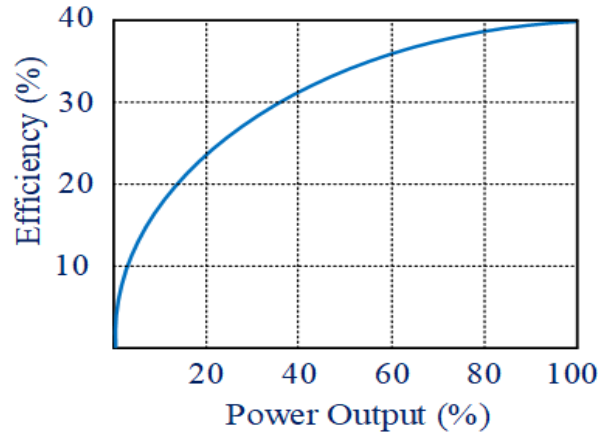


Figure 5-5: Efficiency Curve of a Diesel Genset

The following equation calculates the fuel consumption rate of the diesel generators [194].

$$F = F_i \times P_{rated} + F_s \times P_{out} \quad \text{Eq. 5-30}$$

Where, F is the rate of fuel consumption (L/hr), F_i is the fuel curve intercept coefficient of the diesel generator (L/hr/kW_{rated}), P_{rated} is the rated capacity of the diesel generator (kW), F_s is the fuel curve slope of the diesel generator (L/hr/kW_{out}), and P_{out} is the diesel generator output (kW).

A detailed specification of the diesel generators considered here is recorded in Table 5-13.

Table 5-13: Parameters of the Diesel Generators

Parameter	Value	Reference
Nominal Capacity (kW)	50, 30, 20	N/A
Capital Cost (\$/kW)	800	[200]
Replacement Cost (\$/kW)	800	[200]
O&M Cost (\$/kW/Year)	35	[200]
Lifetime (Years)	2.5	[200]
Fuel Curve Intercept Coefficient (L/hr/kW _{rated})	0.011	[201]
Fuel Curve Slope (L/hr/kW _{out})	0.244	[201]
Diesel Price (\$/L)	0.719	[202]
Electric Efficiency (%)	40	N/A

Chapter 6: Simulation Model

This section formulates the optimization model to find out the optimal configuration of different HESs. The chapter also discusses the decision variables, the optimization constraints, and the optimization problem's boundary conditions. Three different systems are optimized based on three proposed hybridization methods. A diesel-fired MEG is also optimized to analyze and compare with the best configured N-R MHES. The optimization is carried out based on the energy management algorithms outlined in Chapter 4.

6.1. Objective Function

A single-objective N-R MHES planning problem is addressed in this study to minimize the system NPC. The optimization problem formulation consolidates technical and economic parameters. The objective function is the economic KPI (NPC), whereas the optimization constraints include LPSP, SEF, and other technical parameters. To obtain the optimal system configuration with minimal NPC, it is necessary to formulate the fitness function for optimization. The fitness function is the summation of NPC of all system components. The objective function of the minimization problem can be defined as follows.

$$\min f_{NPC} = \sum_{i \in G} NPC_i \quad \text{Eq. 6-1}$$

Where, G is the set of system component and NPC_i is the NPC of the i^{th} component. The system component includes PV panel, WT, MMR, HT, BG, EES, TES, FC, hydrogen tank, electrolyzer, E2H, and H2E unit.

The NPC is the sum of the present worth of total capital cost, replacement cost, O&M cost, and fuel cost. Except for the nuclear reactor, the NPC of other system components can be calculated by the following equation.

$$NPC_i = C_{cap,i} + C_{rep,i} + C_{O\&M,i} + C_{fuel,i} - C_{salv,i} \quad \forall i \in G \quad \text{Eq. 6-2}$$

Where, $C_{cap,i}$ is the capital cost (\$), $C_{rep,i}$ is the total replacement cost (present worth) (\$), $C_{O\&M,i}$ is the total operation and maintenance cost (present worth) (\$), $C_{fuel,i}$ is the present worth of fuel cost (present worth) (\$), and $C_{salv,i}$ is the salvage value of the i^{th} component (\$).

The capital cost of all equipment occurs at the commencement of the project lifetime. It is calculated once in the entire project lifetime. The capital cost of any component is calculated as follows.

$$C_{cap,i} = N_{com,i} \times C_{cap,unit(i)} \quad \forall i \in G \quad \text{Eq. 6-3}$$

Where, $N_{com,i}$ is the number of equipment, and $C_{cap,unit(i)}$ is the capital cost of the unit component (\$).

The replacement cost occurs at the completion of the component lifetime. The number of replacements depends on the project lifetime and the equipment lifetime. The replacement cost (present worth) of system equipment is calculated as follows [174].

$$C_{rep,i} = N_{com,i} \times \sum_{n=1}^{N_{rep}} C_{rep,unit(i)} \times \frac{1}{(1+r)^{j_{rep}}} \quad \forall i \in G \quad Eq. 6-4$$

$$N_{rep} = \left\lceil \frac{T_{project}}{LT_{com,i}} \right\rceil - 1 \quad Eq. 6-5$$

$$r = \frac{i' - f}{1 + f} \quad Eq. 6-6$$

$$j_{rep} = \sum_{n=1}^{N_{rep}} (n \times LT_{com,i}) \quad Eq. 6-7$$

Where, N_{rep} is the number of replacements that occurred for the component, $C_{rep,unit(i)}$ is the unit replacement cost of the i^{th} component (\$), r is the real discount rate (%), $T_{project}$ is the project lifetime (year), $LT_{com,i}$ is the i^{th} component lifetime (year), $ceil(X)$ is a function rounding the element X to the nearest integer which is equal or greater than X , i' is the nominal discount rate/the rate at which the money has been borrowed (%), and f is the inflation rate (%).

The O&M cost of a component in the HESs is counted for each year, and it continues throughout the whole project lifetime. The O&M cost is the same for each year. Therefore, the O&M cost (present worth) is computed by the following equation [174].

$$C_{O\&M,i} = N_{com,i} \times C_{O\&M,annual(i)} \times \frac{\{(1+r)^{T_{project}}\} - 1}{r(1+r)^{T_{project}}} \quad \forall i \in G \quad Eq. 6-8$$

Where, $C_{O\&M,annual(i)}$ is the yearly O&M cost of the i^{th} component (\$/year).

The fuel cost of the system equipment differs from component to component, and it depends on the equipment working principle. Renewable sources do not have any fuel cost. MMRs and fossil-fired generators have fuel cost since they utilize uranium and different fossil fuel, e.g., coal, diesel, and natural gas, to generate electricity. The equation to determine the fuel cost (present value) of equipment can be represented as follows [174].

$$C_{fuel,i} = N_{com,i} \times C_{fuel,annual(i)} \times \frac{\{(1+r)^{T_{project}}\} - 1}{r(1+r)^{T_{project}}} \quad \forall i \in G \quad Eq. 6-9$$

Where, $C_{fuel,annual(i)}$ is the annual fuel cost of the i^{th} component (\$/year).

The salvage value is the worth of a component at the end of its useful life. In this study, the salvage value is estimated for each system component. A linear depreciation is considered in the analysis to calculate the salvage value. In linear depreciation, the amount is evenly distributed over the useful lifetime, and the salvage value of a component is directly proportional to the rest of the component lifetime. The salvage value depends on replacement cost despite the capital cost. The salvage value is calculated as follows [203].

$$C_{salv,i} = N_{com,i} \times C_{rep,unit(i)} \times \frac{LT_{com(i),rem}}{LT_{com,i}} \times \frac{1}{(1+r)^{T_{project}}} \quad \forall i \in G \quad Eq. 6-10$$

$$LT_{com(i),rem} = LT_{com,i} - (T_{project} - LT_{rep,i}) \quad Eq. 6-11$$

$$LT_{rep,i} = LT_{com,i} \times \left[\frac{T_{project}}{LT_{com,i}} \right] \quad Eq. 6-12$$

Where, $C_{salv,i}$ is the salvage value of the i^{th} component (\$), $LT_{com(i),rem}$ is the remaining lifetime of the i^{th} equipment at the end of the project lifetime (year), and $LT_{rep,i}$ is the duration of replacement cost (year).

Cost analysis of MMRs is not as simple as the other energy generation sources. The total deployment cost of an MMR is a sum of several types of cash flows, and each of the cash flows influences the overall cost differently. MMRs involve some new types of expenses, such as decommissioning cost and refueling cost. Therefore, the NPC of an MMR is estimated separately by the following equation.

$$NPC_{MMR} = C_{cap,MMR} + C_{O\&M(fixed),MMR} + C_{fuel,MMR} + C_{decom,MMR} + C_{refueling,MMR} - C_{salv,MMR} \quad Eq. 6-13$$

Where, $C_{cap,MMR}$ is the MMR capital cost (\$), $C_{O\&M(fixed),MMR}$ is the MMR fixed O&M cost (\$), $C_{fuel,MMR}$ is the MMR fuel cost (\$), $C_{decom,MMR}$ is the MMR decommissioning cost (\$), $C_{refueling,MMR}$ is the MMR refueling cost (\$), and $C_{salv,MMR}$ is the salvage value of MMR (\$). All the cost is in the form of present worth.

The O&M cost, the fuel cost, and the salvage value of MMRs are determined by the equations listed above. Though MMRs have a similar type of capital cost like other generation sources, it is calculated uniquely in the study. MMR is a first-of-a-kind product, and the capital cost of an MMR decreases with the increased number of MMR modules. The equation to estimate the MMR capital cost is expressed as follows [137].

$$C_{cap,MMR} = \sum_{n=1}^{N_{MMR}} C_{cap,MMR(1st)} \times (N_{MMR})^{-R} \quad Eq. 6-14$$

Where, N_{MMR} is the number of MMRs required, $C_{cap,MMR(1st)}$ is the capital cost of 1st MMR (\$), and R is the rate of cost reduction (%).

As the decommissioning cost is accrued evenly throughout the project lifetime, it can be calculated by the following equation [174].

$$C_{decom,MMR} = N_{MMR} \times C_{decom,MMR(annual)} \times \frac{\{(1+r)^{T_{project}}\} - 1}{r(1+r)^{T_{project}}} \quad Eq. 6-15$$

Where, $C_{decom,MMR(annual)}$ is the MMR decommissioning cost accrued in each year (\$/year).

The refueling cost occurs every ten years (fuel module lifetime) interval, commencing in the first year, throughout the project lifetime. The following equations calculate the MMR refueling cost [174].

$$C_{refueling,MMR} = N_{MMR} \times \sum_{n=1}^{N_{refuel}} C_{refueling,MMR(unit)} \times \frac{1}{(1+r)^{j_{refuel}}} \quad Eq. 6-16$$

$$N_{refuel} = \left\lceil \frac{T_{project}}{LT_{fuel(MMR)}} \right\rceil - 1 \quad Eq. 6-17$$

$$j_{refuel} = \sum_{n=1}^{N_{refuel}} (n \times LT_{fuel(MMR)}) \quad Eq. 6-18$$

Where, $C_{refueling,MMR(unit)}$ is the refueling cost of a single MMR module (\$), N_{refuel} is the number of refueling of MMR fuel module in the project lifetime, and $LT_{fuel(MMR)}$ is the lifetime of the MMR fuel module (year).

6.2. Constraints

Several optimization constraints are exercised in this research to confirm the utmost reliability and resiliency of the system. The generation by any source must be less or equal to the maximum capacity of that source. It can be presented as:

$$P_{gen}^i(t) \leq P_{gen,max}^i \quad \forall i, \forall t \quad Eq. 6-19$$

$$T_{gen}^i(t) \leq T_{gen,max}^i \quad \forall i, \forall t \quad Eq. 6-20$$

Where, $P_{gen}^i(t)$ and $P_{gen,max}^i$ are the electric generation of the i^{th} component at time t and maximum electricity generation of the i^{th} component, respectively, and $T_{gen}^i(t)$ and $T_{gen,max}^i$ are the thermal power generation of the i^{th} component at time t and maximum thermal power generation of the i^{th} component, sequentially.

The system's cumulative production must be greater or equal to the overall system requirements to ensure the highest reliability of the optimal system. The following equations present the energy management constraints of the optimization problem.

$$\sum P_{gen}^y(t) \geq \sum_{t=1}^{t_{total}} P_{EL}^y(t) \quad \forall t \in t_{total}, \forall y \quad Eq. 6-21$$

$$\sum T_{gen}^y(t) \geq \sum_{t=1}^{t_{total}} P_{TL}^y(t) \quad \forall t \in t_{total}, \forall y \quad Eq. 6-22$$

$$\begin{aligned} \sum P_{gen}^y(t) = & \sum_{t=1}^{t_{total}} N_{PV} P_{pv}(t) + \sum_{t=1}^{t_{total}} N_{WT} P_w(t) \\ & + \sum_{t=1}^{t_{total}} N_{MMR} P_{MMR}(t) + \sum_{t=1}^{t_{total}} P_h(t) \\ & + \sum_{t=1}^{t_{total}} P_{bio}(t) \end{aligned} \quad \forall t \in t_{total}, \forall y \quad Eq. 6-23$$

$$\sum T_{gen}^y(t) = \sum_{t=1}^{t_{total}} N_{MMR} T_{MMR}(t) + \sum_{t=1}^{t_{total}} T_{bio}(t) \quad \forall t \in t_{total}, \forall y \quad Eq. 6-24$$

Where, $P_{gen}^y(t)$ is the electric power generation (kW) at time step t in year y , $P_{EL}^y(t)$ is the electric demand (kW) at time step t in year y , $T_{gen}^y(t)$ is the thermal power generation (kW) at time step t in year y , $P_{TL}^y(t)$ is the thermal demand (kW) at time step t in year y (kW), N_{PV} is the number of PV panels, N_{WT} is the number of WTs, and N_{MMR} is the number of MMRs.

The energy storage systems of the N-R MHESs are subjected to the following constraints to maintain the proper operation of the energy storage systems.

$$SOC_{Htank,min} \leq SOC_{Htank}^y(t) \leq SOC_{Htank,max} \quad \forall t \in t_{total}, \forall y \quad Eq. 6-25$$

$$SOC_{EES,min} \leq SOC_{EES}^y(t) \leq SOC_{EES,max} \quad \forall t \in t_{total}, \forall y \quad Eq. 6-26$$

$$SOC_{TES,min} \leq SOC_{TES}^y(t) \leq SOC_{TES,max} \quad \forall t \in t_{total}, \forall y \quad Eq. 6-27$$

Where, $SOC_{Htank}^y(t)$ is the SOC (%) of hydrogen tank at time step t in year y , $SOC_{Htank,min}$ and $SOC_{Htank,max}$ are the minimum and maximum SOC (%) of the hydrogen tank, respectively, SOC_{EES}^y is the SOC (%) of EES at time step t in year y , $SOC_{EES,min}$ and $SOC_{EES,max}$ are the minimum and maximum SOC (%) of the EES, respectively, $SOC_{TES}^y(t)$ is the SOC (%) of TES at time step t in year y , and $SOC_{TES,min}$ and $SOC_{TES,max}$ are the minimum and maximum SOC (%) of the TES, respectively.

Reliability parameters, such as LPSP and SEF, are inserted as optimization constraints in the problem formulation to confirm the energy systems' reliability and resiliency. The lower values of the LPSP and SEF imply better system reliability. The reliability constraints can be presented as follows.

$$LPSP_{elec} \leq LPSP_{elec,max} \quad Eq. 6-28$$

$$LPSP_{ther} \leq LPSP_{ther,max} \quad Eq. 6-29$$

$$SEF_{elec} \leq SEF_{elec,max} \quad Eq. 6-30$$

$$SEF_{ther} \leq SEF_{ther,max} \quad Eq. 6-31$$

Where, $LPSP_{elec,max}$ and $LPSP_{ther,max}$ are the maximum limit of LPSP for electric and thermal demand, respectively, and $SEF_{elec,max}$ and $SEF_{ther,max}$ are the maximum limit of SEF for electric and thermal demand, respectively. The maximum LPSP and the maximum SEF values are set to 5% and 10%, respectively, in the optimization problem. These are the typically acceptable margins of LPSP and SEF for a reliable energy system [119], [121].

In the second portion of the analysis, the equations for total generation by the diesel-fired MEG can be expressed by Eq. (6-32) -(6-35). The other optimization constraints and the decision variables of the diesel-fired MEG are identical to the MMR-based MEG.

$$\begin{aligned} \sum P_{gen}^y(t) = & \sum_{t=1}^{t_{total}} N_{PV} P_{pv}(t) + \sum_{t=1}^{t_{total}} N_{WT} P_w(t) \\ & + \sum_{t=1}^{t_{total}} P_{diesel}(t) + \sum_{t=1}^{t_{total}} P_h(t) + \sum_{t=1}^{t_{total}} P_{bio}(t) \end{aligned} \quad \forall t \in t_{total}, \forall y \quad Eq. 6-32$$

$$\sum T_{gen}^y(t) = \sum_{t=1}^{t_{total}} T_{diesel}(t) + \sum_{t=1}^{t_{total}} T_{bio}(t) \quad \forall t \in t_{total}, \forall y \quad Eq. 6-33$$

$$\begin{aligned} \sum_{t=1}^{t_{total}} P_{diesel}(t) &= \sum_{i=1}^{t_{total}} N_{50}^{diesel} P_{50}^{diesel}(t) + \sum_{i=1}^{t_{total}} N_{30}^{diesel} P_{30}^{diesel}(t) \\ &+ \sum_{i=1}^{t_{total}} N_{20}^{diesel} P_{20}^{diesel}(t) \end{aligned} \quad \forall t \in t_{total} \quad Eq. 6-34$$

$$\begin{aligned} \sum_{t=1}^{t_{total}} T_{diesel}(t) &= \sum_{i=1}^{t_{total}} N_{50}^{diesel} T_{50}^{diesel}(t) + \sum_{i=1}^{t_{total}} N_{30}^{diesel} T_{30}^{diesel}(t) \\ &+ \sum_{i=1}^{t_{total}} N_{20}^{diesel} T_{20}^{diesel}(t) \end{aligned} \quad \forall t \in t_{total} \quad Eq. 6-35$$

Where, N_{50}^{diesel} , N_{30}^{diesel} , and N_{20}^{diesel} are the number of diesel Genesets rated as 50 kW, 30 kW, and 20 kW, sequentially, $P_{50}^{diesel}(t)$, $P_{30}^{diesel}(t)$, and $P_{20}^{diesel}(t)$ are the electric power generation (kW) by 50 kW, 30 kW, and 20 kW generators, respectively, at time step t , and $T_{50}^{diesel}(t)$, $T_{30}^{diesel}(t)$, and $T_{20}^{diesel}(t)$ are the thermal power generation (kW) by 50 kW, 30 kW, and 20 kW generators, sequentially, at time step t .

6.3. Decision Variables

The optimization problem intends to find out the optimal configuration of the three distinct N-R MHESs. The decision variables include the number of PV panels, number of WTs, number of MMRs, size of the hydro plant (kW), number of hydrogen tank, size of EES and TES (kWh), size of E2H and H2E unit (kW), and the efficiency of the required CHP unit (%). The decision variables of the problem can be written as follows.

$$0 \leq N_{PV} \leq N_{PV,max} \quad N_{PV} \in \mathbb{Z} \quad Eq. 6-36$$

$$0 \leq N_{WT} \leq N_{WT,max} \quad N_{WT} \in \mathbb{Z} \quad Eq. 6-37$$

$$0 \leq N_{MMR} \leq N_{MMR,max} \quad N_{MMR} \in \mathbb{Z} \quad Eq. 6-38$$

$$0 \leq N_{Htank} \leq N_{Htank,max} \quad N_{Htank} \in \mathbb{Z} \quad Eq. 6-39$$

$$0 \leq Capacity_{HT} \leq Capacity_{HT,max} \quad Eq. 6-40$$

$$0 \leq Capacity_{EES} \leq Capacity_{EES,max} \quad Eq. 6-41$$

$$0 \leq Capacity_{TES} \leq Capacity_{TES,max} \quad Eq. 6-42$$

$$0 \leq \eta_{CHP(MMR)} \leq \eta_{CHP(MMR),max} \quad Eq. 6-43$$

Where, $N_{PV,max}$, $N_{WT,max}$, $N_{MMR,max}$, and $N_{Htank,max}$ are the maximum limit of the PV panel, WT, MMR, and hydrogen tank, respectively, $Capacity_{HT}$, $Capacity_{EES}$, and $Capacity_{TES}$ are the required capacity of the hydro plant, EES, and TES, respectively, $Capacity_{HT,max}$, $Capacity_{EES,max}$, and $Capacity_{TES,max}$, are the maximum capacity limit of hydro plant, EES, and TES, respectively, $\eta_{CHP(MMR)}$ is the required CHP efficiency of MMR, and $\eta_{CHP(MMR),max}$ is the maximum CHP efficiency of MMR.

The following equations represent the relationship between thermal power generation and CHP unit's efficiency [204].

$$T_i(t) = \left(\frac{P_i(t)}{\eta_i} - P_i(t) \right) \times HRR \quad \forall t \in t_{total} \quad Eq. 6-44$$

$$\forall i \in G$$

$$\eta_{CHP(i)} = (1 - \eta_i) \times HRR \quad \forall i \in G \quad Eq. 6-45$$

Where, $T_i(t)$ is the thermal power generation from i^{th} source (kW), $P_i(t)$ is the electric power generation from i^{th} source (kW), η_i is the thermal-to-electricity generation efficiency (%), and HRR is the heat recovery ratio (HRR) of the CHP unit.

To analyze the second part, it is mandatory to obtain the optimal system configuration. A new variable, the number of diesel Gensets, is introduced in this part instead of the number of MMRs. The rest of the constraints and the decision variables are kept similar to the MMR-based MEG. The decision variables for diesel Genset can be written as follows.

$$0 \leq N_{50}^{diesel} \leq N_{50}^{max} \quad N_{50}^{diesel} \in \mathbb{Z} \quad Eq. 6-46$$

$$0 \leq N_{30}^{diesel} \leq N_{30}^{max} \quad N_{30}^{diesel} \in \mathbb{Z} \quad Eq. 6-47$$

$$0 \leq N_{20}^{diesel} \leq N_{20}^{max} \quad N_{20}^{diesel} \in \mathbb{Z} \quad Eq. 6-48$$

$$0 \leq \eta_{CHP(diesel)}^{50} \leq \eta_{CHP(diesel),max}^{50} \quad \text{Eq. 6-49}$$

$$0 \leq \eta_{CHP(diesel)}^{30} \leq \eta_{CHP(diesel),max}^{30} \quad \text{Eq. 6-50}$$

$$0 \leq \eta_{CHP(diesel)}^{20} \leq \eta_{CHP(diesel),max}^{20} \quad \text{Eq. 6-51}$$

Where, N_{50}^{max} , N_{30}^{max} , and N_{20}^{max} are the maximum limits of the Gensets with a rated capacity of 50 kW, 30 kW, and 20 kW, respectively, $\eta_{CHP(diesel)}^{50}$, $\eta_{CHP(diesel)}^{30}$, and $\eta_{CHP(diesel)}^{20}$ are the required efficiency of the Gensets with a rated capacity of 50 kW, 30 kW, and 20 kW, respectively, and $\eta_{CHP(diesel),max}^{50}$, $\eta_{CHP(diesel),max}^{30}$, and $\eta_{CHP(diesel),max}^{20}$ are the maximum efficiency limits of the CHP units of the 50 kW, 30 kW, and 20 kW Genset, respectively.

6.4. Implementation of Optimization Algorithm (Particle Swarm Optimization)

PSO implementation steps are discussed in detail as follows.

<i>Step 1:</i>	<p>Read the following input data of the N-R MHES planning problem:</p> <ul style="list-style-type: none"> A. Load system demand data (hourly electric and thermal load data) and meteorological data (hourly solar irradiance, ambient temperature, wind speed, stream flow rate for one year). B. Load system equipment's characteristics (e.g., MMR, battery bank, hydrogen storage, and TES). C. Load economic parameters of each system component, such as capital cost, replacement cost, fuel cost, O&M cost, and lifetime.
<i>Step 2:</i>	<p>Initialize all the parameters of PSO and required system components:</p> <ul style="list-style-type: none"> A. Set the maximum number of iterations and population size to 300 and 250, respectively. B. Set the number of individual runs to 100. C. Set the personal acceleration coefficient (c_1) and global acceleration coefficient (c_2).

	<p>D. Set the inertia coefficient (w).</p> <p>E. Set the value of constriction coefficient (K), where</p> $k = 1, C_1 = C_2 = 2.05$ <p>F. Set the constraints as follows:</p> $LPSP \leq 0.05, SEF \leq 0.10$ <p>G. Set the upper bound and lower bound of the decision variables as follows.</p> <ul style="list-style-type: none"> ▪ Upper bound and lower bound of the number of MMR: [10, 0] for Case-01 [05, 0] for Case-02, Case-03 ▪ Upper bound and lower bound of the number of PV panel: [100, 0] ▪ Upper bound and lower bound of the number of WT: [100, 0] ▪ Upper bound and lower bound of HT (kW): [1000.64, 0] ▪ Upper bound and lower bound of MMR CHP efficiency (%): [50, 0] ▪ Upper bound and lower bound of 50 kW, 30 kW, and 20 kW of Gensets: [50, 0] for all types of Genset ▪ Upper bound and lower bound of the number of hydrogen tank: [25, 0] ▪ Upper bound and lower bound of EES (MW): [100, 0] ▪ Upper bound and lower bound of TES (MW): [25, 0] <p>H. Set the initial global best to "<i>infinity</i>."</p> <p>I. Set the position and the velocity randomly to generate the initial population.</p>
<i>Step 3:</i>	Apply the particle positions to find the value of the objective function.
<i>Step 4:</i>	Update the individual best position by comparing it with the other populations.

<i>Step 5:</i>	Compare the personal best with the global best and update the global best value. The particle with the minimum value of the objective function will be selected as the global best.
<i>Step 6:</i>	Update velocities by using Eq. 2-2. Apply the velocity limits.
<i>Step 7:</i>	Update the position of the particles. Apply the upper bound and lower bound limits. Follow <i>Step 3</i> to <i>Step 7</i> until all the particles (the maximum number of particles is specified initially) are evaluated.
<i>Step 8:</i>	Different particles provide a different value of cost function. Store the best cost value.
<i>Step 09:</i>	If the simulation reaches the maximum number of iterations, then stop. Otherwise, update the iteration variable and continue from <i>Step 3</i> to <i>Step 10</i> . If the program is set to run multiple independent runs, it will run up to the specified number of individual runs.

A static penalty function is also introduced with the objective function. Once the constraints are violated, a fixed value (1×10^{15}) will be added to the objective function no matter how much the violations are. Though several penalty functions, such as static penalty functions, dynamic penalty functions, and adaptive penalty functions, are typically utilized in optimization, the simplest and efficient one- static penalty function- is adopted in this study [205].

Chapter 7: Results and Discussions

In this chapter, the simulation results of different proposed nuclear-renewable integrated systems have been presented. The chapter is primarily segmented into two sections. The first section aims to identify the most effective hybridization method based on the techno-economic parameters explained in earlier chapters. The first section discusses the comparison of the proposed three hybridization methods. The second section compares the designated most efficient nuclear-renewable hybridized system and a diesel-fired MEG. The diesel-fired MEG acts as a representative of conventional fossil-fired technologies. The diesel-fired MEG is developed by only replacing MMRs with diesel Gensets for the second part of the analysis.

Prior to conduct the comparative study, the developed optimization algorithm is verified by employing four benchmark functions. The studied benchmark functions are Rosenbrock function, Ackley function, Michalewicz function, and Eggholder function. Table 7-1. represents the equations and bounds of the corresponding test functions. Different dimensions and types (unimodal and multimodal) of the functions are considered for testing the optimization algorithm. Fig. 7-(1:4) show the convergence plots for all the benchmark functions.

Table 7-1: A list of Studied Benchmark Functions

Function Name	Equation	Upper and lower bounds
Rosenbrock function	$f(x) = \sum_{i=1}^{d-1} [100(x_{i+1} - x_i^2)^2 + (x_i - 1)^2]$	[-2.048, 2.048]
Ackley function	$f(x) = -20 \exp\left(-0.2 \sqrt{\frac{1}{d} \sum_{i=1}^d x_i^2}\right) - \exp\left(\frac{1}{d} \sum_{i=1}^d \cos(2\pi x_i)\right) + 20 + \exp(1)$	[-32.768, 32.768]
Michalewicz function	$f(x) = - \sum_{i=1}^d \sin(x_i) \sin^{2m}\left(\frac{ix_i^2}{\pi}\right)$ $m = 10$	[0, π]
Eggholder function	$f(x) = -(x_2 + 47) \sin\left(\sqrt{\left x_2 + \frac{x_1}{2} + 47\right }\right) - x_1 \sin\left(\sqrt{ x_1 - (x_2 + 47) }\right)$	[-512, 512]

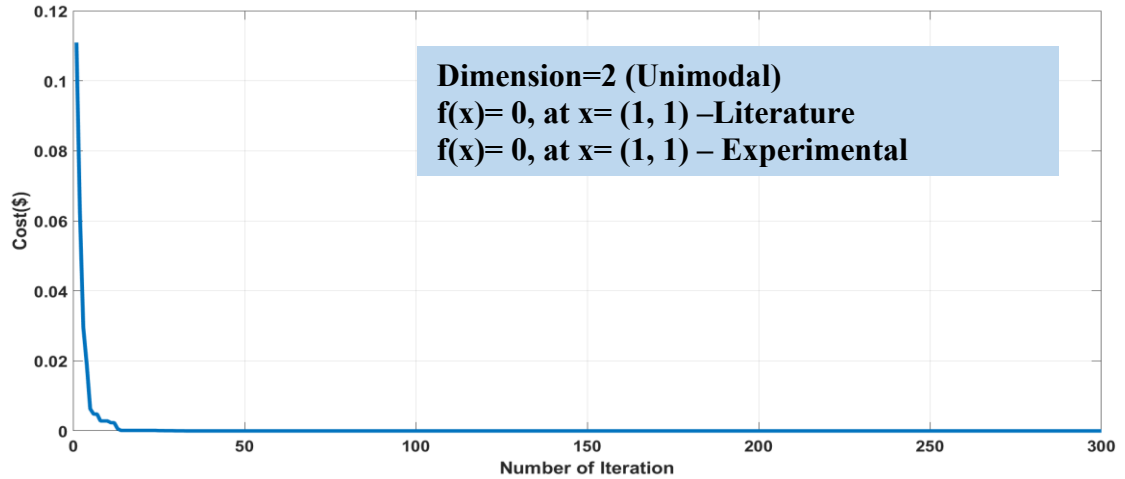


Figure 7-1: Convergence Plot (Rosenbrock Function)

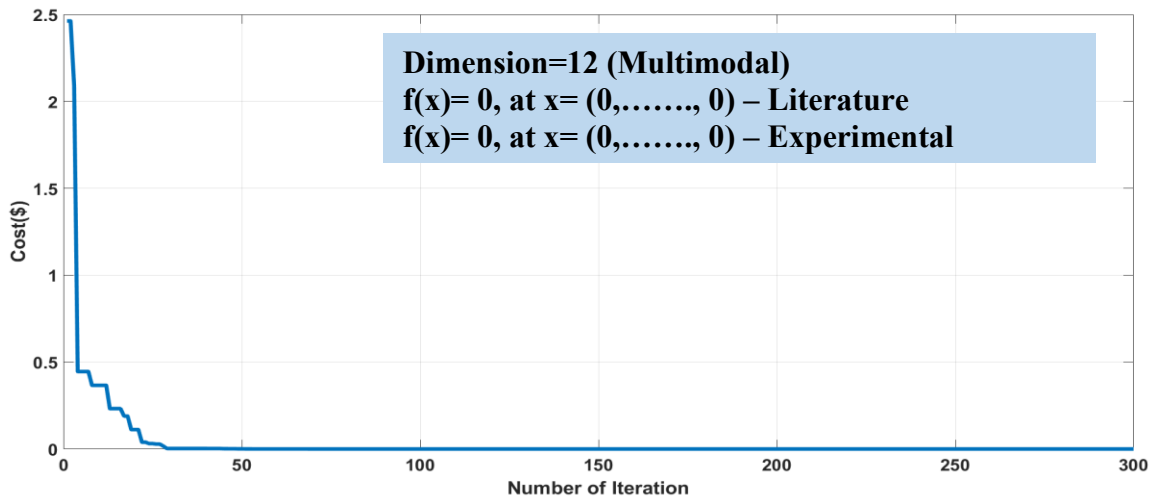


Figure 7-2: Convergence Plot (Ackley Function)

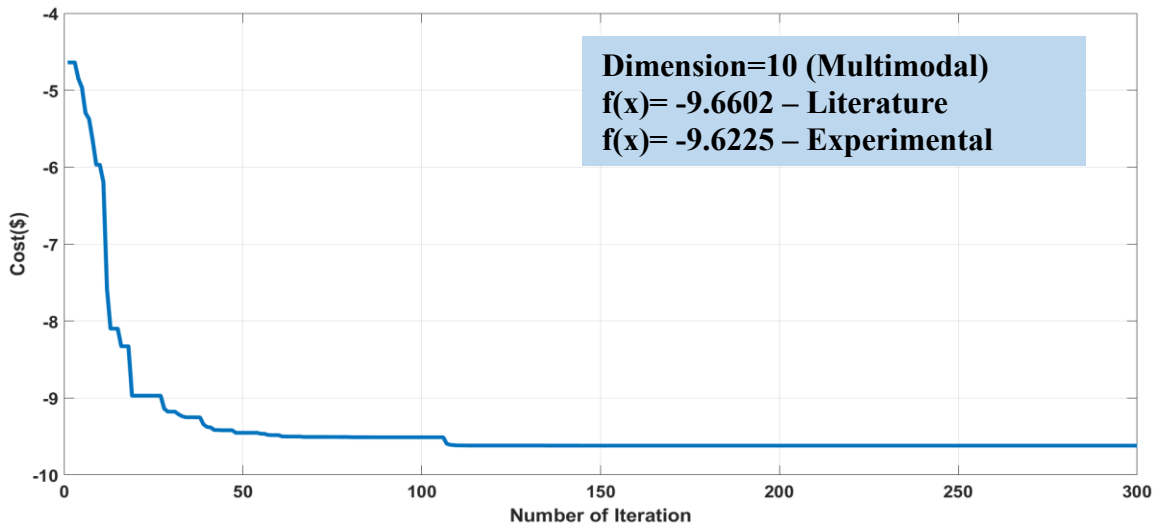


Figure 7-3: Convergence Plot (Michalewicz Function)

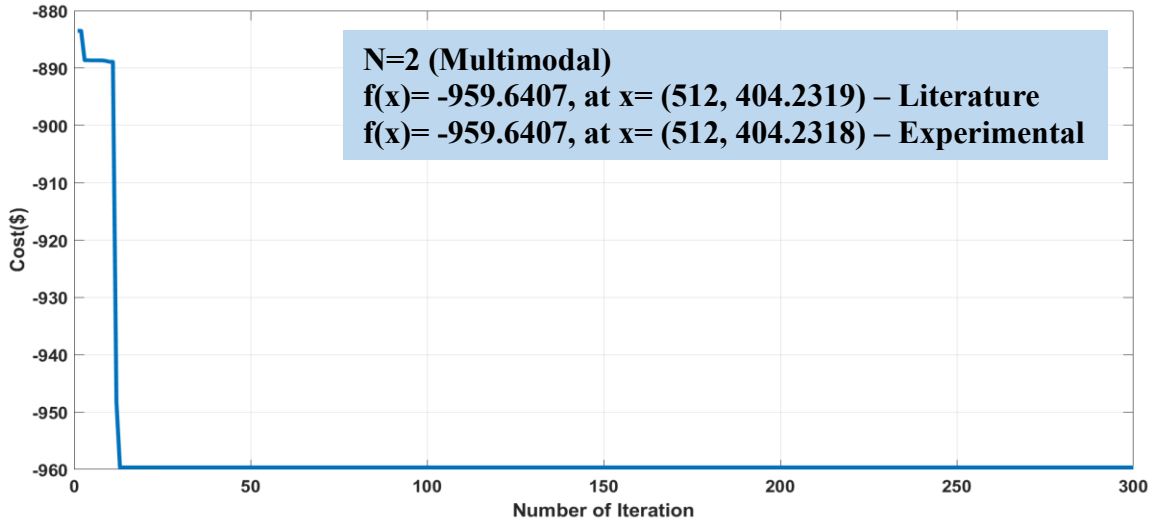


Figure 7-4: Convergence Plot (Eggholder Function)

The results confirm that the expected values are obtained for each case. It certainly verifies that the developed PSO algorithm can identify the optimal results efficiently regardless of the function dimensions and types.

7.1. Comparison between the Proposed Hybridization Methods

An adequate number of population (250) and iterations (300) are considered in the PSO algorithm. The results of PSO assert that the “Multiple Resources and Multiple Products-based coupled N-R MHES (Case-03)” provides the lowest NPC (\$ 201.26 million), while the NPC of “Directly coupled N-R MHES (Case-01)” is the highest (\$ 345.94 million). The “Single Resource and Multiple Products-based coupled N-R MHES” is denoted as “Case-02” in this study. The NPC of the three cases is shown in Fig. 7-5.

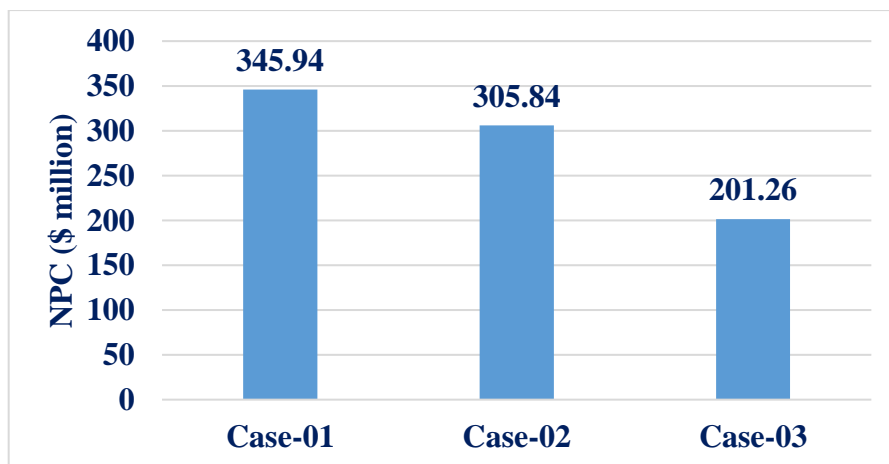


Figure 7-5: Comparison of NPC for the Proposed N-R MHES

Table 7-2 records the details of the optimal configuration of three N-R MHESs. Case-03 includes the least number of MMRs since renewable generation is available in this case. A maximum number (100) of solar PV panels and WTs are utilized in Case-01 since the availability of solar irradiance at the project location is reasonable. Case-02 and Case-03 disregard the EES in the system architecture as the hydrogen storage is sufficient to manage the system demand. The PSO algorithm does not suggest including any E2H and H2E units in any of the system configurations.

Although Case-02 comprises five MMR units in the system, the PSO optimization suggests running one unit at 32% of its rated power; this is one vital drawback of the stand-alone MMR-based energy system (Case-02). If all the five units operate at maximum capacity, the *SEF* will be larger than the defined boundary, and the reliability constraint will be violated. This situation may also include large-scale energy storage systems to store the excess generation with an additional storage cost. Load-following MMRs may overcome the sizing problem of energy storage systems in this case, but the NPC will still be high due to MMRs' substantial capital cost. On the other hand, if four MMR units have been incorporated within the system, the *LPSP* will be higher than the specified limit. Thus, the reliability constraint will also be violated. Since it is required to determine an integer number of MMR units, the PSO selects five MMR units; one of them will run less than its rated capacity. As a significant fraction of MMR total deployment cost is related to sunk cost, the NPC will be roughly comparable whether one of the MMR units runs at 32% of its rated capacity or operates at its full capacity. Therefore, the operation of Case-02 is not a profitable investment, and it is challenging for variable energy demand. It should be noted that MMR units run at the nominal capacity for Case-01 and Case-03.

Table 7-2: Optimal Configuration of different Proposed N-R MHES

Cases	Direct coupling (Case-01)	Single resource and multiple products-based coupling (Case-02)	Multiple resources and multiple products-based coupling (Case-03)
Number of particles	250	250	250
Number of iterations	300	300	300
Number of MMR	5	5	3
Number of PV panels	100	N/A	95
Number of WT	100	N/A	38
HT capacity (kW)	1000.64	N/A	1000.64
Required efficiency of CHP unit (%)	N/A	16.8	24.6
Number of hydrogen tank	25	22	23
EES capacity (MWh)	12.85	0	0
TES capacity (MWh)	N/A	19.90	19.90
BG capacity (kW)	65.10	65.10	65.10
E2H unit capacity (kW)	0	0	0
H2E unit capacity (kW)	N/A	0	0

Table 7-3 presents the KPIs considered in the study. No separate $LPSP$ s, e.g., $LPSP_{elec}$ and $LPSP_{ther}$, are calculated for Case-01 since electric and thermal demand are fulfilled simultaneously by utilizing only electric power. Case-01 considers the electrical demand and the thermal demand as a single entity. The maximum allowable limits of $LPSP$ and SEF are 5% and 10% in the optimization problem. Literature reviews found the specified limits of $LPSP$ and SEF . If HESs have the $LPSP$ and SEF within the defined limits, the system is considered as reliable and resilient. All the system arrangements, recorded in Table 7-3, have the values of $LPSP$ and SEF within the defined limits, signifying the reliability for all cases. However, electric $LPSP$ and SEF of Case-03 are the lowest (4.36% and 1.42%, respectively), referring to the most reliable system. If the GRF is higher than 100% and as much as close to 100%, the system is considered as reliable in terms of GRF . Therefore, Case-03 is also identified as the most reliable system in terms of GRF (GRF_{elec} and GRF_{ther} are 115.31% and 108.71%, respectively). However, Case-02 shows the same thermal GRF as Case-03. The higher value of LA shows better resiliency and operability of the system. Hence, Case-02 (87.85) and Case-03 (76.39) indicates the highest resiliency in terms of electric and thermal LA , respectively.

Table 7-3: KPIs of different Proposed N-R MHESs

Parameters	Directly Coupled System (Case-01)	Single Resource and Multiple Products-based Coupled System (Case-02)	Multiple Resources and Multiple Products-based Coupled System (Case-03)
$LPSP_{elec}$ (%)	5	5	4.36
$LPSP_{ther}$ (%)		5	5
SEF_{elec} (%)	7.16	3.45	1.42
SEF_{ther} (%)		10	10
GRF_{elec} (%)	119.04	118.48	115.31
GRF_{ther} (%)		108.71	108.71
LA_{elec} (%)	87.50	87.85	86.11
LA_{ther} (%)		73.26	76.39
$LCOE$ (\$/kWh)	0.5071	0.4483	0.2950

Fig. 7-6 presents the PSO convergence plot of Case-01 for the best solution. The swarms reach the optimal value with the progression of the iteration number. The best solution is obtained by 100 independent runs of the PSO program. PSO is a natural-inspired optimization algorithm, and the problem contains several constraints. Thus, the PSO shows slightly different values in each run. Therefore, it is imperative to run the PSO program multiple times and identify the best results from the various runs. One hundred individual runs are a reasonable approximation to get a satisfactory solution.

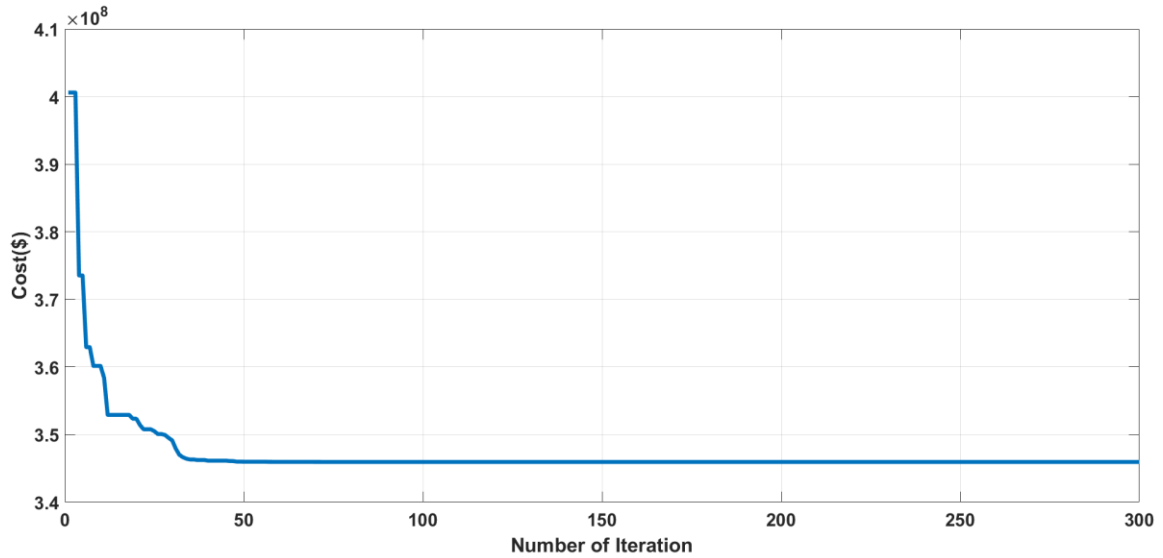


Figure 7-6: Convergence Plot (Case-01)

Fig. 7-7 represents the total energy generation and consumption scenario of Case-01. The figure shows that energy production, along with the support of the energy storage systems, is following the demand. However, there will be a small deficit or excess power within the system due to the allowable *LPSP* and *SEF* limits. Fig. 7-8 depicts the charging and discharging mechanism of the energy storage systems based on the defined energy management algorithm in the earlier chapter. TES is absent in Case-01 since thermal energy production is not possible in this case.

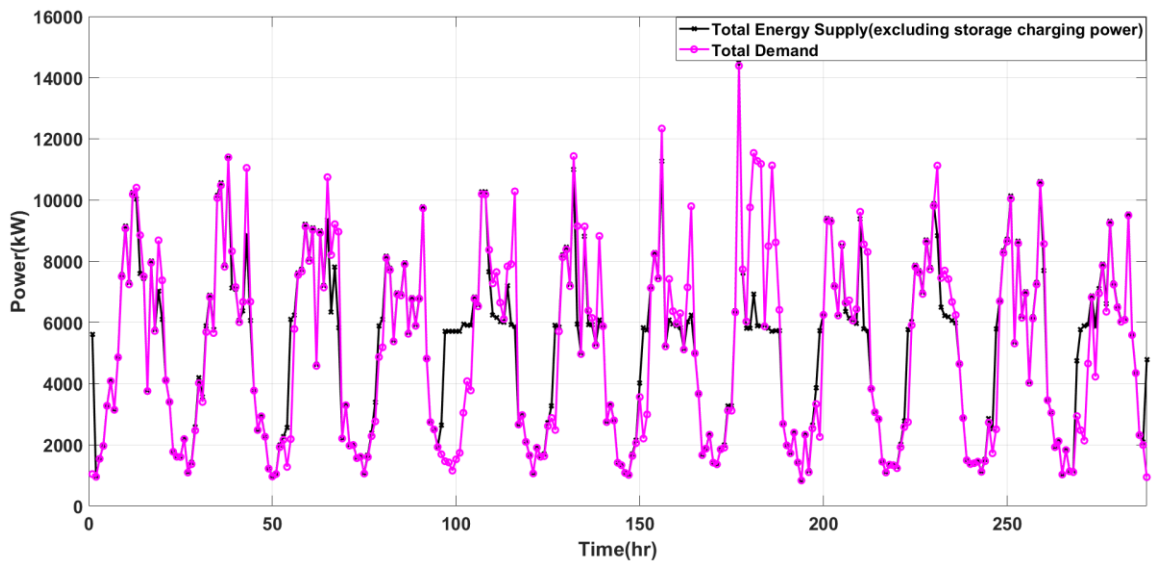


Figure 7-7: Total Energy Generation and Consumption Scenario (Case-01)

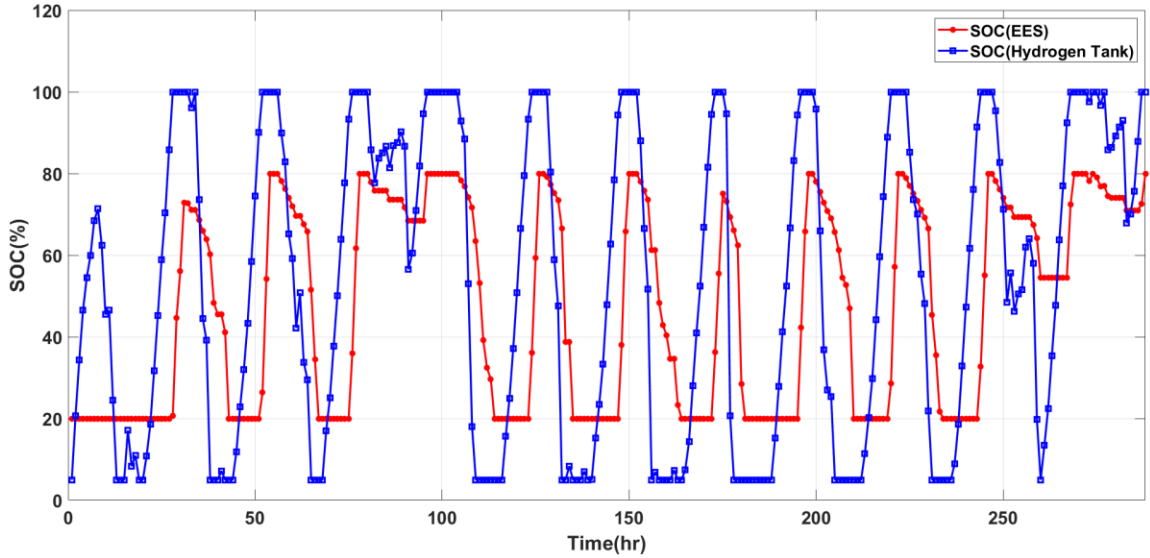


Figure 7-8: Energy Storage Operation (Case-01)

Fig. 7-9 shows the PSO convergence plot of the best run for Case-02. The particles move towards the optimal value very quickly. The multiple independent runs produce almost the same fitness value at each run. Fig. 7-10 represents the total electric power generation and consumption scenario of Case-02. The electrolyzers, hydrogen tanks, and FCs contribute to follow the variable electrical demand based on the energy management algorithm identified in Chapter-04. Fig. 7-11 illustrates the thermal power generation and consumption scenario. The TES always supports to meet the thermal demand by absorbing the excess thermal energy and delivering the required thermal power. The electric generation and the thermal generation have surplus and deficit power due to the permissible limits of *LPSP* and *SEF* constraints. Fig. 7-12 illustrates the charging and discharging scheme of the hydrogen tanks and TES.

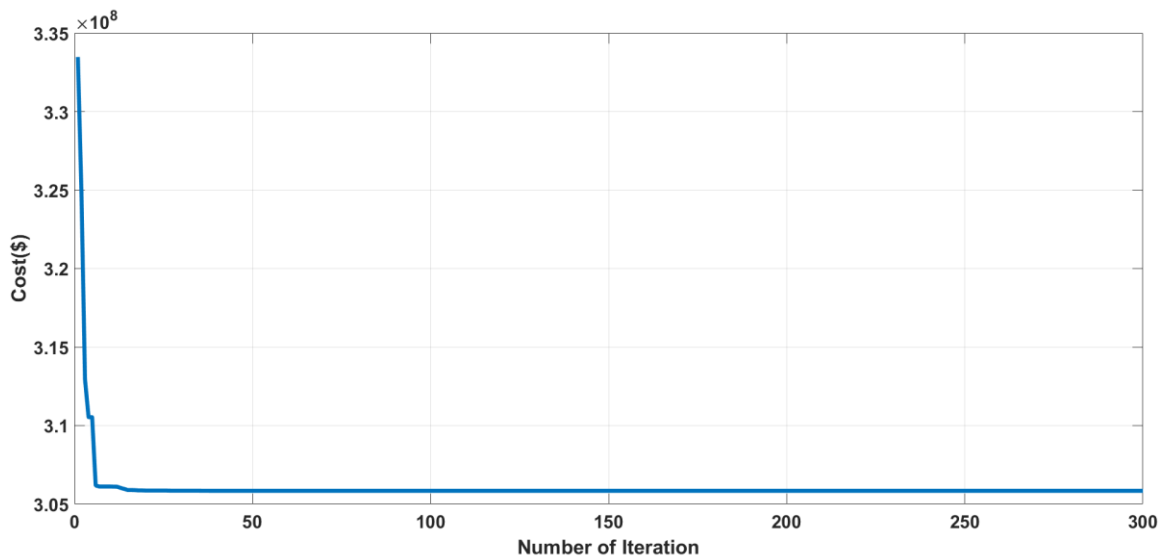


Figure 7-9: Convergence Plot (Case-02)

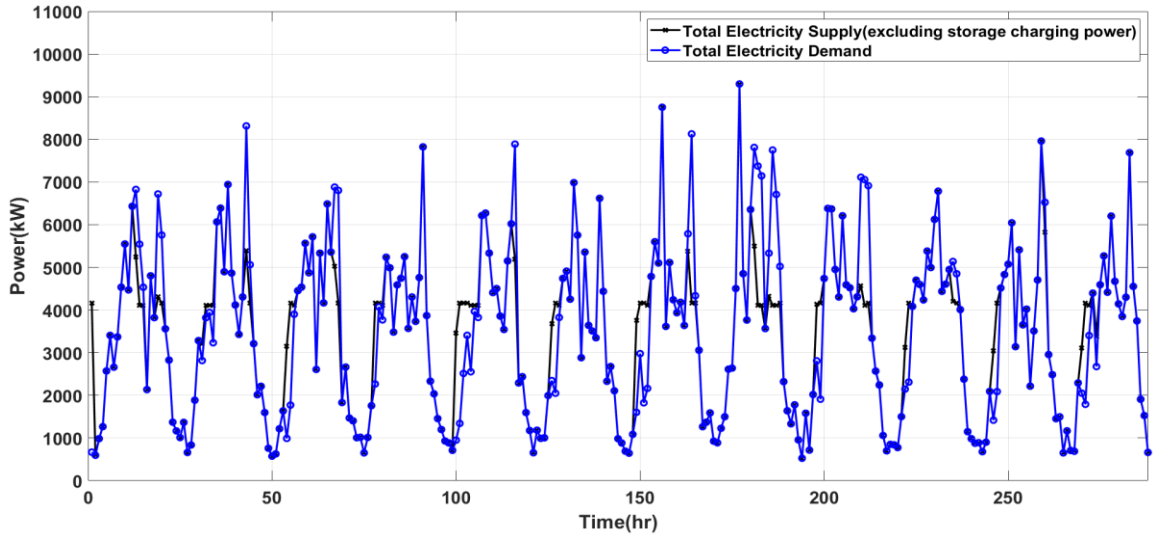


Figure 7-10: Total Electric Energy Generation and Consumption Scenario (Case-02)

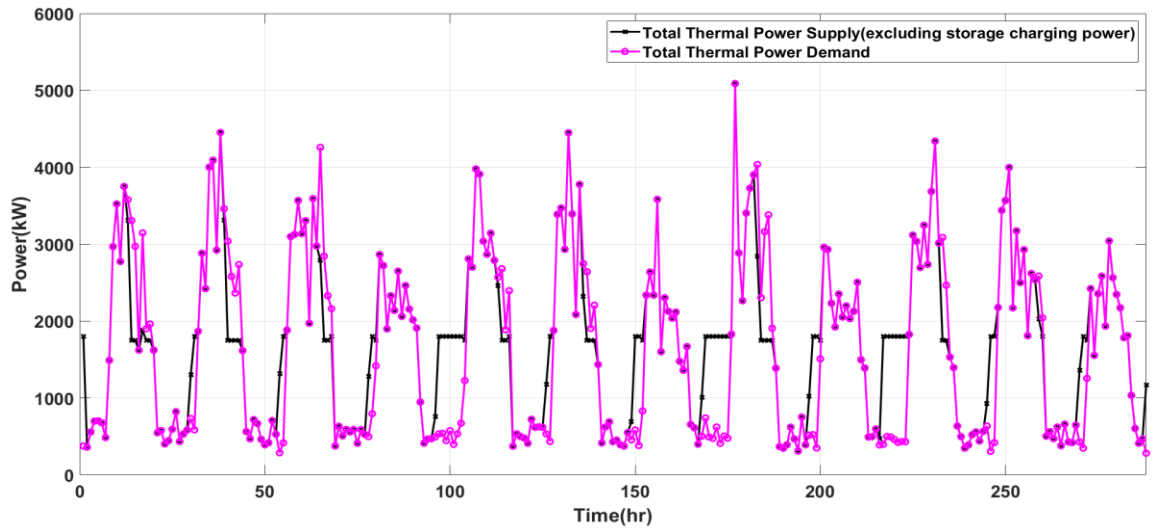


Figure 7-11: Total Thermal Energy Generation and Consumption Scenario (Case-02)

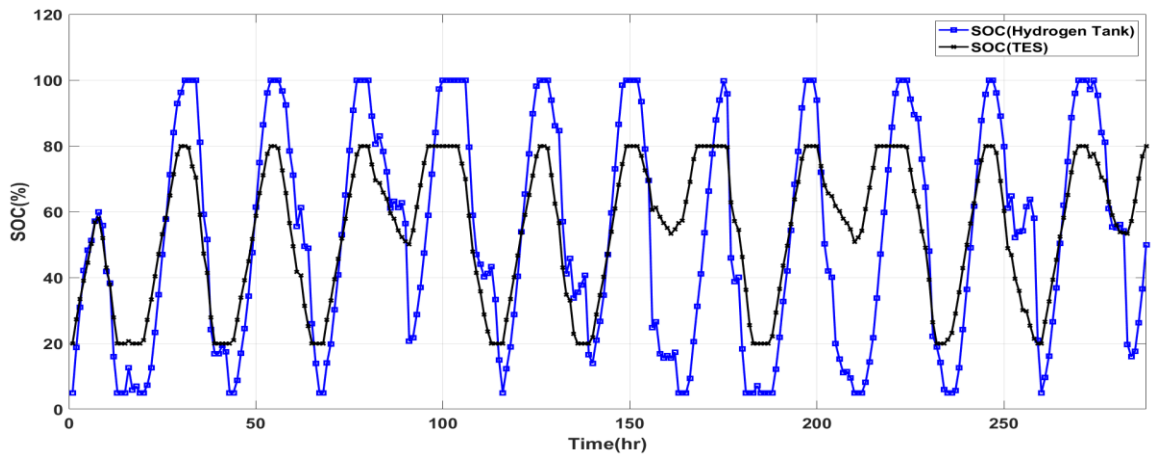


Figure 7-12: Energy Storage Operation (Case-02)

Fig. 7-13 illustrates the PSO convergence plot for Case-03. The particles are able to find the optimal NPC efficiently with less number of iterations. Similar to Case-02, Fig. 7-14 and Fig. 7-15 represent the electric and thermal power generation and consumption processes, respectively. Both the figures show that the production, along with the energy storage systems, is almost always achieving the system demand. Fig. 7-16 illustrates the charging and the discharging scheme of the hydrogen tanks and TES. The energy storage systems always accompany the demand by maintaining the minimum and maximum SOC of the storage.

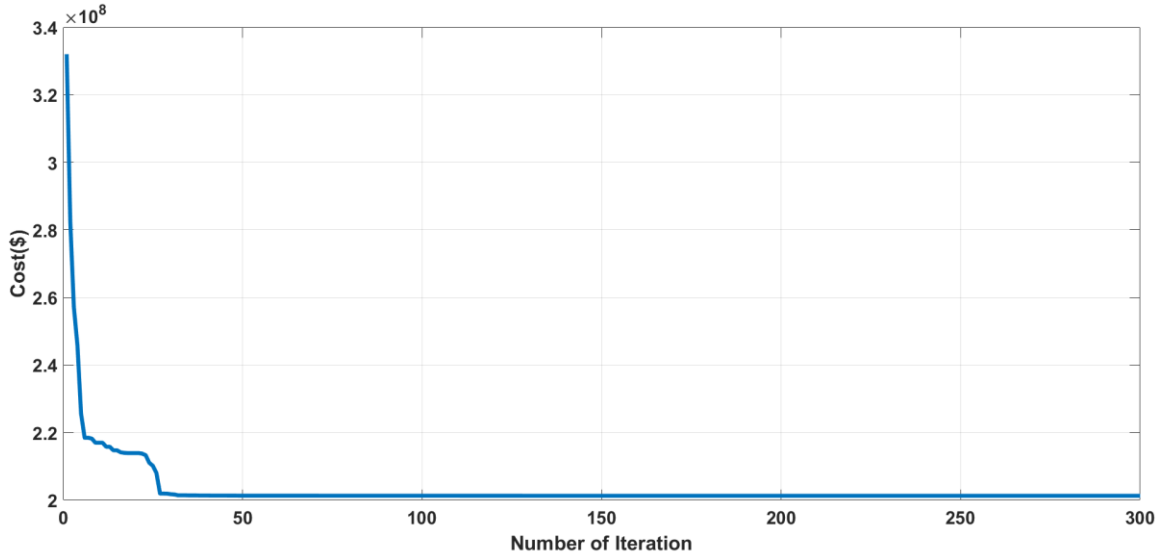


Figure 7-13: Convergence Plot (Case-03)

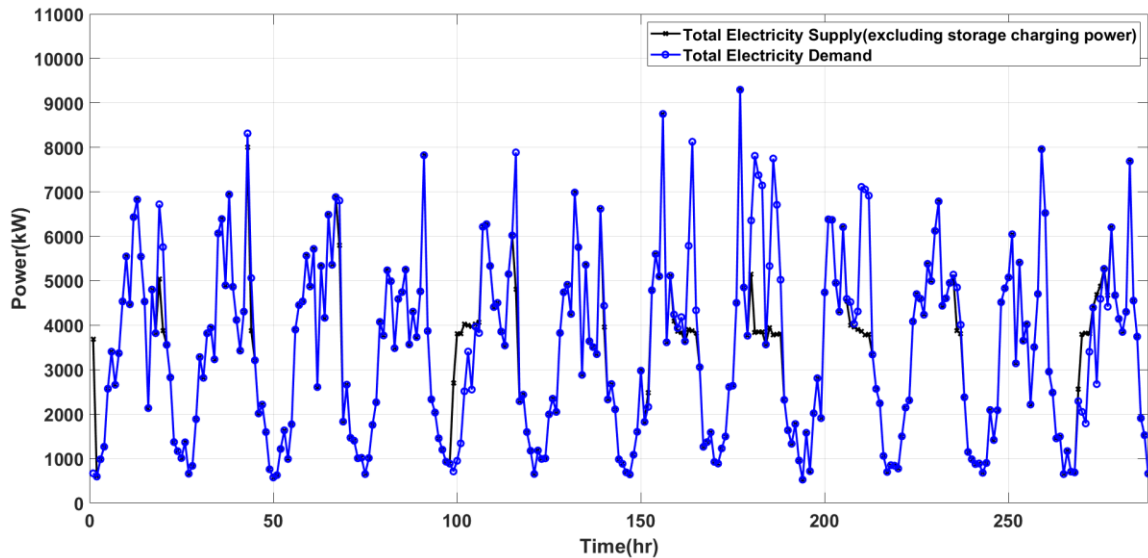


Figure 7-14: Total Electric Energy Generation and Consumption Scenario (Case-03)

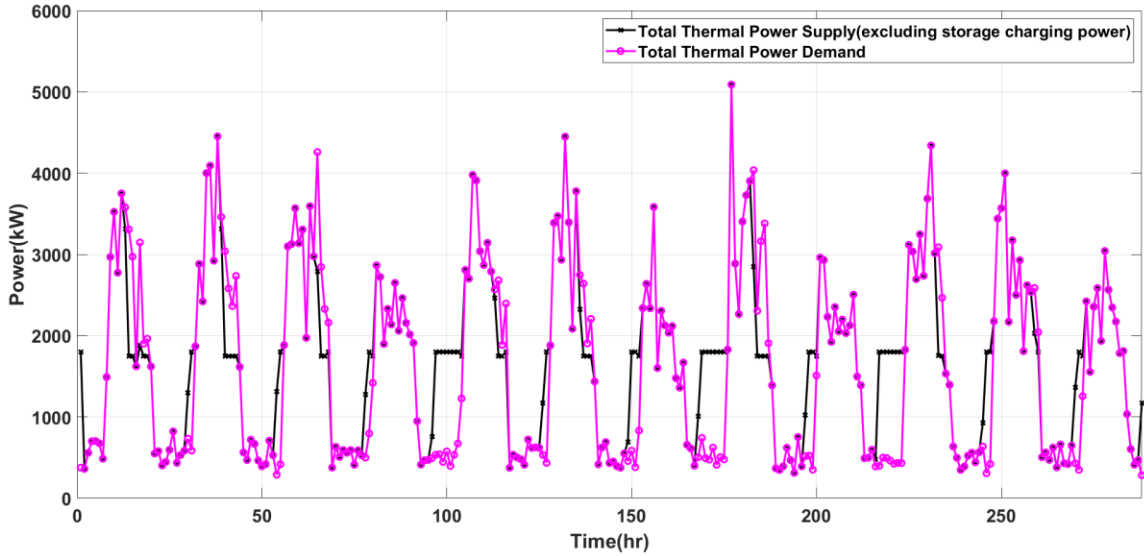


Figure 7-15: Total Thermal Energy Generation and Consumption Scenario (Case-03)

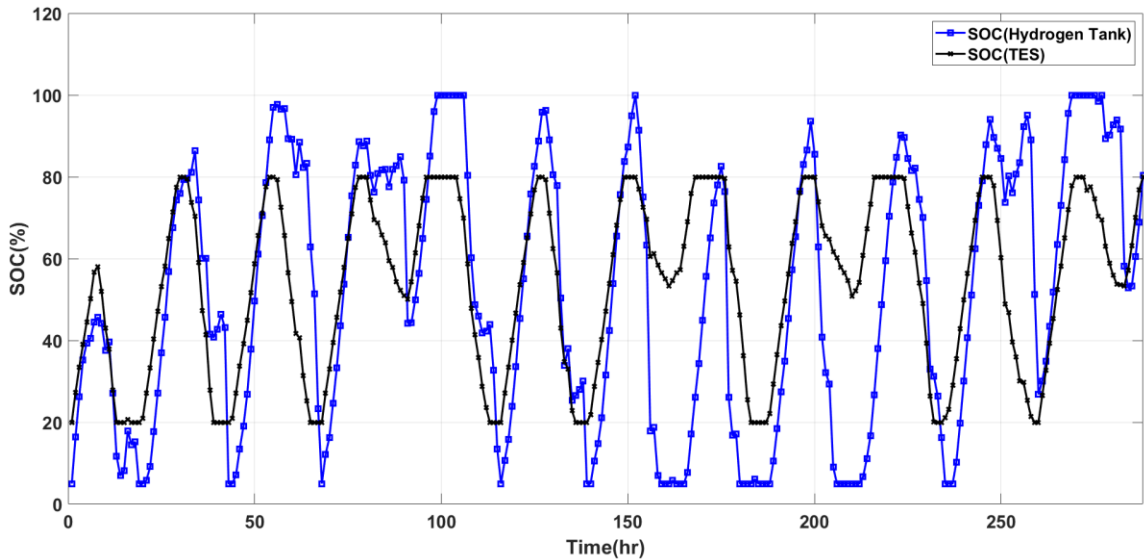


Figure 7-16: Energy Storage Operation (Case-03)

Before going to further analysis, it is necessary to establish the energy management algorithm proposed for different hybridization techniques. To do so, one new set of electric and thermal load data have been collected and utilized. Fig. 7-17 and Fig. 7-18 illustrate the new electric and thermal demand profile.

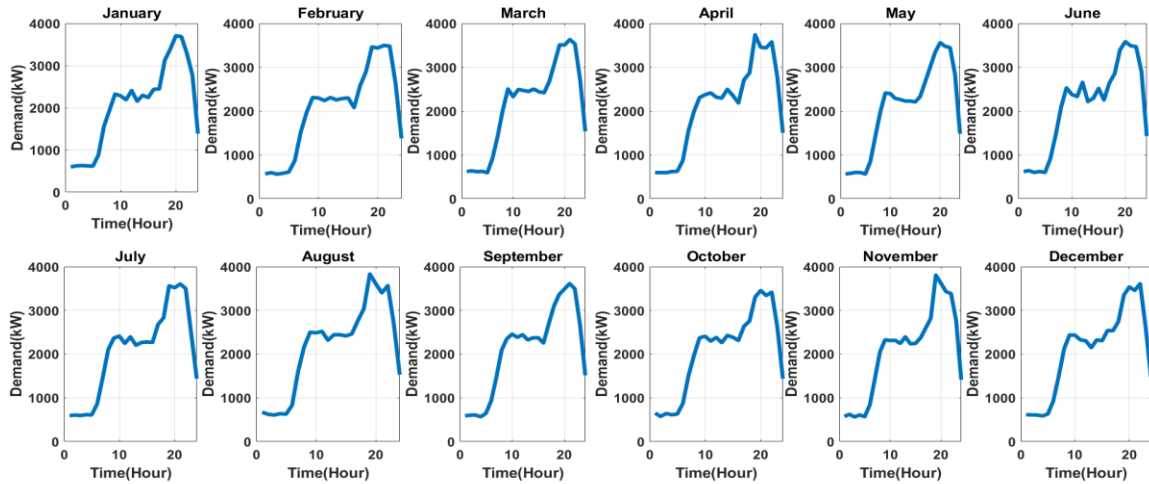


Figure 7-17: Electric Load Profile (for energy management algorithm verification)

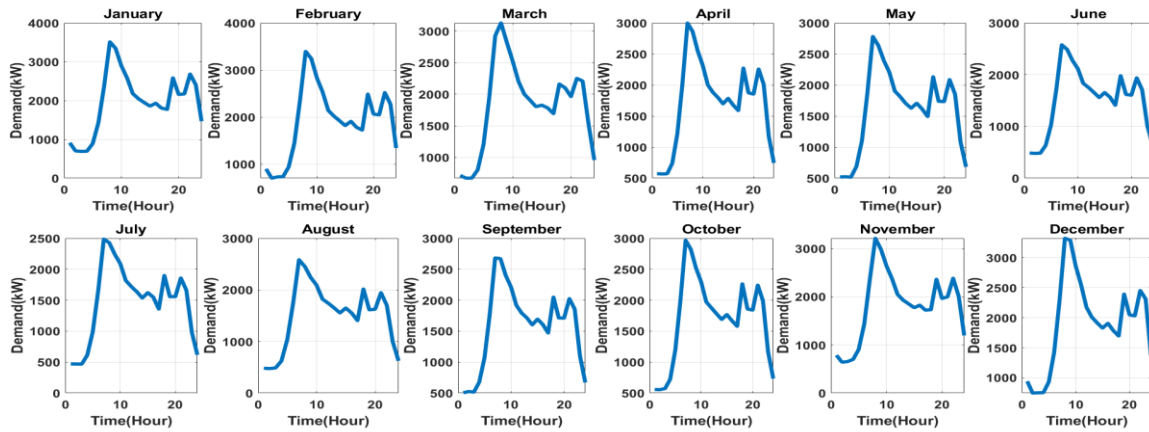


Figure 7-18: Thermal Load Profile (for energy management algorithm verification)

Since the demand profile is changed, the optimization algorithm will find a new set of decision variables for each hybridization technique. The new sets of decision variables are utilized to verify whether the energy supply is accomplishing the system demand or not. Fig. 7-19 shows that the total energy supply fulfills the total system demand effectively with a tolerable margin of reliability. It validates the proposed energy management algorithm for Case-01. Similarly, Fig. 7-(20:21) and Fig. 7-(22:23) depict the energy supply capability of the energy management algorithm proposed for Case-02 and Case-03. The system supply always achieves the electric and the thermal demand with an acceptable reliability limit. This part of analysis also shows that Case-03 has the lowest NPC value.

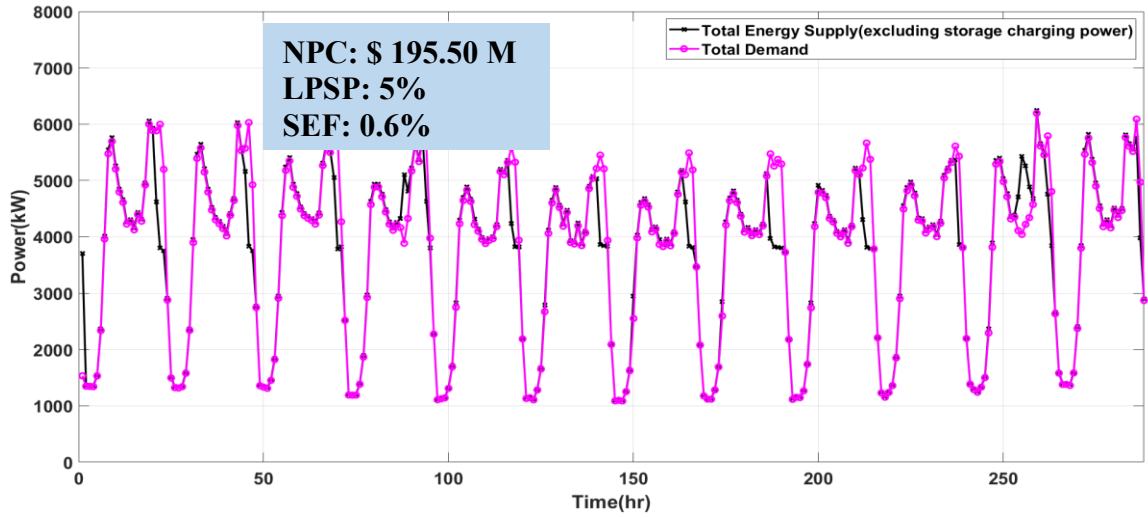


Figure 7-19: Energy Management Algorithm Verification (Case-01)

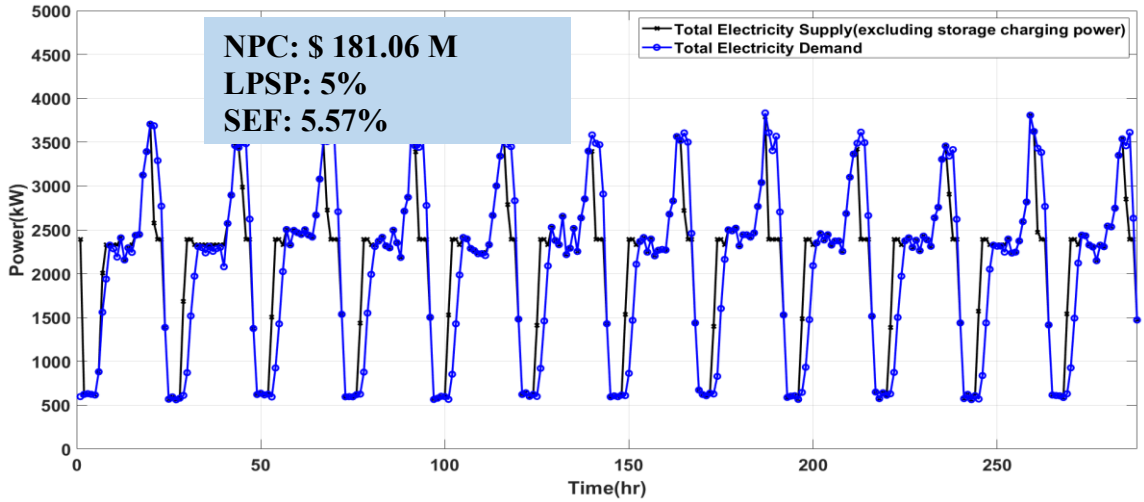


Figure 7-20: Electric Energy Management Algorithm Verification (Case-02)

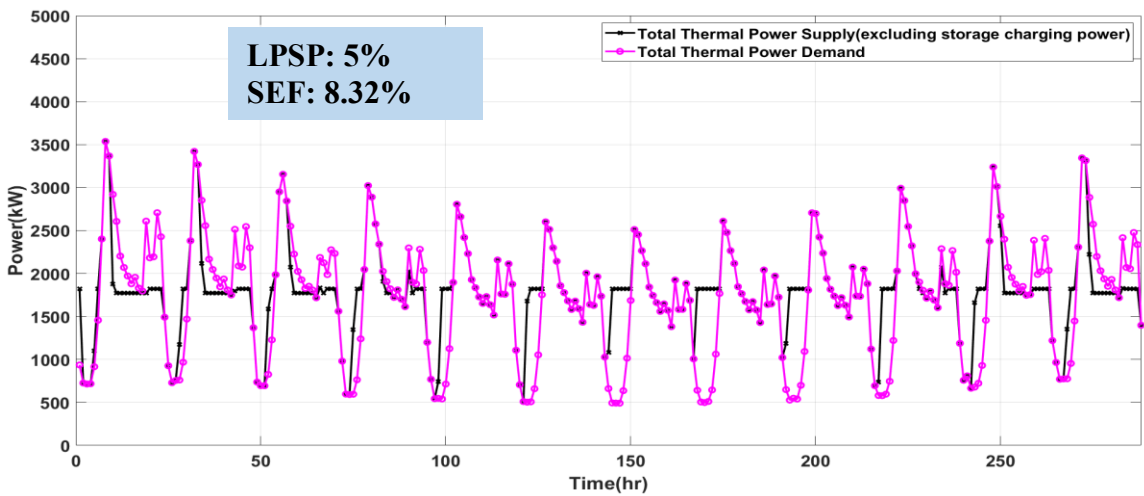


Figure 7-21: Thermal Energy Management Algorithm Verification (Case-02)

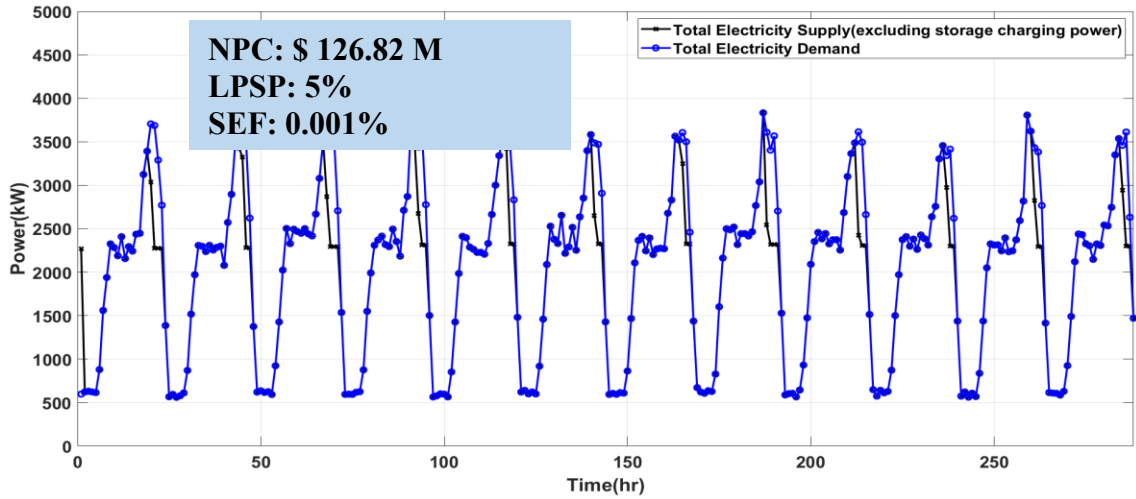


Figure 7-22: Electric Energy Management Algorithm Verification (Case-03)

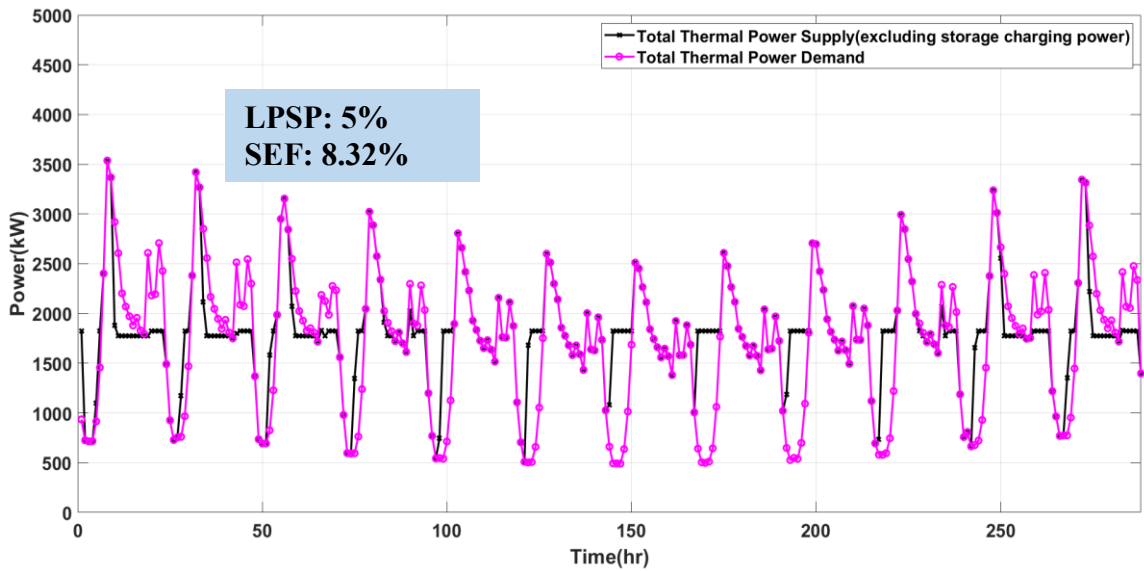


Figure 7-23: Thermal Energy Management Algorithm Verification (Case-03)

Since a nuclear-renewable integrated system's performance depends on several variables, the later sub-sections discuss system performance sensitivity to different parameters. The sensitivity analysis validates the outcomes obtained from the base case analysis. The sensitivity analysis also investigates the impact of various parameters on system economic, reliability, and resiliency. A sensitivity assessment is crucial for a system modeler to model, analyze, and develop the system infrastructure. The most influential parameters are identified in the sensitivity analysis. It helps the research community for future research and development. Several system variables are selected for the sensitivity assessment and presented in later sub-sections. Table 7-4 summarizes the main concepts of the sensitivity analysis conducted in this section.

Table 7-4: A Summary of the Sensitivity Analysis Conducted in Section 7.1

Sub-Section	Summary
7.1.1	This part evaluates the sensitivity of the variation in daily peak demand to NPC.
7.1.2	The sub-section assesses the sensitivity of the variation in annual peak demand to NPC.
7.1.3	This portion of the analysis explores the impact of average demand changes on system NPC.
7.1.4	The sub-section assesses and identifies the influence of different equipment cost on NPC.
7.1.5	This sub-section determines the impact of system economic parameters, such as discount rate, inflation rate, and project lifetime, on NPC.
7.1.6	This part evaluates the impact of the MMR capacity factor on system configuration and system NPC.

7.1.1. Assessment of Sensitivity to Shifting of Daily Peak Demand

Though the peak occurs (both electric and thermal demand) at mid-day in the base cases, it is also reasonable that the peak may occur at the beginning or end of the day. The peak demand for any load depends on the types of load and the project location. Usually, wind speed does not reach zero-level at night, while there will be no solar irradiance at night. Hence, alterations in peak demand cause inclusion or reduction of generation sources depending on geographical regions and the level of system demand. Therefore, a sensitivity analysis has been conducted in this sub-section by shifting the peak demand (both electric and thermal demand) by 12 hours. Fig. 7-24 and Fig. 7-25 depict the shifted peak scenarios of the electrical and the thermal demand, respectively.

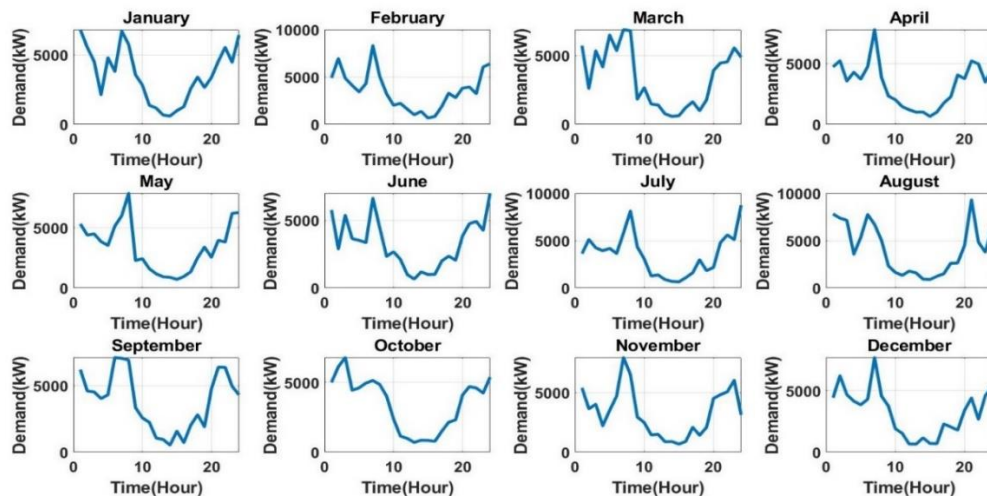


Figure 7-24: Shifted Electric Peak Demand (daily)

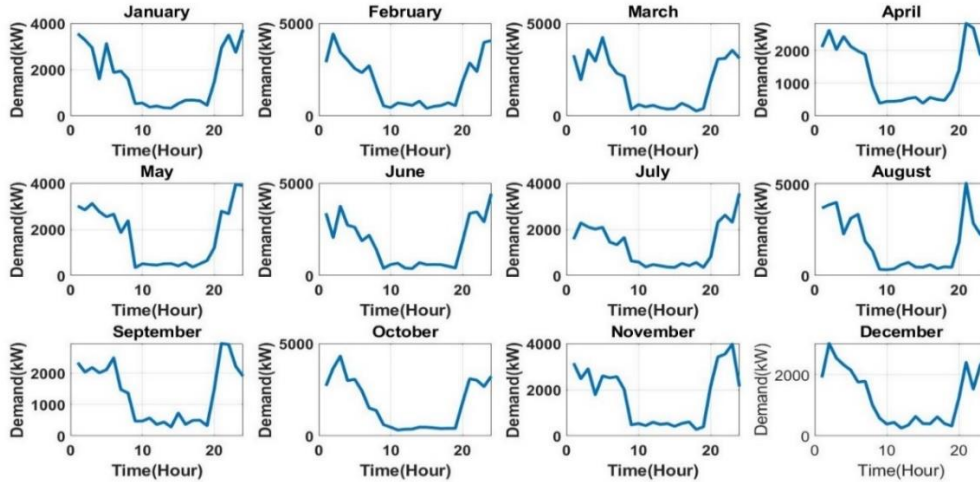


Figure 7-25: Shifted Thermal Peak Demand (daily)

Fig. 7-26 represents the differences in the NPC of three nuclear-renewable hybridized systems due to variation in system peak. The system peak variation analysis is divided into three parts: variation in electric load, variation in thermal load, and variation in both electrical and thermal load. From all the cases of system peak variation, Case-03 provides the lowest system NPC. Since Case-01 and Case-03 include renewables and the demand profile is changing, the NPC will change due to the inclusion or reduction of different generation sources. Therefore, the NPC of Case-01 and Case-03 are varied in Fig. 7-26 compared to the base case NPC mention in Fig. 7-5. The PSO recommends to include four MMR units for Case-02 in electric peak demand variation and thermal peak demand variation. But the PSO includes five microreactors in Case-02 for variation in both electric and thermal demand, while one of the units will run at 27 % of its rated capacity. Conversely, MMR capacity is always fully utilized in Case-01 and Case-03. The hydrogen storage, EES, and TES cost are mainly accountable for the changes in NPC for Case-02 since the sizing of the storage systems changes with the variation in demand. The reliability parameters are regarded as optimization constraints, and the system resiliency is maintained in all cases.

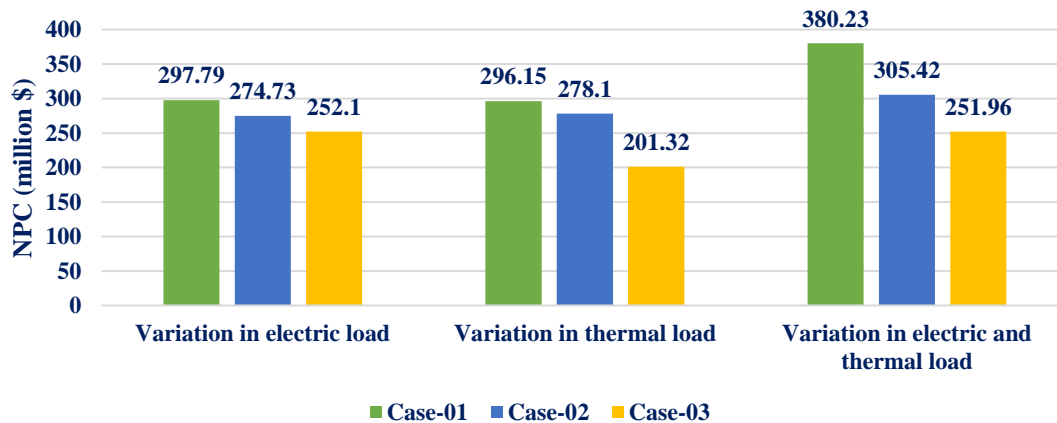


Figure 7-26: Impact of Variation in Daily Peak Demand

7.1.2. Assessment of Sensitivity to Shifting of Seasonal Demand

In the base case analysis, the electric and the thermal annual peak occurs nearby the month of July-August. The seasonal peak demand also depends on the type of load and applications. Hence, the seasonal peak demand is shifted by six months in this sub-section, implying that the annual peak will occur at the starting of the year (around January) in the shifted load demand. Fig. 7-27 and Fig. 7-28 present the electric and the thermal seasonal shifted load profiles, respectively.

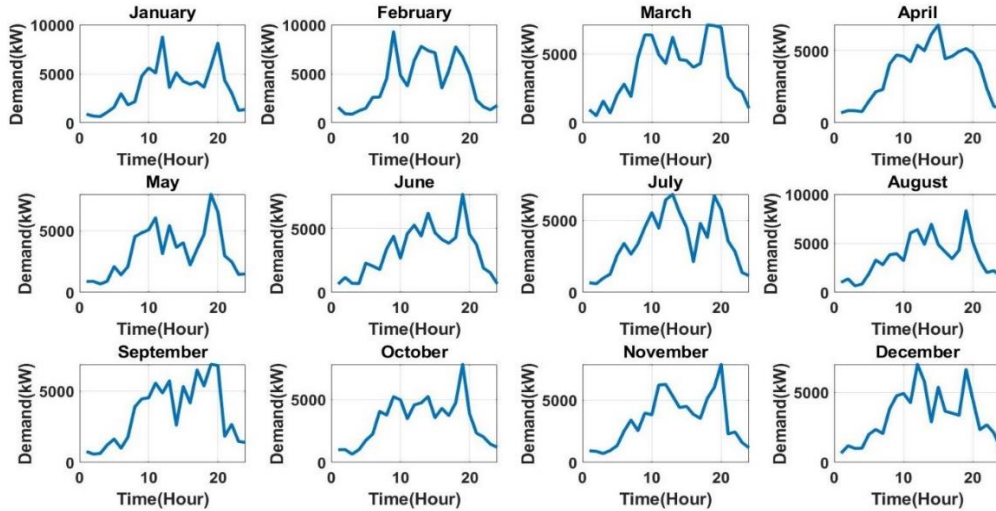


Figure 7-27: Shifted Electric Peak Demand (seasonal)

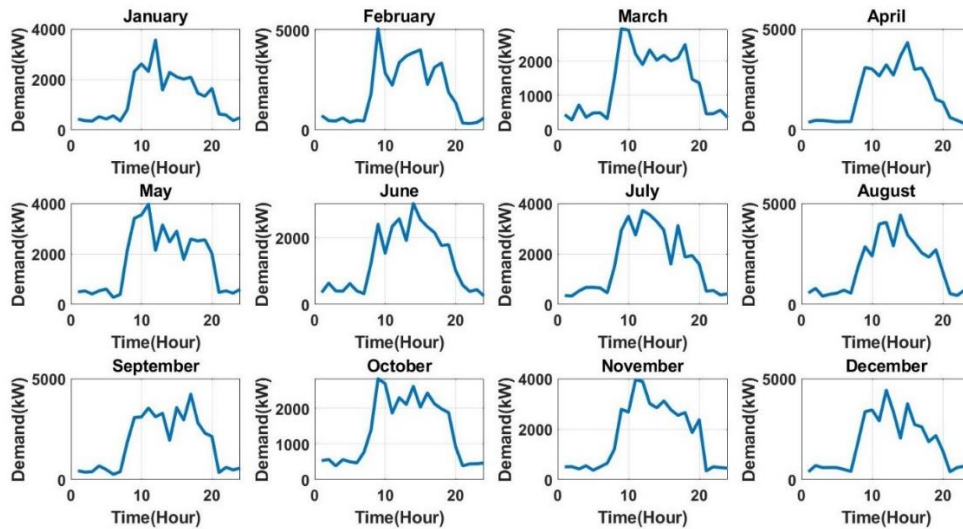


Figure 7-28: Shifted Thermal Peak Demand (seasonal)

Similar to sub-section 7.1.1, this sub-section also divides the sensitivity analysis into three parts. The simulation results also reveal the lowest NPC for Case-03 and the highest NPC for the Case-01 in all sections. Fig. 7-29 summarizes the sensitivity assessment results due to annual peak demand variation. The seasonal peak variation does not affect the NPC of

Case-02 and Case-03. Therefore, the NPC for Case-02 and Case-03 presented in Fig. 7-29 is almost similar to the base case. The seasonal peak variation affects Case-01 since the electric and the thermal load are viewed as a single demand in Case-01; any differences either in electrical demand or thermal demand alter the NPC.

As the Case-02 consists of nuclear and BG, the system peak (daily and yearly) variations can not affect the optimal system configuration and the NPC significantly. PSO includes five MMR units in all types of peak variation in Fig. 7-29 (Case-02). PSO also recommends running one of the MMR units to run at 30%-32% of its maximum capacity for Case-02. The sizing of TES almost remains the same in this sensitivity analysis of all scenarios for Case-02. Thus, the NPC for Case-02 is the same for the seasonal electric demand peak variation, seasonal thermal peak variation, or both. On the other hand, since Case-01 and Case-03 include a considerable number of renewables, seasonal peak variation affects the optimal system architecture and the NPC, as shown in Fig. 7-29.

It should be mentioned that there is a positive co-relationship between typical system demand and availability of renewables, e.g., solar irradiance and wind speed. It indicates that solar irradiance, wind speed, and peak demand usually reach the maximum at the same time, mid-day, in a day. Therefore, daily peak variations impact more severely than seasonal peak variations, as presented in Fig. 7-26 and Fig. 7-29.

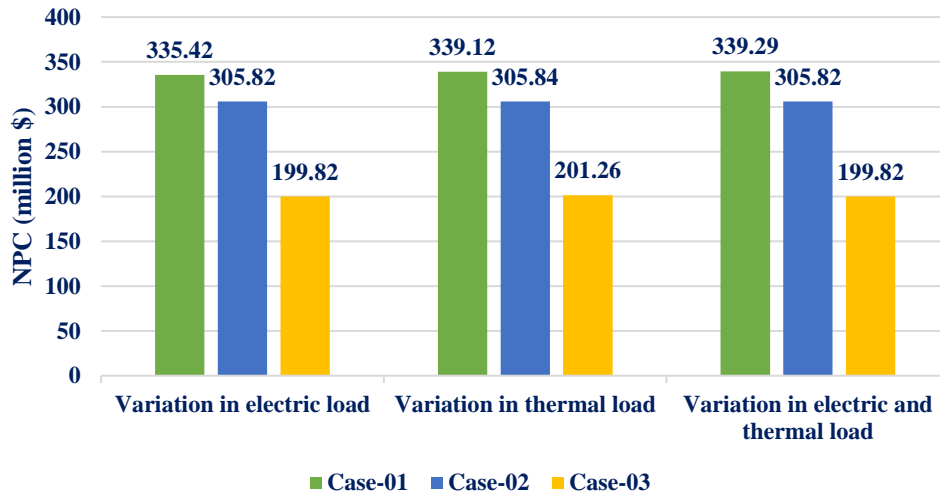


Figure 7-29: Impact of Variation in Seasonal Peak Demand

7.1.3. Assessment of Sensitivity to Variation in Average Energy Demand

Electric and thermal average demand may rise or decrease by a certain percentage at any time or throughout a particular duration. Therefore, a sensitivity analysis is carried out in this sub-section by increasing and decreasing the electric and thermal average demand by 10%.

Fig. 7-30, Fig 7-31, and Fig. 7-32 represent NPC diversity due to changes in the average electric demand, the average thermal demand, and both electrical and thermal average demand, respectively, by $\pm 10\%$. The results show that Case-03 provides the most economical NPC despite increasing or decreasing the electric and the thermal demand by a certain amount. The results also imply that the directly coupled system (Case-01) has the highest NPC for all cases. Fig. 7-30 tells that the NPC of all cases increases proportionately with the increase in electric demand. The augmentation of electrical demand adds more generation components or storage, which ultimately increase the NPC. However, the extension of electric demand does not always affect the NPC of Case-02 evenly. The scenario (Case-02), where the electrical demand is decreased by 10%, comprises four MMR units running at full capacity. On the contrary, the base case and the 10% increase in electric demand (Case-02) include five MMR units. For the base case, one of the MMR units runs at 32% of its nominal capacity. For the 10% increase of electric demand, one of the MMRs operates at 76% of its rated power, and PSO includes more hydrogen storage in this case. Hence, the NPC (\$ 308.18 million) increases due to the inclusion of additional hydrogen storage systems. The sizing of the TES remains the same as the base case.

As illustrated in Fig. 7-31, the thermal demand variation does not significantly affect Case-02 and Case-03 due to MMR's CHP unit. The CHP unit has no additional cost; the CHP unit cost is already incorporated within the component. The optimization only identifies the required efficiency of the CHP unit to fulfill the thermal demand. The PSO selects the same number of MMR units for any kind changes in thermal demand in this case; hence, the NPC of Case-02 is equal in all stages in Fig. 7-31. However, TES contributes to fluctuations in the NPC due to the variation in thermal demand. Since Case-01 meets the thermal requirement by electricity, the thermal demand variation combines more electricity generation sources within the N-R MHES that increase the NPC. Fig. 7-32 simulates both electric and thermal demand variation simultaneously. Since the electrical demand is altering in Fig. 7-32, the NPC increases with the increase of both demands for all three cases. However, Case-03 provides the best performance in terms of NPC for any load variation.

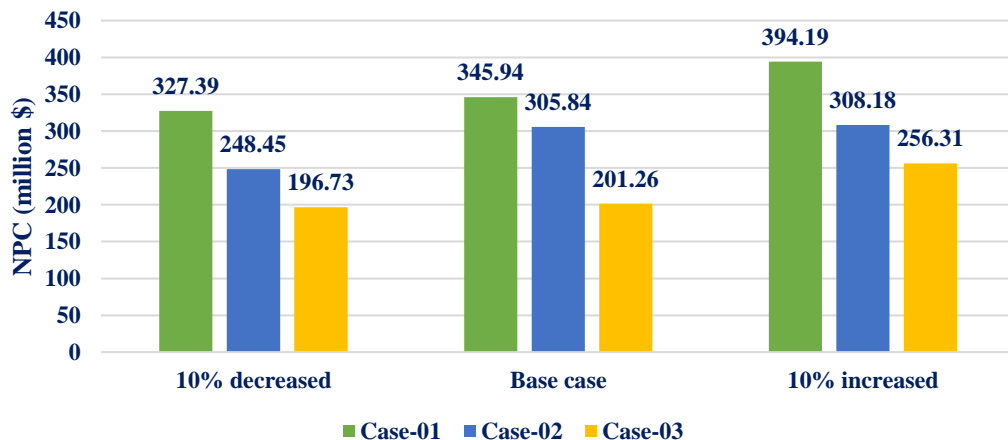


Figure 7-30: Impact of Variation in Average Electric Demand

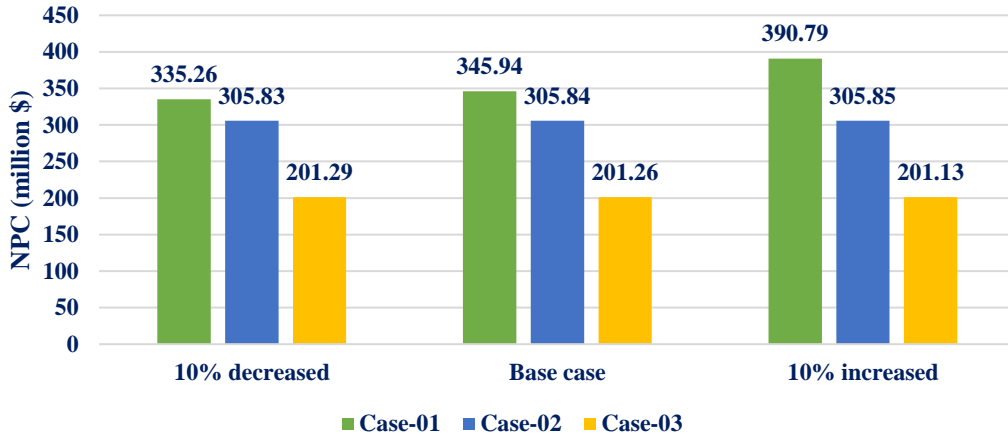


Figure 7-31: Impact of Variation in Average Thermal Demand

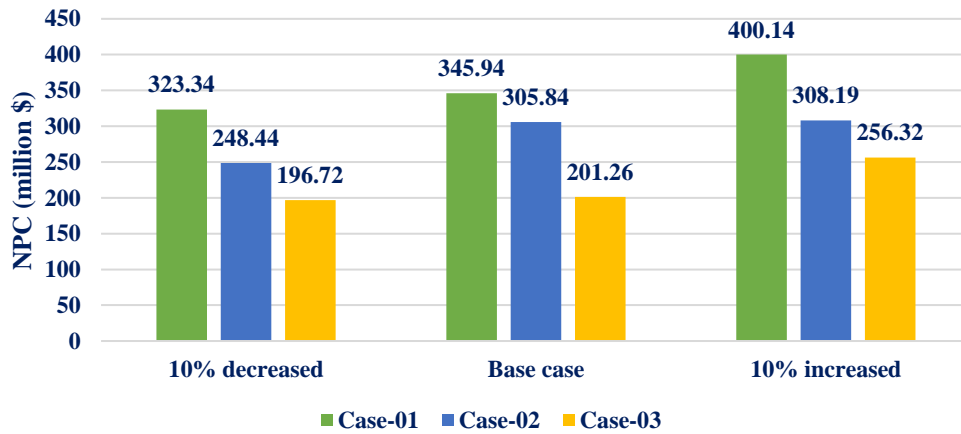


Figure 7-32: Impact of Variation in both Average Electric and Thermal Demand

7.1.4. Assessment of Sensitivity to Variation in System Equipment Cost

This sub-section investigates the impact of different equipment’s cost on system NPC. The discussion also intends to validate the comparison results made for the base case of three proposed hybridization methods. Though the HESs consist of various equipment, the main components are considered in this sensitivity analysis. The overall deployment cost of a single element, such as PV panel, WT, MMR, hydro plant, BG, EES, FC, electrolyzer, and TES, is varied by $\pm 20\%$ of their base values. The impact of changing the component overall installation cost for Case-01 is illustrated in Fig. 7-33. Fig. 7-33 says that the MMR has the highest effect on the NPC. The FC, electrolyzer, and EES also have a moderate impact on the changes in NPC, and the rest of the components do not affect the system NPC significantly. The upper portion of Fig. 7-33 is the amplified version of the dotted part in that figure.

Since the MMR is the primary driver of increasing or lowering the NPC, the MMR total cost is viewed in detail in Fig. 7-34. The different costs of MMRs, e.g., overnight capital cost, fixed O&M cost, refueling cost, fuel cost, and decommissioning cost, are varied by $\pm 20\%$ of their base prices to recognize the main contributor of the MMR total cost. Fig. 7-34 illustrates that refueling cost and overnight capital cost are the primary driver in changing the MMR total cost, while the other expenses are trivial. Fig. 7-35 shows the impact of error in different MMR cost data on system NPC. This part of analysis intends to investigate the influence of each type of cost separately since each type of expense has a different impact on system NPC. Since microreactors are not in reality now and will be available soon, each part of MMRs' total cost may experience differences within a specific range separately. Different technologies may provide a diverse range of cost variation for various cost types, such as capital cost, fixed O&N cost, refueling cost, fuel cost, and decommissioning cost. Therefore, The error in each cost input data (microreactors) is assumed to vary by $\pm 10\%$, a reasonable margin of error used for quality control assessment [206]. This error analysis represents the total system NPC fluctuations due to the inserted errors in different microreactors' cost input.

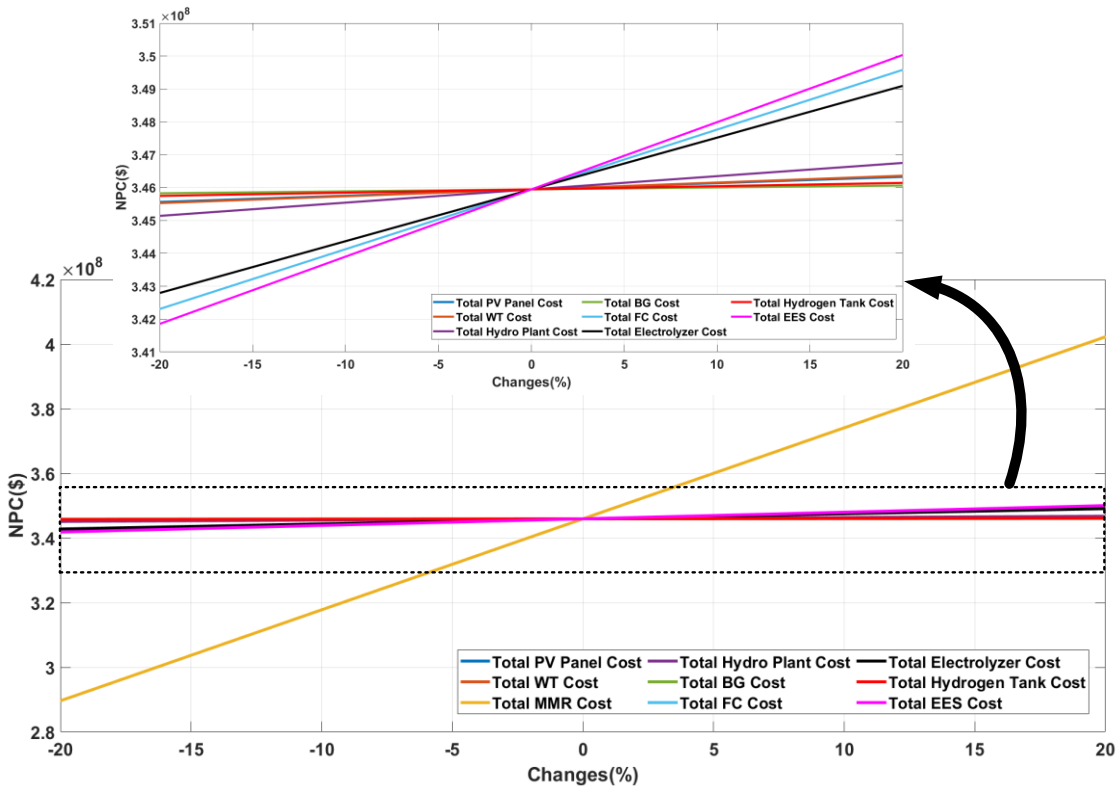


Figure 7-33: Impact of Variation in System Equipment Cost (Case-01)

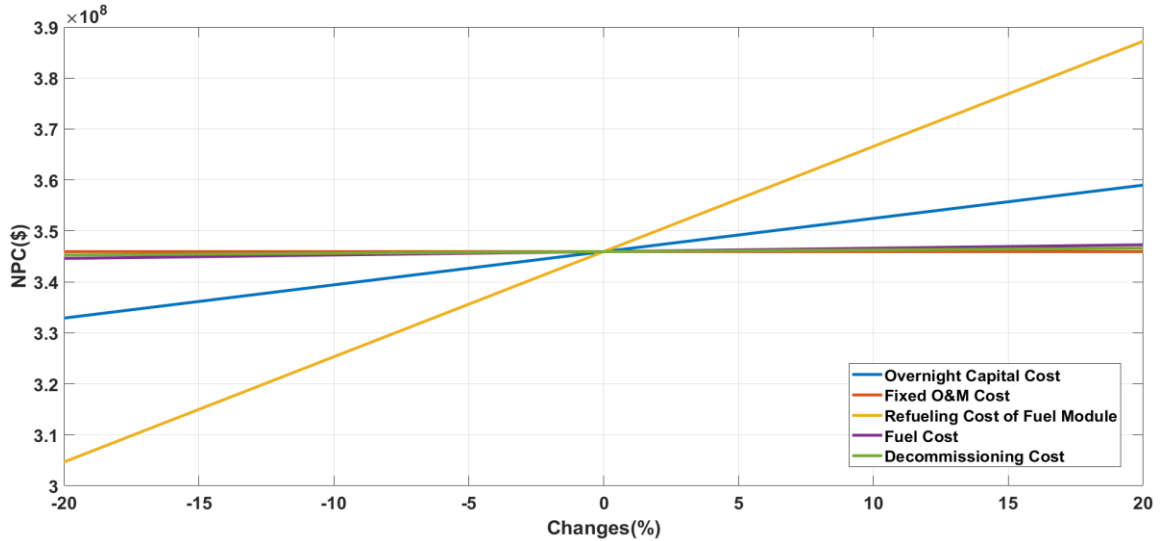


Figure 7-34: Impact of Variation in Different Types of Cost of MMR (Case-01)

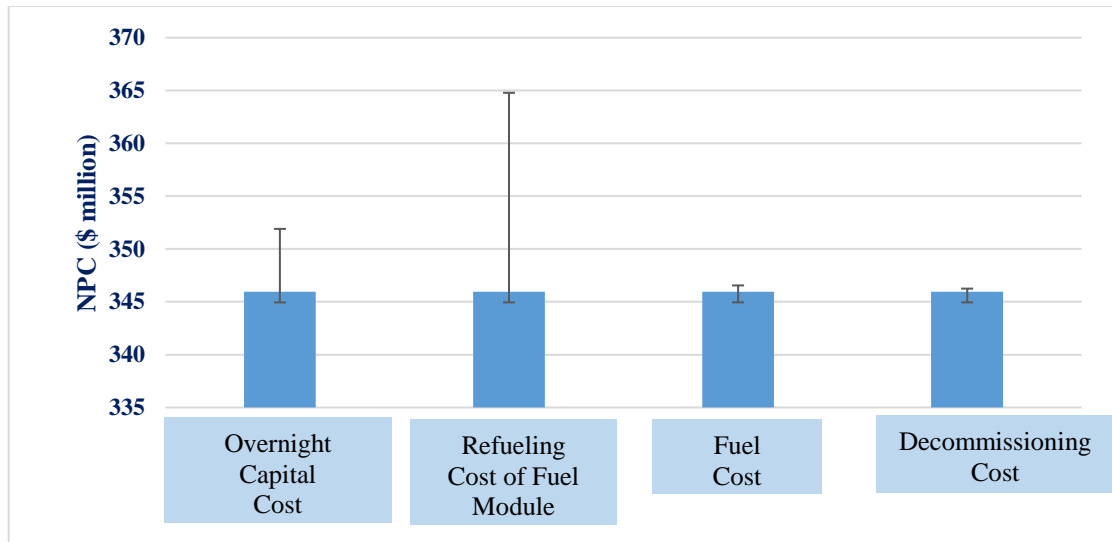


Figure 7-35: Error Analysis of Microreactor Costs (Case-01)

Fig. 7-36 depicts the impact of various components due to the variation of overall component cost for Case-02. Similar to the results of Case-01, the MMR has a tremendous effect on the system NPC. The FC and the electrolyzer have a limited impact on the system economy, but the rest of the components have an insignificant effect on the NPC. Fig. 7-37 illustrates the influence of different types of MMR cost on the total MMR cost. Fig. 7-37 tells that the refueling cost and the capital cost are again the most vital contributor in the MMR deployment for Case-02, similar to the Case-01. Fig. 7-38 shows the effect of error of inputs to various MMR cost data on system NPC. The error is also considered to vary by $\pm 10\%$, a similar assumption made for Case-01 in the previous section.

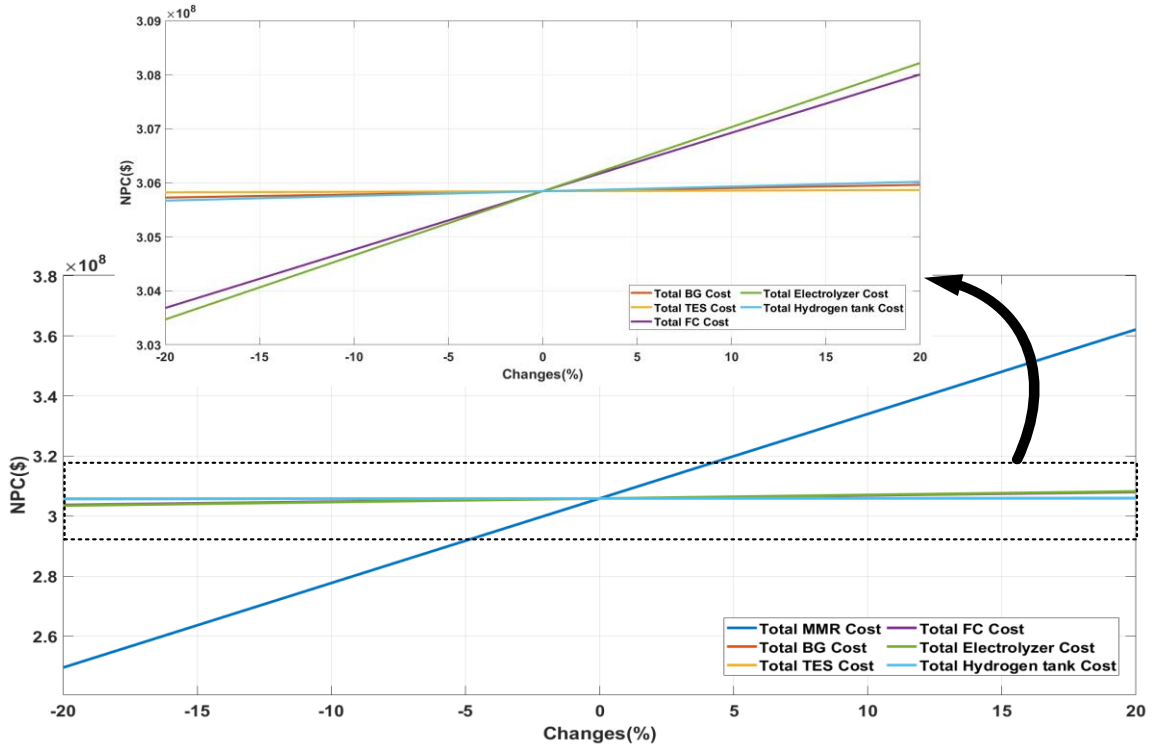


Figure 7-36: Impact of Variation in System Equipment Cost (Case-02)

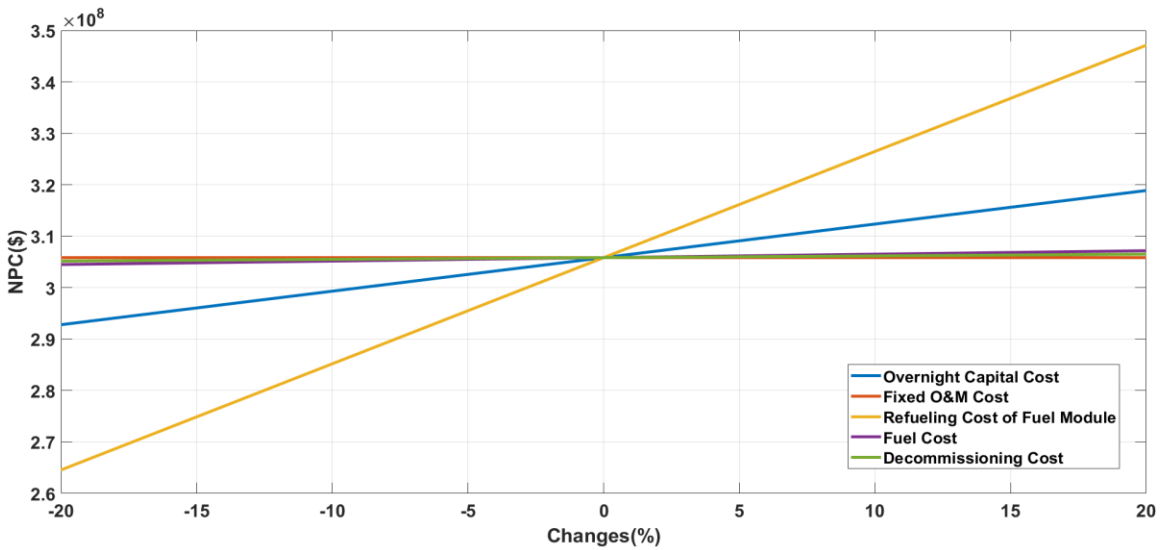


Figure 7-37: Impact of Variation in different types of Cost of MMR (Case-02)

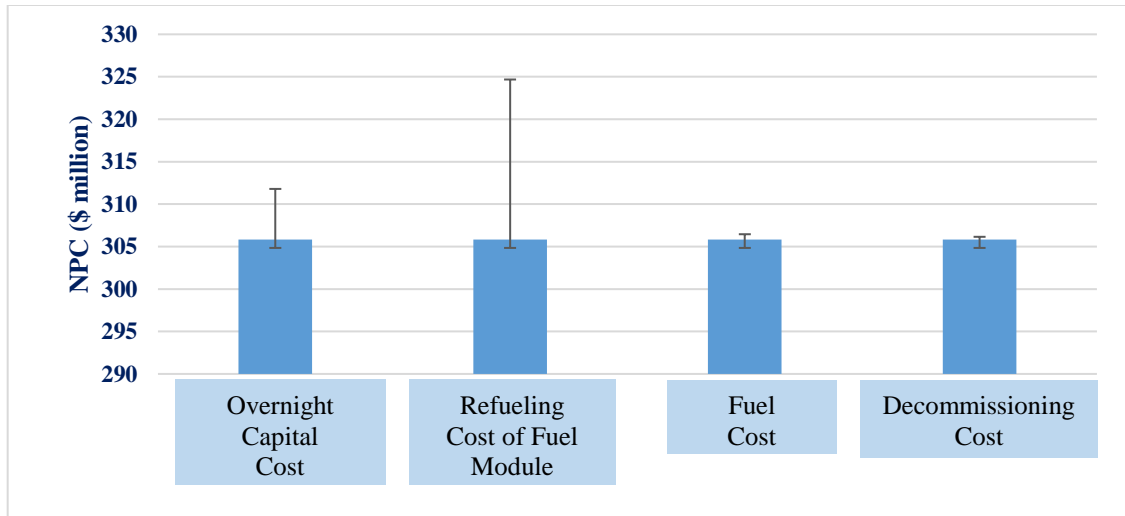


Figure 7-38: Error Analysis of Microreactor Costs (Case-02)

Fig. 7-39 addresses that the MMR has the most critical influence on the NPC, while the FC, electrolyzer, and hydro plant also significantly impact the system economy for Case-03. The PV panels and the TES also affect the NPC. However, the rest of the equipment has a trivial effect on the system NPC. Like Case-01 and Case-02, the refueling and the capital cost of the MMR are the main contributor to raising or lowering the total MMR cost, as illustrated in Fig. 7-40. By observing all the findings from the above discussion, it is said that Case-03 is always superior to the other two hybridization methods for any fluctuations in equipment cost. Fig. 7-41 shows the impacts of error in different cost data (microreactor) on system NPC. The error value is regarded to vary by $\pm 10\%$, similar to the error analysis part for Case-01 and Case-02.

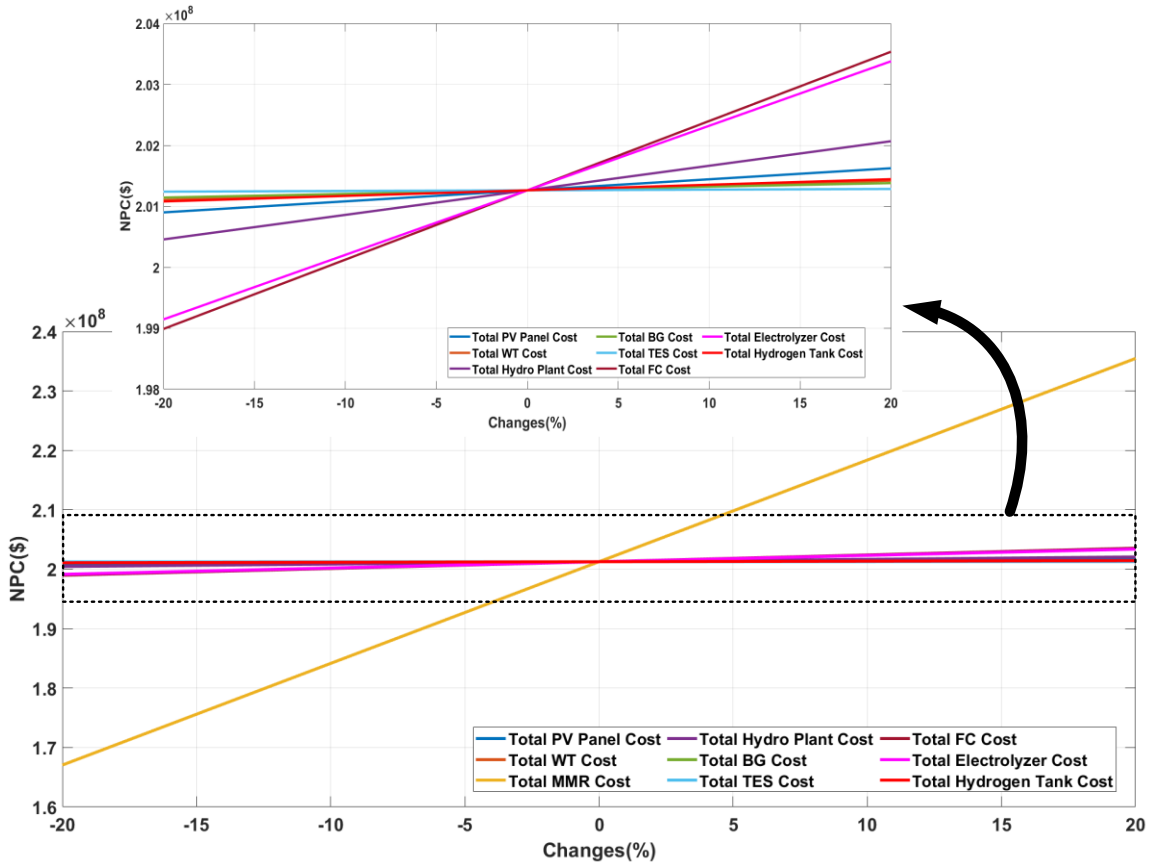


Figure 7-39: Impact of Variation in System Equipment Cost (Case-03)

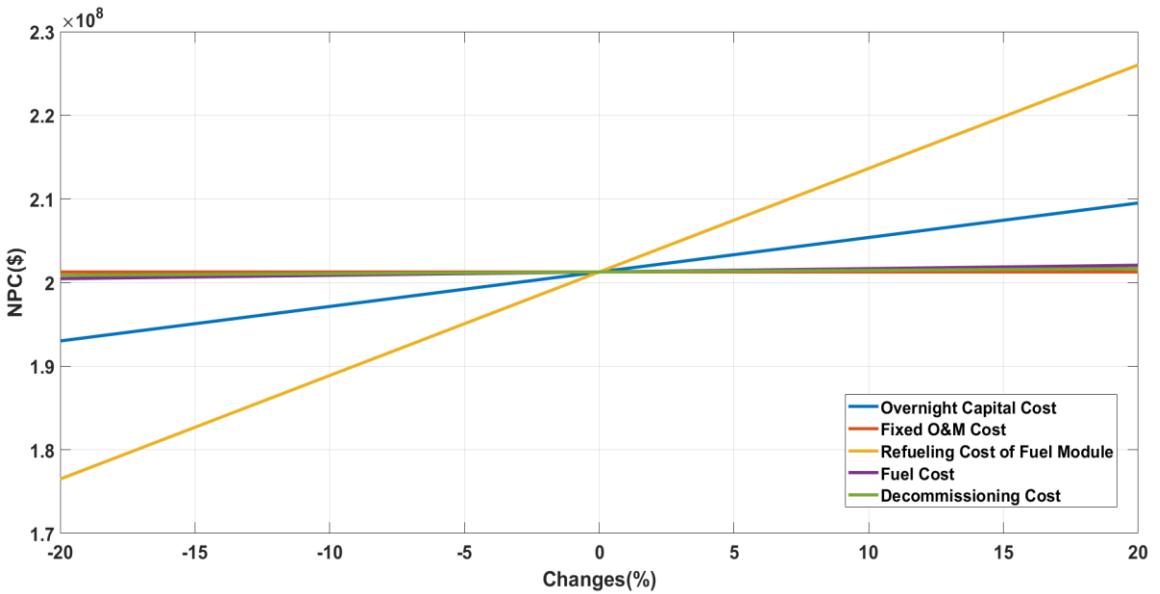


Figure 7-40: Impact of Variation in different types of Cost of MMR (Case-03)

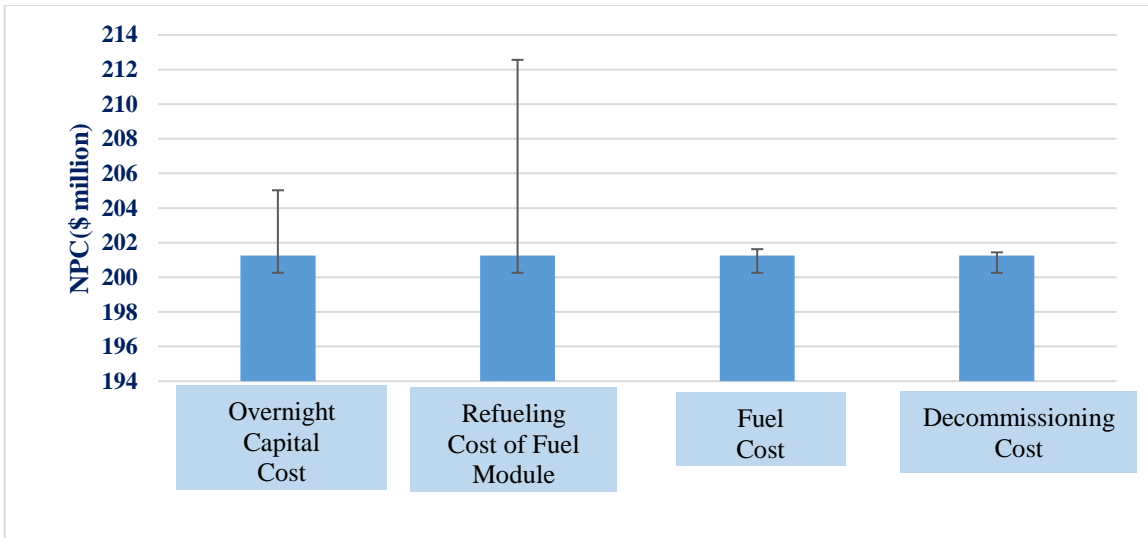


Figure 7-41: Error Analysis of Microreactor Costs (Case-03)

7.1.5. Assessment of Sensitivity to Variation in Economic Parameters

Project lifetime, discount rate, and inflation rate are the three most important economic parameters in the techno-economic analysis of HESs. The project lifetime, discount rate, and inflation rate for the base case are 40 years, 8%, and 2%, respectively.

In this section, a sensitivity analysis is conducted by differing project lifetime, discount rate, and inflation rate from its base case. Fig. 7-42 summarizes the results of sensitivity to the project lifetime. The project lifetime is varied from 20 years to 100 years. The system NPC raises with the increment of the project lifetime. The NPC reaches a stable position for higher project lifetime in N-R MHESs. The figure also tells that the investment in any N-R MHES is also financially profitable for a longer project lifetime. The results show that Case-03 has the least NPC irrespective of the project lifetime. The system reliability is also ensured by executing the reliability constraints into the optimization problem.

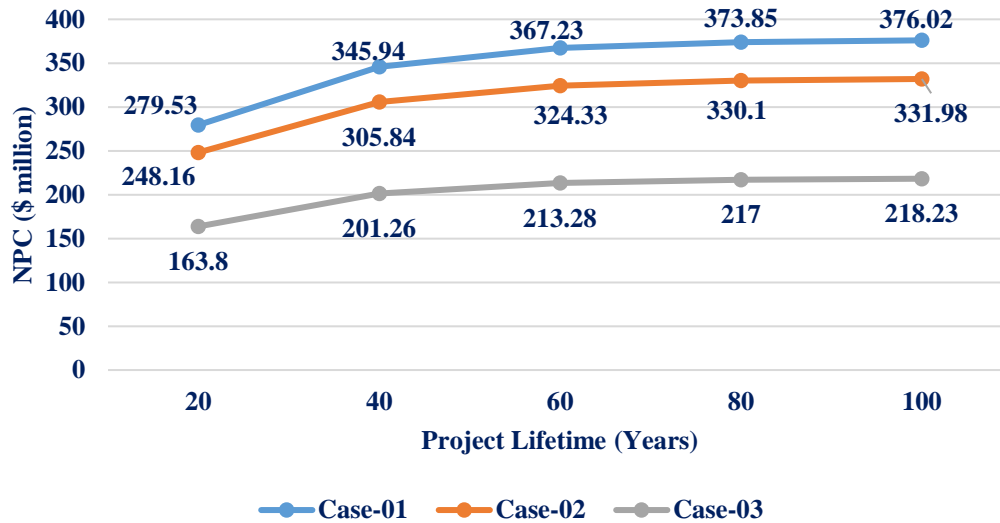


Figure 7-42: Impact of Variation in Project Lifetime

The discount rate is varied from 5% to 10% to evaluate the impact of the discount rate on system planning. The NPC falls with the increase in the discount rate, as shown in Fig. 7-43. It is recommended that system planners should always choose a higher discount rate for economic system modeling. The result tells that Case-03 provides the least NPC irrespective of any value of the system discount rate. The rate of changes in NPC is also more limited for higher values of the discount rate.

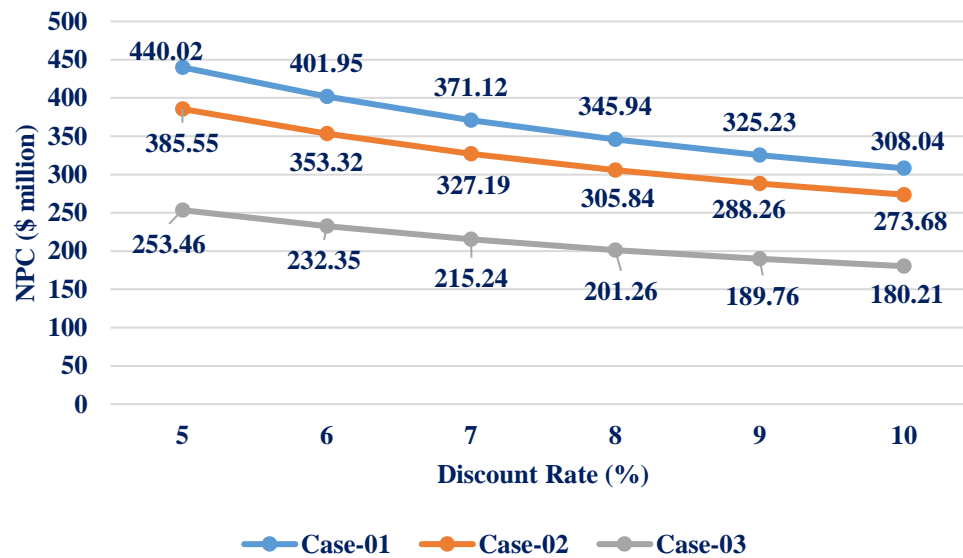


Figure 7-43: Impact of Variation in Discount Rate

The inflation rate is adjusted from 1% to 6% from its' base case value in this sensitivity assessment. The NPC increases significantly with the rise of the inflation rate, presented in Fig. 7-44. Similar to the sensitivity analysis of the project lifetime and the discount rate, the NPC is the lowest for the Case-03, while the Case-01 has the highest NPC, regardless

of any value of the inflation rate. Therefore, the sensitivity assessment of the economic parameters also proves Case-03 as the most economic hybridization method for N-R MHESs.

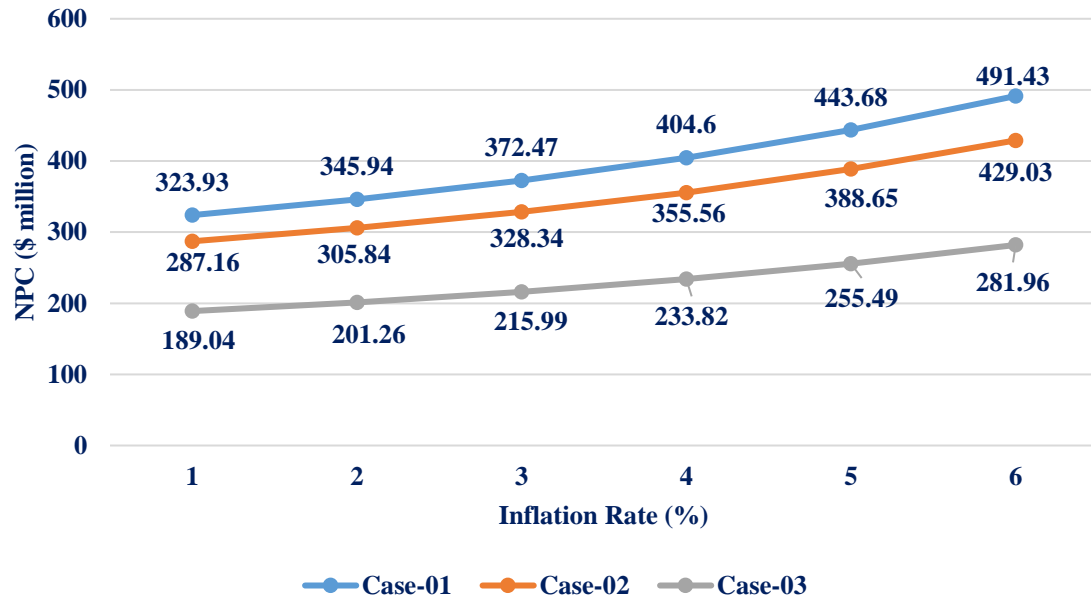


Figure 7-44: Impact of Variation in Inflation Rate

7.1.6. Assessment of Sensitivity to Variation in Capacity Factor (MMR)

A capacity factor indicates how a rated capacity of a generation source is utilized in an energy system. The MMR considered in the research may not always run at maximum rated power. The capacity factor is considered at steady-state mode throughout the operation of microreactors. Therefore, the base capacity factor (95%) would not be achieved. In this circumstance, it is inevitable to conduct a sensitivity analysis by varying the capacity factor to evaluate the N-R MHESs. The goal of this evaluation is to assess the system competency for higher and lower capacity factors. The capacity factors of 65%, 75%, 85%, and 95% have been used in the sensitivity assessment.

Fig. 7-45 represents the NPC of the proposed N-R MHESs due to the difference in capacity factor. The NPC of all systems decreases with the increase of the capacity factor, except at 95% and 85% capacity factor for Case-02. The PSO optimization suggests seven and six MMR units for Case-02 at 65% and 75% capacity factor, respectively. On the other hand, the same number (5 units) of MMRs is combined at 85% and 95% capacity factor for Case-02. Therefore, Case-02 shows the same NPC (\$ 305.84 million) at 85% and 95% of the capacity factor. However, the NPC of Case-02 at the capacity factor of 75% and 65% has been varied (\$ 384.00 million and \$ 360.58 million, respectively) due to the inclusion of the different MMR units. Hence, the capacity factor sporadically affects the NPC

depending on the demand for stand-alone MMR-based HES (Case-02). A stand-alone MMR-based HES makes the reactor selection relatively inflexible.

For Case-01 and Case-03, the reduced capacity factor allows to include more renewable generation sources. The inclusion of a few PV panels, WTs, or HTs can manage a small variation of MMR Capacity. Since the MMR deployment cost is very high, the optimization recommends using renewable sources rather than incorporating a new MMR unit. Therefore, the NPC of Case-01 and Case-03 are also increased with the decreasing of MMR’s capacity factor. However, Case-03 provides the lowest NPC in all values of capacity factor, while Case-01 has the highest NPC in all cases.

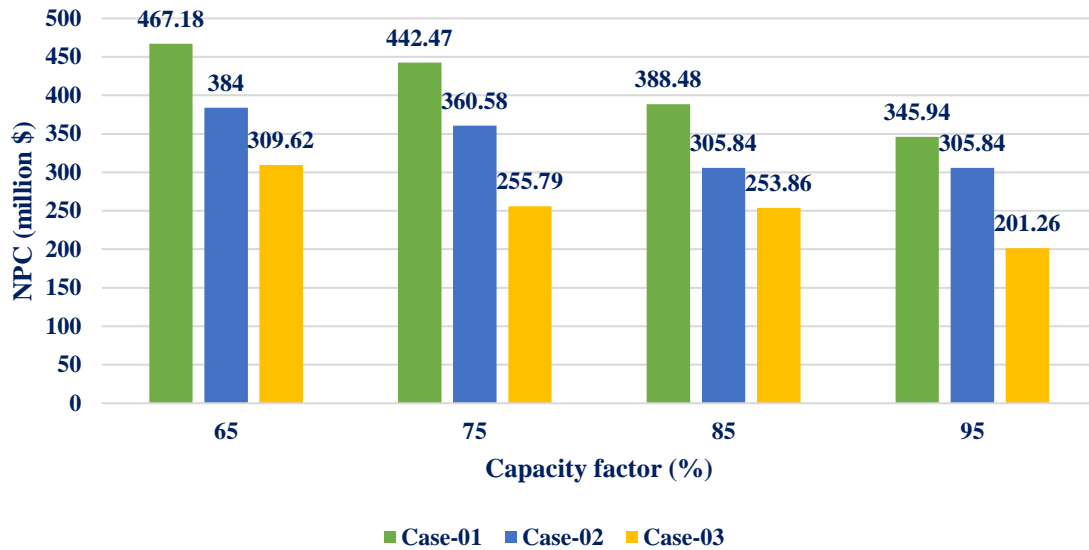


Figure 7-45: Impact of Variation in Capacity Factor (MMR)

7.2. Comparison between the Best Hybridized System and Diesel-based MEG

The study primarily focuses on energy crisis solutions for off-grid applications. Though several types of fuels are available, such as coal, wood, and natural gas, diesel-fired MEGs are often used for remote areas [207]. Therefore, this section intends to evaluate and compare a traditional energy system with the most significant proposed N-R MHES system. To confirm the effectiveness of the proposed N-R MHESs, it is necessary to conduct a comparative study between the proposed most effective N-R MHES and a traditional fossil-fired HES.

In section 7.1, the most suitable nuclear-renewable integrated system configuration, “Multiple Resources and Multiple Product-based Coupling (Case-03),” is identified. Therefore, in this section, a diesel Genset-based MEG (Case-04) is designed and considered as a representative of conventional technology-based MEG to compare with the

most desirable nuclear-renewable integrated system (Case-03). Fig. 7-46 represents a schematic of a typical diesel Genset-based MEG. Diesel Gensets will only replace the MMRs in Case-04; the rest of the system configuration will be identical. The maximum available generation by combining all types of Gensets is kept the same as MMRs (Case-03). Since three classes, 50 kW, 30 kW, and 20 kW, of reduced-size Gensets are used in Case-04 to lessen the NPC, maximum available power is apportioned equally to the 50 kW Genset, 30 kW Genset, and 20 kW Genset. To establish uniformity, the energy management algorithm of diesel Genset-based MEG (Case-04) is considered as same as the multiple resources and multiple products-based coupled N-R MHES (Case-03). The energy management algorithm for Case-04 is outlined in Fig. 7-47.

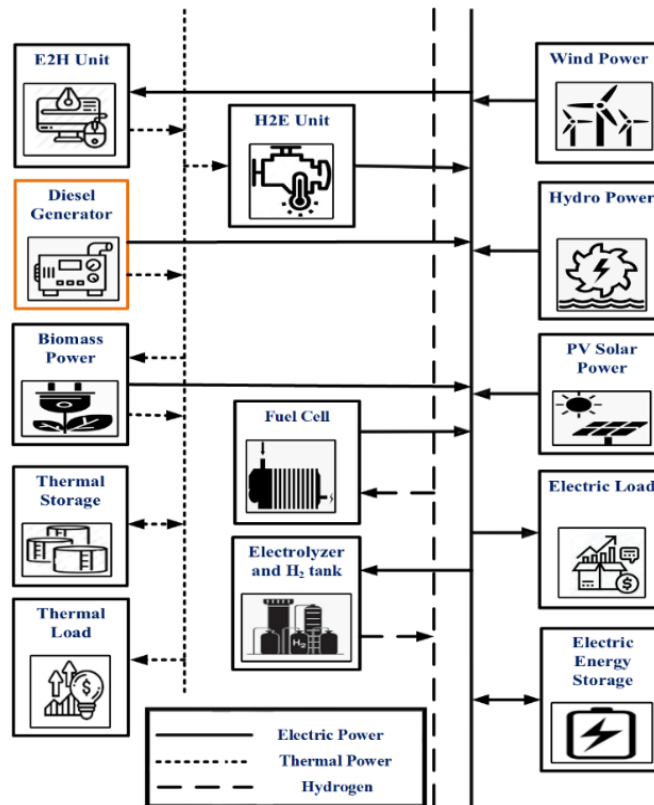


Figure 7-46: Schematic of Diesel Genset-based MEG

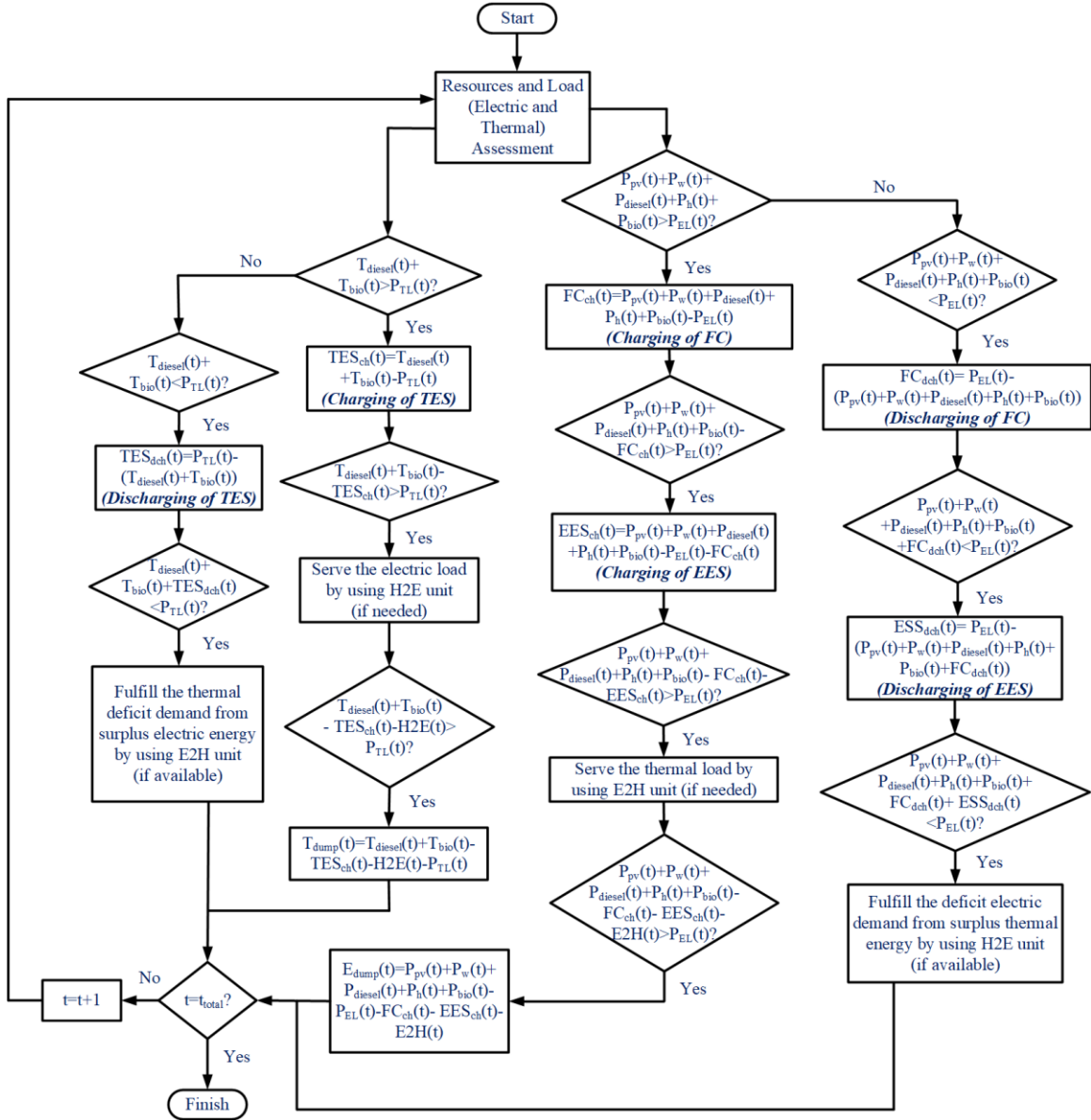


Figure 7-47: Energy Management Algorithm of Diesel Genset-based MEG

The NPC comparison between Case-03 and Case-04 is presented in Fig. 7-48. The NPC of Case-04 (\$ 346.06 million) is about one and half times higher than the NPC of Case-03 (\$ 201.26 million). Though a comprehensive energy-flow model has been exercised in the diesel-fired MEG to reduce the system cost, the NPC of Case-04 is still largely higher compared to Case-03. The results of the optimal configuration of diesel-fired MEG are recorded in Table 7-5. The equal number of populations and iterations with the previous cases are considered in this optimization problem. The PSO optimization results suggest including three types of Gensets, PV panels, WTs, hydro plant, hydrogen storage, EES, and TES. The optimal system intends to utilize multiple small-size generators rather than using a large-scale Genset. A single unit of 50 kW generator is also added to the optimal system. The optimal system utilizes the full availability of all renewable energy generating

components, such as PV panels, WTs, HTs, and BG; the maximum number of these components are incorporated in the optimal configuration. The results do not insert the E2H unit and the H2E unit within the optimal system configuration.

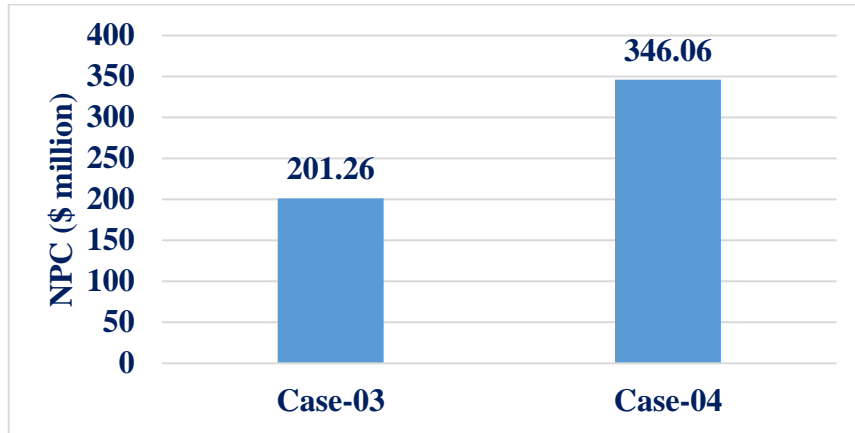


Figure 7-48: Comparison of the NPC between Case-03 and Case-04

Table 7-5: Optimal Configuration of Diesel Genset-bases MEG

Case		Diesel Genset-based MEG (Case-04)
Number of particles		250
Number of iterations		300
Number of Diesel Genset	Genset (50 kW rated)	2
	Genset (30 kW rated)	50
	Genset (20 kW rated)	50
Number of PV panels		100
Number of WT		100
HT capacity (kW)		1000.64
Required CHP Efficiency (%)	Genset (50 kW rated)	29.8
	Genset (30 kW rated)	30.0
	Genset (20 kW rated)	21.6
Number of Hydrogen tank		12
Battery bank capacity (MWh)		12.53
TES capacity (MWh)		19.90
BG capacity (kW)		65.10
E2H unit capacity (kW)		0
H2E unit capacity (kW)		0

Table 7-6 lists the KPIs of Case-04 and compares them with Case-03. Both Case-03 and Case-04 confirm the maximum resiliency within the defined reliability constraint limits. Due to the reduced size of diesel Gensets, Case-04 is more reliable in terms of GRF and LA (electrical); $LPSP_{elec}$ and SEF_{elec} have better values for Case-03 compared to Case-04. Since the total cost of diesel Genset installation and maintenance is high, more RESs are included in Case-04. Hence, the RF of Case-04 is also higher than Case-03. However, the

LCOE of Case-04 (0.5073 \$/kWh) is approximately 1.5 times higher than Case-03 (0.2950 \$/kWh).

Table 7-6: Comparison of KPIs between Case-03 and Case-04

Parameters	Multiple Resources and Multiple Products-based Coupled System (Case-03)	Diesel Genset-based MEG (Case-04)
$LPSP_{elec}$ (%)	4.36	5
$LPSP_{ther}$ (%)	5	5
SEF_{elec} (%)	1.42	8.70
SEF_{ther} (%)	10	10
GRF_{elec} (%)	115.31	113.15
GRF_{ther} (%)	108.71	108.71
LA_{elec} (%)	86.11	90.63
LA_{ther} (%)	76.39	75.00
RF (%)	10.25	15.10
$LCOE$ (\$/kWh)	0.2950	0.5073

Fig. 7-49 illustrates the PSO convergence plot of Case-04 for the best independent run. Fig. 7-50 and Fig. 7-51 demonstrate the electric and the thermal energy generation and consumption plots for the diesel-fired MEG. The electrical and the thermal generation sources accompanying the energy storage systems favorably serve the electric and the thermal demand in Case-04. A few amounts of energy deficiency or surplus happen due to the allowable defined limits of the $LPSP$ and SEF constraints. Fig. 7-52 represents the charging and discharging process of the energy storage systems employed in Case-04.

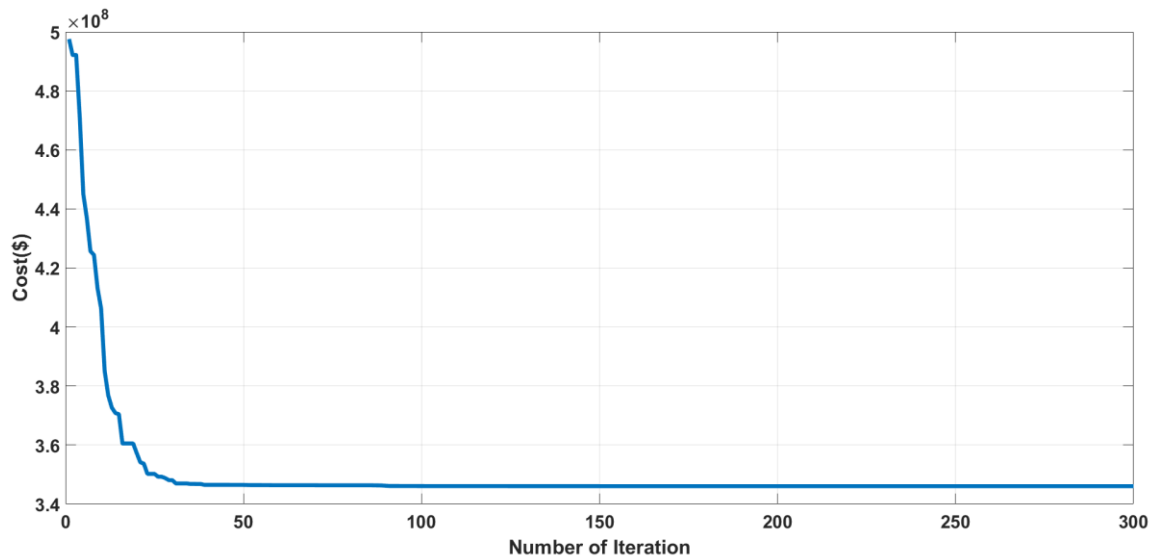


Figure 7-49: Convergence Plot (Case-04)

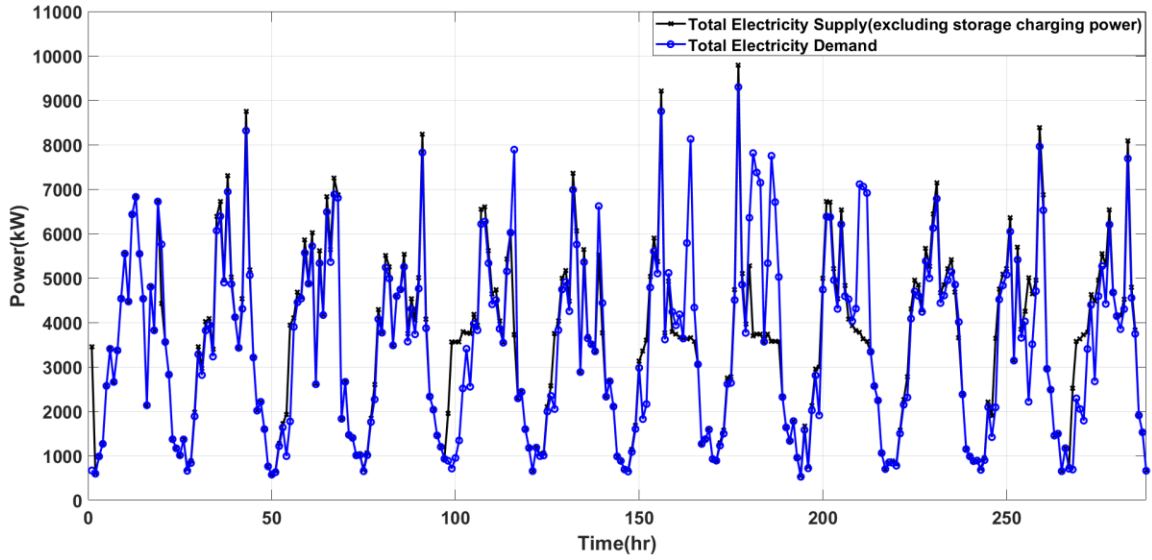


Figure 7-50: Total Electric Energy Generation and Consumption Scenario (Case-04)

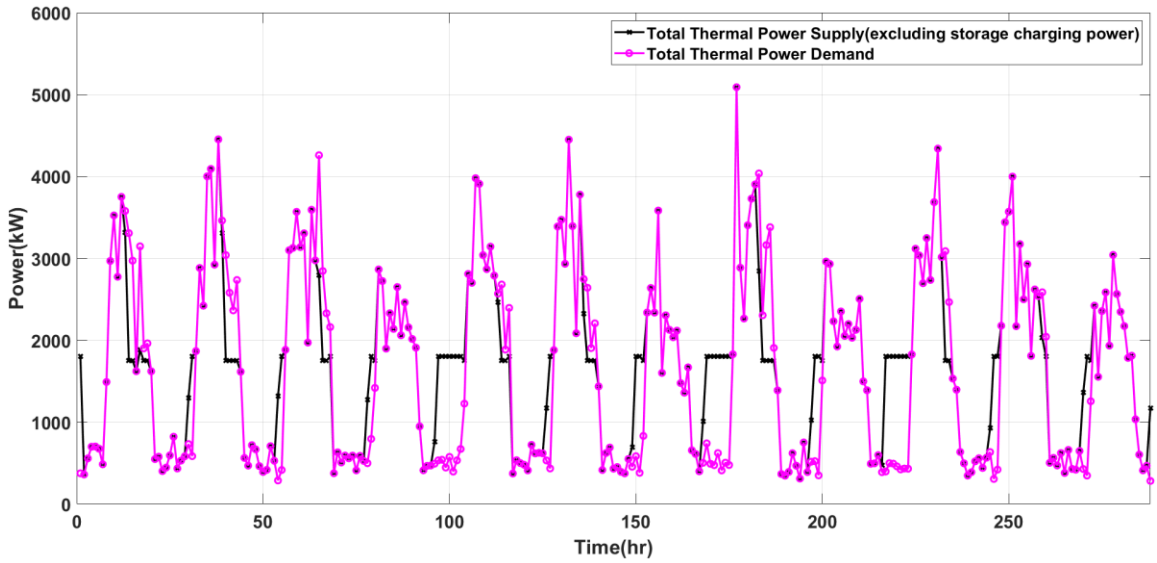


Figure 7-51: Total Thermal Energy Generation and Consumption Scenario (Case-04)

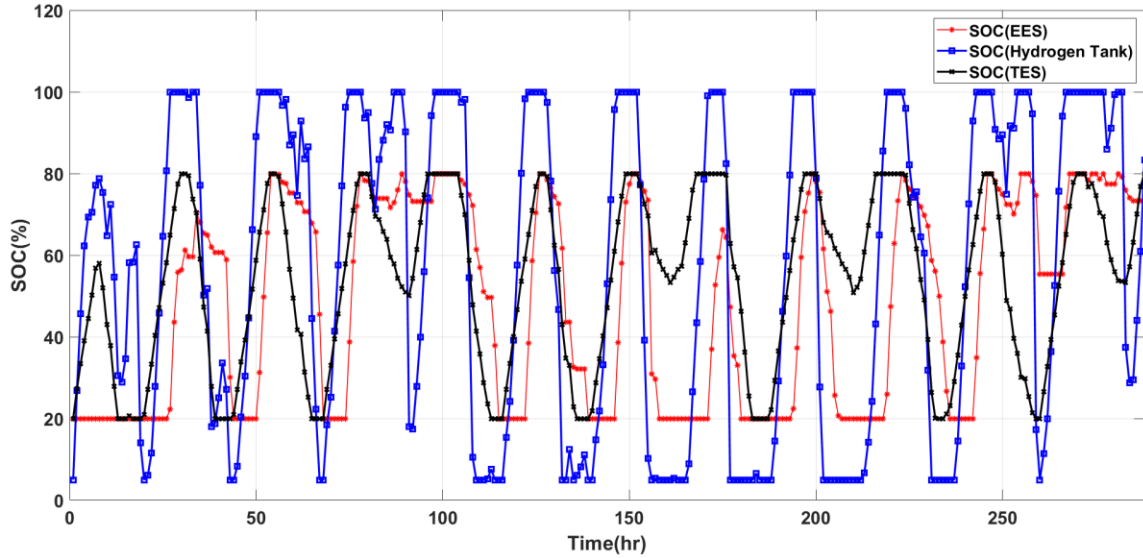


Figure 7-52: Energy Storage Operation (Case-04)

The energy management algorithm proposed in Case-04 has also required validation before additional analysis. Therefore, the same procedure, conducted earlier, is followed here to verify the energy management algorithm by utilizing new sets of load profiles, presented in Fig. 7-17 and Fig. 7-18. As new load profiles are introduced, the PSO will identify a new set of variables for Case-04. By using the new value of the decision variables for Case-04, the supply (electric and thermal) can meet the demand adequately with a fair margin of reliability. Fig. 7-53 and Fig. 7-54 show the energy supply and demand scenario for Case-04 with new electric and thermal profiles. Also, Case-04 still has a higher NPC than Case-03.

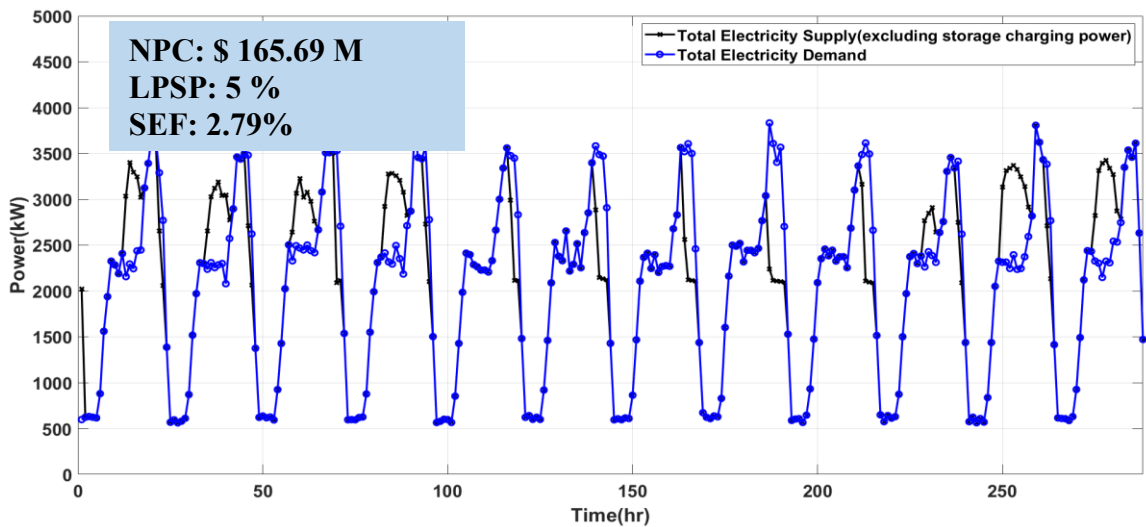


Figure 7-53: Electric Energy Management Algorithm Verification (Case-04)

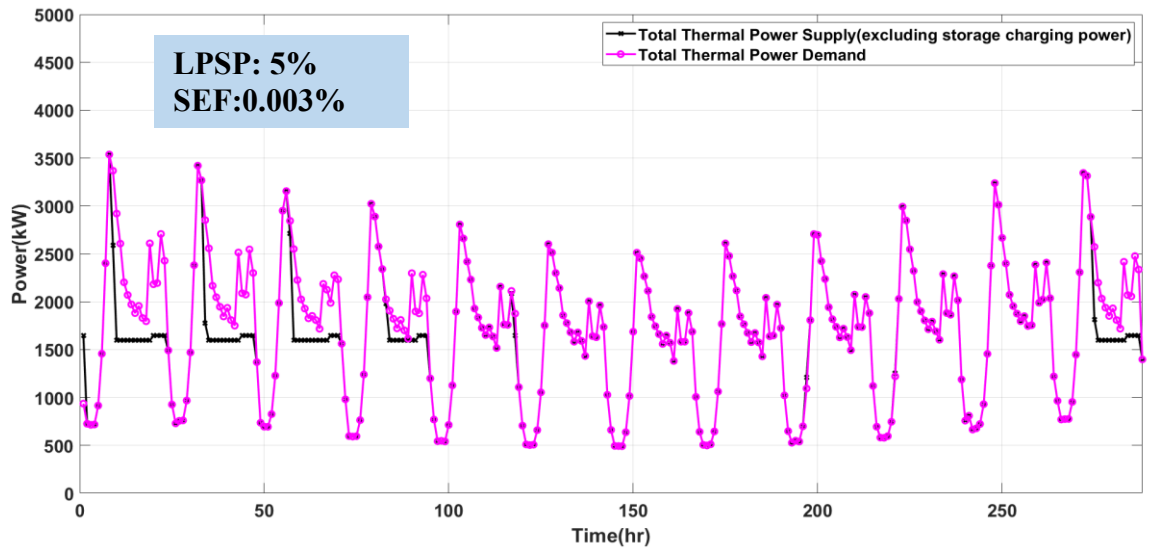


Figure 7-54: Thermal Energy Management Algorithm Verification (Case-04)

Since both the arrangements, Case-03 and Case-04, are dependent on diverse determinants, it is required to carry out a sensitivity analysis by considering the most influential factors. The later sub-sections present the sensitivity analysis in detail for Case-04. This sensitivity analysis's primary purpose is to verify the results obtained from the base case comparison between Case-03 and Case-04. It should be remarked that the cost of environmental impact and the cost of GHG emissions are not considered in this study. Table 7-7 compiles the main idea of the sensitivity assessment carried out in section 7.2.

Table 7-7: A Summary of the Sensitivity Analysis Conducted in Section 7.2

Sub-Section	Summary
7.2.1	This segment compares the NPC of Case-03 and Case-04 due to the shift in daily peak demand.
7.2.2	The sub-section assesses the sensitivity of the difference in seasonal peak demand from base cases to NPC for Case-03 and Case-04.
7.2.3	This piece of assessment estimates the impact of average demand changes on system NPC.
7.2.4	The sub-section evaluates and identifies the impact of different equipment cost on NPC.
7.2.5	This sub-section determines the impact of system economic parameters, e.g., discount rate, inflation rate, and project lifetime, on NPC.
7.2.6	This segment evaluates the influence of renewable resources on system planning and NPC.
7.2.7	This sub-section determines the NPC of Case-03 and Case-04 and analyzes the impact on NPC due to variation in PV panel and WT availability.

7.2.1. Assessment of Sensitivity to Shifting of Daily Peak Demand

Like sub-section 7.1.1, a sensitivity analysis is conducted to evaluate the impact of shifting the daily peak demand. Fig. 7-55 represents the comparison of the NPC for Case-03 and Case-04 for the shifted electric and thermal demand. The sensitivity analysis shows that Case-04 has substantially higher NPC than Case-03, referring Case-03 is more profitable than Case-04.

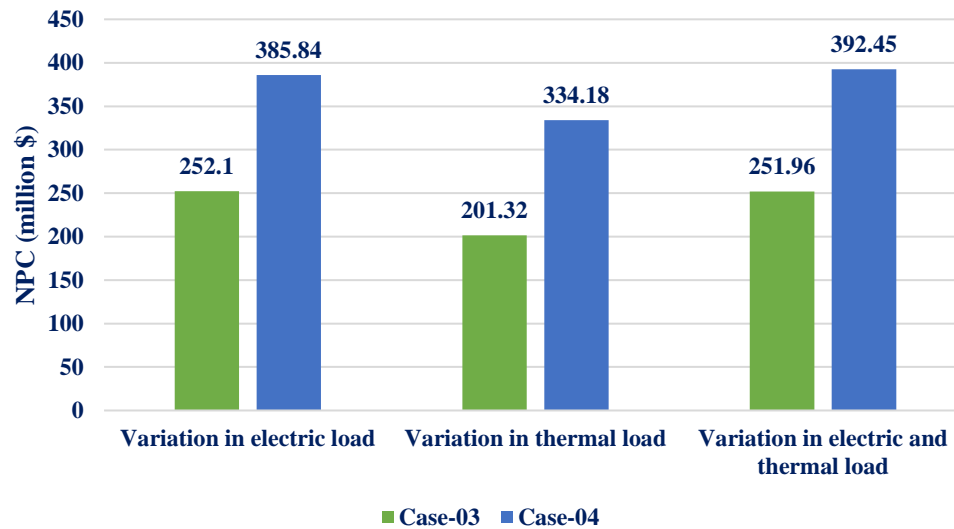


Figure 7-55: Impact of the Shifting of Daily Peak Demand

7.2.2. Assessment of Sensitivity to Shifting of Seasonal Demand

Another sensitivity analysis is conducted here by moving the seasonal demand by six months since it differs from region to region, similar to the study of sub-section 7.1.2. Fig. 7-56 highlights the sensitivity analysis results for Case-03 and Case-04 due to the variation in electric demand, thermal demand, or both. The results affirm that the NPC of Case-03 is still less than Case-04 for all situations. The sensitivity results signify that Case-03 has more financial advantages than Case-04. Similar to the results obtained in sub-section 7.1.2, the annual peak load variation does not widely affect the NPC. Thus, the NPC indicated in Fig. 7-56 for Case-04 are roughly the same as the base case value.

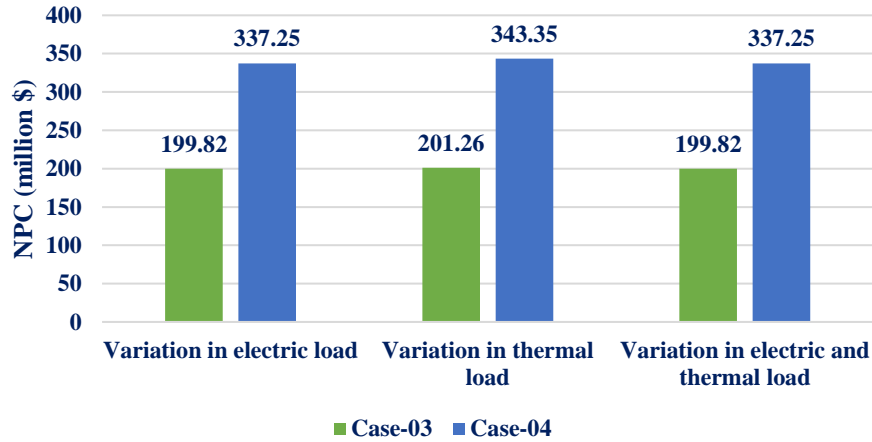


Figure 7-56: Impact of the Shifting of Seasonal Peak Demand

7.2.3. Assessment of Sensitivity to Variation in Average Energy Demand

The electric demand and the thermal demand are altered by $\pm 10\%$ here to evaluate the sensitivity of NPC to system demand for Case-04. Fig. 7-57, Fig. 7-58, and Fig. 7-59 present the NPC of Case-03 and Case-04 due to the modified electric, thermal, and both electric and thermal demand, sequentially. The results again show the cost-efficiency of Case-03 over Case-04 for all cases. Case-03 has less NPC than Case-04 regardless of the increase or decrease of electric demand, thermal demand, or both electrical and thermal demand. The increment of electric demand forces to include more generators. Hence, the NPC increases with the rise of electric demand for Case-04, as shown in Fig. 7-57. Due to the CHP capability and less influence of TES on total NPC, the thermal variation does not alter the NPC significantly, illustrated in Fig. 7-58. Since Fig. 7-59 simulates both the electric and the thermal load variation, the system NPC increases with the extension in system demand.

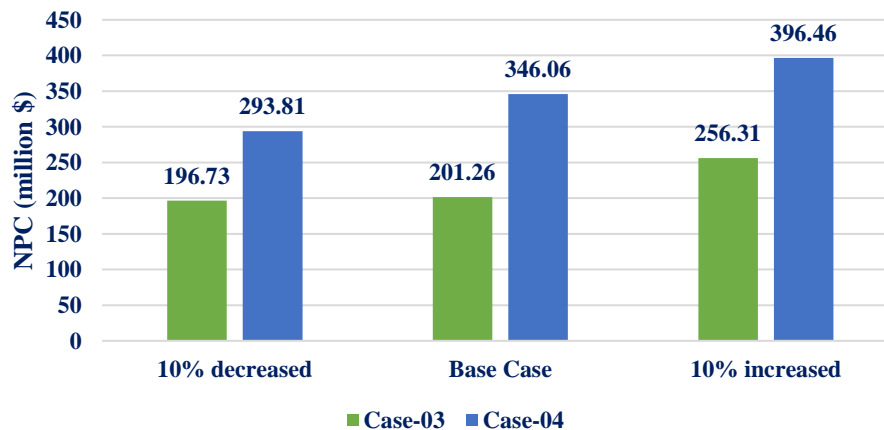


Figure 7-57: Impact of Variation in Average Electric Demand

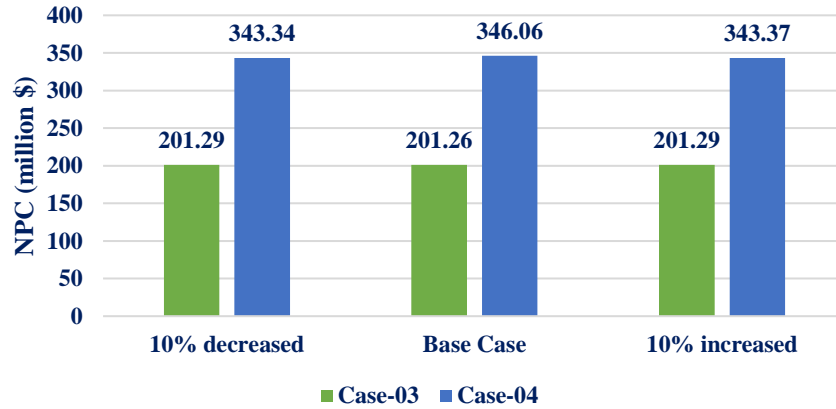


Figure 7-58: Impact of Variation in Average Thermal Demand

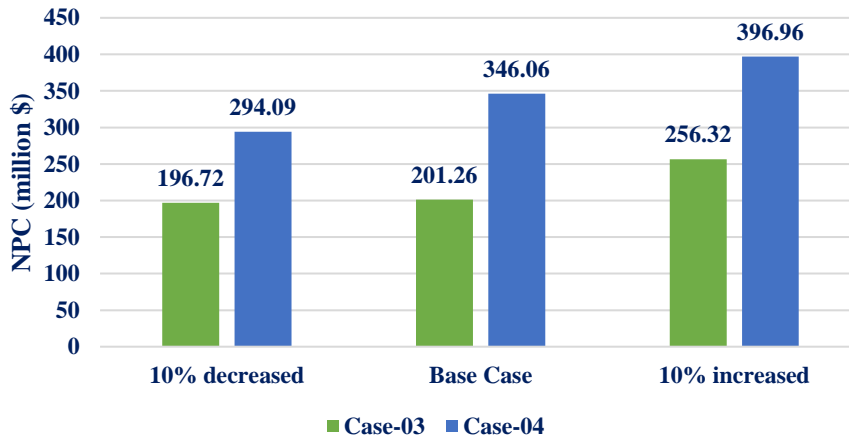


Figure 7-59: Impact of Variation in both Average Electric and thermal Demand

7.2.4. Assessment of Sensitivity to Variation in System Equipment Cost

This section intends to investigate the consequence of the component’s cost on the total system economy for Case-04. The equipment’s impact on NPC for Case-03 has already been studied in sub-section 7.1.4. Therefore, this sub-section investigates the sensitivity of the NPC due to the alteration of different component cost for Case-04. Fig. 7-60 shows that the 30 kW Gensets and the 20 kW Gensets have the highest impact on the system NPC. It is apparent since multiple units of 30 kW generators and 20 kW generators are installed within the HES. Due to two-unit installation of 50 kW Genset, it has reasonable impact on the total system NPC. The EES, electrolyzer, FC, and hydropower plant also have a moderate influence on the NPC. The rest of the components have a limited impact on the NPC. Fig. 7-61 examines the details of the most influential cost contributors, 30 kW and 20 kW Gensets, in Case-04. Fig. 7-61 points that the fuel cost of 30 kW Genset has the most contribution in the NPC variation, followed by fuel cost of 20 kW, O&M cost of 30

kW, and O&M cost of 20 kW, respectively. The capital cost and the replacement cost of the generators are trivial compared to the other investments. By analyzing the discussion stated above, Case-03 is an extensively profitable configuration compared to Case-04.

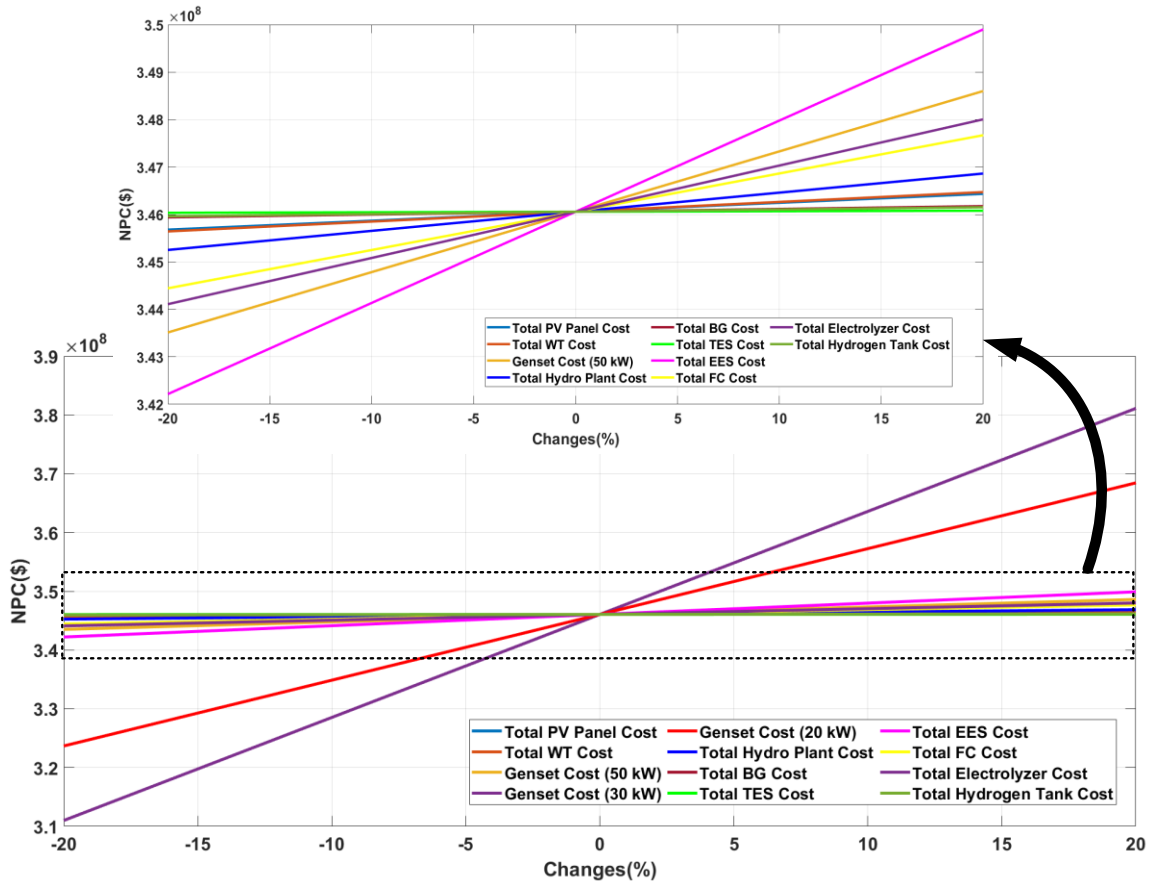


Figure 7-60: Impact of Variation in System Equipment Cost (Case-04)

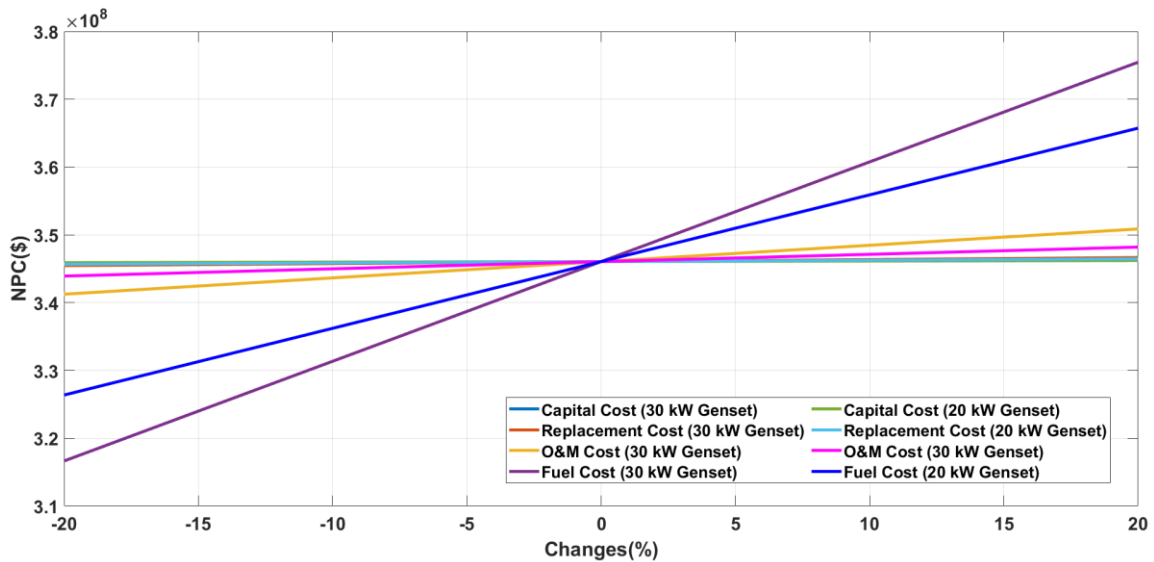


Figure 7-61: Impact of Variation in Diesel Genset Cost

7.2.5. Assessment of Sensitivity to Variation in Economic Parameters

Similar to sub-section 7.1.5, project lifetime, discount rate, and inflation rate are studied here to evaluate these parameters' impact on the system NPC. Fig. 7-62 points out the NPC of Case-03 and Case-04 for different project lifetime. The figure tells that the Case-03 has a lower NPC than Case-04 regardless of the project lifetime. The rate of changes in NPC is very low for a higher project lifetime.

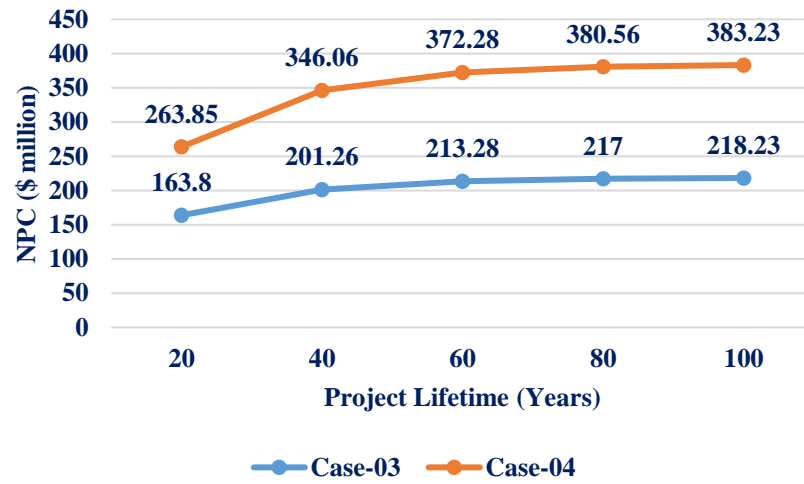


Figure 7-62: Impact of Variation in Project Lifetime

The discount rate varies from 5% to 10% to assess its' sensitivity to the NPC system. The NPC of both cases decreases with the discount rate increase, as indicated in Fig. 7-63. Still, the NPC of Case-04 is always higher than Case-03 for any particular discount rate.

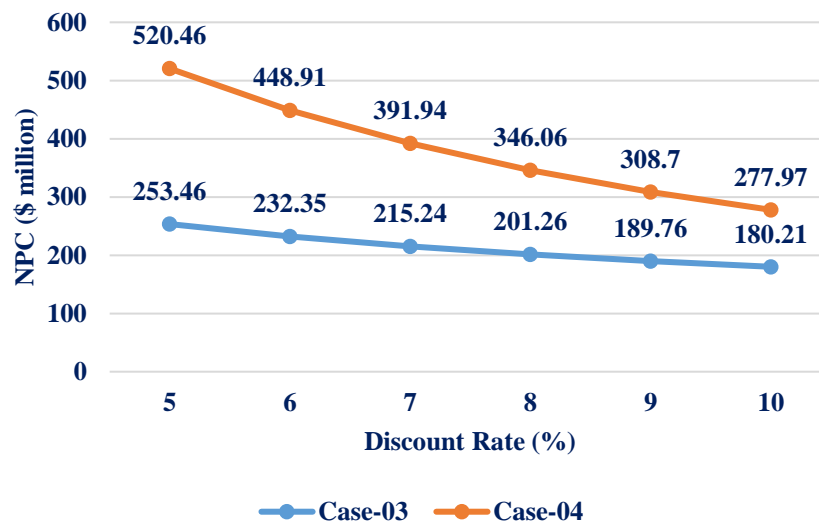


Figure 7-63: Impact of Variation in Discount Rate

The system NPC progresses with the rise of the inflation rate, shown in Fig. 7-64. The base case's inflation rate was assumed to be 2%, and it is adjusted from 1% to 6% in this sensitivity analysis. The results, illustrated in Fig. 7-64, show that Case-03 has a lower NPC than Case-04 for all inflation rate values. The sensitivity assessment of all economic parameters strongly supports that Case-04 is not economically profitable at any point of view, compared to Case-03.

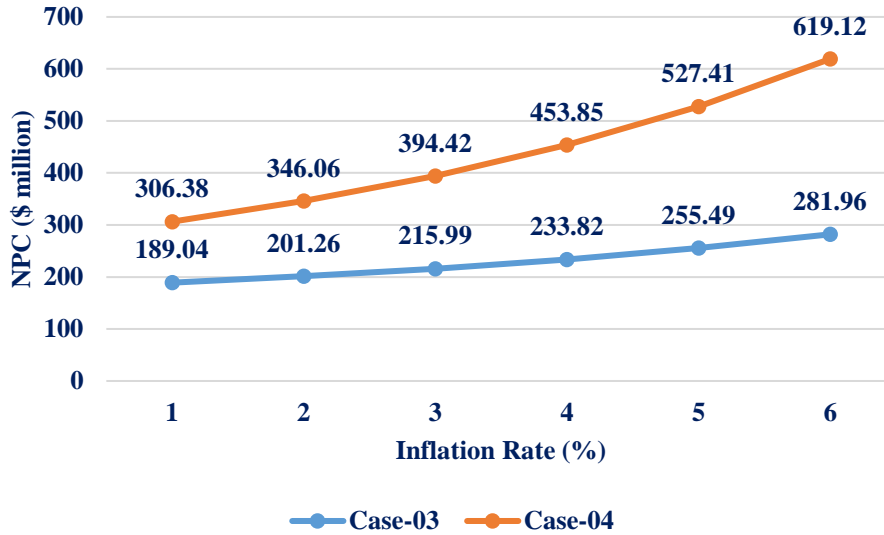


Figure 7-64: Impact of Variation in the Inflation Rate

7.2.6. Assessment of Sensitivity to Variation in Renewable Resources

Solar irradiance, wind speed, and streamflow may rise or fall at any time of the year. Hence, another sensitivity analysis is handled here by changing the solar irradiance and the wind speed by $\pm 10\%$. The purpose of this sensitivity assessment is to evaluate if Case-04 is analogous to Case-03 at any point of resource alteration. The sensitivity assessment is not conducted for the streamflow since it does not fluctuate much throughout a year for small-scale run-of-river hydro plants [157].

The optimization algorithm suggests the number of generation components based on resource availability. If any resource availability is reduced, the optimization either chooses another generation source or incorporates more identical elements to fulfill the demand. The PV panels and WTs are recognized as the least contributor to NPC in the earlier sensitivity analysis. Therefore, due to the unavailability of either solar irradiance or wind speed, the optimization will either pick some other high-priced generation sources or add more WTs and PV panels. Thus, the NPC is increased for the decrease of solar irradiance and wind speed pointed in Fig. 7-65 and Fig. 7-66. Similarly, if the solar irradiance and the wind speed are increased, the PSO optimization will avoid including a large number of PV panels, WTs, and high-cost generation sources. Hence, the NPC will be decreased, as

illustrated in Fig. 7-65 and Fig. 7-66. Though the NPC is decreasing with the increase of solar irradiance and wind speed, the NPC of Case-03 is still not comparable to the NPC of Case-04. Case-04 has a higher NPC than Case-03 for all cases, presented in Fig. 7-65 and Fig. 7-66. It should also be noticed that the wind speed variation strongly affects the NPC compared to the variations in solar irradiance due to the lower installation cost of WT.

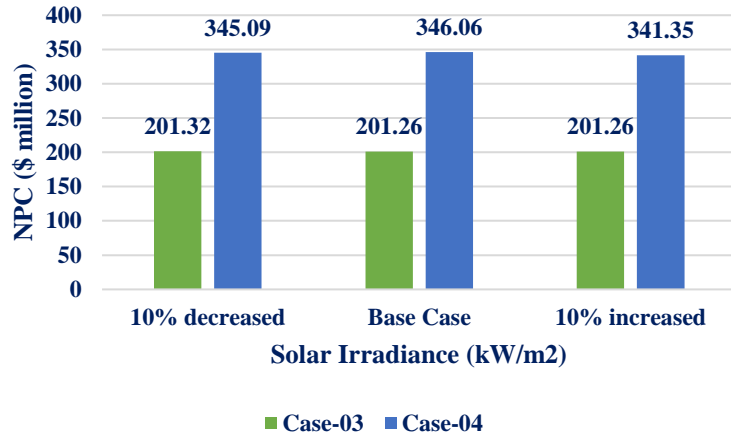


Figure 7-65: Impact of Variation in the Solar Irradiance

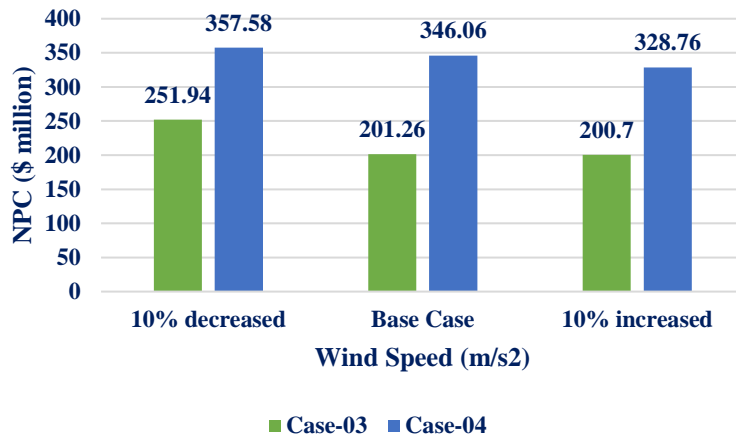


Figure 7-66: Impact of Variation in the Wind Speed

7.2.7. Assessment of Sensitivity to Variation in PV panels and WT Availability

This sub-section assesses the variation in the NPC of Case-03 and Case-04 due to the alteration of PV panel and WT availability. The number of installed PV panels and WTs depends on the available spaces of the project location, user requirements on renewable energy fraction, and the project site's transport facility. The NPC changes with the inclusion or reduction of the PV panels and WTs. Therefore, this sub-section investigates the consequences of variation in PV panel and WT availability for Case-03 and Case-04. The

run-of-river system is kept outside of this analysis since it is not easy to increase the hydroelectric plant size instantly. The BG is also not tested in this part as the generation in BG depends on the number of available cattle.

The maximum available number of the PV panels and the WTs have been adjusted from -50% to 500% in the optimization problem to reflect the variation in PV panel and WT availability. Fig. 7-67, Fig. 7-68, Fig. 7-69 depict the NPC variety due to differences in PV panel availability, WT availability, and both. Fig. 7-67 shows that the NPC of Case-03 does not change much due to the changes in PV panel availability. It implies that the optimization does not include PV panels in the optimal N-R MHES, even if the PV panel availability is extended. The NPC of Case-04 decreases with the increase of PV panel availability. However, the NPC also does not change significantly for Case-04 for the increased number of PV panel availability, signifying PV panel requirement is limited for the optimal diesel-fired MEG (Case-04). Fig. 7-68 shows that the NPC starts decreasing with the increased number of available WTs for both Case-03 and Case-04. However, the NPC reduction sustains for a particular range of WT availability; the NPC does not vary beyond 200% changes of WTs for Case-04. Due to the lower installation cost and reasonable energy conversion efficiency of WTs, compared to solar PV panels, the PSO optimization includes more WTs rather than adding PV panels in this case. Since the increased availability of WTs includes more WTs and discard PV panels, the NPC is reduced. The corresponding NPC values in Fig. 7-68 for 200%, 300%, 400%, and 500% changes in WT availability should not differ, but these values are fluctuating a bit due to the iterative PSO algorithm. Since both the availability of PV panels and WTs have been changed in this case, Fig. 7-69 presents a similar variation, like Fig. 7-68, in the NPC for Case-03 and Case-04. The degree of changes in the NPC is higher in Fig. 7-69 due to the combined effect of both changes.

By analyzing Fig. 7-67, Fig. 7-68, and Fig. 7-69, Case-03 is always more competent in accomplishing the demand. Another finding from this study is that installing a massive number of renewable sources, such as PV panels and WTs, may not be profitable for HESs; optimal planning is mandatory for these kinds of systems. This analysis also verifies that the assumptions made for considering the variable limits in the optimization problem are conservative. Furthermore, this part of the investigation shows that a 100% RES-based energy system may not be an economic system compared to HESs.

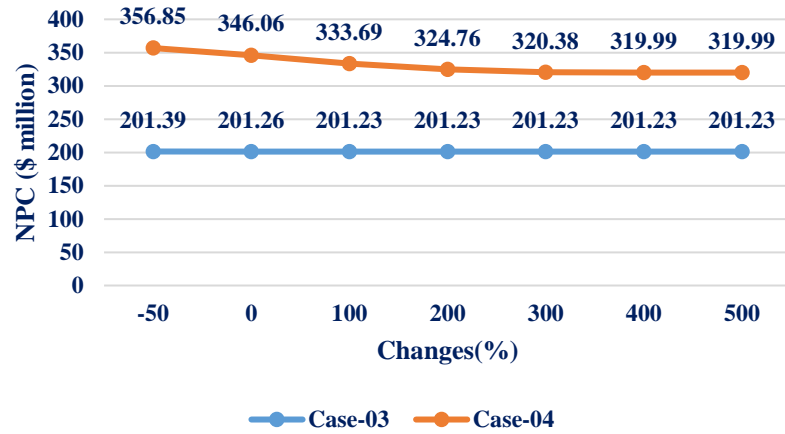


Figure 7-67: Impact of Variation in PV Panels Availability

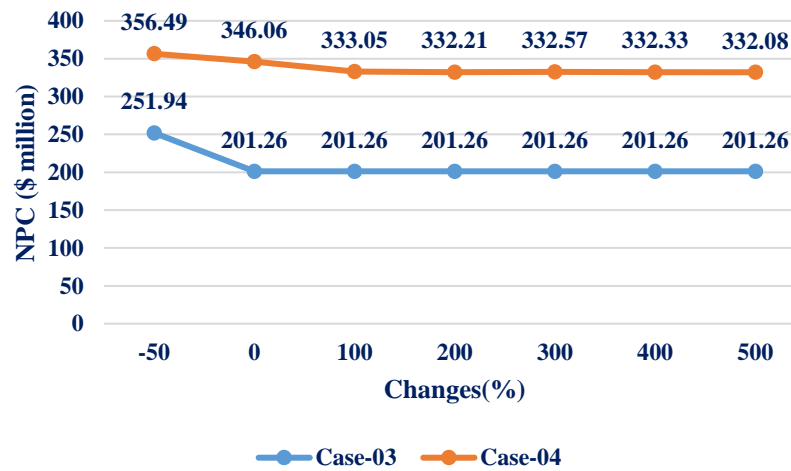


Figure 7-68: Impact of Variation in WT Availability

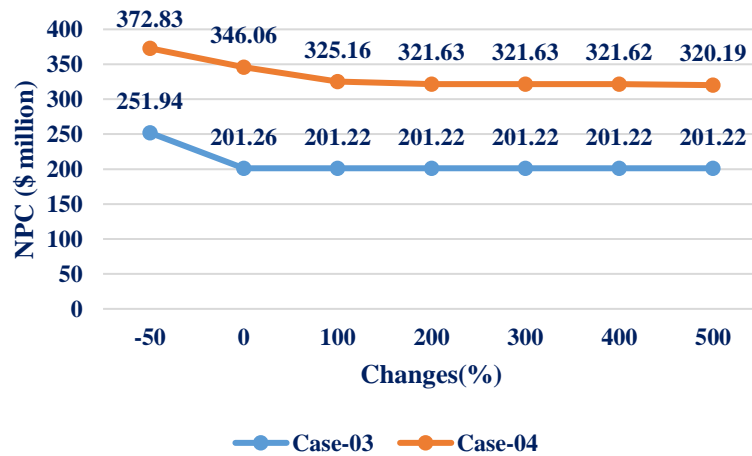


Figure 7-69: Impact of Variation in both PV Panels and WT Availability

Chapter 8: Conclusions and Recommendations

8.1. Summary and Conclusions

This research introduces three distinct nuclear-renewable hybridization approaches, i.e., "Direct Coupling," "Single Resource and Multiple Products-based Coupling," and "Multiple Resources and Multiple Products-based Coupling." The study recognizes "Multiple Resources and Multiple Products-based Coupling" as the most useful hybridization technique. The simulation results show that "Multiple Resources and Multiple Products-based N-R MHES" provides the lowest NPC (\$ 201.26 million) compared to "Directly coupled N-R MHES" (\$ 345.94 million) and "Single Resource and Multiple Products-based N-R MHES" (\$ 305.84 million) for the base case. The results also confirm that all the systems provide an adequate margin of reliability for the base case. The sensitivity analysis proves that "Multiple Resources and Multiple Products-based N-R MHES" remains the most effective hybridization technique despite the variation in key input parameters, such as daily demand peak, seasonal demand peak, average system demand, equipment cost, capacity factor, project lifetime, inflation rate, and nominal discount rate. "Directly coupled N-R MHES" has technical advantages, such as full resource usage, but it is not a profitable investment. "Single Resource and Multiple Products-based Coupled system" is challenging to meet the variable demand; the MMR unit's capacity is not utilized properly in this case. "Multiple Resources and Multiple Products-based Coupled N-R MHES" provides outstanding performance for dynamic load by using the resource capacity suitably.

The second part of the investigation tells that MMRs could be an excellent replacement for diesel Gensets within MEGs in terms of technical, economic, and environmental aspects. The significant fuel cost and the frequent replacement of diesel Gensets cause the diesel-fired MEG extremely expensive. Though MMRs have substantial capital cost, the lower fuel cost and other costs make the MMR-based MEG economical. The environmental issues are not counted in this study, but it is evident that the GHG emissions are excessively high for diesel Gensets. The NPC of the diesel-fired MEG is significantly higher than the most effective MMR-based MEG, and this statement is true for all scenarios investigated in the sensitivity analysis. Diesel Gensets are used as a surrogate of all fossil-fired generators in this study. However, MMRs could also be an ideal replacement for coal-based and natural-gas-based generators within MEGs. The sensitivity analysis reveals that N-R MHESs are more cost-effective and technically reliable than traditional MEGs or stand-alone MMR-based energy systems. The sensitivity assessment considers the key input parameter, e.g., daily peak demand, yearly peak demand, average energy demand, component cost, solar irradiance, wind speed, project lifespan, inflation rate, discount rate, PV panel availability, and WT availability, that has a substantial influence on overall system economy and system resiliency. The hybridization between MMRs and renewables maximizes the benefits of both resources. N-R MHESs also support a more straightforward energy management strategy.

8.2. Contributions of the Thesis

The primary goal of this study is to provide an innovative and sustainable solution to the energy crisis for off-grid applications. To attain such an objective, this study evaluates the potentiality of replacing traditional fossil-fired generators with MMRs within MEGs and proposes three different hybridization techniques for nuclear-renewable integration. Detailed modeling and analysis have been carried out to identify the best hybridization method for micro-level nuclear-renewable integration. The best hybrid nuclear-renewable system is compared with a conventional diesel Genset-based MEG. The results obtained in all cases have been validated by sensitivity analysis. However, the main contribution of this research can be summarized as follows.

- A comprehensive literature review is conducted to identify the problem and gaps in the research topic. A reasonable solution is presented to the identified research problem to bridge the gap.
- Three different coupling methods for nuclear-renewable integration are introduced in this study. The hybridization procedures, along with energy management algorithms, are implemented in the MATLAB environment. Though the previous works on nuclear-renewable integrated systems are carried out on physical component-based simulators, such as Modelica and RAVEN, this study is carried out in the most versatile and popular simulator, MATLAB.
- A metaheuristic optimization algorithm, PSO, is developed and executed in the proposed system arrangements to identify the systems' best configuration. System reliability constraints are efficiently utilized in the optimization problem, rather than using them as an objective function. It reduces optimization complexity.
- One of the most traditional fossil fuel-based power generation sources, diesel Genset, is compared with the best nuclear-renewable hybridized configuration. The study affirms the cost-competency, reliability, performability, and resiliency of the proposed nuclear-renewable hybridized system over the traditional MEG.
- Since the demand varies from region to region and the availability of RESs are highly dependent on the meteorological condition, a sensitivity analysis is carried out widely to determine the system parameters' effect on planning, economy, and resiliency. The sensitivity analysis ensures that the results obtained in the base cases are not confined to a particular project location or specific load demand; the conclusions hold regardless of the demand and project site. The sensitivity analysis also provides ample information to the system planners regarding the impact of different system equipment on system economy and resiliency. It will help in the deployment stage in the future.

8.3. Safety Aspects of N-R MHES

It is important to ensure safety of microreactor operation as the main component within N-R MHES. The safety of microreactors has already been demonstrated in several studies. Microreactors have an enhanced-safety features, and it provide a secure solution to the international energy crisis. MMR plants do not need any active safety system. The natural convection process removes the generated heat of the core. Plants can operate safely without taking support from external electric and water supply systems. The reactor temperature also does not increase suddenly due to the high-performance fuel module. Hence, the fuel module provides a large-scale safety margin. The molten salt is used as thermal storage in MMRs that provide both electric power and process heat. Because of modularity and scalability, multiple MMR units can be rearranged to support different ranges of power demand [77].

Microreactors are new, and it includes several unique characteristics. Therefore, research is progressing to develop regulatory documents for microreactors. Some initial considerations for regulatory review of microreactors have been addressed in [208], but this document only presents limited ideas on microreactor safety assessments. Probabilistic Risk Assessment (PRA) can address the inherent issues related to microreactors. However, PRA model will be relatively simple for microreactors compared to traditional large reactors. Licensing Basic Events (LBE), such as Anticipated Operational Occurrences (AOOs), Design Basis Events (DBEs), and Beyond Design Basis Events (BDBEs), and Design Basic Accidents (DBAs), need to be identified for microreactor sites. The expected frequencies for different events of microreactor sites are listed in Table 8-1 [208].

Table 8-1: Different types of Events Associated with Microreactor Facility

Event Category	Types	Anticipated Frequency (per reactor year)
May challenge safety goals	Rare	$<10^{-5}$
Expected to happen during the lifespan of the population of plants	Infrequent	$<10^{-2}$ to $\geq 10^{-5}$
Expected to happen during lifespan	Frequent	$\geq 10^{-2}$

As microreactors will be operated with less human interventions and managed remotely, several guidelines and operational procedures for MMR may not be the same as traditional NPPs. The anticipated number of accidents and events will be small for microreactors [208]. Some documents that provide preliminary idea on development of new regulatory documents for microreactors are listed below:

- **IAEA-TECDOC-1915:** Considerations for Environmental Impact Assessment for Small Modular Reactors.

- **NEI 18-04:** Risk-Informed Performance-Based Guidance for Non-Light Water Reactor Licensing Basis Development.
- **NRC Draft Regulatory Guide 1353:** Guidance for a Technology-Inclusive, Risk-Informed, and Performance-Based Methodology to Inform the Licensing Basis and Content of Applications for Licenses, Certifications, and Approvals for Non-Light-Water Reactors.
- **NUREG-1860:** Feasibility Study for a Risk-Informed and Performance-Based Regulatory Structure for Future Plant Licensing, Volumes 1 and 2.

Microreactors are still in the R&D stage. Several manufacturers are working on the development and demonstration of microreactors that will be ready in the near future. Possible challenges to the development of microreactor-based energy systems are identified in some studies. “Security by design” is a new and potential approach that can be integrated with the unique microreactor design process [209], while “Safeguards by Design” and “Safety by Design” methods have already been used practiced in traditional large-scale reactors [210]. “Security by design” includes Safety, Security, and Safeguard (3S) features in nuclear reactors' design. “Fault Tree Analysis” can help to achieve the implementation of the “Security by design” approach [211]. A comprehensive review process on proposed nuclear facilities and experts can identify new microreactors' potential risks and solutions. The solution may include verification tools for sealed fuel module, verification of spent fuel tank condition, and confirmation of passive safety system.

Since N-R MHESs occupy small area, the terrestrial impact is also small for these kind of systems. Effects on air quality, sound quality, and dust generation during the microreactor facility's construction stage are limited compared to traditional large-scale NPPs. Water management and waste management facilities are very important parts for N-R MHESs deployment. Although radiological hazards are always identified as a potential risk for nuclear facilities, microreactors' inherent passive safety system reduces the risk significantly. The spent fuel transportation system requires a high level of precaution. N-R MHES development also requires special considerations on fish, fish habitats, aquatic species, and migratory birds around the facility. Moreover, inputs from indigenous peoples of the selected project is also a vital factor in the development of N-R MHES [78].

The operation of renewable energy generation sources is considerably safe. For example, solar panel operation requires glasses and gloves to minimize the risks of electric shock. Metallic jewelry is also avoided during working with electric instruments [212]. In wind power generation, a safety zone is maintained around wind turbines during operation. People are prohibited from entering this zone as a safety precaution [213]. Several regulatory documents for testing, installing, and inspecting solar PV panels and WTs are available from different organizations (e.g., CSA and IEC). These types of regulatory documents should be followed during the development stage of N-R MHESs. By considering the safety aspects of all component of N-R MHESs, it is expected that N-R MHESs are competent in performing safely.

8.4. Future Work and Recommendations

This research intends to consolidate nuclear and renewable sources to operate in tandem. Several works need to be done to determine the specific application of N-R MHESs. The following can be proposed as future works.

- Different electric, electrochemical, mechanical, and thermal energy storage could be combined in N-R MHESs depending on the applications and the availability to make the system more versatile.
- The uncertainty and the variability of the resources input data, e.g., temperature, solar irradiance, wind speed, and mass flow rate, can be introduced in the optimization model in future research.
- The cost associated with alternative energy generation sources that operate during equipment replacement, such as the nuclear fuel module, WT, PV panel, and diesel Genset, should be incorporated in the future work. The energy management procedure during a specific component replacement period should also be documented in future research.
- The cost of real estate for nuclear facilities and renewable generation sources (where applicable) should be included in the future study if demanded to develop a realistic project outline.
- “Traceability Matrix” format can be adopted in the future to arrange the assumptions for extended research of this study.
- Electrification transportation is one of the most crucial issues at present, which has a massive impact on energy systems. Therefore, EV fast-charging stations could be incorporated and evaluated with N-R MHESs for remote locations.
- A Comprehensive licensing procedure for N-R MHESs should be focused on future research.
- The maximum acceptable limits of the reliability constraints used in this research, such as LPSP and SEF, can be varied and conducted another sensitivity analysis to see their impacts on NPC.

- Different energy management algorithms can be employed and tested to quantify the benefits of different N-R MHESs for various applications.
- Alternative artificial intelligent optimization algorithms, e.g. Genetic Algorithm (GA), Ant Colony Optimizer (ACO), PSO, Artificial Bee Colony (ABC) optimization, Cuckoo Search (CS), and Simulated Annealing (SA), can also be utilized in future to obtain the optimal system configuration.
- Flexible operation of MMRs can be adopted in future research for N-R MHESs to evaluate the techno-economic performance analysis.
- The quality of the heat associated with N-R MHESs should be examined and quantified in future investigations to identify specific applications.
- MMR model could be developed in MATLAB Simulink interface for technical and economic evaluation. The developed model could be incorporated with other simulators for techno-economic assessment; this will create a multi-dimensional research area.

REFERENCES

- [1] M. Usman, M. T. Khan, A. S. Rana, and S. Ali, “Techno-economic analysis of hybrid solar-diesel-grid connected power generation system,” *J. Electr. Syst. Inf. Technol.*, vol. 5, no. 3, pp. 653–662, Dec. 2018, doi: 10.1016/j.jesit.2017.06.002.
- [2] H. Ritchie and M. Roser, “Air Pollution,” *Our World Data*, Apr. 2017, Accessed: Aug. 11, 2020. [Online]. Available: <https://ourworldindata.org/air-pollution>.
- [3] H. Ritchie and M. Roser, “Energy,” *Our World Data*, Mar. 2014, Accessed: Jul. 15, 2020. [Online]. Available: <https://ourworldindata.org/energy>.
- [4] L. Freris and D. Infield, *Renewable Energy in Power Systems*. © 2008, John Wiley & Sons, Ltd.
- [5] “What is Sustainable Energy and its types- Conserve Energy Future.” <https://www.conserve-energy-future.com/sustainableenergy.php> (accessed Dec. 09, 2019).
- [6] S. Jarvis, O. Deschenes, and A. Jha, “The Private and External Costs of Germany’s Nuclear Phase-Out,” National Bureau of Economic Research, Cambridge, MA, w26598, Dec. 2019, doi: 10.3386/w26598.
- [7] A. van der Merwe, “Nuclear energy saves lives,” *Nature*, vol. 570, no. 7759, Art. no. 7759, Jun. 2019, doi: 10.1038/d41586-019-01749-8.
- [8] G. Luderer *et al.*, “Environmental co-benefits and adverse side-effects of alternative power sector decarbonization strategies,” *Nat. Commun.*, vol. 10, no. 1, p. 5229, Dec. 2019, doi: 10.1038/s41467-019-13067-8.
- [9] C. McCombie and M. Jefferson, “Renewable and nuclear electricity: Comparison of environmental impacts,” *Energy Policy*, vol. 96, pp. 758–769, Sep. 2016, doi: 10.1016/j.enpol.2016.03.022.
- [10] “Electricity – Global Energy Review 2020 – Analysis,” *IEA*. <https://www.iea.org/reports/global-energy-review-2020/electricity> (accessed Jul. 16, 2020).
- [11] A. Hirsch, Y. Parag, and J. Guerrero, “Microgrids: A review of technologies, key drivers, and outstanding issues,” *Renew. Sustain. Energy Rev.*, vol. 90, pp. 402–411, Jul. 2018, doi: 10.1016/j.rser.2018.03.040.
- [12] H. A. Gabbar and A. Zidan, “Optimal scheduling of interconnected micro energy grids with multiple fuel options,” *Sustain. Energy Grids Netw.*, vol. 7, pp. 80–89, Sep. 2016, doi: 10.1016/j.segan.2016.06.006.
- [13] P. Breeze, “An Introduction to Combined Heat and Power,” in *Combined Heat and Power*, Elsevier, 2018, pp. 1–11.
- [14] M. F. Ruth, O. R. Zinaman, M. Antkowiak, R. D. Boardman, R. S. Cherry, and M. D. Bazilian, “Nuclear-renewable hybrid energy systems: Opportunities, interconnections, and needs,” *Energy Convers. Manag.*, vol. 78, pp. 684–694, Feb. 2014, doi: 10.1016/j.enconman.2013.11.030.
- [15] “Life-cycle emissions - Canadian Nuclear Association.” <https://cna.ca/why-nuclear-energy/clean/life-cycle-emissions/> (accessed Jul. 05, 2020).
- [16] N. Honarmand, “Key Performance Indicators Modeling for Optimized Microgrid Configuration,” p. 141.

- [17] S. M. Bragg-Sitton *et al.*, “Nuclear-Renewable Hybrid Energy Systems: 2016 Technology Development Program Plan,” INL/EXT--16-38165, 1333006, Mar. 2016. doi: 10.2172/1333006.
- [18] Ş. Y. Balaman, “Uncertainty Issues in Biomass-Based Production Chains,” in *Decision-Making for Biomass-Based Production Chains*, Elsevier, 2019, pp. 113–142.
- [19] J. Landsberg and P. Sands, “Modelling Tree Growth,” in *Terrestrial Ecology*, vol. 4, Elsevier, 2011, pp. 221–240.
- [20] “Goal 7: Affordable & Clean Energy - UN SDG.” <https://www.gvicanada.ca/goal-7-affordable-and-clean-energy/> (accessed Dec. 10, 2019).
- [21] H. Blanco and A. Faaij, “A review at the role of storage in energy systems with a focus on Power to Gas and long-term storage,” *Renew. Sustain. Energy Rev.*, vol. 81, pp. 1049–1086, Jan. 2018, doi: 10.1016/j.rser.2017.07.062.
- [22] “The Biggest Batteries Coming Soon to a Grid Near You.” <https://www.greentechmedia.com/articles/read/the-biggest-batteries-coming-soon-to-a-grid-near-you> (accessed Jul. 03, 2020).
- [23] J. P. Deane, B. P. Ó Gallachóir, and E. J. McKeogh, “Techno-economic review of existing and new pumped hydro energy storage plant,” *Renew. Sustain. Energy Rev.*, vol. 14, no. 4, pp. 1293–1302, May 2010, doi: 10.1016/j.rser.2009.11.015.
- [24] “Comparing Fuel Cell Technologies,” *GenCell - Fuel Cell Generators*. <https://www.gencellenergy.com/news/comparing-fuel-cell-technologies/> (accessed Jul. 03, 2020).
- [25] A. M. Eltamaly and M. A. Mohamed, “Optimal Sizing and Designing of Hybrid Renewable Energy Systems in Smart Grid Applications,” in *Advances in Renewable Energies and Power Technologies*, Elsevier, 2018, pp. 231–313.
- [26] “Diesel Engine Generators Life Expectancy - How Long Do They Last?” <https://www.wpowerproducts.com/news/diesel-engine-life-expectancy/> (accessed Jul. 03, 2020).
- [27] S. Suman, “Hybrid nuclear-renewable energy systems: A review,” *J. Clean. Prod.*, vol. 181, pp. 166–177, Apr. 2018, doi: 10.1016/j.jclepro.2018.01.262.
- [28] H. A. Gabbar, M. R. Abdussami, and Md. I. Adham, “Techno-Economic Evaluation of Interconnected Nuclear-Renewable Micro Hybrid Energy Systems with Combined Heat and Power,” *Energies*, vol. 13, no. 7, p. 1642, Apr. 2020, doi: 10.3390/en13071642.
- [29] J. Augutis, L. Martišauskas, and R. Krikštolaitis, “Energy mix optimization from an energy security perspective,” *Energy Convers. Manag.*, vol. 90, pp. 300–314, Jan. 2015, doi: 10.1016/j.enconman.2014.11.033.
- [30] S. Bragg-Sitton, R. Boardman, M. Ruth, O. Zinaman, C. Forsberg, and J. Collins, “Integrated Nuclear-Renewable Energy Systems: Foundational Workshop Report,” INL/EXT--14-32857-Rev.1, NREL/TP--6A20-62778, 1170315, Aug. 2014. doi: 10.2172/1170315.
- [31] T. J. Harrison and M. S. Greenwood, “Nuclear Hybrid Energy Systems Initial Integrated Case Study Development and Analysis,” ORNL/TM--2016/707, 1339399, Dec. 2016. doi: 10.2172/1339399.

- [32] X. Zhou, T. Guo, and Y. Ma, "An overview on microgrid technology," in *2015 IEEE International Conference on Mechatronics and Automation (ICMA)*, Beijing, China, Aug. 2015, pp. 76–81, doi: 10.1109/ICMA.2015.7237460.
- [33] Y. Koraz and A. Gabbar, "Risk analysis and self-healing approach for resilient interconnect micro energy grids," *Sustain. Cities Soc.*, vol. 32, pp. 638–653, Jul. 2017, doi: 10.1016/j.scs.2017.05.010.
- [34] H. A. Gabbar, R. Islam, M. U. Isham, and V. Trivedi, "Risk-based performance analysis of microgrid topology with distributed energy generation," *Int. J. Electr. Power Energy Syst.*, vol. 43, no. 1, pp. 1363–1375, Dec. 2012, doi: 10.1016/j.ijepes.2012.05.061.
- [35] H. A. Gabbar, L. Bower, D. Pandya, A. Agarwal, M. U. Tomal, and F. R. Islam, "Resilient micro energy grids with gas-power and renewable technologies," in *The 2nd IEEE Conference on Power Engineering and Renewable Energy (ICPERE) 2014*, Bali, Indonesia, Dec. 2014, pp. 1–6, doi: 10.1109/ICPERE.2014.7067225.
- [36] "MOBISMART Off-Grid Mobile Power & Storage | Smart Off-Grid Power Technologies | Replace diesel generators in remote locations with mobile clean power | 855-806-0188," *MOBISMART Off-Grid Mobile Power & Storage*. <https://mobismart.ca/> (accessed May 23, 2020).
- [37] G. P. Giatrakos, T. D. Tsoutsos, P. G. Mouchtaropoulos, G. D. Naxakis, and G. Stavrakakis, "Sustainable energy planning based on a stand-alone hybrid renewableenergy/hydrogen power system: Application in Karpathos island, Greece," *Renew. Energy*, vol. 34, no. 12, pp. 2562–2570, Dec. 2009, doi: 10.1016/j.renene.2009.05.019.
- [38] O. H. Mohammed, Y. Amirat, and M. Benbouzid, "Particle Swarm Optimization Of a Hybrid Wind/Tidal/PV/Battery Energy System. Application To a Remote Area In Bretagne, France," *Energy Procedia*, vol. 162, pp. 87–96, Apr. 2019, doi: 10.1016/j.egypro.2019.04.010.
- [39] Mengjun Ming, Rui Wang, Yabing Zha, and Tao Zhang, "Multi-Objective Optimization of Hybrid Renewable Energy System Using an Enhanced Multi-Objective Evolutionary Algorithm," *Energies*, vol. 10, no. 5, p. 674, May 2017, doi: 10.3390/en10050674.
- [40] L. An and T. Tuan, "Dynamic Programming for Optimal Energy Management of Hybrid Wind–PV–Diesel–Battery," *Energies*, vol. 11, no. 11, p. 3039, Nov. 2018, doi: 10.3390/en11113039.
- [41] H. M. K. Al-Masri, A. Al-Quraan, A. AbuElrub, and M. Ehsani, "Optimal Coordination of Wind Power and Pumped Hydro Energy Storage," *Energies*, vol. 12, no. 22, p. 4387, Nov. 2019, doi: 10.3390/en12224387.
- [42] L. M. Halabi, S. Mekhilef, L. Olatomiwa, and J. Hazelton, "Performance analysis of hybrid PV/diesel/battery system using HOMER: A case study Sabah, Malaysia," *Energy Convers. Manag.*, vol. 144, pp. 322–339, Jul. 2017, doi: 10.1016/j.enconman.2017.04.070.
- [43] E. Abdollahi, H. Wang, S. Rinne, and R. Lahdelma, "Optimization of energy production of a CHP plant with heat storage," in *2014 IEEE Green Energy and Systems Conference (IGESC)*, Long Beach, CA, USA, Nov. 2014, pp. 30–34, doi: 10.1109/IGESC.2014.7018636.

- [44] R. Seyed-Ehsan, M. S. Javadi, and A. Esmaeel Nezhad, "Mixed-integer nonlinear programming framework for combined heat and power units with nonconvex feasible operating region Feasibility, optimality, and flexibility evaluation.pdf," *Int. Trans. Electr. Energy Syst.*, vol. 29, no. 3, p. 18, 2019, doi: doi:10.1002/etep.2767.
- [45] P. Hu, C. Cao, and S. Dai, "Optimal dispatch of combined heat and power units based on particle swarm optimization with genetic algorithm," *AIP Adv.*, vol. 10, no. 4, p. 045008, Apr. 2020, doi: 10.1063/1.5145074.
- [46] A. Awad, P. Bazan, and R. German, "Optimized Operation of PV/T and Micro-CHP Hybrid Power Systems," *Technol. Econ. Smart Grids Sustain. Energy*, vol. 1, no. 1, p. 2, Dec. 2016, doi: 10.1007/s40866-016-0004-3.
- [47] T. Fang and R. Lahdelma, "Optimization of combined heat and power production with heat storage based on sliding time window method," *Appl. Energy*, vol. 162, pp. 723–732, Jan. 2016, doi: 10.1016/j.apenergy.2015.10.135.
- [48] S. M. Bragg-Sitton, R. Boardman, and I. N. Laboratory, "Rethinking the Future Grid: Integrated Nuclear Renewable Energy Systems: Preprint," p. 14.
- [49] F. Bienvenu and S. Herring, "Potential of industry for load regulation," Idaho National Laboratory, Idaho National Laboratory, 2014.
- [50] M. Ruth, D. Cutler, F. Flores-Espino, and G. Stark, "The Economic Potential of Nuclear-Renewable Hybrid Energy Systems Producing Hydrogen," NREL/TP-6A50-66764, 1351061, Apr. 2017. doi: 10.2172/1351061.
- [51] H. A. Gabbar and M. R. Abdussami, "Feasibility Analysis of Grid-Connected Nuclear-Renewable Micro Hybrid Energy System," in *2019 IEEE 7th International Conference on Smart Energy Grid Engineering (SEGE)*, Oshawa, ON, Canada, Aug. 2019, pp. 294–298, doi: 10.1109/SEGE.2019.8859925.
- [52] M. Mishra, N. K. Saxena, and P. Mishra, "ANN Based AGC for Hybrid Nuclear-Wind Power System," in *2016 International Conference on Micro-Electronics and Telecommunication Engineering (ICMETE)*, GHAZIABAD, India, Sep. 2016, pp. 410–415, doi: 10.1109/ICMETE.2016.116.
- [53] R. Almalki, J. Piwowar, and J. Siemer, "Geographical Considerations in Site Selection for Small Modular Reactors in Saskatchewan," *Geosciences*, vol. 9, no. 9, p. 402, Sep. 2019, doi: 10.3390/geosciences9090402.
- [54] O. Elma and H. A. Gabbar, "Design and Analysis of Mobile Hybrid Energy System for Off-Grid Applications," in *2019 International Conference on Power Generation Systems and Renewable Energy Technologies (PGSRET)*, Istanbul, Turkey, Aug. 2019, pp. 1–6, doi: 10.1109/PGSRET.2019.8882703.
- [55] M. R. Abdussami and H. A. Gabbar, "Flywheel-based Micro Energy Grid for Reliable Emergency Back-up Power for Nuclear Power Plant," p. 6.
- [56] M. F. Ruth, O. R. Zinaman, M. Antkowiak, R. D. Boardman, R. S. Cherry, and M. D. Bazilian, "Nuclear-renewable hybrid energy systems: Opportunities, interconnections, and needs," *Energy Convers. Manag.*, vol. 78, pp. 684–694, Feb. 2014, doi: 10.1016/j.enconman.2013.11.030.
- [57] C. Rabiti *et al.*, "Strategy and gaps for modeling, simulation, and control of hybrid systems," INL/EXT--15-34877, 1213628, Apr. 2015. doi: 10.2172/1213628.
- [58] J. Chen, H. E. Garcia, J. S. Kim, and S. M. Bragg-Sitton, "Operations Optimization of Nuclear Hybrid Energy Systems," *Nucl. Technol.*, vol. 195, no. 2, pp. 143–156, Aug. 2016, doi: 10.13182/NT15-130.

- [59] W. Binder, C. Paredis, and H. Garcia, “Hybrid Energy System Modeling in Modelica,” Mar. 2014, pp. 979–988, doi: 10.3384/ecp14096979.
- [60] A. Epiney, J. Chen, and C. Rabiti, “Status on the Development of a Modeling and Simulation Framework for the Economic Assessment of Nuclear Hybrid Energy Systems (FY 16).” Idaho National Laboratory, Sep. 2016.
- [61] L. Boldon, P. Sabharwall, S. Bragg-Sitton, N. Abreu, and L. Liu, “Nuclear Renewable Energy Integration: An Economic Case Study,” *Int. J. Energy Environ. Econ.*
- [62] T. E. Baker, A. S. Epiney, C. Rabiti, and E. Shittu, “Optimal sizing of flexible nuclear hybrid energy system components considering wind volatility,” *Appl. Energy*, vol. 212, pp. 498–508, Feb. 2018, doi: 10.1016/j.apenergy.2017.12.061.
- [63] J. S. Kim, R. D. Boardman, and S. M. Bragg-Sitton, “Dynamic performance analysis of a high-temperature steam electrolysis plant integrated within nuclear-renewable hybrid energy systems,” *Appl. Energy*, vol. 228, pp. 2090–2110, Oct. 2018, doi: 10.1016/j.apenergy.2018.07.060.
- [64] H. E. Garcia *et al.*, “Dynamic performance analysis of two regional Nuclear Hybrid Energy Systems,” *Energy*, vol. 107, pp. 234–258, Jul. 2016, doi: 10.1016/j.energy.2016.03.128.
- [65] A. Borisova and D. Popov, “An option for the integration of solar photovoltaics into small nuclear power plant with thermal energy storage,” *Sustain. Energy Technol. Assess.*, vol. 18, pp. 119–126, Dec. 2016, doi: 10.1016/j.seta.2016.10.002.
- [66] A. Epiney, C. Rabiti, P. Talbot, and A. Alfonsi, “Economic analysis of a nuclear hybrid energy system in a stochastic environment including wind turbines in an electricity grid,” *Appl. Energy*, vol. 260, p. 114227, Feb. 2020, doi: 10.1016/j.apenergy.2019.114227.
- [67] J. D. Jenkins *et al.*, “The benefits of nuclear flexibility in power system operations with renewable energy,” *Appl. Energy*, vol. 222, pp. 872–884, Jul. 2018, doi: 10.1016/j.apenergy.2018.03.002.
- [68] D. Mikkelsen, C.-W. Chang, SacitM. Cetiner, A. L. Qualls, J. M. Doster, and T. N. Dinh, “Small Modular Reactor Modeling Using Modelica for Nuclear-Renewable Hybrid Energy Systems Applications.” Idaho National Laboratory, Oct. 2015.
- [69] Technical Meeting on Nuclear-Renewable Hybrid Energy Systems for Decarbonized Energy Production and Cogeneration and International Atomic Energy Agency, Eds., *Nuclear-renewable hybrid energy systems for decarbonized energy production and cogeneration: proceedings of a technical meeting held in Vienna, 22-25 October 2018*. 2019.
- [70] A. S. Epiney, C. Rabiti, P. W. Talbot, J. S. Kim, S. M. Bragg-Sitton, and J. Richards, “Case Study: Nuclear-Renewable-Water Integration in Arizona,” INL/EXT--18-51359-Rev000, 1495196, Sep. 2018. doi: 10.2172/1495196.
- [71] J. S. Kim and H. E. Garcia, “Nuclear-Renewable Hybrid Energy System for Reverse Osmosis Desalination Process\,” *Trans. Am. Nucl. Soc.*, vol. 112, p. 5, 2015.
- [72] M. Ruth *et al.*, “The Economic Potential of Two Nuclear-Renewable Hybrid Energy Systems,” p. 275.
- [73] M. Ruth, D. Cutler, F. Flores-Espino, G. Stark, and T. Jenkin, “The Economic Potential of Three Nuclear-Renewable Hybrid Energy Systems Providing Thermal Energy to Industry,” NREL/TP-6A50-66745, 1335586, Dec. 2016. doi: 10.2172/1335586.

- [74] E. K. Redfoot and R. A. Borrelli, “Analysis of Nuclear Renewable Hybrid Energy Systems Modeling and Nuclear Fuel Cycle Simulators,” *Nucl. Technol.*, vol. 204, no. 3, pp. 249–259, Dec. 2018, doi: 10.1080/00295450.2018.1478590.
- [75] “Small nuclear power reactors - World Nuclear Association.” <https://www.world-nuclear.org/information-library/nuclear-fuel-cycle/nuclear-power-reactors/small-nuclear-power-reactors.aspx> (accessed Dec. 08, 2019).
- [76] N. Edson, P. Willson, B. Rakshi, and I. Kekwick, “Technology and Market Assessment of Micro Nuclear Reactors,” Nuvia Limited, Mar. 2016. [Online]. Available: <https://www.gov.uk/government/publications/market-and-technical-assessment-of-micro-nuclear-reactors>.
- [77] “USNC.” <https://usnc.com/> (accessed Dec. 09, 2019).
- [78] “Project Description for the Micro Modular Reactor™ Project at Chalk River,” p. 52.
- [79] “Nuclear Reactors | Nuclear Power Plant | Nuclear Reactor Technology - World Nuclear Association.” <https://www.world-nuclear.org/information-library/nuclear-fuel-cycle/nuclear-power-reactors/nuclear-power-reactors.aspx> (accessed Jul. 12, 2020).
- [80] “U-Battery.” <https://www.u-battery.com/> (accessed Jun. 07, 2019).
- [81] “Super-Heaters, Economisers & Air Heaters - Primasonics International Ltd.” <https://www.primasonics.com/applications/super-heaters-economisers-air-heaters> (accessed Aug. 03, 2020).
- [82] djysrv, “Karios, Moltex, See Progress in Funding; First Canadian SMR, an HTGR, Submits License Application to CNSC,” *Neutron Bytes*, Apr. 06, 2019. <https://neutronbytes.com/2019/04/06/karios-moltex-see-progress-in-funding/> (accessed Aug. 03, 2020).
- [83] IAEA, *Opportunities for Cogeneration with Nuclear Energy*. Vienna: IAEA, 2017.
- [84] *Opportunities for Cogeneration with Nuclear Energy*. Vienna: INTERNATIONAL ATOMIC ENERGY AGENCY, 2017.
- [85] “USNC.” <https://usnc.com/FCM.html> (accessed Jul. 14, 2020).
- [86] J. J. Powers and B. D. Wirth, “A review of TRISO fuel performance models,” *J. Nucl. Mater.*, vol. 405, no. 1, pp. 74–82, Oct. 2010, doi: 10.1016/j.jnucmat.2010.07.030.
- [87] D. Petti, A. Languille, P. Martin, and R. Ballinger, “DEVELOPMENT OF IMPROVED MODELS AND DESIGNS FOR COATED-PARTICLE GAS REACTOR FUELS,” Idaho National Engineering and Environmental Laboratory (INEEL), Idaho National Engineering and Environmental Laboratory (INEEL), Massachusetts Institute of Technology (MIT), INEEL/EXT-02-01493, Nov. 2002.
- [88] D. Petti *et al.*, “The DOE advanced gas reactor fuel development and qualification program,” *JOM*, vol. 62, no. 9, pp. 62–66, Sep. 2010, doi: 10.1007/s11837-010-0140-5.
- [89] P. Breeze, “Renewable Energy Combined Heat and Power,” in *Combined Heat and Power*, Elsevier, 2018, pp. 77–83.
- [90] H. Cho, A. D. Smith, and P. Mago, “Combined cooling, heating and power: A review of performance improvement and optimization,” *Appl. Energy*, vol. 136, pp. 168–185, Dec. 2014, doi: 10.1016/j.apenergy.2014.08.107.
- [91] H. I. Onovwiona and V. I. Ugursal, “Residential cogeneration systems: review of the current technology,” *Renew. Sustain. Energy Rev.*, vol. 10, no. 5, pp. 389–431, Oct. 2006, doi: 10.1016/j.rser.2004.07.005.

- [92] P. Breeze, “Combined Heat and Power Principles and Technologies,” in *Combined Heat and Power*, Elsevier, 2018, pp. 21–32.
- [93] M. A. Iqbal, M. Ahmadi, F. Melhem, S. Rana, A. Akbarzadeh, and A. Date, “Power Generation from Low Grade Heat Using Trilateral Flash Cycle,” *Energy Procedia*, vol. 110, pp. 492–497, Mar. 2017, doi: 10.1016/j.egypro.2017.03.174.
- [94] K. M. Laughlin and G. P. Reed, “BEHAVIOUR OF COAL ASH IN A PRESSURISED FLUIDISED BED GASIFIER,” in *1991 International Conference on Coal Science Proceedings*, Elsevier, 1991, pp. 396–399.
- [95] P. Breeze, *Combined Heat and Power*. Elsevier Ltd, 2018.
- [96] S. C. Bhatia, “19.5 Classification of cogeneration systems,” p. 16.
- [97] B. F. Tchanche, Gr. Lambrinos, A. Frangoudakis, and G. Papadakis, “Low-grade heat conversion into power using organic Rankine cycles – A review of various applications,” *Renew. Sustain. Energy Rev.*, vol. 15, no. 8, pp. 3963–3979, Oct. 2011, doi: 10.1016/j.rser.2011.07.024.
- [98] D. Emad, M. A. El-Hameed, M. T. Yousef, and A. A. El-Fergany, “Computational Methods for Optimal Planning of Hybrid Renewable Microgrids: A Comprehensive Review and Challenges,” *Arch. Comput. Methods Eng.*, Jul. 2019, doi: 10.1007/s11831-019-09353-9.
- [99] M. D. A. Al-falahi, S. D. G. Jayasinghe, and H. Enshaei, “A review on recent size optimization methodologies for standalone solar and wind hybrid renewable energy system,” *Energy Convers. Manag.*, vol. 143, pp. 252–274, Jul. 2017, doi: 10.1016/j.enconman.2017.04.019.
- [100] R. Siddaiah and R. P. Saini, “A review on planning, configurations, modeling and optimization techniques of hybrid renewable energy systems for off grid applications,” *Renew. Sustain. Energy Rev.*, vol. 58, pp. 376–396, May 2016, doi: 10.1016/j.rser.2015.12.281.
- [101] N. A. C., R. Jyoti, and A. B. Raju, “Economic analysis and comparison of proposed HRES for stand-alone applications at various places in Karnataka state,” in *ISGT2011-India*, Kollam, Kerala, India, Dec. 2011, pp. 380–385, doi: 10.1109/ISET-India.2011.6145346.
- [102] W. L. Theo, J. S. Lim, S. R. Wan Alwi, N. E. Mohammad Rozali, W. S. Ho, and Z. Abdul-Manan, “An MILP model for cost-optimal planning of an on-grid hybrid power system for an eco-industrial park,” *Energy*, vol. 116, pp. 1423–1441, Dec. 2016, doi: 10.1016/j.energy.2016.05.043.
- [103] Q. Wu, H. Ren, W. Gao, and J. Ren, “Multi-objective optimization of a distributed energy network integrated with heating interchange,” *Energy*, vol. 109, pp. 353–364, Aug. 2016, doi: 10.1016/j.energy.2016.04.112.
- [104] H. Ren, Q. Wu, W. Gao, and W. Zhou, “Optimal operation of a grid-connected hybrid PV/fuel cell/battery energy system for residential applications,” *Energy*, vol. 113, pp. 702–712, Oct. 2016, doi: 10.1016/j.energy.2016.07.091.
- [105] E. Koutroulis, D. Kolokotsa, A. Potirakis, and K. Kalaitzakis, “Methodology for optimal sizing of stand-alone photovoltaic/wind-generator systems using genetic algorithms,” *Sol. Energy*, vol. 80, no. 9, pp. 1072–1088, Sep. 2006, doi: 10.1016/j.solener.2005.11.002.

- [106] S. Upadhyay and M. P. Sharma, "Development of hybrid energy system with cycle charging strategy using particle swarm optimization for a remote area in India," *Renew. Energy*, vol. 77, pp. 586–598, May 2015, doi: 10.1016/j.renene.2014.12.051.
- [107] M. B. Shadmand and R. S. Balog, "Multi-Objective Optimization and Design of Photovoltaic-Wind Hybrid System for Community Smart DC Microgrid," *IEEE Trans. Smart Grid*, vol. 5, no. 5, pp. 2635–2643, Sep. 2014, doi: 10.1109/TSG.2014.2315043.
- [108] A. Askarzadeh and L. dos Santos Coelho, "A novel framework for optimization of a grid independent hybrid renewable energy system: A case study of Iran," *Sol. Energy*, vol. 112, pp. 383–396, Feb. 2015, doi: 10.1016/j.solener.2014.12.013.
- [109] S. Ahmadi and S. Abdi, "Application of the Hybrid Big Bang–Big Crunch algorithm for optimal sizing of a stand-alone hybrid PV/wind/battery system," *Sol. Energy*, vol. 134, pp. 366–374, Sep. 2016, doi: 10.1016/j.solener.2016.05.019.
- [110] J.-H. Cho, M.-G. Chun, and W.-P. Hong, "Structure Optimization of Stand-Alone Renewable Power Systems Based on Multi Object Function," *Energies*, vol. 9, no. 8, p. 649, Aug. 2016, doi: 10.3390/en9080649.
- [111] Y. A. Katsigiannis, P. S. Georgilakis, and E. S. Karapidakis, "Hybrid Simulated Annealing–Tabu Search Method for Optimal Sizing of Autonomous Power Systems With Renewables," *IEEE Trans. Sustain. Energy*, vol. 3, no. 3, pp. 330–338, Jul. 2012, doi: 10.1109/TSST.2012.2184840.
- [112] M. Tahani, N. Babayan, and A. Pouyaei, "Optimization of PV/Wind/Battery stand-alone system, using hybrid FPA/SA algorithm and CFD simulation, case study: Tehran," *Energy Convers. Manag.*, vol. 106, pp. 644–659, Dec. 2015, doi: 10.1016/j.enconman.2015.10.011.
- [113] A. Khare and S. Rangnekar, "A review of particle swarm optimization and its applications in Solar Photovoltaic system," *Appl. Soft Comput.*, vol. 13, no. 5, pp. 2997–3006, May 2013, doi: 10.1016/j.asoc.2012.11.033.
- [114] D. P. Rini and S. M. Shamsuddin, "Particle Swarm Optimization: Technique, System and Challenges," *Int. J. Appl. Inf. Syst.*, vol. 1, no. 1, pp. 33–45, Sep. 2011, doi: 10.5120/ijais-3651.
- [115] J. L. Bernal-Agustín and R. Dufo-López, "Simulation and optimization of stand-alone hybrid renewable energy systems," *Renew. Sustain. Energy Rev.*, vol. 13, no. 8, pp. 2111–2118, Oct. 2009, doi: 10.1016/j.rser.2009.01.010.
- [116] D. Kaur and P. S. Cheema, "Software Tools for Analyzing the Hybrid Renewable Energy Sources:-A Review," p. 4.
- [117] R. Islam, "Feasibility Study of Small Nuclear Power Plant within Modern Microgrids," p. 146.
- [118] R. Luna-Rubio, M. Trejo-Perea, D. Vargas-Vázquez, and G. J. Ríos-Moreno, "Optimal sizing of renewable hybrids energy systems: A review of methodologies," *Sol. Energy*, vol. 86, no. 4, pp. 1077–1088, Apr. 2012, doi: 10.1016/j.solener.2011.10.016.
- [119] R. K. Rajkumar, V. K. Ramachandaramurthy, B. L. Yong, and D. B. Chia, "Techno-economical optimization of hybrid pv/wind/battery system using Neuro-Fuzzy," *Energy*, vol. 36, no. 8, pp. 5148–5153, Aug. 2011, doi: 10.1016/j.energy.2011.06.017.

- [120] C.-T. Tsai, T. M. Beza, W.-B. Wu, and C.-C. Kuo, “Optimal Configuration with Capacity Analysis of a Hybrid Renewable Energy and Storage System for an Island Application,” *Energies*, vol. 13, no. 1, p. 8, Dec. 2019, doi: 10.3390/en13010008.
- [121] H. Borhanazad, S. Mekhilef, V. Gounder Ganapathy, M. Modiri-Delshad, and A. Mirtaheri, “Optimization of micro-grid system using MOPSO,” *Renew. Energy*, vol. 71, pp. 295–306, Nov. 2014, doi: 10.1016/j.renene.2014.05.006.
- [122] “7.133 Renewable Fraction.” https://www.homerenergy.com/products/pro/docs/latest/_renewable_fraction.html (accessed Sep. 28, 2020).
- [123] “HOMER - Hybrid Renewable and Distributed Generation System Design Software.” <https://www.homerenergy.com/> (accessed Jan. 02, 2020).
- [124] W. Ko and J. Kim, “Generation Expansion Planning Model for Integrated Energy System Considering Feasible Operation Region and Generation Efficiency of Combined Heat and Power,” *Energies*, vol. 12, no. 2, p. 226, Jan. 2019, doi: 10.3390/en12020226.
- [125] P. W. Stackhouse, “Surface Meteorology and Solar Energy (SSE) Data Release 5.1.” Accessed: Jul. 24, 2020. [Online]. Available: <https://ntrs.nasa.gov/search.jsp?R=20080012141>.
- [126] “Group Picnics at Lakeview Park,” Jul. 30, 2020. <https://www.oshawa.ca/en/things-to-do/Group-Picnics.asp> (accessed Aug. 12, 2020).
- [127] “Flows,” *International Joint Commission*, Sep. 25, 2018. <https://ijc.org/en/loslrb/watershed/flows> (accessed Aug. 12, 2020).
- [128] S. M. Bragg-Sitton *et al.*, “Nuclear-Renewable Hybrid Energy Systems: 2016 Technology Development Program Plan,” INL/EXT--16-38165, 1333006, Mar. 2016. doi: 10.2172/1333006.
- [129] K. Lee and J. Park, “Application of Particle Swarm Optimization to Economic Dispatch Problem: Advantages and Disadvantages,” in *2006 IEEE PES Power Systems Conference and Exposition*, Atlanta, Georgia, USA, 2006, pp. 188–192, doi: 10.1109/PSCE.2006.296295.
- [130] O. H. Mohammed, Y. Amirat, and M. Benbouzid, “Particle Swarm Optimization Of a Hybrid Wind/Tidal/PV/Battery Energy System. Application To a Remote Area In Bretagne, France,” *Energy Procedia*, vol. 162, pp. 87–96, Apr. 2019, doi: 10.1016/j.egypro.2019.04.010.
- [131] “Solar resource data – time series data vs monthly averages.” <https://solargis.com/blog/best-practices/solar-resource-data-time-series-data-vs-monthly-averages> (accessed Sep. 28, 2020).
- [132] “Cost Competitiveness of Micro-Reactors for Remote Markets.” Nuclear Energy Institute, Apr. 15, 2019.
- [133] T. Minkiewicz and A. Reński, “Nuclear power plant as a source of electrical energy and heat.” Faculty of Electrical and Control Engineering, Gdansk University of Technology, Oct. 2011.
- [134] M. F. Sherlock, “The Renewable Electricity Production Tax Credit: In Brief,” p. 16.
- [135] P. Lang, “Nuclear Power Learning and Deployment Rates; Disruption and Global Benefits Forgone,” *Energies*, vol. 10, no. 12, p. 2169, Dec. 2017, doi: 10.3390/en10122169.

- [136] A. McDonald and L. Schratzenholzer, “Learning rates for energy technologies,” *Energy Policy*, vol. 29, no. 4, pp. 255–261, Mar. 2001, doi: 10.1016/S0301-4215(00)00122-1.
- [137] E. S. Rubin, I. M. L. Azevedo, P. Jaramillo, and S. Yeh, “A review of learning rates for electricity supply technologies,” *Energy Policy*, vol. 86, pp. 198–218, Nov. 2015, doi: 10.1016/j.enpol.2015.06.011.
- [138] Q. Lee, “Learning & Experience Curves In Manufacturing,” p. 15, 2012.
- [139] “Latest Oil, Energy & Metals News, Market Data and Analysis | S&P Global Platts.” <https://www.spglobal.com/platts/en> (accessed Jul. 13, 2020).
- [140] G. Locatelli, S. Boarin, F. Pellegrino, and M. E. Ricotti, “Load following with Small Modular Reactors (SMR): A real options analysis,” *Energy*, vol. 80, pp. 41–54, Feb. 2015, doi: 10.1016/j.energy.2014.11.040.
- [141] “Load Following Power Plant,” *Nuclear Power*. <https://www.nuclear-power.net/nuclear-power/reactor-physics/reactor-operation/normal-operation-reactor-control/load-following-power-plant/> (accessed Jul. 13, 2020).
- [142] C. Lewis, R. MacSweeney, M. Kirschel, W. Josten, T. Roulstone, and G. Locatelli, “Small modular reactors: Can building nuclear power become more cost-effective?,” National Nuclear Laboratory, Mar. 2016. [Online]. Available: https://www.researchgate.net/publication/321715136_Small_modular_reactors_Can_building_nuclear_power_become_more_cost-effective.
- [143] S. Bragg-Sitton, “Hybrid energy systems (HESs) using small modular reactors (SMRs),” in *Handbook of Small Modular Nuclear Reactors*, Elsevier, 2015, pp. 319–350.
- [144] C. L. Archer and M. Z. Jacobson, “Supplying Baseload Power and Reducing Transmission Requirements by Interconnecting Wind Farms,” *J. Appl. Meteorol. Climatol.*, vol. 46, no. 11, pp. 1701–1717, Nov. 2007, doi: 10.1175/2007JAMC1538.1.
- [145] B. Upadhyaya and T. Kerlin, *Dynamics and control of nuclear reactors*, 1st ed. San Diego: Academic press is an imprint of Elsevier, 2019.
- [146] N. El Bassam, P. Maegaard, and M. L. Schlichting, “Solar Energy,” in *Distributed Renewable Energies for Off-Grid Communities*, Elsevier, 2013, pp. 91–109.
- [147] A. Heydari and A. Askarzadeh, “Optimization of a biomass-based photovoltaic power plant for an off-grid application subject to loss of power supply probability concept,” *Appl. Energy*, vol. 165, pp. 601–611, Mar. 2016, doi: 10.1016/j.apenergy.2015.12.095.
- [148] N. E. B. Government of Canada, “NEB – Market Snapshot: The cost to install wind and solar power in Canada is projected to significantly fall over the long term,” Feb. 13, 2020. <https://www.cer-rec.gc.ca/nrg/ntgrtd/mrkt/snpst/2018/11-03cstnstllwnd-eng.html> (accessed Jul. 24, 2020).
- [149] “Solar Panel Maintenance Costs | Solar Power Maintenance Estimates,” *Fixr.com*. <https://www.fixr.com/costs/solar-panel-maintenance> (accessed Apr. 16, 2020).
- [150] “What Is the Lifespan of a Solar Panel?” <https://www.engineering.com/DesignerEdge/DesignerEdgeArticles/ArticleID/7475/What-Is-the-Lifespan-of-a-Solar-Panel.aspx> (accessed Apr. 16, 2020).
- [151] “SUN2000-(25KTL, 30KTL)-US, User Manual.” HUAWEI TECHNOLOGIES CO., LTD., Apr. 01, 2017, [Online]. Available:

- https://www.huawei.com/minisite/solar/en-na/service/SUN2000-25KTL-30KTL-US/User_Manual.pdf.
- [152] S. Diaf, G. Notton, M. Belhamel, M. Haddadi, and A. Louche, “Design and techno-economical optimization for hybrid PV/wind system under various meteorological conditions,” *Appl. Energy*, vol. 85, no. 10, pp. 968–987, Oct. 2008, doi: 10.1016/j.apenergy.2008.02.012.
- [153] R. N. S. R. Mukhtaruddin, H. A. Rahman, M. Y. Hassan, and J. J. Jamian, “Optimal hybrid renewable energy design in autonomous system using Iterative-Pareto-Fuzzy technique,” *Int. J. Electr. Power Energy Syst.*, vol. 64, pp. 242–249, Jan. 2015, doi: 10.1016/j.ijepes.2014.07.030.
- [154] “US wind O&M costs estimated at \$48,000/MW; Falling costs create new industrial uses: IEA | New Energy Update.” <https://analysis.newenergyupdate.com/wind-energy-update/us-wind-om-costs-estimated-48000mw-falling-costs-create-new-industrial-uses-iea> (accessed Apr. 17, 2020).
- [155] T. Stehly, P. Beiter, D. Heimiller, and G. Scott, “2017 Cost of Wind Energy Review,” *Renew. Energy*, p. 61, 2018.
- [156] “Small wind turbines,” *Eocycle*. <https://eocycle.com/our-wind-turbines/> (accessed Jul. 24, 2020).
- [157] “Run of River Power - Energy BC.” <http://www.energybc.ca/runofriver.html> (accessed Aug. 03, 2020).
- [158] H. A. Gabbar, M. R. Abdussami, and Md. I. Adham, “Techno-Economic Evaluation of Interconnected Nuclear-Renewable Micro Hybrid Energy Systems with Combined Heat and Power,” *Energies*, vol. 13, no. 7, p. 1642, Apr. 2020, doi: 10.3390/en13071642.
- [159] “RENEWABLE ENERGY TECHNOLOGIES: COST ANALYSIS SERIES (Hydropower),” International Renewable Energy Agency (IRENA), Power Sector Issue 3/5 Volume 1, Jun. 2012.
- [160] A. Acakpovi, “Original Framework for Optimizing Hybrid Energy Supply,” *J. Energy*, vol. 2016, pp. 1–10, 2016, doi: 10.1155/2016/8317505.
- [161] A. Wu, D. Lovett, M. McEwan, F. Cecelja, and T. Chen, “A spreadsheet calculator for estimating biogas production and economic measures for UK-based farm-fed anaerobic digesters,” *Bioresour. Technol.*, vol. 220, pp. 479–489, Nov. 2016, doi: 10.1016/j.biortech.2016.08.103.
- [162] R. L. Grando, F. V. da Fonseca, and A. M. de S. Antunes, “Mapping of the Use of Waste as Raw Materials for Biogas Production,” *J. Environ. Prot.*, vol. 08, no. 02, pp. 120–130, 2017, doi: 10.4236/jep.2017.82010.
- [163] L. Jarrar, O. Ayadi, and J. Al Asfar, “Techno-economic Aspects of Electricity Generation from a Farm Based Biogas Plant,” *J. Sustain. Dev. Energy Water Environ. Syst.*, vol. 8, no. 3, pp. 476–492, Sep. 2020, doi: 10.13044/j.sdewes.d7.0302.
- [164] M. K. Shahzad, A. Zahid, T. ur Rashid, M. A. Rehan, M. Ali, and M. Ahmad, “Techno-economic feasibility analysis of a solar-biomass off grid system for the electrification of remote rural areas in Pakistan using HOMER software,” *Renew. Energy*, vol. 106, pp. 264–273, Jun. 2017, doi: 10.1016/j.renene.2017.01.033.

- [165] “A geographical profile of livestock manure production in Canada, 2006.” <https://www150.statcan.gc.ca/n1/pub/16-002-x/2008004/article/10751-eng.htm> (accessed Jul. 23, 2020).
- [166] “Biogas Basics - energypedia.info.” https://energypedia.info/wiki/Biogas_Basics (accessed Jul. 23, 2020).
- [167] M. Lantz, “The economic performance of combined heat and power from biogas produced from manure in Sweden – A comparison of different CHP technologies,” *Appl. Energy*, vol. 98, pp. 502–511, Oct. 2012, doi: 10.1016/j.apenergy.2012.04.015.
- [168] German Solar Energy Society, *Planning and Installing Bioenergy Systems: A Guide for Installers, Architects and Engineers*, 1st ed. Routledge, 2004.
- [169] Y. R. Chen, “Thermal properties of beef cattle manure,” *Agric. Wastes*, vol. 6, no. 1, pp. 13–29, May 1983, doi: 10.1016/0141-4607(83)90003-3.
- [170] A. Al-Rousan and A. Zyadin, “A Technical Experiment on Biogas Production from Small-Scale Dairy Farm,” *J. Sustain. Bioenergy Syst.*, vol. 04, no. 01, pp. 10–18, 2014, doi: 10.4236/jsbs.2014.41002.
- [171] H. M. Morgan *et al.*, “A techno-economic evaluation of anaerobic biogas producing systems in developing countries,” *Bioresour. Technol.*, vol. 250, pp. 910–921, Feb. 2018, doi: 10.1016/j.biortech.2017.12.013.
- [172] P. Lako, “Biomass for Heat and Power,” Energy Technology Systems Analysis Program (ETSAP), May 2010. [Online]. Available: <https://iea-etsap.org/>.
- [173] A. Fathy, “A reliable methodology based on mine blast optimization algorithm for optimal sizing of hybrid PV-wind-FC system for remote area in Egypt,” *Renew. Energy*, vol. 95, pp. 367–380, Sep. 2016, doi: 10.1016/j.renene.2016.04.030.
- [174] A. M. Abdelshafy, H. Hassan, A. M. Mohamed, G. El-Saady, and S. Ookawara, “Optimal grid connected hybrid energy system for Egyptian residential area,” in *2017 International Conference on Sustainable Energy Engineering and Application (ICSEEA)*, Jakarta, Indonesia, Oct. 2017, pp. 52–60, doi: 10.1109/ICSEEA.2017.8267687.
- [175] S. Kharel and B. Shabani, “Hydrogen as a Long-Term Large-Scale Energy Storage Solution to Support Renewables,” *Energies*, vol. 11, no. 10, p. 2825, Oct. 2018, doi: 10.3390/en11102825.
- [176] “California Hydrogen Business Council – CHBC – Hydrogen Means Business in California.” <https://www.californiahydrogen.org/> (accessed Jul. 24, 2020).
- [177] H. S. Das, C. W. Tan, A. H. M. Yatim, and K. Y. Lau, “Feasibility analysis of hybrid photovoltaic/battery/fuel cell energy system for an indigenous residence in East Malaysia,” *Renew. Sustain. Energy Rev.*, vol. 76, pp. 1332–1347, Sep. 2017, doi: 10.1016/j.rser.2017.01.174.
- [178] “Efficiency Water Electrolysis,” *DeepResource*, Jan. 02, 2019. <https://deepresource.wordpress.com/2019/01/02/efficiency-water-electrolysis/> (accessed Jul. 24, 2020).
- [179] S. C. Johnson *et al.*, “Selecting Favorable Energy Storage Technologies for Nuclear Power,” in *Storage and Hybridization of Nuclear Energy*, Elsevier, 2019, pp. 119–175.
- [180] X. Luo, J. Wang, M. Dooner, and J. Clarke, “Overview of current development in electrical energy storage technologies and the application potential in power system

- operation,” *Appl. Energy*, vol. 137, pp. 511–536, Jan. 2015, doi: 10.1016/j.apenergy.2014.09.081.
- [181] “PV Performance Modeling Collaborative | CEC Inverter Test Protocol.” <https://pvpmmc.sandia.gov/modeling-steps/dc-to-ac-conversion/cec-inverter-test-protocol/> (accessed Jul. 24, 2020).
- [182] A. Zidan, H. A. Gabbar, and A. Eldessouky, “Optimal planning of combined heat and power systems within microgrids,” *Energy*, vol. 93, pp. 235–244, Dec. 2015, doi: 10.1016/j.energy.2015.09.039.
- [183] “Thermal Energy Storage Technology Brief.” IEA-ETSAP and IRENA© Technology Brief E17, Jan. 2013, [Online]. Available: <https://www.irena.org/publications/2013/Jan/Thermal-energy-storage>.
- [184] W.-D. Steinmann and M. Eck, “Buffer storage for direct steam generation,” *Sol. Energy*, vol. 80, no. 10, pp. 1277–1282, Oct. 2006, doi: 10.1016/j.solener.2005.05.013.
- [185] “Technology Roadmap Energy storage,” INTERNATIONAL ENERGY AGENCY, 9 rue de la Fédération 75739 Paris Cedex 15, France, 2014. [Online]. Available: <https://speicherinitiative.at/assets/Uploads/20-technologyroadmapenergystorage.pdf>.
- [186] “Learn how much it costs to Install a Steam Shower or Steam Room.” <https://www.homeadvisor.com/cost/plumbing/steam-shower-installation/> (accessed Apr. 24, 2020).
- [187] “Combined Heat and Power Technology Fact Sheet Series.” US Department of Energy, [Online]. Available: <https://betterbuildingssolutioncenter.energy.gov/sites/default/files/attachments/CHP-Steam%20Turbine.pdf>.
- [188] “Steam Generator Efficiency,” *Power Engineering*, Jun. 01, 2007. <https://www.power-eng.com/2007/06/01/steam-generator-efficiency/> (accessed Jul. 24, 2020).
- [189] *A-to-Z Guide to Thermodynamics, Heat and Mass Transfer, and Fluids Engineering: AtoZ*. Begellhouse, 2006.
- [190] “Electricity Generating and Distribution Efficiency.” https://www.mpoweruk.com/energy_efficiency.htm (accessed Jul. 24, 2020).
- [191] “LION ELECTRIC BOILER 28KW | Boilers | Northern Hydronics.” <http://www.northernhydronics.com/Boilers/LION-ELECTRIC-BOILER-28KW/flypage.tpl.html?pop=0> (accessed Apr. 24, 2020).
- [192] “Are electric boilers better than gas boilers? - VHL,” *Village Heating LTD Facilities*, Oct. 30, 2015. <https://www.villageheating.co.uk/alternate-heating-are-electric-boilers-better-than-gas-boilers/> (accessed Jul. 24, 2020).
- [193] N. H. Lipman, “Overview of wind/diesel systems,” *Renew. Energy Elsevier*, vol. 5, Part I, no. 1–4, pp. 595–617, Aug. 1994.
- [194] F. Katiraei and C. Abbey, “Diesel Plant Sizing and Performance Analysis of a Remote Wind-Diesel Microgrid,” in *2007 IEEE Power Engineering Society General Meeting*, Tampa, FL, USA, Jun. 2007, pp. 1–8, doi: 10.1109/PES.2007.386275.
- [195] “Transporting Generators to Remote Locations in an Emergency Situation - New & Used Generators, Ends and Engines | Houston, TX | Worldwide Power Products.”

- <https://www.wpowerproducts.com/news/transporting-generators-to-remote-locations-in-an-emergency-situation/> (accessed Aug. 22, 2020).
- [196] “Generator.”
<https://www.homerenergy.com/products/pro/docs/latest/generator.html> (accessed Aug. 17, 2020).
- [197] “Generator Sizing Guide For Off-Grid Solar Systems,” *Wholesale Solar*, Mar. 22, 2019. <https://www.wholesalesolar.com/blog/generator-sizing-guide> (accessed Aug. 17, 2020).
- [198] K. Kusakana and H. J. Vermaak, “Hybrid diesel generator/renewable energy system performance modeling,” *Renew. Energy*, vol. 67, pp. 97–102, Jul. 2014, doi: 10.1016/j.renene.2013.11.025.
- [199] “How HOMER Creates the Generator Efficiency Curve.”
https://www.homerenergy.com/products/pro/docs/latest/how_homer_creates_the_generator_efficiency_curve.html (accessed Aug. 08, 2020).
- [200] S. J. Ericson and D. R. Olis, “A Comparison of Fuel Choice for Backup Generators,” NREL/TP--6A50-72509, 1505554, Mar. 2019. doi: 10.2172/1505554.
- [201] “Generator Fuel Curve Intercept Coefficient.”
https://www.homerenergy.com/products/pro/docs/latest/generator_fuel_curve_intercept_coefficient.html (accessed Aug. 23, 2020).
- [202] “Canada diesel prices, 18-Nov-2019 | GlobalPetrolPrices.com.”
https://www.globalpetrolprices.com/Canada/diesel_prices/ (accessed Nov. 25, 2019).
- [203] “Salvage Value.”
https://www.homerenergy.com/products/pro/docs/latest/salvage_value.html (accessed Jul. 13, 2020).
- [204] “Generator Heat Recovery Ratio.”
https://www.homerenergy.com/products/pro/docs/latest/generator_heat_recovery_ratio.html (accessed Aug. 21, 2020).
- [205] A. W. Mohemmed and M. Y. Alias, “Particle Swarm Optimization for Constrained and Multiobjective Problems: A Brief Review,” p. 5.
- [206] N. Facchiano, A. Kingman, A. Olore, and D. Zuniga, “Sampling Strategies for Error Rate Estimation and Quality Control,” Worcester Polytechnic Institute, 2008.
- [207] “Applications & Uses of Industrial Diesel Engine Generators.”
<https://www.wpowerproducts.com/news/industrial-diesel-engine-applications/> (accessed Aug. 02, 2020).
- [208] P. Samanta, “Regulatory Review of Micro-Reactors - Initial Considerations,” BNL-212380-2019-INRE, 1581244, Jan. 2020. doi: 10.2172/1581244.
- [209] “4.1 Implementing Security by Design at Nuclear Facilities – WINS.” ,
<https://wins.org/document/4-1-security-by-design/> (accessed Nov. 17, 2020).
- [210] International Atomic Energy Agency, *International safeguards in nuclear facility design and construction*. Vienna: IAEA, 2013.
- [211] G. Bentoumi, “SAFETY AND SECURITY FOR SMALL MODULAR NUCLEAR REACTORS IN CANADA,” p. 8.
- [212] W. Kit, “The easiest kit you’ve ever installed!,” p. 2.
- [213] M. Ragheb, “SAFETY OF WIND SYSTEMS,” p. 41.

